UNIVERSITÉ DU QUÉBEC À MONTRÉAL

POROUS POLYMERIC HOST-MATRICES FOR HIGHLY DISPERSED METAL SUBNANOPARTICLES WITH ANTIBACTERIAL ACTIVITY: MECHANISTIC INSIGHTS

DISSERTATION

PRESENTED

AS PARTIAL FULFILLMENT

OF THE DOCTORATE IN CHEMISTRY

BY

FARZANEH NOORI

JULY 2023

UNIVERSITÉ DU QUÉBEC À MONTRÉAL

MATRICES HÔTES POLYMÉRIQUES POREUSES POUR DES SOUS-NANOPARTICULES MÉTALLIQUES HAUTEMENT DISPERSÉES À ACTIVITÉ ANTIBACTÉRIENNE : ASPECTS MÉCANISTIQUES

THÈSE

PRÉSENTÉ(E)

COMME EXIGENCE PARTIELLE

DU DOCTORAT EN CHIMIE

PAR

FARZANEH NOORI

JUILLET 2023

ACKNOWLEDGEMENTS

I am extremely grateful to my supervisors – **Pr. Mircea A. Mateescu and Pr. Abdelkrim Azzouz** for their invaluable supervision, support, tutelage and patience during the course of my PhD degree. Their immense knowledge and plentiful experience have encouraged me in all the time of my academic research and daily life. I also could not have undertaken this journey without the jury committee – **Pr. Mohamed Siaj and Pr. David Dewez**, who generously provided knowledge and expertise.

My gratitude extends to the Swine and Poultry Infectious Diseases Research Center (CRIPA) of Université de Montréal (UdeM) for three times awarding of the " TOGETHER FOR THE NEXT GENERATION" scholarship to undertake my studies. Additionally, this endeavor would not have been possible without the generous support from Université du Québec à Montréal (UQAM) for " UNIVERSAL DOCTORAL SUPPORT" foundation, who financed my research.

I would like to thank **Dr. Lihong Shang** (McGill University), **Dr. Jean-Philippe Massé** (Polytechnique Montreal) and **Dr. G. Chamoulaud** (Nanoqam) for their technical assistance. My appreciation also goes out to **Pr. Younes Chorfi** and **Dr. Armelle Tchoumi Neree** for their cooperation with our research group in a joint project between UQAM and UdeM. I am also grateful to my colleagues – **Marc-André Labelle** and **Meriem Megoura** for their collaboration which was influential in shaping my experiment methods and analyzing my results. I would be remiss in not mentioning my lab mates from **Pr. Mircea A. Mateescu, Pr. Abdelkrim Azzouz and Pr. René Roy** research groups who impacted and inspired me.

Finely, words cannot accurately express my gratitude to my mom and dad – **Lida** and **Rasoul Noori** who set me off on the road to this PhD a long time ago. Without their tremendous understanding and encouragement in the past few years, it would be impossible for me to complete my study. To conclude, I cannot forget to thank my little brother – **Pooya Noori** who kept my spirits up in the difficult conditions of my studies via his own brand of humor.

To my parents and my brother – it would be an understatement to say that, as a family, we have experienced some ups and downs in the past three years. Every time I was ready to quit, you did not let me and I am forever grateful. This PhD thesis stands as a testament to your unconditional love.

DEDICATION

I would like to dedicate this thesis to my parents, Rasoul and Lida Noori whose words of encouragement and push for tenacity ring in my ears. You have been my source of inspiration, support, and guidance. You have taught me to be unique, to believe in myself, and to always persevere. I am truly thankful and honored to have you as my parents.

To take a quote from Albert Schweitzer,

"At times our own light goes out and is rekindled by a spark from another person. Each of us has cause to think with deep gratitude of those who have lighted the flame within us."

You, mom and dad, have been that spark for me when my light blew out. Thank you for your unwavering love and support along this journey I have taken. I love you both always and forever.

TABLE OF CONTENTS

LIST OF FIGURES

LIST OF SCHEMES

LIST OF TABLES

LIST OF ABBREVIATIONS

MMI	Metal-Matrices Interaction
RT	Room Temperature
CRC	CO_2 Retention Capacity
FCC	Face-Centered Cubic
WL	Weight Loss
ROS	Oxygen Reactive Species
H20	Boltorn™ H20
CFU	Colony Forming Units
PS	Particle Size
CT	Cellulose Tissue
CMS	Carboxymethyl Starch
CMC	Carboxymethyl Cellulose
NaMt	Sodium Montmorillonite
MSNP	Metal Subnanoparticle
MNP	Metal Nanoparticle
IZD	Inhibition Zone Diameter
LAB	Lewis Acid-Base Interaction
TPD	Thermal Programmed Desorption
XPS	X-Ray Photoelectron Spectroscopy
TGA	Thermogravimetric Analysis
SEM	Scanning Electron Microscopy
ZS	Zetasizer
ZP	Zeta Potential
TEM	Transmission Electron Microscopy
XRD	X-Ray Diffraction
EX-XRF	Energy-Dispersion X-Ray Fluorescence
EDAX	Energy Dispersive X-Ray Analysis
OD_{600}	Optical Density at 600 nm
LB	Lysogeny Broth
ZVM	Zero-Valent Metal

CM	Carboxymethyl group
Gu	Glucose Unit
CEC	Cation Exchange Capacity
GP	Gram-Positive
GN	Gram-Negative
HSAB	Hard–Soft Acid Base Theory
DHP	Dihydropteroate Synthase
OM	Outer Membrane
AMR	Antibiotic Microbial Resistance
DS	Degree of Substitution
PP	Polarizing Power
BE	Binding Energy
SPC	Standard Plate Count
XANES	X-ray Absorption Near-edge Structure Spectroscopy

LIST OF SYMBOLS AND UNITS

µV	Microvolt
℃	Degree Celsius
mg	Milligram
mL	Millilitre
cm	Centimeter
nm	Nanometer
mol/g	Mole per gram
eV	Electronvolt
h	Hour
mmol/g	Millimole per gram
CFU/mL	Colony Forming Units per milliliter
rpm	Revolutions or rotations per Minute
W	Watt
kHz	Kilohertz
kDa	Kilodalton
µW	Microwatt
µmol/g	Micromole per gram
Å	Angström
µm	Micrometer
°C/min	Degree Celsius per Minute
mL/min	Millilitre per Minute
mm^2	Square millimeter
wt. %	Weight Percent
w/v	Weight per volume
w/w	Weight per weight
M	Molar

ABSTRACT

This doctoral research was devoted to design of new metal-loaded clay and cellulose materials with antibacterial activity intended to overcome the issue of bacteria resistance to conventional antibiotics. This research tackled an unprecedented approach by correlating the metal retention strength to the antibacterial activity against two microorganisms (*E. coli* and *B. subtilis*), and has been crowned by the production of two publications. The first one was focused on the role of the interactions of host matrices such as montmorillonite and cellulose-supported polyol dendrimers with metal nanoparticles such as CuNP and AgNP and their cationic form (Cu^{2+} and Ag^{+}) in the antibacterial activity. Deeper insights in the role of the oxygen atoms of the organic moiety allowed achieving a second publication by extending the concept of Metal:Oxygen interaction to carboxymethyl groups of two different biopolymers, namely carboxymethylcellulose (CMC) and carboxymethylstarch (CMS). CMS and CMC were found to behave as effective host matrices for metal sub-nanoparticles (MSNP) with diameters smaller than 1 nm. A judicious strategy involved a combination of instrumental techniques such as X-ray Photoelectron Spectroscopy (XPS) and Transmission Electron Microscopy (TEM). The results revealed that the antibacterial activity expressed in terms of inhibition zone diameter (IZD) in the first paper and of IZD and viability tests in the second publication increases with decreasing metal binding energy with the different atoms of the host-matrices and decreasing metal particle size (Metal-PS). The antibacterial activity was found to depend on the metal types as well as their oxidation. The highest performances were registered for both zero-valent and cationic forms of Cu and for Ag^{+}. This provided a significant finding that the antibacterial activity of MNPs is enhanced by weak retention strength and high contact surface with the microorganisms. Another combination involving Zeta potential, particle size and pH measurements allowed stating that enhanced repulsive forces between metal-loaded grains, reduces the material granulometry, improves its dispersion in less acidic aqueous media and raises the contact surface with microorganisms and antibacterial activity. A judicious compromise between metal retention and release by the host matrices in culture media and an increased hydrophilic character turned out to be essential requirements for achieving high biocidal effect. Competitive Lewis acid-base interactions are involved between MNPs and the oxygen atoms of the host materials, and can explain the antibacterial efficiency of the dispersed metals. These findings offer promising prospects for designing effective MNP-loaded matrices to treat dermatological and gastrointestinal infections.

Keywords: Organoclays; Montmorillonite; Carboxymethylcellulose; Carboxymethylstarch; Metal subnanoparticles; X-ray Photoelectron Spectroscopy; Antibacterial activity.

RÉSUMÉ

Cette recherche doctorale était dédiée à l'élaboration de nouveaux matériaux à base d'argile et de cellulose, chargés en métaux et ayant une activité antibactérienne, pour résoudre le problème de résistance bactérienne avec les antibiotiques conventionnels. Ce travail de recherche présente une nouvelle approche qui relie la capacité de rétention des métaux à leur activité antibactérienne sur deux microorganismes (*E. coli* and *B. subtilis*), et a été couronné de deux publications. La première publication traite des interactions entre la matrice hôte de montmorillonite ou des dendrimères de polyols sur support de cellulose, avec des particules de métal comme CuNP, AgNP et leur forme cationique, ainsi que de leurs rôles dans l'activité antibactérienne. Des analyses approfondies du rôle de l'atome d'oxygène ont permis d'obtenir une deuxième publication en étendant le concept d'interaction Métal:Oxygène jusqu'aux fonctions carboxyméthyle de deux différents polymères, notamment la carboxyméthylcellulose (CMC) et le carboxyméthylamidon (CMS). Il fut observé que le CMS et la CMC étaient des bonnes matrices hôtes pour des particules métalliques sub-nanométriques dont le diamètre est plus petit que 1 nm. À ces fins, une combinaison de techniques instrumentales comme la spectroscopie photo électronique des rayons-X et la microscopie électronique à transmission était une stratégie judicieuse. Les résultats ont révélé que l'activité antibactérienne, exprimée en termes de diamètre de zone d'inhibition (IZD) dans la première publication et en termes de IZD et tests de viabilité dans le second article, augmente lorsque l'énergie de liaison des métaux avec les différents atomes diminue et lorsque la taille des particules de métal diminue. L'activité antibactérienne dépend du type de métal mais aussi de leur état d'oxydation. Les meilleures performances ont été enregistrées pour le cuivre cationique et métallique ainsi que pour Ag^{+}. Il fut observé que l'activité antibactérienne des nanoparticules métalliques (MNPs) était plus grande quand la force de rétention était faible et quand la surface de contact avec les micro-organismes était grande. Le potentiel zêta, la taille des particules et les mesures de pH permettent d'affirmer qu'une force de répulsion plus grande entre les grains chargés en métaux réduit la granulométrie, améliore la dispersion en solution moins acide, augmente la surface de contact avec les micro-organismes et donc, améliore l'activité antibactérienne. Un judicieux compromis entre la rétention des métaux, leur libération par la matrice hôte dans le milieu de culture et leur caractère hydrophile s'est avéré être une exigence essentielle pour obtenir un effet virucide prononcé. Des interactions acide-base de Lewis compétitives sont impliquées entre les MNPs et les atomes d'oxygène de la matrice hôte, et peuvent expliquer l'efficacité antibactérienne des métaux dispersés. Ces découvertes permettent de sélectionner des candidats prometteurs pour la conception de matrices chargées en MNPs, efficaces pour traiter les infections dermiques (cutanées) et gastro-intestinales.

Mots clés : Organoargiles; Montmorillonite; Carboxyméthylcellulose; Carboxyméthylamidon; Particules métalliques sous-nanométriques; Spectroscopie photoélectronique par rayons X; Activité antibactérienne.

INTRODUCTION

1. General considerations and context

Antibiotics can be found in nature in many vegetal sources particularly in fungi, but nowadays a major part of pharmaceutical industries are devoted to the manufacture of molecules exhibiting biocidal effect against pathogenic bacteria. These molecules have brought major improvements in health standards for both humans and animal. Abusive utilization of antibiotics in clinical medicine, agriculture, aquaculture, veterinary practice, and poultry and even in the composition of some household products raised many environmental issues. Among these, the unavoidable release of antibiotics in nature generated pollution sources with negative effects on biodiversity and human health. In both nature and animal body, antibiotics act not only as an organic pollutant in inadequate concentrations but also lead to drug-resistance of pathogenic bacteria (Allen *et al.*, 2010; Courvalin, 1994; Karkman *et al.*, 2018). The genes that induce such a resistance arise from the very defense mechanism of the host bacteria against antibiotics. Since bacteria contribute to almost all biological processes in nature, resistance genes persist in the environment and are continuously produced by bacteria in soils (Knapp *et al.*, 2010; Van Goethem *et al.*, 2018). These genes rapidly spread in nature, unavoidably affecting other species of normal bacteria.

There are four main categories of general mechanisms of bacteria resistance against antibiotics: 1. Limiting uptake of drug; 2. Modifying a drug target; 3. Inactivating a drug; 4. Active drug efflux (Lima *et al.*, 2013; Mcmanus, 1997). Each of these mechanisms will be deeply analyzed in the theoretical chapter of the present PhD thesis. Resistance mechanisms used by Gram negative bacteria versus Gram positive are expected to be different according to the structure of bacteria cell wall. All four above-mentioned mechanisms are supposed to be involved by Gram negative strains. The absence of lipopolysaccharide outer membrane (LPS) in Gram positive bacteria cell wall caused them to act less via mechanisms 1 and 4 (Reygaert, 2018).

Bacteria defense mechanisms also involve a resistance against heavy metals, even though most metals excluding ‘’xenobiotic metals can be metabolized in suitable concentrations where and when required. Here also, four possible mechanisms can be involved such as 1. extracellular efflux by pumps; 2. formation of complexes with other components; 3. redox reactions; 4. intra and extra-cellular sequestration. Bacteria actively pump these toxic elements out of the bacterial cells by developing efflux

mechanisms to prevent the accumulation and concentration of heavy metal. Another defense mechanism of bacteria is defined as enzymatic reduction of cations into less toxic oxidation states. To avoid metal re-oxidation, the reduced metal cation should be expelled out of the cell (Ji et Silver, 1995; Nanda *et al.*, 2019). However, such a defensive property of bacteria has major limitations, inasmuch as continuous metal injection within the bacteria cell turns out be to be toxic and harmful for the micro-organism due to their accumulation and concentration (Seiler et Berendonk, 2012; Sharma et Agrawal, 2005).

2. Problematics and issues to be addressed

Drastic increase of antibiotic-resistant bacteria has raised mortality and morbidity rates and created major economic issues for both developing and developed countries (Amabile-Cuevas, 2010; Byarugaba, 2004; Gandra *et al.*, 2014; Groot et Van't Hooft, 2016; Hart et Kariuki, 1998; Iszatt *et al.*, 2021). There exists an ample literature related to the particular cases of Gram-negative bacteria such as *Klebsiella pneumoniae*, *Escherichia coli*, *Acinetobacter*, and *Pseudomonas aeruginosa* which developed resistance against all available antibiotics. These strains currently can be found in some Asia and Mediterranean countries and their number have increased at a critical rate over the recent decades (Ash *et al.*, 2002; Hsu *et al.*, 2010; Mcgowan Jr, 2006). This has become a major environmental and health issue that has stimulated research for developing new alternative to conventional molecular antibiotics that can prevent microorganisms to acquire drug-resistance.

3. Approach and strategies

Metals are known to exhibit toxicity towards living organisms, which are sensitive to even low concentrations of metals due to their capacity to be chelated by sulfur-based groups more particularly of proteins. This was the starting hypothesis of the present doctoral research that incited to focus towards the capacity of metals to bind to thiol or amine groups of cellular proteins leading to their deactivation. The metal concentration inside the bacteria cell increases inducing cell death with increasing tendency of proteins to attract metal ions. Metals such as silver and copper are capable to break the bacterial defense barriers through interaction with sulfhydryl groups (Ref). This is known to deactivate proteins and enzymes functions inducing cell death (Mittapally *et al.*, 2018). Copper ions were found to deform the cell wall via binding to negatively charged groups before accessing and causing damages inside the cell.

Employing this biocidal properties of metals is a judicious approach to synthesize surrogates to conventional antibiotics and address the issue of bacterial resistance (Pang *et al.*, 2019). Silver and copper focus interest more than other metals mainly because of their effective antibacterial activities (Johanson, 2006; Khodakarami et Bagheri, 2021). It would be interesting investigating the effect of the metal valence on its biocidal properties. Positively charged metal cations are supposed to easily penetrate into the bacteria cell wall through diverse pathways among which two seem to prevail in aqueous media: (***i)*** strong electrostatic interaction that alter bacteria membrane equilibrium, and (***ii***) Lewis acid-base interaction with water molecules that generates Brønsted acidity ($M^{n+} + xH_2O \rightarrow [M(H_2O)_{(x-1)}OH]^{(n-1)+} + H^+$) with potential negative impact on the metabolic processes of bacterial cells . In contrast, zero-valent metals can alter the cell wall equilibrium via Lewis acid-base interactions (LAB) with atoms bearing available electron pairs (O, S, and N) that act as Lewis base (Alavi et Rai, 2020; Feng *et al.*, 2000; Harun *et al.*, 2020; Khorsandi *et al.*, 2021; Phan *et al.*, 2020). Such interactions are assumed to affect the normal cell exchange through bacteria membrane (Greiner *et al.*, 2012; Turel et Kljun, 2011).

This special feature of metals opens promising prospects to develop metal-based antibiotics with pharmacological applications (Jarosz *et al.*, 2022; Yu *et al.*, 2019; Zhang et Lippard, 2003). This requires highly effective metal-based antibacterial agents and imposes specific strategies for this purpose. Unlike metal cations, zero-valent metals are bulky aggregates that interact with surrounding species only through their limited outer surface. One of these strategies resides in achieving high metal dispersion even at a subnanometric scale for improving the contact surface between metal particles and bacteria. Highly porous metal-loaded matrices displaying high surface-to-volume ratios are expected to provide a large number of active sites per area unit accessible to microorganisms compared to their massive counterparts (Alavi et Rai, 2019; Gallo et Schillaci, 2021). This first strategy imposes another one, which consists in overcoming the great tendency of metal nanoparticles to aggregate into bulky inactive clusters (Ravindran *et al.*, 2013; Ribeiro *et al.*, 2022). The use of adequate host-matrices bearing high number of chelating groups is a judicious route to address this issue (Soler-Illia et Azzaroni, 2011). Such host-matrices could be hyperbranched polyol dendrimers and carboxylated biopolymers. The performances of their hydroxyls and carboxyls, respectively, will be studied in the present doctoral research, being expected to act as chelating and stabilizing groups for MNPs and metal ions (Qureshi *et al.*, 2020; Zare-Akbari *et al.*, 2016). The interest of this research consists in using low-cost and widely available natural alumino-silicates such as clay minerals. They are also known for their harmlessness, chemical inertness, sorptive capabilities and large specific surface area. The latter may also act as host-matrices for metals through the negative charges

that can capture metal cations through ion-exchange and through the silanols and lattice oxygen atoms that can chelate both cations and zero-valent metals (Uddin, 2018; Varadwaj et Parida, 2013). Mixing clay minerals with dendrimers and/or biopolymers is a comprehensive strategy that offers not only highly dispersed metal particles but also pH-dependent material dispersity that allows tailoring optimum contact surface in the infected media.

4. Main objective

This Ph.D. research is based on three hypotheses 1. Metals are toxic for living organisms; 2. Metals block sulfide and sulfhydryl groups of proteins through Lewis-Acid-Base interaction (LAB) and affect the enzymatic processes and metabolisms; 3. biocidal effect of metals depends on the metal accessibility and contact surface with the infected media. These hypotheses allowed orientating the research undertaken to demonstrate the proof-of-concept of the beneficial roles of increased metal dispersion and of the contact surface on the antibacterial activity. This is the major objective of this research.

5. Specific objectives

As specific objectives, these investigations are intended to provide evidence that the use of host-matrices with intrinsic microporosity such as clay minerals or with induced porosity like metal-loaded clay-dendrimer and clay-biopolymer composites or metal-loaded biopolymers can induce significant improvement of the antibacterial activity against two non-pathogenic bacterial strains. Another specific objective resides in correlating the antibacterial activity to many factors such as the metal, type, oxidation state, particle size and concentration of the metal and the pH of the cultivation media. A final specific objective consists in demonstrating that the biocidal effect results from an optimum compromise between sufficiently strong metal-matrix interaction for stability reason in dry media and sufficiently strong and competitive matrix-water and metal-bacteria interactions for metal mobility and accessibility to micro-organisms.

6. Methodology

Optimizing the physicochemical structure of host matrices is a key factor to tailor the biocidal effect of metals by favoring the metal and dispersion, contact surface and accessibility to micro-organisms**.** This aspect required an ample documentation that allowed building an entire methodology briefly summarized

on the basis of two successive steps. First, preparation of clay-based and clay-cellulose based host materials and dispersion of metals. For this purpose, sodium montmorillonite (NaMt) and cellulose biopolymer (CT) were intercalated with a Boltorn polyol dendrimer denoted as H20. The resulting both clay-dendrimer and polyol-functionalized cellulose composites were further loaded with Ag^{+} and Cu^{2+} to obtain the first series of samples. The second series of samples were prepared by adding $NaBH_4$ for cation reduction to metal zero. The experiments results were obtained mainly from measurements through X-ray Photoelectron Spectroscopy (XPS), Transmission Electron Microscopy (TEM) and determination of the Zeta potential (ZP) and particle size (PS).

Additional measurements were performed through Thermal Programed Desorption (TPD), Thermogravimetric Analysis (TGA) and X-ray diffraction (XRD) to investigate changes in the host matrix basicity and hydrophilicity before and after dispersion of different metals. The particle morphology was screened by Scanning Electron Microscopy (SEM) to investigate the effect of polyol incorporation in metal dispersion. Energy-Dispersive X-ray Fluorescence (EX-XRF) was employed to assess the amount of incorporated metal and particle size.

The antibacterial tests against Gram-positive (*Bacillus subtilis168*) and Gram-negative (*E coli DH5α*) bacteria were evaluated only in terms of inhibition zone diameter (IZD). These results allowed demonstrating a part of the proof-of-concept of the beneficial roles of metal dispersion and of Metal:Matrix and Matrix:water interactions on the antibacterial activity. These results were published as a first paper that offers the basis for the second step of the methodology.

The same approach with more advanced requirements were involved in a second step of this methodology by extending the concept copper and silver dispersion in the entanglement of two biopolymers, namely carboxymethylcellulose (CMC) and carboxymethylstarch (CMS) and their combination with Na^{+}-exchanged montmorillonite. Using the same instrumental characterization techniques, the results allowed correlating the physicochemical structure and properties of host materials with metal dispersion in cultivation media. The hypothetical ‘’metal release’’, if any, was only suggested by the weak retention strength as assessed through XPS data, but still remains to be confirmed by deeper insights in this direction.

Deeper insights into the role of the constituting atoms of the metal loaded matrices on the metal-matrix interaction were achieved by using XPS, ZP and PS measurements. The results allowed highlighting the judicious compromise between the pH induced by the biocidal agent and its particle size in the liquid media

(PS). XPS signal deconvolution was useful to establish the existence of a particle size distribution with strongly depends on the types of metal and of biopolymers. TEM-XPS combination turned to be a judicious strategy to provide evidence of the occurrence of predominant subanoparticles in biopolymers bearing high number of chelating groups.

Here also, the antibacterial activity was expressed in terms of inhibition zone diameter (IZD) against both Gram-positive (*Bacillus subtilis168*) and Gram-negative (*E coli DH5α*) bacteria, and was discussed in correlation with the physicochemical properties of the metal-loaded materials investigated herein. Due to the non-circular shape of most inhibition zone obtained, graphical measurements were carried out using image j software. The effects of pH and metal content on the antibacterial activity were also evaluated through impregnation of the discs of blotting paper with aqueous suspensions of similar amounts of metal cation-loaded biopolymer but with different metal contents for different periods.

An additional set of samples was prepared by mixing the same amount of metal-loaded biopolymer with similar metal content at different pH adjusted with HCl or NaOH aqueous solutions. The viability rate of bacteria in the presence different concentrations of metal-loaded host matrix was evaluated at different times. The results obtained in this second step of the methodology allowed publishing a second paper, which provides valuable evidence that the capacity of carboxylated biopolymer to host metal subnanoparticles is due to the contributions of a higher density of carboxyl group and of the silanol that promote biopolymer dispersion via clay-polymer interaction. In other words, the methodology employed herein allowed achieving the targeted objectives (**Scheme 1**). This methodology imposed the following structure to the present doctoral thesis.

7. The structure of the thesis

The content of the present Ph.D. thesis is structured in six chapters. These chapters are devoted to a critical review of literature data, an experimental part, two sections gathering the results & discussion of publications, general discission and a general conclusion that synthesizes the main findings making emphasis on the most important ones. The descriptions of the different chapters are provided here below.

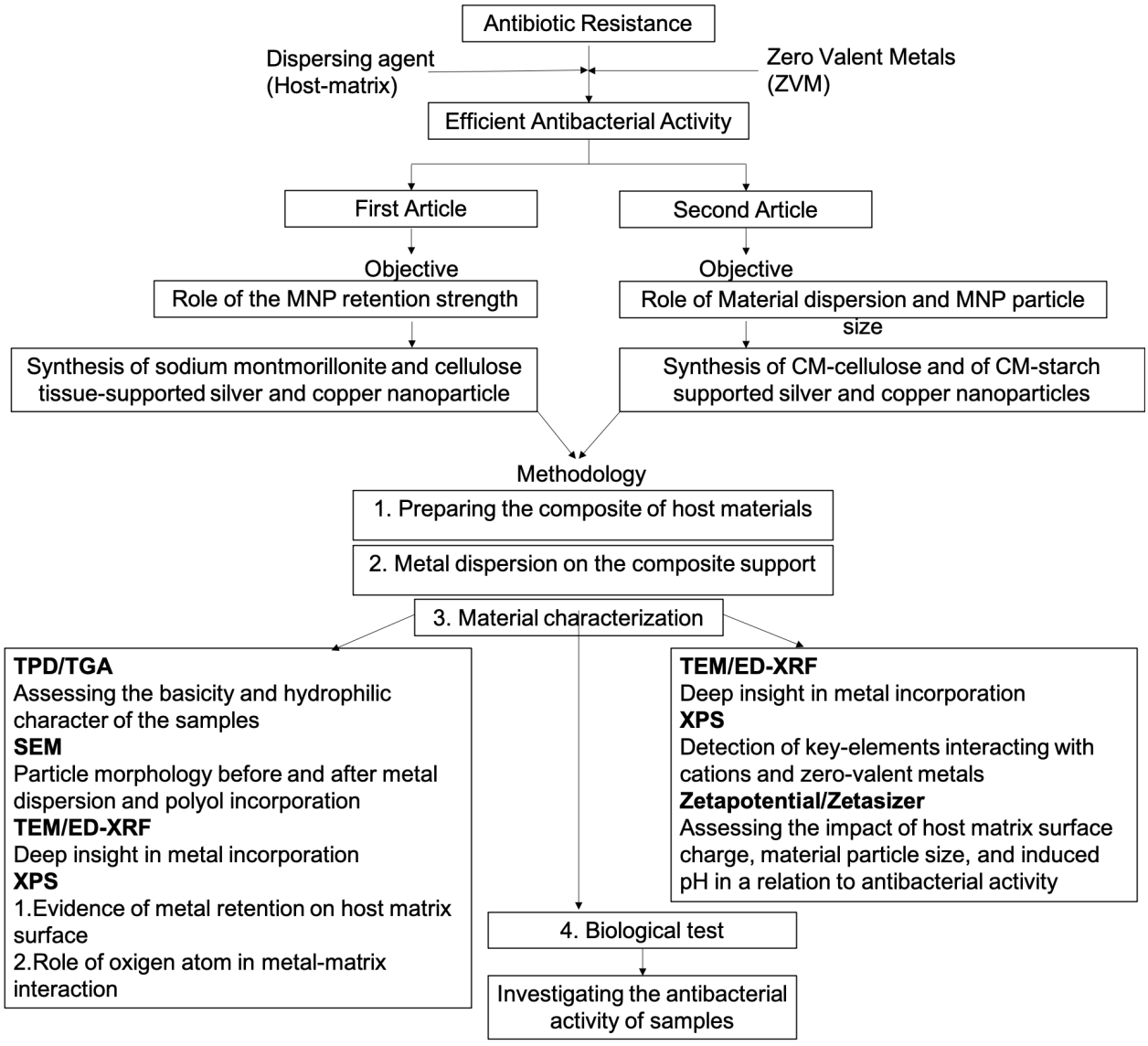

Scheme 0.1. Synthetical methodology for the targeted objectives.

Chapter 1. Critical review of literature data

It contains ten sub-chapters focused on general information about: 1. the mechanisms and causes of bacterial resistance; 2. Attempts to address bacteria resistance; 3. antibacterial mechanisms of metal cations and zero-valent metals; 4. Adverse pathophysiological outcomes of metals; 5. The general advantages of metal nanoparticles as antibacterial materials; 6. Physical and chemical synthetic methods and their effects on MNP structure; 7. Main drawbacks of nano-particulate system and necessity of using support matrices; 8. Overview of different biomaterials modified with metal ions and/or metallic

nanoparticles and the concept of metal release/retention and its effect on antibacterial activity; 9. General information about the chemical structure and biomedical applications of the host materials (Hyperbranched dendritic polymers, Natural alumina silicates, Carboxylated biopolymers, Porous organoclay host materials with high metal capturing abilities); 10. Role of dispersion and stabilizing agents in MNP size.

Chapter 2. Experimental part

It involves the following sections: 1. List of chemicals and materials employed in both steps of this research; 2. Protocols for the preparation of cation- and metal-loaded materials; 3. Introducing the instrumental techniques and analytical methods for the characterization of the synthesized materials; 4. Strategy used to evaluate the antibacterial activity in terms of inhibition zone diameter and viability rate.

Chapter 3. **First article:** Insights in metal retention role on the antibacterial behavior of montmorillonite and cellulose tissue supported copper and silver nanoparticles

This chapter is structured in the form of the first publication including comparative studies of the role of metal-matrix interaction (MMI) on the antibacterial performance expressed in terms of inhibition zone of copper and silver in both cationic and zero-valent form supported by sodium montmorillonite (NaMt) and cellulose tissue (CT) and their combinations with dendrimer Boltorn^{TM}H20.

Chapter 4. **Second article:** Synthesis of metal-loaded carboxylated biopolymers with antibacterial activity through metal subnanoparticle incorporation

This chapter contains the second publication that was an extension of the concept demonstrated in the first one to carboxymethylcellulose (CMC) and carboxymethylstarch (CMS) as stabilizing agents for metals. However, the second paper differs from the previous one by new findings related to the synthesis metal sub-nanoparticles (MSNPs) and to the key-role of the degree of substitution (DS) defined as the number of carboxyls per glucose unit that turned out to govern the metal capturing ability of the two biopolymers. A comprehensive characterization through sophisticated techniques in combination with additional antibacterial tests involving viability allowed demonstrating the significant contributions of the metal retention strength and the particle size distribution of both the metal and metal-loaded materials.

Chapter 5. General discussion

The goal of including a general discussion chapter in the current thesis is to provide a comprehensive overview and interpretation of the results presented in Chapter 3 and Chapter 4. This chapter allows the reader to synthesize the findings from these two chapters, explore their implications, and discuss their significance in the broader context of my research topic.

Chapter 6. General conclusion

The last chapter of this Ph.D. thesis is devoted to an inventory of the main conclusions withdrawn in each step of this research followed by a synthetical analysis of the most important findings with emphasis on what remains to be elucidated through future investigations. Judiciously tailored Lewis acid-base interactions turn out to govern material dispersion in the infected media and antibacterial activity. Notwithstanding that weak [–Oxygen:Metal] interaction reduces MNP retention strength, the suggested metal release in the liquid media or directly on the bacterial cell membrane still remains to be elucidated.

All of these valuable findings allowed demonstrating that matrices hosting sub-metal nanoparticles could be regarded as promising surrogates to conventional antibiotics. This can be achieved if the physico-chemical interactions occurring within the matrix and liquid media are also taken into account in future research in this direction.

CHAPTER 1

CRITICAL REVIEW OF LITERATURE DATA

1.1 Challenge of Bacterial Resistance

Over the world, infections are a major cause of death and the rise of more pathogenic germs and development of antibiotic microbial resistance (AMR) have become challenging public health issues. AMR is an inevitable evolutionary outcome because all organisms undergo self-protective genetic alterations. The causes of bacterial resistance to various classes of antibiotics are examined in this section (Uddin *et al.*, 2021).

1.1.1 General Mechanisms of Antibacterial Activity of Conventional Antibiotics

Antibiotics damaging the bacterial Cell Wall Synthesis

The cell wall of a bacterial cell mainly consists of cross-linked peptidoglycans which act as mechanical supports (Zapun *et al.*, 2008). The cross-linking is achieved by transpeptidases upon recognition of a D-Ala-D-Ala dipeptide (**Scheme 1.1a-c**). Glycopeptides (vancomycin) and β-lactams are two different kinds of antibiotics that prevent the production of cell walls. The β-lactams have a structure similar as that of the D-Ala-D-Ala dipeptide (**Scheme 1.1d**). They bind covalently and are quite difficult to be hydrolyzed, thereby hindering the production of cell wall. Vancomycin and other glycopeptide antibiotics inhibit the formation of cell walls by binding to the D-alanyl D-alanine part of the peptide side chain of the precursor peptidoglycan subunit (Ghooi et Thatte, 1995; Liu et Breukink, 2016).

Inhibitors of Protein Biosynthesis

Through the transcription process, the information in bacterial DNA is first used to create messenger RNA (mRNA). Further, through a process known as translation, 70S ribosomes allows the synthesis of proteins of mRNA. The 30S and 50S subunits of the ribonucleic protein are known to build the bacterial 70S ribosome and are the target of antimicrobials that prevent protein production.

Aminoglycosides (AGs) are positively charged antibiotics that bind to the negatively charged outer membrane (OM) and allow the entry of antibiotics into the bacterium. However, oxygen and an active proton motive force are needed to flow through the cytoplasmic membrane. Therefore, AGs only function

under aerobic conditions. They allow for higher penetration within the cell and work in synergy with antibiotics that block the formation of cell walls (such as β-lactam and glycopeptides). Through hydrogen bonds, AGs associate with the 30S subunit's 16S rRNA close to the A site, which is the first location where the tRNA binds during protein synthesis. Other antibiotics, such as tetracyclines, act in a similar way.

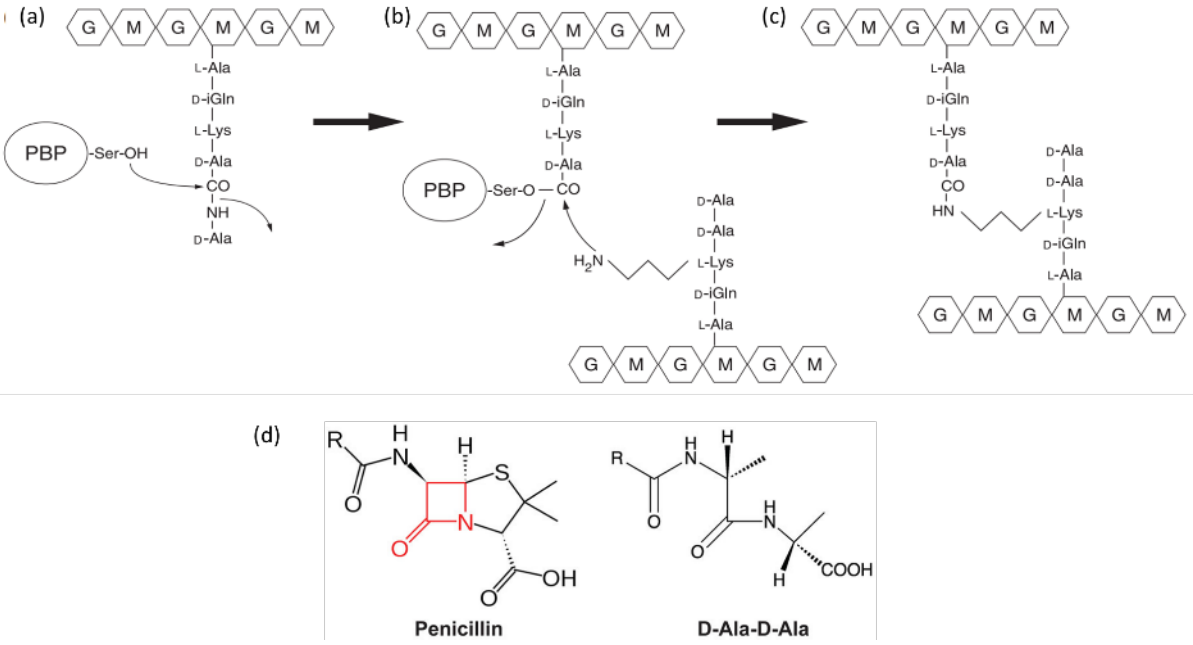

Scheme 1.1. Transpeptidase is part of the penicillin binding proteins (PBPs) of the microorganism. This family has a serine in the active site. This serine attacks the carbonyl of the first D-Ala (on the peptidoglycan), releasing the last D-Ala (a). The D-Ala forming a bridge with the active site serine has a carbonyl that can be attacked by a primary amine from another peptide (b). It is then released by the PBP to create a peptide bridge (c). The structure of β-lactams is similar to the structure of the D-Ala-D-Ala sequence (d) *(* Zapun et al., 2008). G= N-Acetylglucosamine; M= N-Acetylmuramic acid

The second class are macrolides, namely that of 50S subunit inhibitors that impact on the initial stages of protein synthesis. Macrolides, lincosamides and streptogramin B exhibit a similar mode of action.

The third category of antibiotics known as oxazolidinones, prevent many stages of protein synthesis, including: 1. binding to 23S rRNA of the 50S subunit; 2. suppressing 70S ribosomes via interaction with peptidyl-tRNA (Franklin et Snow, 1989; Vázquez, 2012).

Inhibitors of DNA Replication

Fluoroquinolones (FQ) prevent the bacterial DNA gyrase enzyme from nicking double-stranded DNA, adding negative supercoils, and then resealing the nicked ends. This is required to stop the strands from being excessively positively supercoiled when they separate to allow for transcription or replication. The strand cutting and resealing function of the DNA gyrase is hampered by the high affinity binding of the FQs. Greater potency against Gram-positive bacteria might result from greater affinity for this enzyme. Mammalian cells have topoisomerase II instead of DNA gyrase or topoisomerase IV, which have relatively low affinity for FQ and are less hazardous to cells (Baranovskiy *et al.*, 2014; Drlica et Franco, 1988; Kurose *et al.*, 2006).

Folic Acid Metabolism Inhibitors

Sulfonamides and trimethoprim are two types of antibiotics that prevent folic acid metabolism in several ways. Dihydropteroate synthase (DHP) is involved in the folate synthesis, essential for bacterial nucleic acid synthesis. DHP is not expressed in most eukaryotes and has a high affinity for sulfonamides, making it a good target. Trimethoprim inhibits the folic acid synthesis pathway by binding with dihydrofolate reductase (Mazel et Davies, 1999). **Table 1.1** shows targets and mode of actions of different antibiotics.

1.1.2 Causes of Bacterial Resistance

Natural selection has led to an increase in the prevalence and spread of resistance, which should be seen as a predicted effect of the Darwinian biological principle of "survival of the fittest". Several bacterial populations have small number of cells with characteristics that confer them protection against harmful toxins. The capacity to resist the effects of the antibiotic can be used to explain this. The long-term use of antibiotics will significantly alter the bacterial communities in a given environment, leading to a rise in the population of resistant species. As a result, an infection that was once easily curable may not respond well to an antimicrobial when next required (Uddin *et al.*, 2021; Wright, 2010).

Table 1.1. Mode of Action of Different Classes of Antibiotics

Drug class	Targets	Mode of action	Ref.
Beta-lactams	Penicillin-binding protein	Cell wall synthesis inhibition	(Saravolatz *et al.*, 2011)
Glycopeptides, Aminoglycosides and Tetracyclines	Peptidoglycan subunits 30 s subunits	Inhibition of protein synthesis	(Macone *et al.*, 2014; Saravolatz *et al.*, 2009)
Macrolides, Chloramphenicol and Oxazolidinones	50 s subunit	Inhibition of protein synthesis	(Moellering Jr, 2014; Wolter *et al.*, 2005)
Rifamycin (rifampicin)	RNA	Inhibition of nucleic acid synthesis	(Robertson *et al.*, 2008)
Fluoroquinolones	DNA	Inhibition of nucleic acid synthesis	(Abbanat *et al.*, 2008)
Sulfonamides and trimethoprim	Folic acid synthesis enzymes	Anti-metabolites	(Sköld, 2001)
Polymyxins	Lipopolysaccharides	Disrupt membranes	(Velkov et Roberts, 2019)
Lincosamides	30 s subunit and 50 s subunit	Inhibition of protein synthesis	(Zhao *et al.*, 2014)
Sulfamethoxazole	DNA , 30 s subunit and 50 s subunit	Inhibition of nucleic acid and protein synthesis	(Moghaddam *et al.*, 2021)

There are some main causes of bacterial adaptation over time. Natural causes may result in bacterial changes in two ways. The first one is genetic mutation, where base pair changes can take place during bacterial reproduction. By replacing one or a few amino acids in a vital target (enzyme, cell wall, or cell structure) and by regulating genes or chromosomal structures, a phenomenon known as point mutation, leads to the formation of novel resistant strains. The second microbial-based explanation is genetic material transfer. Here, a previously vulnerable strain may develop resistance from a different species or genus. Most of the genes that cause antibiotic resistance are found on plasmids and other mobile genetic components, which can and frequently do transfer to various genera and species of bacteria (Chinedum, 2005).

Selective pressure is a term used to describe an environmental factor that promotes the growth of microorganisms with unique mutations or newly evolved traits. Antimicrobials either kill microorganisms or allow them to survive if they have resistant genes. The newly generated resistant bacteria will proliferate quickly and become the predominant form among the germs (Kolář *et al.*, 2001; Witte, 2000).

Inaccurate treatment is possible when administering an antibiotic or a wide-spectrum antibiotic whereas a specific narrow spectrum antibiotic may be more suited. It amplifies the selective pressure and speed up

the development of antibiotic resistance (Hornischer et Häußler, 2016). There are also some other reasons as self-medication, inadequate or inappropriate prescription of antibiotics, their overuse, their extensive use in agriculture, poor hospital environments and the small number of new antibiotics available.

1.1.3 Main Mechanisms of Bacterial Resistance

Infections that call for the use of second- and third-line treatments frequently arise as a result of antibacterial resistance. In the USA alone, antibiotic-resistant bacteria like methicillin-resistant *Staphylococcus aureus* cause ~19,000 fatalities annually. Therefore, the use and prescription of antibiotics must be changed immediately. Antibiotic resistance will continually pose a serious hazard even if new medications are created. **Table 1.2** provides a summary of some of the most dangerous species showing multiple drug resistance (MDR) that have developed resistance to many types of antimicrobial agents (Galletta *et al.*, 2020).

Bacteria that are susceptible to antibiotics can develop resistance through genetic mutation or by transferring antibiotic-resistant genes from other bacteria (natural resistance or acquired resistance). There are three main types of genetic mutation: a) Mutation; b) Inactivation or Destruction; and c) Efflux. In addition, bacteria can exchange resistant genetic material through 1. Transformation; 2. Transduction; and 3. Conjugation (Pitton, 1972; Reygaert, 2018; Van Duijkeren *et al.*, 2018).

Mutation - A mutation is a change in the DNA that may result in a change to the gene product, which is the antimicrobial's target. Antimicrobials, no longer bind effectively when spontaneous mutations arise in regions of the genes encoding DNA gyrase. As a result, the bacterium can carry on with DNA replication (Fernández et Hancock, 2012).

Destruction or Inactivation - Numerous bacteria have genes that produce enzymes that chemically break down or inactivate the antibiotic. The two primary ways are deterioration of the drug and/or transfer of a chemical group to the drug. The broad category of drug-hydrolyzing enzymes is known as β-lactamases. As example, tetracyclines of the fourth generation gave promising clinical trials but were found to be inactivated in presence of a gene called tetX, originating from a plasmid found in *Bacteroides fragilis* (Markley et Wencewicz, 2018).

Table 1.2. Mechanism of Resistance of Different Bacteria Strains.

The name of bacteria	Resistant to	Mechanism of resistance	Ref.
P. aeruginosa	Aminoglycoside	Enzymatic modification	(Hancock, 1998)
S. aureus and S. pneumoniae	Beta-lactams	Enzymatic Degradation	(Shortridge *et al.*, 1996)
E. faecium and E. faecalis	Glycopeptides	Altered target	(Al-Obeid *et al.*, 1990)
S. aureus, S. pneumoniae and S. pyogenes	Macrolides	Altered target	(Farrell *et al.*, 2002)
S. pneumoniae, S. pyogenes, S. faecium and S. aureus	Oxazolidinones	Efflux pumps and altered target	(Camilli *et al.*, 2008)
S. aureus **and *S. pneumoniae***	Quinolones	Altered target and efflux	(Shortridge *et al.*, 1996)
S. pneumoniae	Chloramphenicol	Antibiotic inactivation and efflux pump	(Widdowson *et al.*, 2000)
E. coli, S. aureus and S. pneumonie	Sulfonamide drugs	Altered target	(Levy *et al.*, 2008)
Neisseria gonorrhea	Cephalosporins	Mutation	(Allen *et al.*, 2014)
Shigella species	Fluoroquinolones	Mutation	(Azmi *et al.*, 2014)
Klebsiella	Cephalosporin and Carbapenems	Loss of porin	(Pfeifer *et al.*, 2010)
Staphylococcus ***aureus***	Oxacillin, Vancomycin and Linezolid	Altered target	(Azhar *et al.*, 2017)
E. coli	Cephalosporins and Fluroquinolones	Antibiotic inactivation	(Shaheen *et al.*, 2013)
Streptococcus ***pneumoniae***	Penicillin	Altered target	(Hakenbeck *et al.*, 1999)

Efflux - An efflux pump is a channel that actively exports antibacterial agents and other chemicals from the cell. Once the compound has entered through a channel known as a porin, the efflux pump forces the antibiotic back out of the bacterium. Therefore, by aggressively pumping out antimicrobials, the efflux pumps stop the intracellular build-up required for them to carry out their bactericidal activity in the cell (Levy, 1992; Longley et Johnston, 2005).

Transformation - Bacterial cells transform when they acquire genetic materials from their surroundings. These genetic materials typically originate from nearby lysed bacteria in nature, and it may also comprise plasmid DNA or fragments of DNA that have been discharged into the environment. The receiving cell inserts the new DNA into its own chromosome (homologous) and becomes pathogenic if a harmless bacterium takes up the DNA for a poisonous gene from a pathogenic type of bacterium. Different bacteria are naturally transformed by a variety of conditions, such as cell growth stage or the presence of specific chemicals.

Transduction - Transduction takes place when a virus or viral vector introduces foreign DNA or RNA into bacterial or eukaryotic cells. Bacteriophages embed their genetic materials inside bacterial cells after

adhering to their membranes. Once within, phages can go through either the lytic or lysogenic life cycle. Lytic phages use the machinery of their bacterial hosts to produce more virus particles. The phage's genetic material is incorporated into the host's genome. Once inside the infected bacteria, the transferred DNA can either persist as temporary extra-chromosomal DNA, similar to a plasmid, on merge with the host bacterium's genome by homologous or site-directed recombination.

Conjugation - Direct contact of two bacteria during conjugation allows the transfer of genetic material from one to the other. The donor bacterium has the Fertility Factor DNA sequence (F-factor) which encodes genes for sexual pili, thin rod-like structures serving the F-carrying male (or donor) bacteria to attach to female (or recipient) cells for conjugative transfer.

Plasmids are frequently the genetic materials transferred and can confer genetic “benefits” to the bacteria, like antibiotic resistance (Adekunle, 2012; Sultan *et al.*, 2018; Tenover, 2006).

1.1.4 Attempts to address bacteria resistance

Health institutions are required to develop strategies for controlling the spread of antibiotic resistance. The most frequently suggested methods include improving hand cleanliness, controlling antibiotic availability over-the-counter, rationing antimicrobial use, and infection prevention and control. However, those are insufficient to achieve the goal of eliminating bacterial resistance. Antimicrobial resistance must be reduced, which calls for multidisciplinary solutions. To curtail bacterial resistance, various approaches are being pursued, including the use of new generations of antibiotics, combination therapy, naturally occurring compounds with antibacterial capabilities, and tailored drug delivery systems **(Table 1.3)**.

Development of Natural Compounds and Novel Antibacterial Agents

Scientific methods of introducing new antibacterial compounds and the development of novel antibacterial agents have been moving slowly over the past few years. Finding and creating really novel antibiotics is difficult since the generation of chemicals which are not harmful to humans takes a long time, costs a lot of money, and fails frequently. As a result, natural substances are currently attracting more research attention as standalone or combined antibacterial agents. While semi-synthetic and synthetic antibiotics show greater therapeutic efficacy and lower toxicity when compared to herbal supplements, natural antibiotics present a significant drawback due to their high toxicity against bacteria. Even with the

existence of natural antimicrobials, the issue of resistance persists since combining several natural antibiotics may cause interactions or undesirable side effects (Butler et Buss, 2006; Guglielmi *et al.*, 2020; Moloney, 2016).

Table 1.3. Approaches for Combating Bacterial Resistance.

Strategies Against Bacterial Resistance			
Natural compounds	**Novel antibacterial agents**	**Nanoparticulate drug delivery systems**	**Combination therapy**
Epigallocatechin gallate Piperine Resveratrol Tannic acid Novobiocin Berberine and harmane Sesquiterpenes	Plazomicin Delafloxacin Nemonoxacin Tedizolid Radezolid Omadacycline Eravacycline Cethromycin Solithromycin Telavancin Dalbavancin Oritavancin Ceftaroline	Lipid-based NPs Liposomes Solid lipid NP (SLN) Polymeric particles Nitric oxide-releasing NPs Metal nanoparticles (MNP)	
Reference			
(Khameneh *et al.*, 2016)	(Khameneh *et al.*, 2016)	(Ramasamy et Lee, 2016; Susanti *et al.*, 2022)	(Mouton, 1999)

Combination Therapy

Antibiotic combination therapy is one method of treating infections with high death rates. The main benefits of using combination therapy include: an increased antibiotic activity by achieving a synergistic effect, prevention of resistance emergence, providing antibacterial activity against microorganisms forming biofilms, enhancing antibacterial agent penetration to cell and tissues, toxin production inhibition, and reduction of enzyme production. Combination therapy broadens the antibacterial spectrum, but there are drawbacks that limit the efficacy of this approach, including hypersensitivity and/or adverse reactions to an antibiotic (like penicillin) and/or metabolic products that cause serious issues ranging from urticaria (hives) to anaphylactic shock (Mouton, 1999; Namivandi-Zangeneh *et al.*, 2021).

Nano-particulate Drug Delivery Systems

Recently in nanotechnology, advances have been made in the creation of nanoparticles with appropriate physico-chemical properties for better medication administration. By loading antibacterial agents in

nanoparticles, some related mechanisms for improving therapeutic potency may include: 1. Modifying the activity of the bacterial efflux pump; 2. Nanoparticles' anti-biofilm activity; 3. Enhanced penetration through biofilm structures; 4. Protection from enzymatic degradation and inactivation via polyanionic compounds; 5. Intracellular bacterial killing; and 6. Specific targeting (Aberdein *et al.*, 2013; Marquez, 2005; Martinez-Gutierrez *et al.*, 2013). The primary systems that have been used in this regard include metal nanoparticles, polymeric nanoparticles, nitric oxide-releasing nanoparticles, and lipid-based nanoparticles.

1.2 Metal species for addressing the bacteria resistance to drugs

So far, a wide variety of metal nanoparticles (MNP) have been tested in attempts to address the issue of drug-resistant bacteria. The main chemical properties of metals for this research reside in their acceptor/donor atom selectivity depending on their oxidation state, their redox potential and speciation diversity with specific effects on living cells (Lemire *et al.*, 2013). The acceptor/donor atom selectivity often arises from strong and selective interactions involving a central metal ion binding to surrounding O, N and/or S atoms that act as ligands and electron pair donors. These interactions are based on coordination chemistry and confer specific roles to metals in protein folding or function.

The “Ligand Field Theory” is useful to predict how the electronic arrangement results in bonding interactions with specific configurations (Griffith et Orgel, 1957). This very metal binding to electron pair donors is one of the causes of intoxication of living organisms that are constituted of macromolecules bearing such chelating groups such as proteins, fats and polysaccharides. There exists an ample literature devoted to the use of metal cations, oxides or zero-valent metals (ZVM) in the form of MNP. This is one of the most common strategies to prevent abusive administration of antibiotics and rise of bacteria resistance.

The speciation of metals occurs as multiple chemical species depending on pH, redox potential, ionic strength and temperature. In a cell, speciation of essential metals is restricted by transporters, metal-regulator sensors and metal-chaperones. Parameters that affect the oxidation state of metals can also vary between the subcellular compartments and microorganisms (Baun et Christensen, 2004; Davidson *et al.*, 1994). Some works have been focused on the interesting capacity of AgNP, CuNP, ZnONP, MnONP, TiO_2NP and their cationic counterparts to kill bacteria (Patel *et al.*, 2017; Rai *et al.*, 2012; Rudramurthy *et al.*, 2016). This antibacterial activity of metals was already discovered and tested by human in past civilizations. Zero-valent metals (ZVM) induce potential and permeability changes in the bacteria

membrane via leakage in lipopolysaccharides, proteins, intracellular biomolecules and proteins (Mello-Filho et Meneghini, 1991).

Cationic forms of metals also exhibit intrinsic antimicrobial effect against bacteria by: 1. ''bridging'' DNA segments into complexes with nucleotides and disrupting H-bonds between base pairs; 2. The production of Adenosine triphosphate (ATP) to alter the DNA replication (Mello-Filho et Meneghini, 1991). Vessels releasing Cu^{2+} and Ag^{+} cations were already employed for water disinfection and food preservation since the time of the Persian kings. Transition metals are still used as antibacterial agents today in treating wounds, burns, rashes and many other health issues.

1.3 Metal cations with antibacterial activity

The mere presence of heavy metals in the environment is a pollution with multiple negative impact, and has become a major ecological, evolutionary, nutritional, and environmental concern (Duruibe *et al.*, 2007; Sharma et Agrawal, 2005). Metals in cationic form are soluble species that can be easily dispersed in living organisms. Unlike light alkali and alkaline-earth metals, the so-called heavy metals are metal cations with high toxicity for the environment and biodiversity, with negative impacts on human, fauna and flora. Transition metal cations in very low concentrations are quintessential to maintain various biochemical and physiological functions in living organisms. They however become noxious when they exceed specific threshold concentrations with several health risks for human and animals. Metal toxicity may be acute or chronic depending on the absorbed dose, type, speciation and exposure duration.

This type of metal cations is of great interest for investigating the behavior of some of them for biomedical purposes. Diverse attempts to synthesize materials for hosting metal cations with enhanced biocidal efficacy and reduced side effects have been achieved so far. In this regard, during the last few decades, different types of supporting materials such as inorganic mesoporous silica and organic micelles, liposomes, biopolymers and dendrimers were used as host matrices for metal with controllable release capacity **(Table 1.4).**

Table 1.4. The State-of-the-Art on biomedical applications of metal cations.

Cations	Host matrices	**Operation conditions**	**Targeted microorganismes**	Measured toxicity parameter	**Ref.**
Ag^{+}, Cu^{2+} and Zn^{2+}	Aluminosilicate zeolites	10.0 g of zeolite was suspended in 500 mL of 0.3 M of metal salts	*Escherichia coli and Staphylococcus aureus*	Determination of Minimal Bactericidal Concentration (MBC)	(Suleiman et Haddadin, 2019)
Fe^{3+}	Montmorillonite (MT)	20 g of Na^{+}-MT and 150 mL of 0.1 mol/L $FeCl_3$ aqueous solution were mixed for 1 h	*E. coli, coliforms, and SPC bacteria*	measuring the number of viable bacteria and total bacteria using a fluorescent staining method	(Suzuki *et al.*, 2021)
Cu^{2+} and Zn^{2+}	Cetylpyridinium and N-lauroylsarcosinate intercalated Mt	1 g Mt-CP-SR was added to 50 mL of the metal ion solutions at the 300-ppm initial concentration	*S. aureus, E. coli*	The ASTM E2149 "Standard Test Method	(Özdemir et Yapar, 2020)
Zn^{2+}	Cuban zeolite	1M of Cuban zeolite was mixed with 0.5 M solution of $ZnSO_4{\cdot}7H_2O$	*Helicobacter pylori*	In-vitro tests. Measuring the minimum inhibitory concentration (MIC)	(Cerri *et al.*, 2021)
Ag^{+}, Cu^{2+} and Zn^{2+}	Synthetic zeolite A (A)	Zeolite was mixed with the corresponding metal solution in a weight ratio of 1:100 and shaking the suspension at 25–45 °C in a thermostatic water bath	*Escherichia coli*	Measuring minimal inhibitory concentration (MIC) values by VITEK 2 Compact 15 automated system	(Milenkovic *et al.*, 2017)
Ag^{+}, Cu^{2+}	Natural zeolitised tuff (NZ)	treatment of 2 mol/L of NaNZ with 6 mmol/L of $Cu(NO_3)_2$ or $AgNO_3$ solution in a water bath at 25°C for 24h	*Acinetobacter baumannii*	Bacterial counting by matrix-assisted laser desorption/ionisation – time of flight mass spectrometry	(Hrenović *et al.*, 2020)
Cr^{3+}, Cu^{2+}, Fe^{3+} and Zn^{2+}	Mesoporous silica MCM-41	5 g of non-calcined MCM41 and 100 mL of metallic solution was prepared and stirred for 2 h under room temperature	*P. aeruginos, E. coli, B. cereus, and S. aureus*	Calculation of bacteria inhibition zone diameter (IZD)	(Hachemaoui *et al.*, 2020)
Cu^{2+} and Pb^{2+}	Chemically modified cellulose	2 g of DTD was added to the 1000 mg/L of $CuSO_4{\cdot}5H_2O$, $Pb(NO_3)_2$ solution	*E coli, E. faecalis and S. aureus*	Standard disc diffusion method	(Saravanan et Ravikumar, 2015)

Table 1.4b

Cations	Host matrices	**Operation conditions**	**Targeted microorganisms**	**Measured toxicity parameter**	**Ref.**
Ni^{2+}, Co^{2+}, Cu^{2+}, Zn^{2+}, Pt^{2+}, Cd^{2+} Pd^{2+}	N,N-di-n-propyl-N0 -(2-chlorobenzoyl)-thiourea (HL1) and N,N-diphenyl-N0 -(2-chlorobenzoyl) thiourea (HL2)	metal acetate (0.01 mole) in ethanol (30 cm3) was added dropwise to a solution of the ligand in a 1 : 2 mol ratio	*Escherichia coli, Enterobacter cloacae, Enterococcus faecalis, Pseudomonas aeruginosa, Staphylococcus aureus and Staphylococcus epidermidis*	In vitro antibacterial test via using the agar dilution procedure	(Binzet *et al.*, 2006)
Cu^{2+}, $Ni^{2+,}$, Co^{2+}, Mn^{2+}, Fe^{3+}	Isonicotinic acid (2- hydroxy benzylidene) hydrazide	Metal salt solution as added to the ligan solution in the molar ratio 1:2 (metal:ligand)	Staphylococcus aureus and Escherichia coli	In vitro evaluation of antimicrobial activity was carried by measuring minimum inhibitory concentration (MIC)	(Abou-Melha, 2008)
Co^{2+}, Ni^{2+}	-	5 ml of metal solution was added to 2 ml of cultivation media	*Helicobacter pylori*	Measuring the minimum inhibitory concentrations	(Bruggraber *et al.*, 2004)
Co^{2+}, Ni^{2+}, Mn^{2+}, Cu^{2+}, Cd^{2+}	2-Acetylpyridine o-Hydroxybenzoyl-hydrazone	0.3 mmol of metal salt solution was mixed with o.3 mmol in 50 mL absolute ethanol	*Escherichia coli, Bacillus subtilis*	Measuring inhibition zone diameter (IZD)	(Nawar et Hosny, 1999)
Cu^{2+}, Co^{2+}, Ni^{2+}, Mn^{2+}, Fe^{3+}	Hydrazone 7-chloro-4-(benzylidene-hydrazo) quinoline	The complexes were prepared using of 2:2:1 molar ratios of Li(OH)-ligand-metal salt. 2.82 g. 10 mmol of ligand was added to the 5mmol of metal solution	*Staphylococcus aureus and Escherichia coli*	The ligand and complexes were tested on solid media using the diffusion technique	(Al-Sha'alan, 2007)
Cu^{2+}, Ni^{2+}, Co^{2+}, Mn^{2+}, Zn^{2+}, $Hg^{2+}$and Cd^{2+}	Schiff base (L) derived from 4-aminoantipyrine, 3-hydroxy-4-nitrobenzaldehyde and o-phenylenediamine	A solution of metal(II) chloride in ethanol (2 mM) was refluxed with an ethanolic solution of the Schiff base (2 mM) for ~5 h	*Salmonella typhi, Staphylococcus aureus, Escherichia coli, and Bacillus subtilis*	The in vitro biological screening effects were investigated via the well-diffusion method, using agar nutrient as the medium	(Raman *et al.*, 2007)
Fe^{3+}, Cu^{2+}, Mn^{2+}, and Zn^{2+}	Kaolin-rich clay from the Colombian Amazon (AMZ)	Exchangeable cations in the AMZ were extracted using 1 M NaCl (100 mg of clay/mL of NaCl solution	*Escherichia coli*	Measuring Minimum Inhibitory (MIC) and Minimum Bactericidal Concentrations (MBC)	(Londono *et al.*, 2017)

For divalent transition metal ions of the fourth period, the order of preference for donor ligands is called the Irving–Williams series (Mn^{2+}< Fe^{2+} < Co^{2+} < Ni^{2+} < Cu^{2+} < Zn^{2+}). A second theory, called "Hard–soft Acid Base Theory" (HSAB), is based on the reactivity of metals (Mani, 2018). This theory classifies transition metals according to their affinity for specific organic ligands, e.g., soft acidic (Hg^{2+}, Cu^{2+}, Ag^{+} and Cd^{2+}); and borderline acidic cations (Co^{2+}, Ni^{2+}, Cu^{2+} and Zn^{2+}) tend to associate tightly with soft bases, such as the sulfhydryl (R-SH) groups in proteins. Consequently, the toxicity of these metal cations is approximately proportional to their affinity for the S atom (Lapasam *et al.*, 2019). The oxidation/reduction potential is a thermodynamic parameter that describes the tendency of metals to lose or acquire electrons from an acceptor or donor, respectively.

1.3.1 Disruption of bacteria cell wall

Disruption of bacteria cell wall may occur in contact with metals. The external sides of Gram-Positive (GP) and Gram-Negative (GN) bacteria have net negative charge due to the presence of functional groups such as carboxyl, phosphate, and hydroxyl. GP bacteria cell wall has a tick peptidoglycan layer consisting of linear chains of N-acetylglucosamine (NAC) and N-acetylmuramic acid (NAM). The cell wall of GN bacteria consists of a phospholipid outer membrane bearing negative surface charges.

An electrostatic attraction is induced between metal cations and bacteria cell wall whose negatively charged functional groups strongly bind to metals via ion-dipole interaction. This leads to shrinkage of the cytoplasm membrane or disruption of the cell wall.

Dispersion of both cationic and zero-valent metals in aqueous media where bacteria grow naturally alters bacteria membrane equilibrium through Lewis acid-base interaction with : 1. water molecules generating Brønsted acidity that affects the bacteria functions; 2. O, S and N atoms that act as Lewis acids (Glauert et Thornley, 1969; Gold *et al.*, 2018). The initial damage caused by the metal to the bacterial envelope is crucial for the consecutive penetration inside the cell, where the metal can inflict additional damage on vital cellular functions. Metal ions will bind to proteins and nucleic acids affecting their function.

1.3.2 ROS generation and intracellular damages

Metals are known to induce oxidative stress in the bacteria cell by producing reactive oxygen species (ROS) such as superoxide anion radical ($\bullet O_2^-$), hydrogen peroxide (H_2O_2), and hydroxyl radical (HO•). The high reactivity of oxygen radicals towards phosphates, thiol and carboxyl groups causes them to oxidize some

antioxidant species such as glutathione (GSH), suppressing the antioxidant defense mechanism of the intrinsic ROS naturally produced by the cell. Bacterial growth and cell cycle are also inhibited by oxygen radicals through the dephosphorylation of some key proteins displaying enzymatic activities.

Many relevant studies (Refs – from those already listed) have shown that the free radicals generated on the metal surface would interact with the proteins of the bacterial cell membrane, and oxidize the unsaturated fatty acids, impacting the fluidity and stability of the membrane. Surface-associated ROS production was also found to cause cell membrane rupture. The ROS generated by metals can inactivate the membrane bound enzymes and cause dysfunction of the electron transport chain and proton motive force. This has also an impact on ATP synthesis, interfering with many vital cell functions. In addition, increased ROS levels appear to induce chemical reactions with various cellular components such as DNA, proteins and other biomolecules.

1.3.3 Antibacterial activity of copper cations

Copper is an important cofactor for several key enzymes such as cytochrome C oxidase involved in respiration and photosynthetic processes. Copper cations are involved in several processes depending on the oxidation state. While the reduced Cu^{+} has affinity to thiols and thiol-ether groups, as in cysteine and methionine side chains, the oxidized Cu^{2+} cation induce preferable interactions with oxygen atoms or nitrogen containing-groups belonging to aspartate and glutamate, or the imidazole ring of histidine, respectively. Several pathways which lead to bacteria cell death are suggested for copper ions, including disruption of the cell membrane, intracellular alteration of biochemical processes and induction of DNA damage (Esteban-Cubillo *et al.*, 2006). Copper binds to phospholipids and alters the physicochemical properties of the membrane (fluidity and/or flexibility).

This may also enhance the oxidative stress by generating more hydroxyl radicals at the membrane surface. High concentrations of copper are toxic for prokaryotic cells, partly due to its redox properties. Various studies showed that the antibacterial activity of copper and its transition capacity between Cu^{+} and Cu^{2+} can produce ROS under aerobic conditions. The so-called Fenton chemistry of copper provides valuable data on the decomposition of H_2O_2 in •OH generated by the metal oxidized states. In higher dose, they cause various disorders and result in excessive damage due to the oxidative stress induced by free radical formation (**Scheme 1.2)**.

Although Cu^{2+} is the most stable oxidation state, copper itself cannot sufficiently sustain redox processes. A reducing agent ($\bullet O_2^-$, NADPH oxidase from the respiratory chain or intracellular thiols) is therefore needed to reduce Cu^{2+} into Cu^+ in order to complete the redox cycle and to maintain the •OH radical production. These free oxygen radicals may then cause lipid peroxidation damages, reducing the membrane flexibility and leading to membrane rupture (Godoy-Gallardo *et al.*, 2021). The antibacterial mechanisms of Cu^{2+} and Cu^+ cations in aqueous media containing *S. aureus, E. coli and P. aeruginosa* were elucidated by using XANES spectroscopy. It was demonstrated that the antibacterial activity of copper mainly results in Cu^+:S binding and minor Cu^+ interactions with phosphate groups such as those in ATP, if any. For GN bacteria, the antibacterial activity of Cu^+ was found to mainly originate from its redox behavior (Allan et Jarrell, 1989).

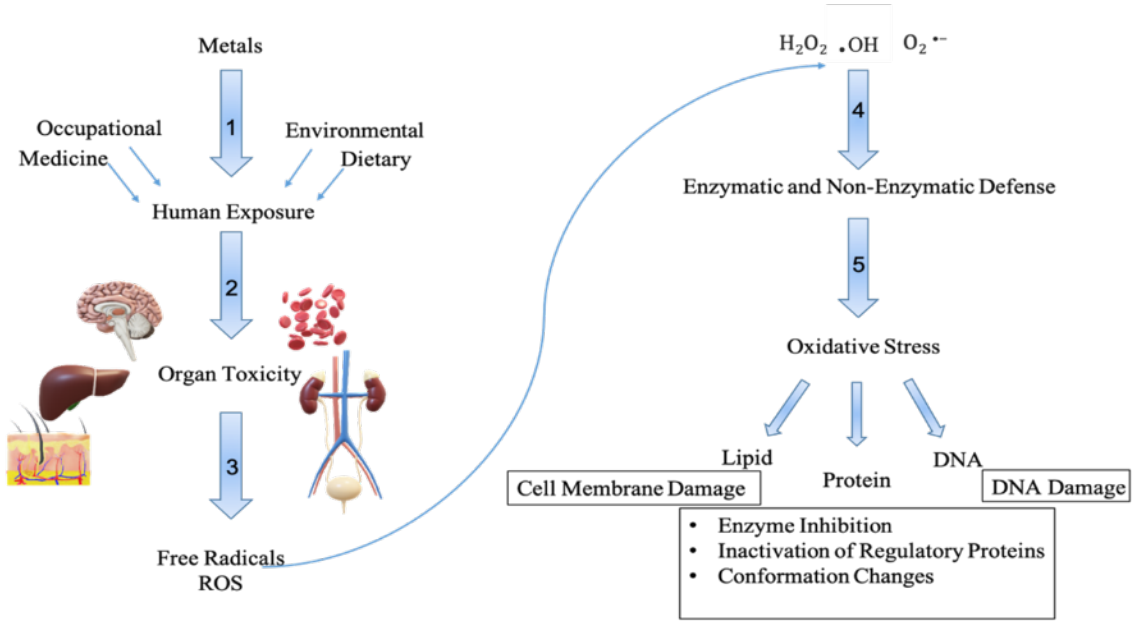

Scheme 1.2. Oxidative stress by exposure to heavy metals.

The accumulation of copper ions also inhibits the aerobic pathway for nucleotide synthesis. During the cell effort to remove the metal from the cytoplasm, the inhibition of the ribonucleoside-diphosphate reductase reduces the cell replication and bacterial growth. Copper toxicity can also be attributed to the disaggregation of the metal clusters. Copper ion can competitively disrupt the Iron-sulfur bridges in proteins which are important targets of isopropyl malate-dehydratase, involved in the enzymatic biosynthesis of branched-chain amino acids. The DNA of *E. coli* was found to be a minor target of copper

ions, given the minimal damage produced by prolonged exposure this cation even in the presence of H_2O_2. However, it appears that copper ions released from CuO-NP can bind to the DNA double helix, causing disorder in DNA strands, and even affecting both transcription and replication up to cell death (Linder, 2001; Theophanides et Anastassopoulou, 2002).

1.3.4 Antibacterial activity of silver cation

Silver has long been recognized as an effective antimicrobial agent, being employed in numerous formulations. Silver is known to exhibit very low and even no toxicity to human cells at certain concentrations. Silver was found to be effective against various pathogens occurring in implant sites, including *Pseudomonas aeruginosa, Escherichia coli, Staphylococcus aureus, and Staphylococcus epidermidis*. In spite of the extensive research on both silver ions and silver nanoparticles, the mechanisms of their antimicrobial actions are still supposed to be similar and remain to be elucidated (Wakshlak *et al.*, 2015).

Cell membrane disruption by both metals is assumed to involve similar pathways. Ag^+ show lower antibacterial activity against GP bacteria than against the GN bacteria, probably due to their thicker PGN (peptidoglycan) layer. Ionic silver may interact with proteins associated with the bacterial cell wall and membrane, thereby forming detrimental complexes that alter the physicochemical properties of the cell wall. Silver is known to readily react with the sulfhydryl groups on the bacterial cell membrane by exchanging the terminal hydrogen atom. This ought to generate a stable S:Ag interaction that fully blocks the respiratory process, electron transfer, protein secretion and lipid biosynthesis (Yamanaka *et al.*, 2005).

Ag^+ cation can provoke a denaturation of intracellular proteins and DNA disruption. Some studies suggested the association of sulfur of thiol groups of nucleotide-associated proteins with silver ions and alteration of chromatin-regulating proteins, thus affecting mRNA transcription and DNA replication. Reportedly (Barros *et al.*, 2019; Godoy-Gallardo *et al.*, 2021), silver-induced decrease of S2 protein (Spike Glycoprotein) leads to altered ribosomes and protein synthesis. This is expected to hinder the production of key cellular enzymes, to deplete adenosine triphosphate (ATP) in the cells, leading to metabolism malfunction and ultimately cell death (Cronholm *et al.*, 2013).

The production of reactive oxygen species by Ag^+ ions could cause DNA damages involving deletions, insertions, point mutations, single-strand breaks, double-strand breaks, fragmentation and adduct

formation. Interactions with DNA-binding proteins were also reported. In addition, Ag^{+} ions may weaken the intracellular Fe:S interaction up to disruption. This should result in an intracellular release of Fe^{2+} that unavoidably enhances the formation of •OH via Fenton reaction (Park *et al.*, 2009).

1.4 Zero-valence metals with antibacterial activity

Metal nanoparticles (MNP) have commonly particle size smaller than 100 nm can also be used as antimicrobial agents since they display antibacterial activity by inducing severe bacteria malfunctions and slowing their growth. Their antibacterial activity seems to be favored by decreasing particle and subsequently higher contact surface with the infected media supported AgNP and CuNP already turned out to be quite effective against both Gram-negative and Gram-positive bacteria by inhibiting their cell growth and ability to develop resistance towards drugs (Alavi et Rai, 2019; Allafchian et Hosseini, 2019; Staroń et Długosz, 2021; Wan *et al.*, 2021). Their action appears to follow rather a bactericidal than a bacteriostatic mechanism, but other potential action pathways can also be involved depending on the types of metals and microorganisms (Noori *et al.*, 2022; Noori *et al.*, 2021).

1.4.1 MNP preparation methods

The reverse proportionality between the antibacterial activity and particle size is now well established. This has stimulated research for developing effective synthesis methods targeting the finest MNP possible. The most common methods to produce MNP include ball milling, co-precipitation, thermal decomposition, hydrothermal treatment, micro-emulsion, sol-gel and biological routes (Alavi et Rai, 2019; Ali *et al.*, 2021). Comparison of the merits and shortcomings of the different MNP synthesis routes (**Table 1.5**) clearly shows that MNP are difficult to obtain through physical methods. Tunable parameters can allow tailoring the particle size and shape (Akhtar *et al.*, 2013; Decastro et Mitchell, 2012; Shah *et al.*, 2015).

The physical methods can involve a “top-down” or “bottom-up” approach. In the top-down approach, the bulk materials are broken into smaller particles by mechanical crushing and grinding (Ball milling). In the bottom-up approach, well dispersed Nano-scaled tiny particles can be obtained *i.e.,* using laser evaporation (Biehl *et al.*, 2018; Decastro et Mitchell, 2002). The particles have wide size distribution as compared to that obtained by chemical synthesis (Benjamin, 1970; El-Eskandarany, 2001). Another physical technique for MNP preparation resides in laser evaporation (also laser ablation); nanoparticles are formed through condensation from liquid or gaseous phase (Amendola et Meneghetti, 2009; Biehl *et al.*, 2018; Shin *et al.*, 2004). The wire explosion method is a one-step productive process that does not

require any additional steps as separation or retreatment. It is often used to prepare iron oxide MNP for water treatment (Kotov, 2003).

Table 1.5 Advantages and shortcomings of the different synthesis methods of MNP.

Synthesis methods	Advantages	Shortcomings	Ref.
Ball milling method	Simple, widely used, Produce fine powder	Contamination of product	(Sarwat, 2017)
Laser evaporation	Low experimental cost, no use of chemicals, no pollutant products	High price of laser system, needs high amount of energy	(Yang *et al.*, 2017)
Wire explosion method	Ecologically safe, clean, and highly productive	A little contamination of product may occur	(Kotov, 2003)
Co-precipitation	Simple, large quantity	impurities, time consuming	(Jiang *et al.*, 2004)
Thermal decomposition	Controllable size, high yield	Toxic solvents	(Odularu, 2018)
Micro-emulsion synthesis	Thermodynamically table	Low yield	(Stubenrauch *et al.*, 2008)
Hydrothermal/solvothermal	Good crystallinity	Needs high temp, and pressure	(Mamaghani *et al.*, 2019)
Sol-gel method	High pure, good crystallinity	Longer time, toxic organic solvents	(Parashar *et al.*, 2020)
Sonochemical reaction	High crystallinity, saturation magnetization, narrow size distribution	Mechanism is still not well understood	(Fujimoto *et al.*, 2001)
Microwave	Fast, rapid kinetic for crystallization	Homogenous nucleation due to uniform heating	(Motshekga *et al.*, 2012)
Chemical reduction	Simplicity, safe	Environmental pollution	(Guzmán *et al.*, 2009)
Chemical vapor deposition	Wide range production of materials	Low productivity, impurities	(Seipenbusch et Binder, 2009)
Arc discharge	Simple, low cost	Difficult to control particle size	(Mao *et al.*, 2019)
Laser pyrolysis	Highly localized heating and rapid cooling	Expensive	(Dumitrache *et al.*, 2005)
Combustion synthesis	Simple, fast, low cost	Generate impurities	(Li *et al.*, 2015)
Annealing	Controllable particle size and chemical composition	Generate impurities	(Stepanov *et al.*, 2000)
Biological method	Efficient, clean process, ecofriendly	Poor dispersion of NPs	(Thakkar *et al.*, 2010)

The chemical synthesis methods usually consist of different bottom-up approaches. A comprehensive literature review allows highlighting the co-precipitation as being one of the most employed methods for preparing MNP of controlled size. Metal ions are dissolved and reduced in a solvent to produce MNP.

Different factors such as the pH of the liquid medium, the types of metal cation and salt, their concentrations, the reaction temperature, the reducing agent can influence MNP particle size and shape (Jiang *et al.*, 2004; Sandeep Kumar, 2013). Here the main role of the co-precipitation resides in achieving high metal oxide dispersion before the reduction reaction. Another chemical method involves the thermal decomposition of organometals. Stabilizing agents such as fatty acids (i.e. oleic acid) and hexadecylamine can attenuate the nucleation velocity favoring the production of spherical particles with adaptable size (less than 30 nm). The stabilizing agent is then removed upon heating. This technique often generates smaller particle size than by co-precipitation (Effenberger *et al.*, 2017; Ren *et al.*, 2019).

The micro-emulsion method uses isotropic systems of lipophilic and hydrophilic phases stabilized with surfactants or co-surfactants. The main micro-emulsion types are oil in water (O/W), water in oil (W/O) and both water and oil in comparable amount. Small MNP amounts but uniformly dispersed depending on the surfactant type are usually obtained (Mosayebi *et al.*, 2017).

Aqueous methods, also called solvothermal, involves hydrolysis and oxidation, and are usually carried out under high pressure and temperature. Uniform particles sizes were obtained from various metals and their morphology was found to depend on the solvent, time, pressure, and temperature. This method is often preferred over others because it can produce MNP with controllable composition, size and shape (Zahid *et al.*, 2019; Zhang *et al.*, 2016).

The sol-gel method involves gel formation through precursor hydrolysis and metal alkoxide polycondensation followed by metal reduction. Here, metal salts are dissolved in a solvent which is further evaporated giving rise to a gel. This is a low cost process that produces large quantities of MNP with tailored size and shape, but the regeneration of the three-dimensional oxide networks is a major shortcoming that limits its applications (Ansari *et al.*, 2019; Gu *et al.*, 2006).

MNP can also be synthesized by plants. This is a very interesting biological route whose various mechanisms involving the activity of nitrate reductase and/or quinones acting as electron shuttle still remain to be elucidated (Gericke et Pinches, 2006; Thakkar *et al.*, 2010; Verma *et al.*, 2021). This category of procedures is however restricted by the culture of plant, which is an energy-consuming agricultural step. Using specific plants and related biomasses can also provide valuable and low lost sources of reducing agents for MNP synthesis. Coffee or green tea already showed reducing capacity in the synthesis of CuNP and AgNP within the channels of SBA-like silica (Santa Barbara Amorphous) (Sekkal *et al.*, 2021). This

property made tea and coffee to be regarded as beneficial for human health by reducing the oxidative stress (Yan *et al.*, 2020b) and as valuable raw materials for food, pharmacological and cosmetic purposes (Aree, 2019; Chacko *et al.*, 2010; Rahman *et al.*, 2018). This reducing property arises from the capacity of phenolic acids in coffee and that of flavonoids in green tea to be oxidized, thereby playing a key role as antioxidants in living organisms (Scalbert et Williamson, 2000).

Regardless to the dispersion technique of the MNP precursors (metal cation or oxides), a thorough chemical reduction requires a powerful reducing agent (Jamkhande *et al.*, 2019). This allows preventing the presence of undesirable less or no reduced species. The most common reducing agents are glucose, ethylene glycol, ethanol, hydrazine, molecular hydrogen, metal hydride such as LiH, NaH, $LiAlH_4$, CaH_2, sodium borohydride ($NaBH_4$) and ''green'' reducing agents such as phenolic acids in coffee and flavonoids in green tea (Scalbert et Williamson, 2000).

1.4.2 Role of the stabilizing agent

It is well-known that fine MNP are generally more active against microorganisms than their bulkier counterparts because their offer high contact surface with the infected media (Alavi et Rai, 2019; Wu *et al.*, 2019). AgNP constitutes one of the most frequently used nanomaterials, mainly due to their high antimicrobial activity. The latter supposedly involves a release of Ag^+ cation in the infected medium due to increased contact surface (Yan et Chen, 2019; Yu *et al.*, 2013). In aqueous dispersions, MNP can be prone to many processes such as dissolution that unavoidably modifies their size, shape, surface properties, reactivity, fate, transport, bioavailability and uptake. MNP stability is difficult to be preserved because of their strong tendency to aggregate into bulkier clusters. This growth rate depends on interfacial interactions.

MNP aggregation and sedimentation can significantly affect their antibacterial activity (Peng *et al.*, 2019; Zhang *et al.*, 2018). Changes in the particle size, shape, composition and crystallographic arrangement can significantly modify their plasmonic properties. The literature shows that MNP are rarely used alone and their stabilization is therefore essential, requiring chemical species and host-matrices bearing sufficient chemical functions display optimum chelating capacity (**Table 1.6**) (Keller *et al.*, 2010; Prathna *et al.*, 2011; Zhang, 2014). Such chemical functions should be capable to promote not only a high dispersion of MNP into smaller particles but also their stabilization by favoring MNP accessibility to the infected media at the

expense of Metal:Metal interactions. Such an optimum stabilization should also prevent MNP oxidation into cations.

Too weak MNP retention strength is major shortcoming for their stabilization, and conversely too strong interaction with the chelating chemical group can strongly encapsulate MNP, thereby blocking their contact surface and impeding their exchanges with surrounding medium. Unlike entrapped in solid support, MNP are often stabilized by surfacing agents that impede Metal:Metal interaction, detrimental MNP aggregation and reduced antimicrobial efficiency (Chen *et al.*, 2021; Wang *et al.*, 2010; Yuan *et al.*, 2018).

1.4.3 MNP antibacterial mechanisms

MNP antimicrobial activity can involve different mechanisms. A first mechanism is promoted by interactions between Lewis acids (electron pair acceptors) and Lewis bases (electron pair donors), between opposite surface charges or between hydrophobic/hydrophilic species on the MNM-Cell membrane interface.

Lewis acid-base interactions (LAB) are particularly interesting, because they take place through competitive MNP attraction by stronger chelating groups belonging to the cell membrane and enzymes such as sulfhydryl at the expense of that exerted by the mother-matrix. LAB is probably the most common cause of intoxication (poisoning) by both ZVM and metal cation, and is known to affect the fundamental cellular functions and metabolisms. A second mechanism resides in the production of reactive oxygen species (ROS) by MNP and requires no contact with the microorganisms. ROS can diffuse through the cell membrane and can react with DNA, lipids and proteins, leading to cell death. However, exposition to ROS is not constant and is not effective against ROS-resistant strains. Another mechanism is that involving MNP oxidation into metal ions, whose solubility is known to ease their diffusion through the cell membrane. Once reaching the cell nucleus, metal ions can interact with DNA and/or proteins with potential genetic damages (Alavi et Rai, 2019; Gabrielyan et Trchounian, 2019; Slavin *et al.*, 2017a).

Table 1.6. The State-of-the-Art on biomedical applications of metal nanoparticles.

MNPs	Host matrices	Operation conditions	Microorganisms	Toxicity criteria	Ref.
AgNPs	Modified Gum Tragacanth/Graphene Oxide composite hydrogel	0.5 g of dried hydrogels was mixed with 50 mL $AgNO_3$ (0.85 g/50 mL) aqueous solution and 50 mL of flower extract solution	*Staphylococcus aureus*	*In vitro* antibacterial activity (direct contact test with agar diffusion)	(Sahraei et Ghaemy, 2017)
CrNPs, ZnNPs	Ultrasonic-assisted Spirulina platensis (UASP)	One gram of UASP powder was added to the metal solution (1.69g metal salts in 20 mL distilled water)	*Staphylocicus aureus, Klebsiella pneumonia, Proteus vulgaris, Pseudomonas aeruginosa and Escherichia coli*	Agar well diffusion method	(Gunasundari *et al.*, 2017)
ZnONP	Cellulose acetate (CA) films	0.2 percent (w/v) solution of cellulose acetate in DMF (solvent dimethylformamide) was added to a precalculated amount of $ZnCl_2$	*Escherichia coli*	Evaluation of antibacterial action by zone inhibition method	(Chaurasia *et al.*, 2010)
AgNPs	Calcium oxide (CaO) nanocrystals	1g of Silver was mixed with 3g of calcium oxide	*Bacillus cereus, Bacillus subtilis, Enterococcus feacalis, E. coli, Klebsiella sp, Pseudomonas fluorescens, Enterobacter sp, Micrococcus leteus*	Measuring inhibition zone diameter	(Alsohaimi *et al.*, 2020)
AgNPs	Chitosan (CS)	0.1 g chitosan was dissolved in 50 mL of ultrapure water under vigorous stirring at 90 °C, followed by adding 0.5 mL of 0.1 M $AgNO_3$ solution	*Escherichia coli, Staphylococcus aureus*	Measuring minimal inhibitory concentration (MIC)	(Chen *et al.*, 2020)
ZnONPs	Chitosan films	chitosan film was placed in 2% (w/v) aqueous solution of zinc chloride for 12 h at 30°C	*Escherichia coli*	Zone inhibition method	(Bajpai *et al.*, 2010)
ZnONPs	Alginate-chitosan biofilm (CS/Alg)	2 g of chitosan and alginate was dissolved into the 100mL DI water. Then, ZnO nanoparticles (1mg/ml) were added drop wise to the solution of chitosan- alginate	*Bacillus subtilis*	Inhibition zone diameter	(Gong *et al.*, 2019)
CuNPs, PbNPs, AgNP and ZnNPs	Activated carbon (AC)	0.478 g of metal salt was dissolved in 25 mL of fresh distilled water. Then 1 g of AC was added to metal solution	*Staphylococcus aureus, Staphylococcus epidermidis, Pseudomonas aeruginosa and Escherichia coli*	Agar well diffusion method	(Saravanan *et al.*, 2016)

Table 1.6b

MNPs	Host matrices	Operation conditions	Microorganisms	Toxicity criteria	Ref.
AgNPs	Chitosan-alginate	3.0% (w/v) Na-alginate was well dissolved in water, and the equivalent volume of AgNP was added to the Na-alginate solution	*Staphylococcus aureus, Pseudomonas aeruginosa, Klebsiella pneumoniae, Acinetobacter baumannii, Morganella morganii and Haemophilus influenza.*	The AATCC Anti-Bacterial Test Method	(Bilal *et al.*, 2017)
ZnONPs	Calcium-alginate films	20 ml of 4% (w/v) solution of sodium alginate, definite quantity of zinc oxide nanoparticles was added and the solution was mixed thoroughly under high stirring rate of 160 rpm for 1 h	*Escherichia coli*	Zone of inhibition method	(Bajpai *et al.*, 2012)
AgNPs, ZnONP	Bentonite clay	20 g of the sieved clay was chemically activated by dispersing in 3 M H_2SO_4 solution	*Escherichia coli and Enterococcus faecalis*	Disk diffusion method	(Motshekga *et al.*, 2013)
AgNPs	Intercalated clay (saponite)/poly acrylamide (PAAm) nanocomposite (NC) hydrogels	AAm (1 g), and various amounts of inorganic clay content (1–3 wt% according to monomer) were dissolved into the 3 mL water. 0.1% $AgNO_3$ was added to the former solution	*Staphylococcus and Escherichia coli*	Disc method	(Bandla *et al.*, 2017)
AgNPs	Agar-carboxymethylcellulose-montmorillonite nanocomposite (Agar-CMC/MMT)	Ag-MMT was prepared by dispersing 1 g of MMT in 100 ml of 10 mM $AgNO_3$ solution for 24 h. Film solutions were prepared by dissolving 3 g of agar and 1 g of CMC in 100 ml of distilled water	*Bacillus subtilis, Escherichia coli*	Calculating bacteria inhibition zone diameter	(Makwana *et al.*, 2020)
ZnONPs	Zeolite	Zeolite/ZnO NCs was obtained by preparing five different solutions of $Zn(acetate)_2 .2 H_2O$ with different wt.% of ZnO: Zeolite (1, 3, 5 and 8 wt.%) in 100 ml deionized water	*Escherichia coli, Bacillus Subtilis, Staphylococcus aureus and Salmonella choleraesuis*	Agar disc diffusion method	(Alswat *et al.*, 2016)
CuONPs	Montmorillonite-chitosan (MMT-Cs)	MMT and $CuSO_4.5H_2O$ at the ratio of 1:1 (w/w) were mixed for 20, 90 min. Then, 2 g of chitosan was added into the solution	*S.aureus, B.cereus, E.coli and P.aeruginosa.*	Viable cell colony count method (CFU)	(Nouri *et al.*, 2018)

1.4.4 Role of MNP particle size

The non-solubility of ZVM makes that MNP act only through their particle external surface. Therefore, it clearly appears that MNP exchanges with the surrounding liquid media containing bacteria are narrowly related to MNP dispersion. In other words, MNP display size-dependent toxicity towards bacteria. The size is also related to their pharmaceutical use for "*in vivo* "administration purposes. Through intravenous injection, MNP with size smaller than 50 nm can reach faster all tissues and exhibit stronger toxic effect. MNP with particle size higher than 6 nm are known to accumulate in specific organs because they cannot be excreted by the kidneys. Reducing the size of nanoparticles below 1 nm (metal-subnanoparticles MSNPs) facilitates their penetration and enhances their interactions with proteins, nucleic acids and other biomolecules with potential cell damages. It results that MNP particle size controls their toxicity. For instance, cadmium selenide quantum dots were found to accumulate in living tissues and to cause hepatotoxicity, fine gold nanoparticles (AuNP) showed increased accumulation in organs while larger ones (more than 1nm) cannot easily enter the cell (Auría-Soro *et al.*, 2019; Khurana *et al.*, 2014).

1.5 Approach for the synthesis of metal-loaded antibacterial agents

Hence, over the last years, many investigations have been focused on the stabilization of MNP and of metal cations by organic and inorganic biomaterials to improve their antimicrobial properties (Carbone *et al.*, 2016; García-Ivars *et al.*, 2019; Karbowniczek *et al.*, 2017; Wang *et al.*, 2020). This stabilization is known to be promoted by different types of metal or metal ion interactions involving LAB, electrostatic interactions and/or hydrophilic/hydrophobic attraction forces. Three different strategies have been developed for the incorporation and entrapment of MNP and M^{n+} cations in a porous matrix bearing interactive chemical functions (Godoy-Gallardo *et al.*, 2021). This Ph.D. thesis has been focused on the stabilization of metal cation and of metal zero via using solid supports such as natural and lamellar microporous alumino-silicates like sodium montmorillonite (NaMt) and carboxylated biopolymers like carboxymethylcellulose (CMC) and carboxymethylstarch (CMS). In both cases, MNP and M^{n+} cations dispersion and stabilization involve mainly optimum Lewis acid-base interactions (LAB). Moderate LAB should be sufficiently strong to hinder MNP re-aggregation and re-oxidation but also sufficiently weak for easy MNP release in the infected media.

1.5.1 Clay-based host matrices

Each montmorillonite lamella is constituted by two tetrahedral silica layers sandwiching an octahedral alumina layer (**Scheme 1.3 a**). In aqueous media, NaMt highly swells and expands due to water molecules

adsorbed in the interlamellar space. This often induces a more or less weakening of Lamella:Lamella attraction forces even up to total delamination and exfoliation depending on the exchangeable charge compensating cation (Eirish et Tret'yakova, 1970; Lou et Huang, 1988).

A beneficial feature of NaMt in the synthesis of metal-loaded antimicrobial agents resides in the cation exchange capacity (CEC) arising from the isomorphous substitution of Al^{3+}-centered octahedra by Mg^{2+} ones (Bergaya et Lagaly, 2013). Here, Na^{+} can conveniently be exchanged by cations such as Ag^{+} and Cu^{2+}.

Once incorporated on the clay mineral surface, Ag^{+} and Cu^{2+} can display their intrinsic antibacterial activity in the cationic form or can be converted into MNP . Both MNP and M^{n+} can be dispersed on the clay mineral surface owing to the presence chelating sites, namely lattice oxygen atoms of siloxy groups (-S-O-Si-), terminal oxygen atoms belonging to the hydroxyl groups both the in-plane and out-plane silanols (-S-O-H) (**Scheme 1.3 b**).

These oxygen atoms can act as Lewis base (electron-pair donor), exhibiting LAB interaction through their electron pairs with both MNP and metal cation that act as Lewis acids (electron-pair acceptor) (Malla *et al.*, 1991; Noori *et al.*, 2021). The clay dispersion capacity was found to be improved by the incorporation of OH-functionalized organic moieties such as Boltorn polyol dendrimers (Noori *et al.*, 2022).

1.5.2 Biopolymer-based host matrices

Functionalized polysaccharides as carboxymethylstarch (CMS) and carboxymethylcellulose (CMC) can also be employed in the synthesis of efficient metal-loaded antimicrobial agents. CMC and CMS (**Scheme 1.4)** are low-cost, conveniently modifiable potential, non-toxic and highly biodegradable and biocompatible polymers. They consist of a chain of D-glucose monomers that link each other via β-1, 4 or α-1, 4 glycosidic bonds respectively (Pooresmaeil et Namazi, 2021; Stojanović *et al.*, 2000; Su *et al.*, 2010).

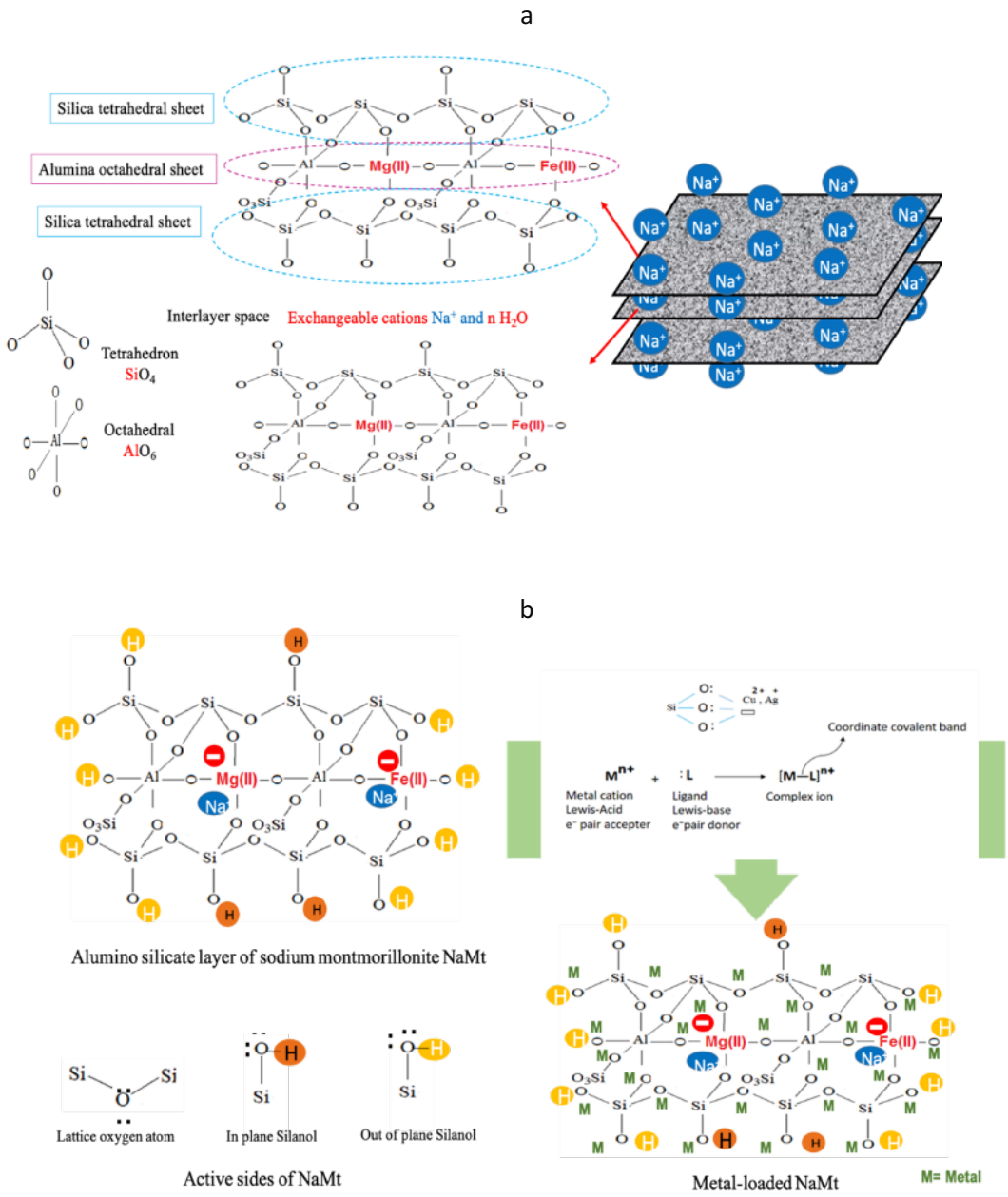

Scheme 1.3. Chemical structure of NaMt (a), metal dispersion into the alumino silicate layers of NaMt (b).

Chemical functionalization of CMC and CMS by CH_2COOH groups is a key factor to improve their metal retention capacity. This property strongly depends on their degree of substitution (DS) which accounts for the number of carboxymethyl groups (CM) per glucose unit (GU) (Casaburi *et al.*, 2018; Spychaj *et al.*, 2013; Stojanović *et al.*, 2005).

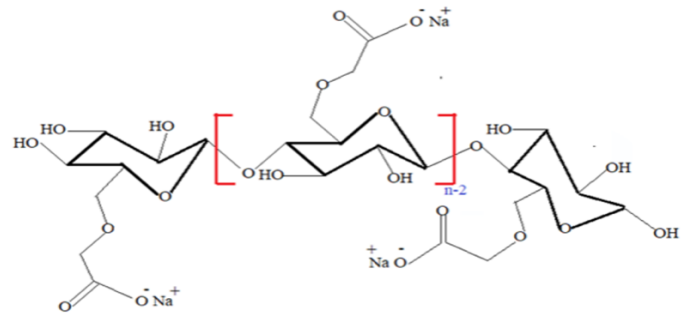

Sodium-Carboxymethyl Cellulose CMC

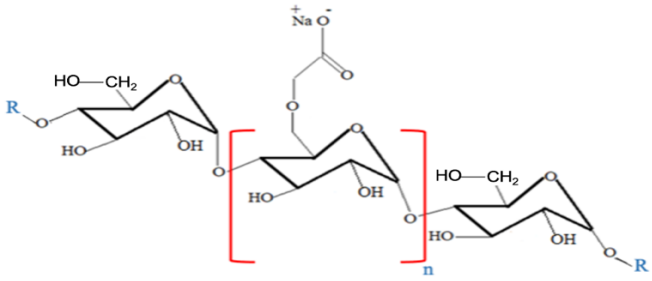

Sodium-Carboxymethyl Starch CMS

Scheme 1.4. Chemical structure of CMC and CMS

CM groups can capture and stabilize MNP and M^{n+} through Lewis acid-base interaction and ion-exchange, respectively. Therefore, increasing the Degree of Substitution (DS) of biopolymers is a judicious strategy to favor the metal dispersion through particle size reduction. The acidic properties of CM groups cause CMC and CMS to have pH-dependent behavior which governs the metal retention strength and the dispersion of not only the metal within the host-matrices but also that of the metal-loaded biopolymer in the aqueous medium. The pH-sensitivity is also expected to influence the antibacterial activity of the polymers by controlling (1) The contact surface of the metal-loaded biopolymer with the infected media and (2) The metal release, if any, on the bacteria cell membrane and/or into the aqueous medium (Cai *et al.*, 2020; Rao *et al.*, 2018; Tan *et al.*, 2010).

Biopolymers such as CMC and CMS have a tendency to aggregate in aqueous media because of the unavoidable interparticle H-bridge interactions between their carboxyl and hydroxyl functional groups (Anirudhan et Parvathy, 2014; Saboktakin *et al.*, 2009). The resulting porosity decrease can be attenuated by MNP or metal cation incorporation. Both zero-valent and cationic forms of metals are known to behave as Lewis acids and can interact with basic chemical groups. Hence, a combination of HO-bearing clay

minerals with biopolymers is an effective procedure to avoid polymer compaction and improve metal dispersion and stabilization. Intercalation of inorganic solid surfaces such as NaMt with CMC or CMS along with MNP or M^{n+} dispersion paves the way to synthesize metal-loaded inorganic–organic materials (metal-based organoclays) with probably even higher antibacterial activity (**Scheme 1.5. a**). This involves the formation of competitive H-bridges of the OH groups of NaMt with the oxygen atoms on the polymers that improves both the metal dispersion within the organoclay structure and material porosity (Noori *et al.*, 2022).

That is why the use of hyper-branched polymer such as Boltorn H20 polyol is particularly interesting in the present research. This is due to the appreciable metal retention capacity induced by an additional number of terminal -OH groups (end-groups) that promotes Metal:Clay:Polymer ternary interaction. The incorporation of Boltorn H20 with clay lamellae was acquired via H-bridge interaction for hosting MNP and metal cations, resulting in appreciable antibacterial activity (Noori *et al.*, 2020) (**Scheme 1.5. b)**. According to an ample literature, polyalcohol and polyol incorporation could enhance the hydrophilic character of montmorillonite and its affinity towards metals (Polyol refers to an organic compound with three or more hydroxyl functional groups, whereas polyalcohol is an alcohol that contains multiple hydroxyl groups). Increasing number of OH groups in the host matrix turned out to be a key factor for the metal retention capacity (Azzouz *et al.*, 2013b; Bouazizi *et al.*, 2018b; Yan *et al.*, 2020a).

1.5.3 Concept of optimal metal release/retention compromise

The metal type, oxidation state and chemical features of the solid support are expected to strongly influence the biocidal effect. This can be explained in terms of the interdependency between the metal retention strength by the host matrix and antibacterial activity. Optimal interactions between the metals (in both MNP and cationic forms) and active sites of the host matrices are expected to be beneficial for achieving high antibacterial performances (Noori *et al.*, 2022; Noori *et al.*, 2021). This is the major objective of the present doctoral research. It is believed that strong metal-host interaction reduces the material porosity, metal accessibility and contact surface with bacteria-containing media.

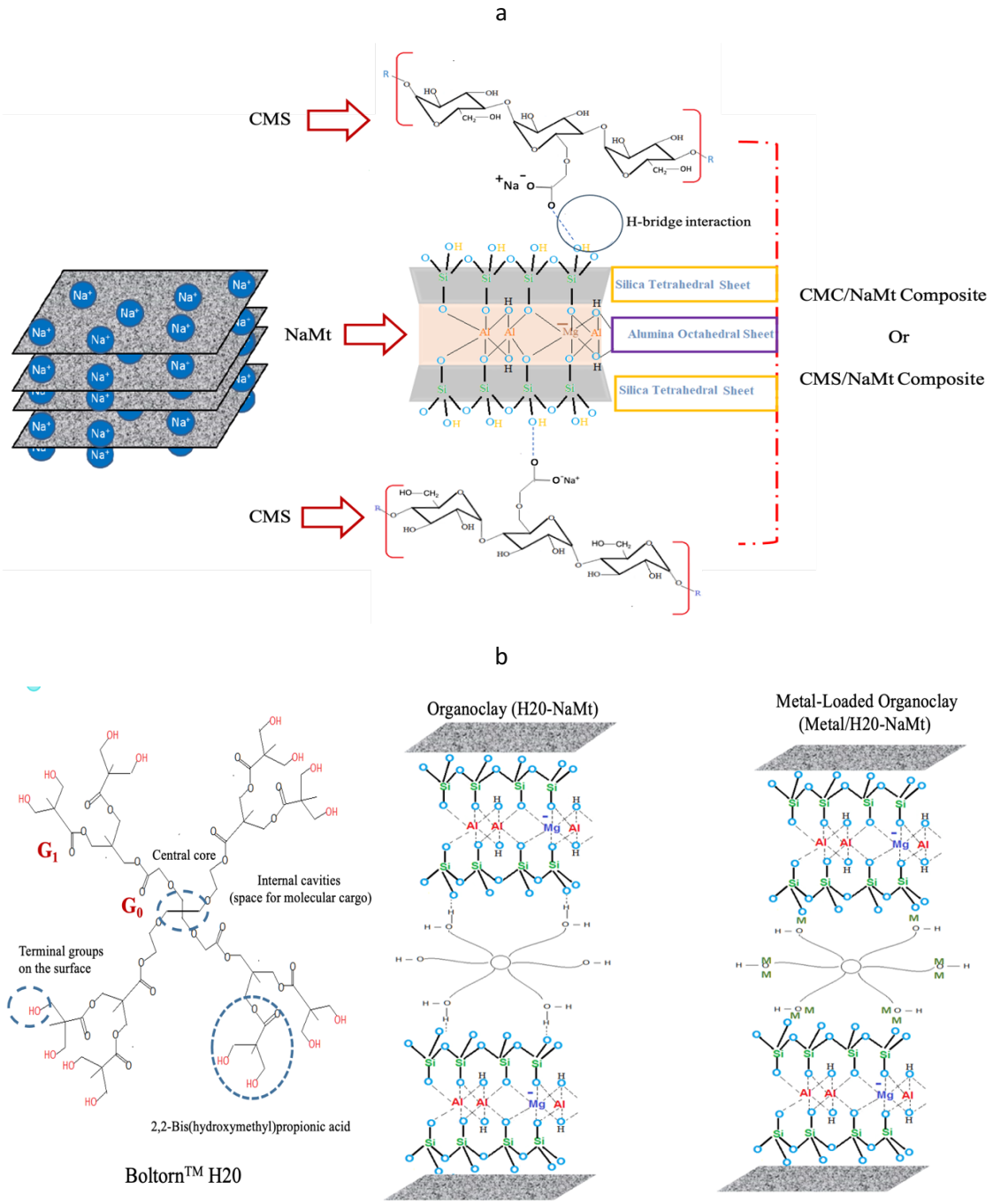

Scheme 1.5. Incorporation of NaMt with CMC or CMS (a) and NaMt impregnation with polyol and metal dispersion (b).

The use of clay minerals to attenuate the Biopolymer:Metal interaction can allow promoting the metal diffusion with consecutive release and subsequently the antibacterial activity. To provide evidence in favor of this concept, the main objective of the present PhD thesis resides in understanding how the

antibacterial activity can be optimized by simultaneously controlling a compromise between the material dispersion in aqueous media and the metal retention strength and dispersion inside the host-matrices

CHAPTER 2

EXPERIMENTAL PART

This chapter provides a detailed overview of the materials & methods used for the preparation, characterization, and biological test of the metal-loaded host materials in both article 1 (chapter 3) and article 2 (chapter 4).

2.1 List of chemicals and materials employed in both steps of this research

Article 1

All chemicals were of analytical grade used without previous purification. Crude bentonite (Sigma-Aldrich, Oakville, Canada), sodium chloride (NaCl) (ACP chemicals, Montreal, Canada), copper acetate ($Cu(CH_3COO)_2$) (Fisher chemicals, Ottawa, Canada), silver nitrate ($AgNO_3$) (Fisher chemicals), sodium borohydride 98% ($NaBH_4$) (Acros organics, Ottawa, Canada), copper nitrate ($Cu(NO_3)_2$) (Anachemia VWR company, Montreal, Canada), Boltorn H20 (Perstorp, Malmo, Sweden), absolute methanol (MeOH) (Sigma-Aldrich), toluene (Sigma-Aldrich) were used. All experiments were performed in distilled water. Cellulose tissue (gauze) denoted as CT was purchased from Jean Coutu group (PJC), Canada.

Article 2

Copper acetate: $Cu(CH_3COO)_2$, silver nitrate: $AgNO_3$ and sodium borohydride: $NaBH_4$ 98 % were supplied by Fisher chemicals, Canada. Sodium carboxymethylcellulose (CMC) with a degree of substitution (DS) of 0.30 carboxymethyl group (CM) per glucose unit (Gu) and 90 kDa MW was purchased from Sigma Aldrich, Canada. Sodium carboxymethylstarch (CMS) with a DS value of 0.167 CM/Gu and 100 kDa MW was prepared by treatment of High Amylose Starch (Hylon VII) with sodium monochloroacetate and the degree of substitution of -OH by the carboxymethyl groups was measured by back titration, as previously described (Alothman *et al.*, 2021). Both biopolymers (**Fig. S1**) were used without further purification. Lysogeny Broth medium and agar was purchased from Biobasic (Markham, ON, Canada). *Escherichia coli DH5Alpha* and *Bacillus subtilis S168* bacterial strains were purchased from American Type Culture Collection (ATCC, Manassas, VA, USA). Na^+-montmorillonite (NaMt) used in combination with the

investigated biopolymers was prepared through purification of an Aldrich bentonite according to the same procedure as previously reported (Noori *et al.*, 2021).

2.2 Protocols for the preparation of cation- and metal-loaded materials

Article 1

Sodium-montmorillonite (NaMt) was prepared by combined ion-exchange and purification of crude bentonite (Aldrich) in aqueous NaCl solution using an effective procedure fully described elsewhere (Azzouz *et al.*, 2010; Thuc *et al.*, 2010). NaMt (200 mg) was immersed in a methanol/water mixture containing 200 mg of Boltorn H20 polyol dendrimer (41.2:58.8 V/V ratio) under continuous stirring for 1h at 40-60°C, resulting in Boltorn H20-NaMt organoclay which was dried overnight in a freeze-drying device. Similarly, impregnation of a CT patch of 1×0.5 mm^2 surface in 20 mL of an aqueous solution of 0.01mol/L Boltorn^{TM}H20 at room temperature (RT) for 1h resulted in dendrimer dispersion into a Boltorn H20-CT composite.

Article 2

Cation-loaded CMC samples (Cu^{2+}/CMC and Ag^{+}/CMC) with 1 mmol/g cation content were prepared by adding dropwise 10 mL of 0.1 mol/L $Cu(CH_3COO)_2$ or $AgNO_3$ solutions in CMC solutions (1 g CMC in 50 mL water) at 50-60 °C under stirring for 3h. Further addition of 4 mL of 0.5 mol/L $NaBH_4$ under nitrogen stream for 10 min allowed obtaining MNP-loaded CMC (Cu^0/CMC or Ag^0/CMC) with 1 mmol/g metal content through cation reduction into zero-valent metal (ZVM). Given that the DS value of CMC is approximately twice higher than that of CMS (0.3 versus 0.17), cation-loaded CMS samples (Cu^{2+}/CMS and Ag^{+}/CMS) reduced cation content of 0.4 mmol/g were obtained by adding 250 mg of CMS to 10 mL of 0.01 mol/L $Cu(CH_3COO)_2$ or 0.01 mol/L $AgNO_3$ aqueous solutions under vigorous stirring at 25 °C for 1h. Both mixtures were sonicated for 50 min (500 W, 20 kHz) at room temperature for homogenization. Consecutive cation reduction by adding 10 mL of 0.02 mol/L $NaBH_4$ resulted in MNP-loaded CMS (Cu^0/CMS and Ag^0/CMS). The metal polarizing effect was investigated through zeta potential measurements of various CMC and CMS samples previously treated with aqueous solutions of other cations such as Zn^{2+}, Co^{2+}, Pt^{2+}, Ti^{2+} and Au^{+}. Biopolymer/clay composites (CMC/NaMt and CMS/NaMt) with 1:1 Wt. ratio were prepared by previous

dispersion of 0.5 g of CMC or CMS in 50 mL distilled water at 50-60 °C and slow addition of an aqueous suspension containing 0.5 g of NaMt under vigorous stirring for 1h. Cu^{2+}/CMC/NaMt, Ag^{+}/CMC/NaMt, Cu^{2+}/CMS/NaMt and Ag^{+}/CMS/NaMt were obtained by addition 10 mL of 0.1 mol/L $Cu(CH_3COO)_2$ or $AgNO_3$ at room temperature under vigorous stirring for 3h. Consecutive reduction of Cu^{2+} or Ag^{+} by adding 4 mL of 0.5 mol/L $NaBH_4$ gave rise to Cu^0/CMC/NaMt, Ag^0/CMC/NaMt, Cu^0/CMS/NaMt, Ag^0/CMS/NaMt. All samples were dried by lyophilisation and stored in a sealed desiccator containing O_2-free dry nitrogen.

2.2.1 Metal dispersion on composite supports

Article 1

An amount of 0.2 g of NaMt or Boltorn H20-NaMt was slowly mixed in a 50 mL beaker with 15 mL (33.33% and 66.66% toluene/water) aqueous solution with a metal salt concentration of 0.12mol/L Cu $(CH_3COO)_2$ or $(AgNO_3)$ under vigorous stirring for 2 h. For comparison some antibacterial tests were only performed with the resulting Cu^{2+}/NaMt@H20 and Ag^{+}/NaMt@H20. Both cation-loaded organoclay suspensions were treated by dropwise adding 10 mL aqueous solution of $NaBH_4$ (0.2mol/L) during 15 min under a nitrogen stream at ambient conditions. The resulting metal-zero-loaded clay minerals (Cu^0/NaMt and Ag^0/NaMt) and organoclays (Cu^0/H20-NaMt and Ag^0/H20-NaMt) were repeatedly washed with distilled water to eliminate the excess of Cu^{2+} and Ag^{+} salts and then dried overnight. Further, metal loaded H20-CT samples were obtained by dissolving 0.8 g of $AgNO_3$ or 1.24g of $Cu(NO_3)_2$ in 30 mL of distilled water and adding with 1 g and 1.5 g of $NaBH_4$, respectively. Cu^{2+} and Ag^{+} reduction into Cu^0 and Ag^0 nanoparticles (AgNP and CuNP) was achieved under stirring for 5-6h at RT, under nitrogen stream to prevent MNP oxidation. The resulting Ag^0/H20-CT and Cu^0/H20-CT samples were dried overnight at RT in a sealed enclosure with dry O_2-free nitrogen dried with NaOH pellets.

Article 2

The effects of the metal dispersion on both biopolymers and their NaMt-composites and material size distribution in aqueous suspension were assessed through Zeta potential (BrookHaven Instrument Corp., ZetaPlus / Bl-PALS) and Dynamic Light Scattering measurements (DLS) (Malvern, Zetasizer Nano S90), respectively. Deeper insights in MNP incorporation were achieved through Transmission Electron Microscopy (TEM) and Energy-dispersion X-ray fluorescence (ED-XRF) by means of JEOL JEM-2100F equipment (with an accelerating voltage of 200 kV) coupled to an EDAX X-ray fluorimeter. The samples

were previously dispersed in methanol and dried on holey carbon-coated Ni grids. The ED-XRF spots were denoted as ***eds1*** and ***eds2***.

Additional analyses were performed by X-ray Photo-electron Spectroscopy (Thermo Scientific K-Alpha) XPS of 400 µm spots and a monochromatic Aluminum-kα X-ray source (260 watts in constant pass energy mode in two 200 eV and 1 eV steps). High resolution scans (Ag3d, C1s, O1s, Cu2p) were recorded at a constant pass energy of 50 eV and 0.1 eV steps. XPS data were processed using the software Thermo-Advantage. Deconvolution was applied for all symmetric and asymmetric XPS signals for detecting potentially overlapped peaks for the key-element interacting with cations and zero-valent metals (**Fig. S2-S3**).

2.3 Introducing the instrumental techniques and analytical methods for the characterization of the synthesized materials

Article 1

The basicity and hydrophilic character of the as-prepared samples were assessed in terms of carbon dioxide (CO_2) retention capacity (CRC) through Thermal Programmed Desorption (TPD) and moisture content by thermogravimetric analysis (TGA). The basicity of diverse materials is commonly defined as the surface affinity towards an acidic gas such as CO_2. This is herein assessed by TPD in terms of CRC or total basicity, which accounts for the total amount of desorbed of CO_2 within the investigated temperature range. The basicity strength accounts for CO_2 retention strength, and is proportional to CO_2 desorption temperature (Arus *et al.*, 2018; Azzouz *et al.*, 2013a; Azzouz *et al.*, 2010; Azzouz *et al.*, 2006; Azzouz *et al.*, 2013b; Azzouz *et al.*, 2013c; Azzouz *et al.*, 2013d; Beltrao-Nunes *et al.*, 2019; Ghomari *et al.*, 2015; Ghomari *et al.*, 2017; Nousir *et al.*, 2019; Nousir *et al.*, 2013a; Nousir *et al.*, 2013b; Nousir *et al.*, 2014; Noussir *et al.*, 2017; Terrab *et al.*, 2016) For this purpose, 45-50 mg of each material sample was prone to previous saturation with dry and O_2-free CO_2 and then to a 5 °C/min heating rate from 20 °C to a given temperature threshold under 5 mL/min nitrogen stream. This temperature threshold was evaluated as stability range through TGA by means of a TA Instruments TGA (Q500)/Discovery MS equipment. This was achieved by heating 4-7 mg samples in platinum (Pt) pan in the temperature range of 20-500 °C at a 10 °C/min heating rate under a 30 mL/min dry argon stream. The particle morphology was screened by Scanning Electron Microscopy (SEM) using a Jeol JCM-6000 PLUS instrument on samples spread as powder on conductive double adhesive carbon tapes at 1.0 kV voltage for non-conductive samples and 15 kV for metal-containing

materials (conductive). Deeper insights in MNP incorporation were achieved through Transmission Electron Microscopy (TEM) and Energy-dispersion X-ray fluorescence (EX-XRF) by means of JEOL JEM-2100F equipment (with an accelerating voltage of 200 kV) coupled to an EDAX X-ray fluorimeter. The samples were previous dispersed in methanol and dried on holey carbon-coated Ni grids. The ED-XRF spots were denoted as eds1 and eds1. This denotation arises from a shortening of this acronym into Energy-Dispersive Spectroscopy (eds). Additional analyses were performed by X-ray diffraction (XRD) in 2-Theta range 10-80 degrees (XRD D8 Advance device and CuK_{alpha} radiation at 1.5406 Å), X-ray Photo-electron Spectroscopy (XPS) XPS of 7800 × 300 µm spots (AXIS-ULTRA instrument, KRATOS Analytical Ltd, UK) and a monochromatic Al-based X-ray source (260 watts in constant pass energy mode in two 160eV and 1eV steps.

Article 2

The effects of the metal dispersion in both biopolymers and their NaMt-composites on the behavior of their suspensions in aqueous media were assessed in terms of surface charge and average particle size in correlation with the induced pH. This was achieved through triplicate measurements of the Zeta potential (BrookHaven Instrument Corp., ZetaPlus / Bl-PALS) and Dynamic Light Scattering measurements (DLS) (Malvern, Zetasizer Nano S90), respectively. Deeper insights in MNP incorporation were achieved through Transmission Electron Microscopy (TEM) and Energy-dispersion X-ray fluorescence (ED-XRF) using a JEOL JEM-2100F equipment (with an accelerating voltage of 200 kV) coupled to an EDAX X-ray fluorimeter. The samples were previously dispersed in methanol and dried on holey carbon-coated Ni grids. The ED-XRF spots were denoted as ***eds1*** and ***eds2***.

Additional analyses were performed by X-ray Photo-electron Spectroscopy (Thermo Scientific K-Alpha) XPS of 400 µm spots and a monochromatic Aluminum-kα X-ray source (260 watts in constant pass energy mode in two 200eV and 1eV steps). High resolution scans (Ag3d, C1s, O1s, Cu2p) were recorded at a constant pass energy of 50 eV and 0.1 eV steps. XPS data were processed using the software Thermo Avantage. Deconvolution was applied for all symmetric and asymmetric XPS signals for detecting potentially overlapped peaks for the key-element interacting with cations and zero-valent metals (**Fig. S2-S5**).

2.4 Strategy used to evaluate the antibacterial activity in terms of inhibition zone diameter and viability rate

Article 1

The antimicrobial behavior of the as-prepared samples was evaluated by the extent of the diffusion and inhibition zone tests towards *Bacillus subtilis168* and *Escherichia coli DH5α* bacterial strains. Almost similar wall structures and behavior were reported between Gram+ pathogenic and non-pathogenic strains (Grün et Dirr, 1967; Lorenz *et al.*, 2020). Non-pathogenic strains also appear to influence intestinal homeostasis through anti-inflammatory responses and mild inflammation (Behrouzi *et al.*, 2018). This justified their use herein for assessing MNP toxicity on bacteria integrity and providing the proof-of-concept of the key role of Metal-Matrices interaction on the antibacterial behavior. Copper and silver ions have the capacity to kill bacteria by destroying their walls and membranes in the presence of both pathogenic and non-pathogenic strains.

The assay is a semi-quantitative method where 5 mg metal-loaded clay materials or 1×0.5 mm^2 CT-based samples were inoculated in Petri dishes pre-seeded by approximatively 74 x 10^6 colony forming units CFU/mL of each bacteria strain with a cell optical density of 0.5 at 600 nm. Negative controls were included in each assay. All experiments were performed in triplicate involving three independent growth cultures with at least two technical replicates for each growth culture. After 24 h of incubation at 37 °C, the antibacterial activity was assessed through measurements of the inhibition zone diameter (IZD). The effect of the material amount on the IZD values was investigated by inoculating 1-9 mg of metal-loaded clay materials in both series of pre-seeded Petri dishes.

Article 2

Bacillus subtilis S168 and *Escherichia coli DH5α* were cultivated in Lysogeny Broth (LB) overnight in an incubator shaker at 37 °C, 100 rpm. The antimicrobial behavior of the as-prepared samples was first evaluated in terms of inhibition zone diameter (IZD) for two bacteria strains in 10 cm diameter Petri dishes. The latter were pre-inoculated with approximatively 74 x 10^6 CFU/mL of each strain with an optical density at 600 nm (OD_{600}) of 0.5 as measured by a UV-vis spectrophotometer (Biochrom Libra S50 UV/VIS Instrument). A preliminary test was performed by seeding 1 g of each lyophilized sample directly into the center of the as-prepared Petri dishes. All experimental runs were performed in triplicate at 37 °C for 24

h. The influence of various variables (pH and metal contents) was evaluated through impregnation of the discs of blotting paper with aqueous suspension of similar amounts of metal cation-loaded biopolymer but with different metal contents (0.1, 0.2, 0.5, 1.0, 2.0 and 5.0 mmol/g biopolymer). Another set of samples was prepared by mixing the same amount of metal-loaded biopolymer with similar metal content of 1 mmol/g biopolymer) at different pH (1, 3, 5, 7 and 9) adjusted with HCl or NaOH aqueous solutions. The discs were placed on the pre-inoculated agar and incubated for 24 h at 37 °C. Negative controls were performed in each assay. As the inhibition zones (IZ) were not circular, the area of the inhibition zone was estimated using Image J software for a 10 cm scale (**Fig. S4**). The average IZD and standard deviation were assessed through triplicate graphical measurements. Additional evaluation of the antibacterial capacity was performed. Practically, the tests were done using silver and copper CMC based materials with *E. coli* as bacterial model in LB broth with an OD_{600nm} of 0.5. The nanoparticles were added to the *E. coli* suspension at two different concentrations (0.1 and 1 mg/mL), and incubated at 37 °C, 180 rpm for 24h. During this period, samples were collected at 3, 6, 9 and 24h. Then, dilution series were carried-out and 0.1 mL was spread on LBA Petri dishes. The plates were then incubated at 37˚C for 24 hours and CFUs were counted.

CHAPTER 3

INSIGHTS IN METAL RETENTION ROLE ON THE ANTIBACTERIAL BEHAVIOR OF MONTMORILLONITE AND CELLULOSE TISSUE SUPPORTED COPPER AND SILVER NANOPARTICLES

Farzaneh Noori[a], Armelle Tchoumi Neree[b], Meriem Megoura[b], Mircea Alexandru Mateescu[a,b*], Abdelkrim Azzouz[a,]

Chemistry Dept, [a]Nanoqam and [b]CERMO-FC Centers, University of Quebec at Montreal, QC, H3C 3P8.

**Corresponding authors:*

Pr. Abdelkrim AZZOUZ, E-mail : azzouz.a@uqam.ca; Tel: 1 514 987 3000 Ext. 4119, Fax: 1 514 987 4054

Pr. Mircea Alexandru MATEESCU, E-mail : mateescu.m-alexandru@uqam.ca; Tel: 1 514 987-4319

Author contributions

Farzaneh Noori: Investigation, Data curation, Writing- Original draft preparation.

Armelle Tchoumi Neree: Investigation, Data curation.

Meriem Megoura: Investigation, Data curation.

Mircea Alexandru Mateescu: Supervision, Conceptualization, Methodology, Writing- Reviewing and Editing.

Abdelkrim Azzouz: Supervision, Conceptualization, Methodology, Writing- Reviewing and Editing, corresponding author.

Published by the Royal Society of Chemistry (RSC Advances) on July 9th, 2021, 11(39), pp.24156-24171

Abstract

The role of the retention strength of Cu^0 and Ag^0 nanoparticles on the induced antibacterial properties of montmorillonite and cellulose-supported polyol dendrimer against *Escherichia coli DH5α* and *Bacillus subtilis* 168 was comparatively investigated. An unprecedented approach involving X-Ray photoelectron spectroscopy, thermal analyses and surface charge measurements allowed correlating the host-matrices features to the different antibacterial activities of Cu^0 and Ag^0 nanoparticles against both bacteria strains. Optimal metal-matrice interactions appear to favor high dispersion of both metal particles and material grains. Improved contact surface with the cultivation media was explained in terms of hydrophilic character and a compromise between metal retention by the host-matrices and release in impregnating media. Competitive Lewis acid-base interactions appear to occur between MNP, solid surface and liquid media. These findings are of great importance providing a deeper understanding of the antibacterial activity of metal-loaded materials. This opens promising prospects for vegetal fibers and clay-supported drugs to treat dermatological and gastro-intestinal infections.

Keywords: Organoclays; Montmorillonite; Cellulose; Metal Nanoparticles; Copper; Silver; Antibacterial Properties; X-ray Photoelectron Spectroscopy; Thermal programmed desorption.

Highlights

1. Metal-loaded polyhydroxylic matrices displayed antibacterial activity.
2. Cellulose and clay mineral act as host matrices for metal and cation dispersion.
3. Polyol showed chelating and stabilizing ability for both metal and cation.
4. Metal cations are more effective than metal-zero against *E. coli* and *B. subtilis*.
5. Natural aluminosilicates and vegetal fibers are potential drug delivery matrices.

Graphical abstract

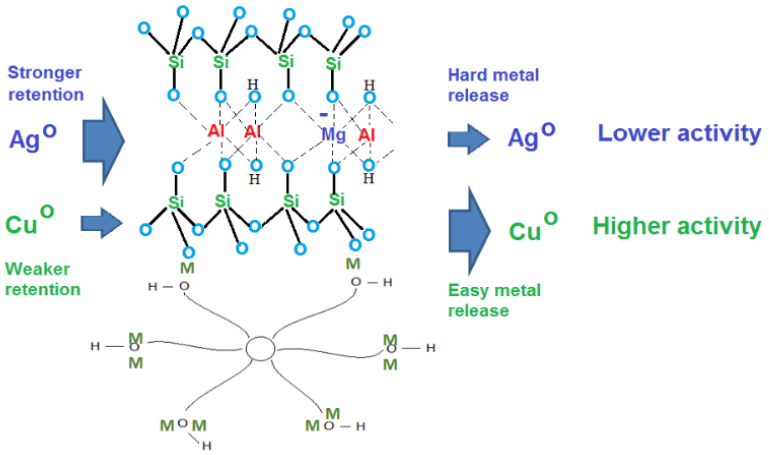

3.1 Introduction

Overuse of conventional antibiotics has led to pathogenic bacteria adaption and rise of resistance was found to be a direct cause of a series of outbreaks of infectious diseases (Levy, 1998). This has become a major medical issue that imposed a great challenge to be addressed (Cragg et Newman, 2013). Some metals nanoparticles (MNP) can behave as potential surrogates for organic antibiotics, given the well-known toxicity of heavy metals in certain concentrations in aqueous media. Metals are known as metabolism disturbing agents, some of them being harmful for animals and human (Martin et Griswold, 2009). Certain zero-valence metals (metal-zero) such as silver in high dispersion state have long been used in treating skin bacterial infections (Rai *et al.*, 2009). Nanoparticles of gold, zinc and titanium have showed high bioactivity. In this context, silver (Ag) and copper (Cu) are also promising nanoparticles that have shown broad-spectrum activity against many species of Gram positive and Gram-negative bacteria (Carretero, 2002; ČíK *et al.*, 2001; Čík *et al.*, 2006; Costa *et al.*, 2011; Dizman *et al.*, 2007; Gupta *et al.*, 1998; Herrera *et al.*, 2000). High antibacterial activity against pathogenic were already reported for finely dispersed MNP (España *et al.*, 2019) and more particularly AgNP which appear to generate free radicals that inhibit microbial growth (Kim *et al.*, 2007). Reportedly, eco-friendly and cost-effective cotton fabric–based composite materials doped with copper oxide showed antibacterial action against S*taphylococcus epidermis* and *Escherichia coli* (Nabil *et al.*, 2018). Preliminary unpublished tests provided arguments that metal-loaded polyhydroxylic matrices act as antibacterial agents (Noori *et al.*, 2020).

These performances were often explained in terms of contribution of the antibacterial properties of metal without sufficient emphasis on metal dispersion. In spite of the wide literature reported in this regard, the effect of the interactions occurring between the host matrix and both MNP on the infected media has scarcely been tackled so far. Furthermore, the role of metal retention strength in the antibacterial activity has never been evaluated and still remained to be elucidated. That is the present was undertaken.

MNPs have a strong tendency to aggregate into bulky inactive clusters (Rees *et al.*, 2011). So far, a wide variety of metal-loaded materials with antibacterial activity have been synthesized (Biegański *et al.*, 2021). Both zero-valent and cationic metal forms are known to behave as Lewis acids, and can interact with basic chemical groups. Polyols and polyamines bear specific chemical groups that confer them chelating and stabilizing properties for metals (Crooks *et al.*, 2001). Besides, unavoidable interparticle H-bridges interactions often lead to structure compacted and enhanced metal encapsulation that impede direct metal interaction with the infected area, thereby reducing their antibacterial activity. MNP dispersion and

stabilization on inorganic solid surfaces and/or specifically functionalized polymers provide metal-loaded inorganic-organic materials that allow overcoming this significant drawback (Hellmann *et al.*, 1998). Their synthesis has become one of the main targets of the present research.

Such a novel class of solid antibacterial agents are supposed to act as MNP reservoir. A wide variety of materials has been more or less successfully tested as host matrices for MNP so far, and an ample literature has been reported in this direction. Nevertheless, the use of natural and organically modified clay minerals has barely been investigated. These materials display high surface-to-volume ratio, chemical stability, thermal resistance, non-toxicity and recyclability (Bragg et Rainnie, 1974). Among these, smectite-type sodium montmorillonite (NaMt) is of particular interest due to its natural abundance, cost effectiveness, chemical inertness, sorptive capabilities, large specific surface area (Komadel, 2016) and even beneficial medicinal effects (Carretero, 2002; Nadziakiewicza *et al.*, 2019). This crystalline alumino-silicate is also known to be harmless for human health and biodiversity, and has already found some applications in biochemical and biomedical fields. Successful attempts against bacteria were already achieved using other clay minerals such as allophane and imogolite doped with metals like Ag, Cu, Co, Zn (Kim *et al.*, 2007; Stavitskaya *et al.*, 2019; Williams *et al.*, 2011). Attempts were also achieved using functionalized clay minerals and vegetal fibers for the dispersion of silver and copper ions (Joshi *et al.*, 2015).

The adsorptive properties of NaMt are governed by a large specific surface area bearing net negative charges and both in-plane and out-of-plane silanol groups. The latter are known to act as Lewis base and effective chelating groups for metals due the electron pair of the oxygen atoms. Additional hydroxyl groups can be brought by clay intercalation with dendritic polyols (Arus *et al.*, 2016a; Azzouz *et al.*, 2015; Sennour *et al.*, 2017b; Tahir *et al.*, 2017) or by direct use of polyhydroxylic polymers. .

Deeper insights in metal-matrices interaction (MMI) were achieved herein through a comparative study of the antibacterial activity of two metals (Copper and Silver) in both cationic and zero-valence form dispersion on a clay mineral, a vegetal polymer and their combination against two pathogenic bacteria strains. Diverse analysis techniques are expected to provide complementary data for demonstrating the proof-of-concept that the antibacterial activity requires optimal MMI, i.e. a judicious compromise between a strong metal retention by the host-matrices but a paradoxically easy metal release due to a high contact surface with the cultivation media. This is a comprehensive approach that is expected to allow tailoring optimal interactions with MNP-matrices by modifying the surface type and number of hydroxyl groups of

the incorporated organic moiety. This should provide valuable data for correlating the influence the metal retention strength and release velocity to the induced antibacterial activity. This is a new concept that opens new prospects for controlled release of diverse medicinal substrates.

3.2 Results and discussion

3.2.1 Metal dispersion on unmodified supports

CuNP and AgNP dispersion into polyol-based matrices in the presence of $NaBH_4$ was first noticed by color changes from blue to black for Cu^{2+} conversion into Cu^0 and from colorless to light grey for Ag^+ conversion into Ag^0 **(Fig. S1)**. Almost similar color change was observed for MNP dispersion in H20-CT-based samples **(Fig. S2).** Metal incorporation was confirmed by visible modification of the morphology of surface of the host-material. Preliminary observations through optical microscopy revealed a transition from a clean and almost soft surface of NaMt to the appearance of grains on the surfaces of both Cu^0/NaMt and Ag^0/NaMt (**Fig. S3**) and on CT-based materials (**Fig. S4**).

SEM analysis revealed larger amounts of spheroidal grains smaller than 100 nm and fewer quantities of crystalline rods of residual metal salt on both MNP-loaded NaMt (**Fig. 3.1a2-3**) as compared to CT samples (**Fig. 3.1b2-3)**. CT samples showed non-uniform dispersion of the spheroidal grains suggesting a weak CT-MNP interaction. The relatively high amount of Ag salt needles must originate from the lower capacity of silver to undergo redox processes indicating a lower amount of incorporated Ag^0NP. Thus, Ag-based materials are expected to exhibit a weaker antibacterial activity of as compared to their Cu-counterparts, as this will be examined further.

The rise of metal-loaded dendrimer scales not anchored on CT surface may be due to weak CT interaction with dendrimer H20, if any (**Fig. 3.2**). The most plausible explanation resides in a deficiency in OH groups on CT surface. This is expected to rather promote [H20:H20] H-bridges and [H20:MNP] attraction forces at the expense of binary [CT:H20] and ternary [CT:H20:CuNP] interactions within the polymer entanglement.

a	b
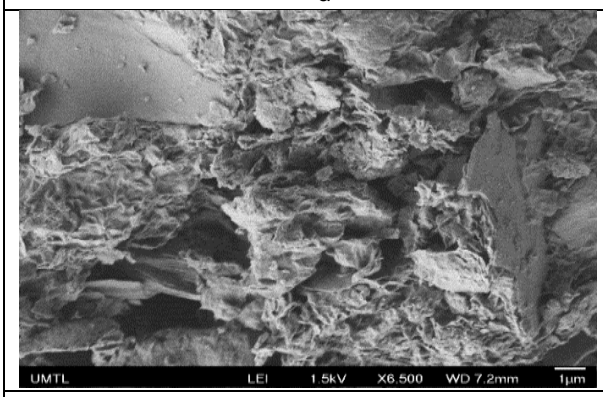	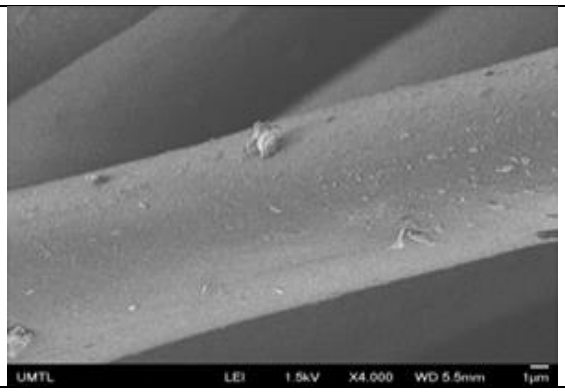
1. NaMt	1. CT
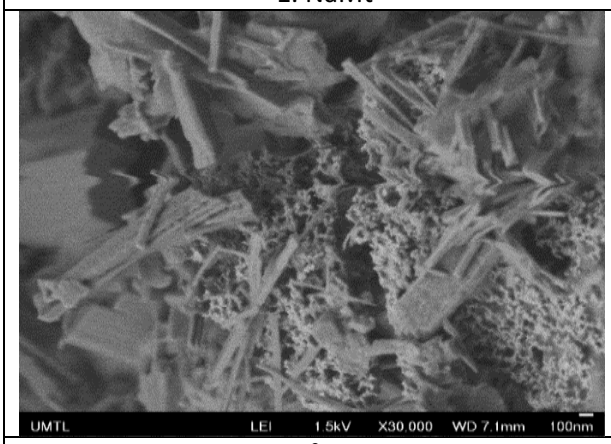	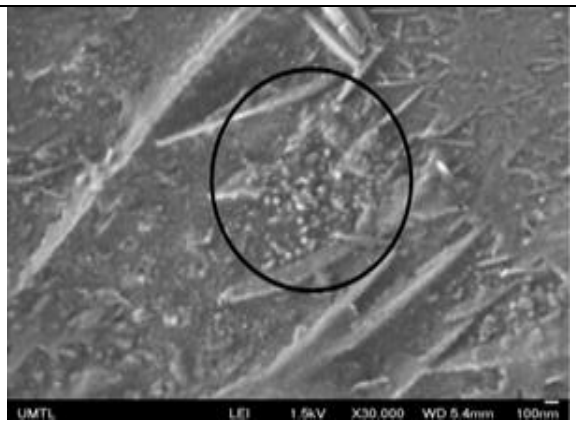
2. Cu^0/NaMt	2. Cu^0/CT
	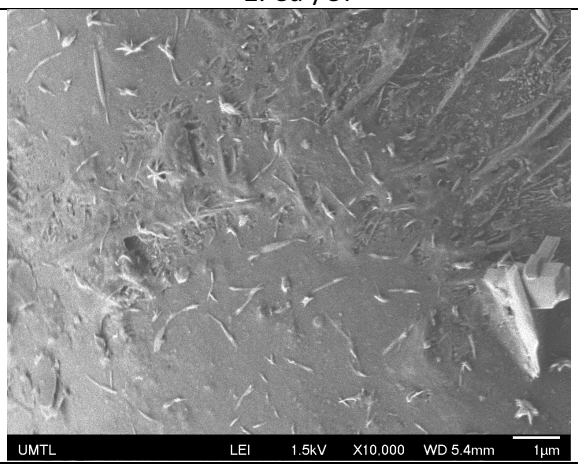
3. Ag^0/NaMt	3. Ag^0/CT

Figure 3.1. SEM images of NaMt, CT and their metal-loaded counterparts

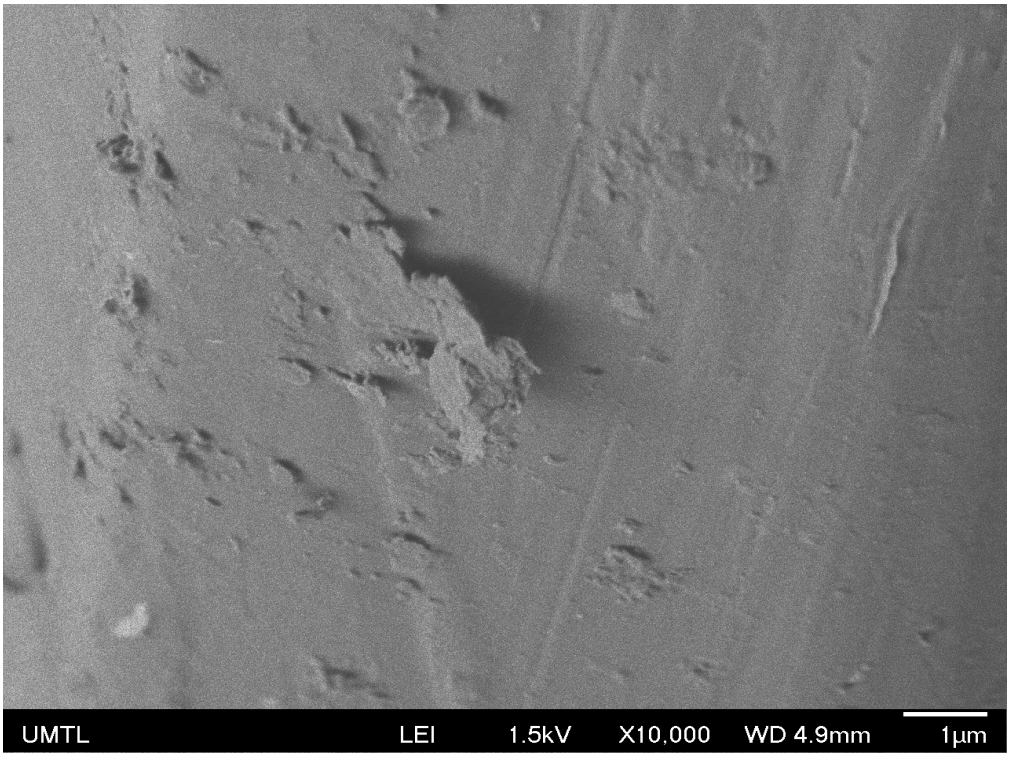

Figure 3.2. SEM images of Cu^0/H20-CT.

3.2.2 Effect polyol incorporation on metal dispersion

Dendrimer H20 incorporation induced a total disappearance of such crystalline rods on Cu^0/H20-CT. Their persistence in trace amounts on Ag^0/H20-CT confirms the lower amount of Ag^o particles. This beneficial effect of dendrimer H20 on MNP dispersion appears to markedly mitigate this drawback, presumably through a previous dispersion of metal cation even before reduction. This was followed by instant entrapment and stabilization of the rising MNP within the dendrimer entanglement, resulting in a pronounced improvement of metal dispersion on H20-NaMt (**Fig. 3.3**). This higher capacity of H20-NaMt to host MNP should arise from the contributions of the OH groups of both clay surface and dendrimer branches in the formation of ternary [NaMt-polyol-MNP] interactions.

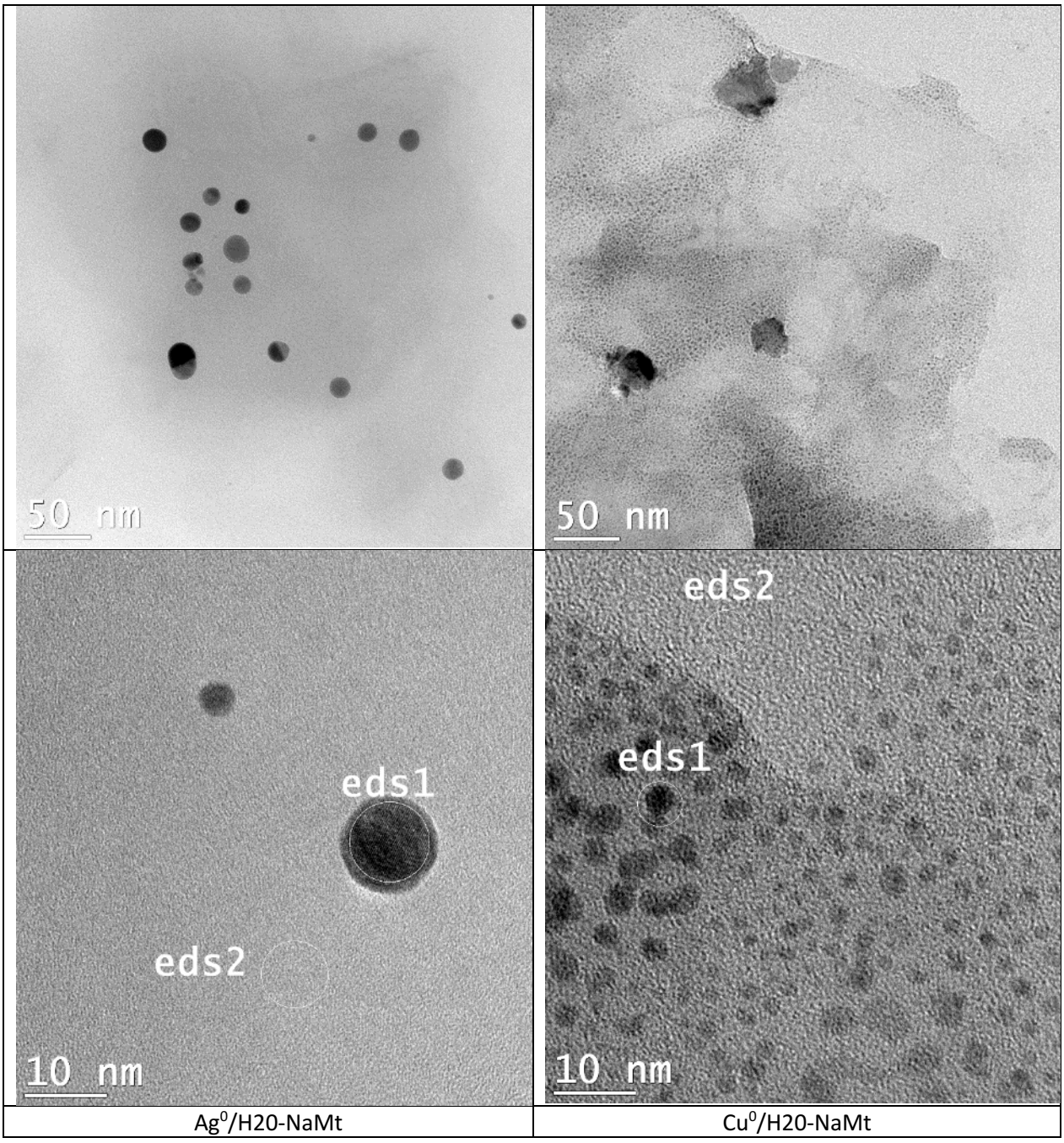

Ag^0/H20-NaMt	Cu^0/H20-NaMt

Figure 3.3. TEM images of metal-loaded H20-NaMt composites. The ED-XRF spots were denoted as eds1 and eds1 as previously defined. This result is of great importance, because it provides evidence that the presence of OH group on the surface of the support is an essential requirement for high MNP dispersion. Deeper TEM insights on H20-NaMt samples revealed a higher copper dispersion as reflected by a much lower average particle diameter not exceeding 5.5 nm as compared to silver (30 nm) (**Fig. 3.4**). Close-up analysis on **eds2** spots between in the grey surface between the black stains through EX-XRF revealed the

presence of metal sub-nanometric particles (MSNP) in Cu^0/H20-NaMt. No MSNP were detected in Ag^0/H20-NaMt, thereby confirming its much weaker dispersion capacity as compared to that of copper.

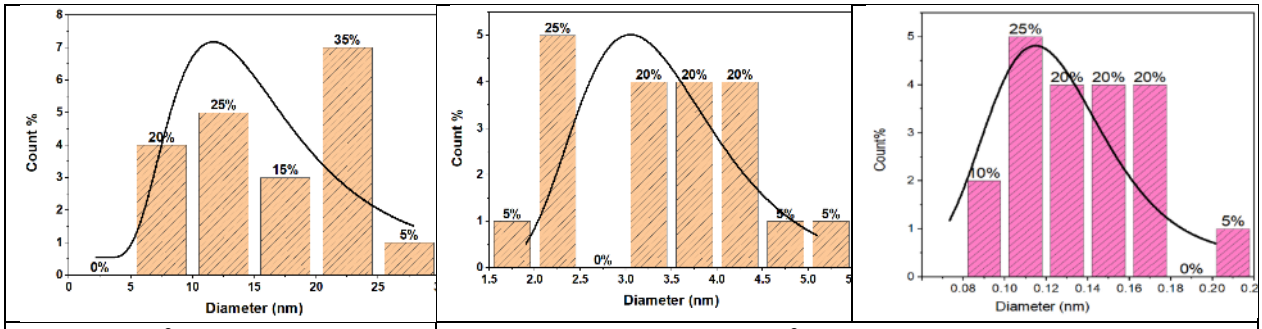

Ag^0/H20-NaMt | Cu^0/H20-NaMt

Figure 3.4. Average particle diameter of metal-loaded H20-NaMt composites as assessed by Image-J software.

Attempts to assess the size of copper sub-nanometric particles (CuSNP) using image G software on metal-free blank samples and Cu-H20-NaMt resulted in average particle diameter values ranging from 0.08 to 0.22 nm. The expected Face-Centered Cubic (fcc) symmetry and 0.74 compactness factor of Cu^0 suggest the occurrence of CuSNP with less than 5 copper atoms, given that one 0.5 nm particle and one 1 nm particle are supposed to have ca. 5 and 38 Cu^0 atoms, respectively (Sennour *et al.*, 2017b). Calculations based on ED-XRF measurements on two samples of each metal-loaded composite (**Fig. S5-S6**) gave O/Cu^0 atom ratio ranging from 1.4 to 1.7 in eds1 spot and from 3.8 to 9.6 in eds2 spot. For comparison, the average O/Cu^0 value was found to be ca. three folds higher than O/Ag^0 atom ratio, thereby explaining the higher antibacterial activity of Cu^0/H20-NaMt in spite of its lower Cu^0 content as expressed in term Cu/(Si+Al+O) mole ratio of 0.18 versus 0.24 for Ag/(Si+Al+O) value. Here, the metal particle size appears to play a key role, provided that the material particle size is sufficient to afford optimal surface contact with the aqueous media.

3.2.3 Changes in clay surface basicity

The involvement of the OH groups in metal stabilization is expected to induce changes in the hydrophilic character and basicity of the host materials. Insights through TPD revealed the occurrence of at least four desorption peaks for NaMt. This should account for four basicity strengths, namely weakly (below 100°C), medium (between 100 and 250°C), medium-to-strong (between 300 and 450°C) and strong basicity (between 450 and 550°C). The slight shift of the desorption peak from 60-200°C towards higher

temperatures (170-220°C) was noticed from bentonite to NaMt (**Fig. S7a**). This indicates a slight enhancement and strengthening of the surface basicity, most likely due to the removal of acidic silica phases (quartz, sand, cristobalite). This agrees with the slight increase in the CRC value from 2101 to 2261 $\mu mol.g^{-1}$ after bentonite purification (**Table 3.1**).

Table 3.1. CO_2 retention capacity (µmol/g) and weight loss for the synthesized materials

Material	TPD measurements	TGA measurements**	
	CRC (µmol/g)*	Temperature (°C)	Weight loss (%)
Bentonite	2101	-	-
Residual ash	1752	-	-
NaMt	2261	20-140	1.0-1.2
Cu^0/NaMt	55.5	20-140	0.5-0.6
		140-480	6.6
Ag^0/NaMt	662	20-90	1.9
		90-470	9.4
CT	-	47-130	0-0.1
H20-CT	38.4	47-185	0.275
Cu^0/CT	-	43-190	8.25
Ag^0/CT	-	47-200	8.74
Cu^0/H20-CT	14,5	32-200	4.675
Ag^0/H20-CT	5.6	40-200	8.525

***** CRC: CO_2 retention capacity.

**TGA measurements were performed between 25 and 700 °C for clay-based samples and between 25 and 200 °C for CT-based materials. The weight loss measured for each material within the lowest temperature range accounts for dehydration, and provides the moisture content.

Silica phase removal was supported by the marked depletion of the XRD lines assigned to Quartz (denoted as Q) after bentonite purification and presence of the main XRD lines of crystalline silica in the pattern of the residual ash (**Fig. S8**). The shift of the 001 XRD line from a 2θ value of 7.357˚ for bentonite to 9.142˚ for NaMt indicates a decrease in the interlayer spacing. This must originate from the replacement of bulky impurity particles and diverse cations by Na^+. This was confirmed by the noticeable sharpening and increased intensity of the main XRD lines of NaMt, which is a special feature of homo-ionic form of montmorillonite and almost perfect parallel arrangements of the clay sheets. This somehow explains the lower moisture content value observed for NaMt compared to bentonite, given that Na^+ cation has a lower polarizing power and thereby weaker capacity to attract water molecules than multivalent cations. MNP incorporation in NaMt induced a marked decrease in CRC from 2261 µmol/g down to 662 µmol/g for Ag^0/NaMt and 55.5 µmol/g for Cu^0/NaMt, providing clear evidence of the occurrence of competitive interaction of CO_2 and metal with the clay surface. Here, metal dispersion must involve at least two kinds of interactions. Some MNP interactions occur with the lattice oxygen atoms (-Si-O-Si- with strong Lewis

basicity), while others should take place with the OH groups of both in-plane silanols and out-of-plane Si-OH of the surface (Sulpizi *et al.*, 2012).

3.2.4 Changes in CT surface basicity

CT-based samples exhibited much lower surface basicity as compared to clay materials. TDP measurements for untreated cellulose tissue revealed no CO_2 desorption peak in the temperature range 20-100 °C. Polyol incorporation induced a marked change in the TPD profile, reflected by the appearance of a wide desorption peak between 20 and 110 °C (**Fig. S7b**). This accounts for the rise of weakly basic adsorption sites, most likely amphoteric to slightly basic OH groups belonging to the inserted polyol dendrimer. As, expected, OH groups were found to dramatically decline after CuNP insertion and totally disappear after AgNP incorporation. This is a confirmation of the occurrence of [-HO:MNP] interaction. This pronounced OH decay accounts for stronger [AgNP:OH-] interaction and a stronger entrapment as compared to CuNP, and allows predicting a less intense Ag^0 release and weaker antibacterial activity as compared to CuNP.

3.2.5 Changes in hydrophilic character

The hydrophilic character is expected to favor the material dispersion in aqueous media, while the antibacterial activity must be strong dependently on the material affinity towards aqueous media where bacteria naturally grow. This affinity towards water can be evaluated by TGA (Fu *et al.*, 2015), which revealed a single and small weight loss (WL) of at most 1.0-1.2 % for NaMt between 20 and 120 °C corresponding to reversible dehydration (**Fig. S9.a, Pattern 1**). Rehydration was found to revive the WL as supported by similar TGA patterns obtained after repeated TGA analysis-rehydration cycles. The total absence of other weight losses at higher temperature and more particularly of dihydroxylation (2 -Si-OH → Si-O-Si- + H_2O) provided evidence that NaMt is stable throughout the entire range of temperature investigated.

A noticeable decay of dehydration was noticed after CuNP incorporation, as reflected by the pattern flattening with a WL not exceeding 0.7-1.0% in the temperature range 20-120 °C (**Pattern 2**). This is concordance with the depletion of unoccupied OH groups due to the rise of competitive [-HO: metal] interaction, as previously stated. MNP insertion into NaMt also gave rise to a marked endothermic process at ca. 140-480 °C for Cu^0/NaMt and 90-470 °C for Ag^0/NaMt with a 6.6 % and a 9.4 % WL, respectively (**Table 3.1**). A possible explanation should consist in a delayed and slow moisture release from the internal

surface due to weak moisture diffusion across a compacted structure of MNP-loaded clay mineral (Bouazizi *et al.*, 2017b). Another WL was noticed at 470-480 °C and could be related to a dihydroxylation of terminal Metal-OH groups of possible metal oxide particles. The latter may unavoidably be produced during the synthesis procedure through slight metal oxidation when contacted to air. Both WL were found to shift towards lower temperatures but with higher WL values in Ag^0/NaMt, indicating a slightly higher hydrophilic character. This suggests less the formation of less AgNP and [-HO:Ag^0] interaction, and thereby more available hydrophilic OH groups

In contrast, CT-based samples were mostly characterized by a much lower moisture loss **(Fig. 3.9.b)**, which indicates a much weaker hydrophilic character. This must be due to a negligible surface density of hydroxyl groups on the commercial untreated CT. Polyol incorporation allowed overcoming this drawback by introducing hydrophilic OH groups, as reflected by the noticeable increase in moisture content from ca 0.1 % up to 0.277 % (**Table 3.1**).

Further incorporation of MNP in CT or in H20-CT induced a marked enhancement of the hydrophilic character. This is supported by more pronounced WL in the temperature range of 47-200 °C up to 8.25 % (Cu^0/CT), 9.74 % (Ag^0/CT), 4.675 % (Cu^0/H20-CT) and 8.525 % (Ag^0/H20-CT) (**Table 3.2**). Here, in spite of competitive [-HO:Metal] and [-HO:H_2O] interactions, the mere presence of OH groups in the vicinity of MNP seems to enhance the surface affinity towards water (Zhu, 1995). This confirms the narrow interdependence between the moisture content that reflects the hydrophilic character is expected to favor the material dispersion in aqueous media and surface basicity that promotes the metal retention.

3.2.6 Evidence of metal retention on clay surface

Evidence of metal dispersion in NaMt was provided by X-Ray photoelectron spectroscopy. Changes in the binding energy (BE) of the electrons belonging to the material atoms before and after metal dispersion are expected to provide valuable information about MNP retention strength and subsequently on the antibacterial activity. The values of the BE shift is considered as being proportional to the interaction strength. Metal incorporation in NaMt was revealed by new XPS signals, i.e. $Cu2p_{3/2}$ at 931.42 eV for Cu^0/NaMt and $Ag3d_{5/2}$ at 367.99 eV for Ag^0/NaMt **(Table 3.2)**. Other signals for $Cu2p_{1/2}$ at 953.00 eV, $Ag3d_{5/2}$ at $Ag3d_{3/2}$ at 373.89 eV provide confirmation of the presence of Cu^0 and Ag^0 particles. No loss feature was detected between Ag3d5/2 and $Ag3d_{3/2}$ and for higher BE, suggesting the occurrence of Ag^+ cations and incomplete reduction by $NaBH_4$, in agreement with SEM data.

Table 3.2. Binding energy (eV) shifts for key elements in the synthesized materials

Electron type	Binding energy (eV)								
	Theoretical data		NaMt			Cellulose tissue (CT)			
	Matrice	Alone	Alone	+Cu^0	+Ag^0	Alone	+H20	+Cu^0/H20	+Ag^0/H20
O 1s	SiO_2	532.9[a]	532.60	531.48	531.59	532.71	532.71	531.65	531.74
	Al_2O_3	531.1	-	-	-	-	-	-	-
	C=O	531.5	-	-	-	-	-	531.65	531.74
	C-O-H	532.9	-	-	-	-	-	533.54	533.66
	Unknown	-	-	-	-	-	-	536.11	535.85
C 1s	C-C	284.8[b]	-	-	-	285.05	285.01	281.61	285
	C-O-C	286[c]	-	-	-	286.45	286.16	282.96	
	O-C=O	288.5	285.05	285.03	289.49	288.98	288.96	285.71	
Al 2p	Alumino silicate	74.4[b]	75.25	76.00 (low)	74.99	-	-	-	-
Si2s	149	-	154.55	152.00	149	-	-	-	-
Si 2p	SiO_2	103.5	103.25	103.00	103.4	-	-	-	-
	Alumino-silicate	102.7	103.55			-	-	-	-
Ag $3d_{5/2}$*		368.2	-	-	367.99	-	-	-	368
Ag $3d3_{/2}$*		374.5	-	-	373.89	-	-	-	368
$Cu2p_{3/2}$**		933	-	931.42	-	932.65	-	932.97	-
$Cu2p_{1/2}$**		952.5	-	953.00	-	-	-	940	-
Cu satellite				943.50					

*XPS data for silver metal: $Ag3d_{5/2}$=368.2 eV; **XPS data for copper metal: $Cu2p_{3/2}$= 933 eV.

Weak satellite was barely detected around 943.50 eV, indicating the presence of trace amounts of Cu_2O. The C1s signals noticed at 285.05 eV for NaMt at and 285.03 eV for Cu^0/NaMt were both assigned to O-C=O groups and indicate to the presence of carbonates (CO_3^{2-}) as supported by the XRD pattern of bentonite with 113, 202 and 018 plane families between 40-45 degrees (**Fig. S8**). The marked BE increase of C1s signal for Ag/NaMt from 285.05 to 289.49 suggests a strong interaction between carbonate and silver, presumably through the formation of metal carbonate.

3.2.7 Role of oxygen atom in metal-clay interaction

The most important XPS results reside in the shifts of the binding energy (BE) of the key elements (oxygen, silicon and aluminum) providing evidence of the occurrence of metal interaction with the host surface. For oxygen, the BE value decreased from 532.66 eV down to 531.48 eV and 531.59 eV upon Cu^0 and Ag^0 incorporation, respectively. The larger BE shift of the O1s signal for Cu/NaMt suggests a stronger Cu^0 retention by the clay surface as compared to Ag^0 (**Fig. 3.5**). Such a BE weakening indicates must be due to an attraction by next-neighboring species and can be explained in terms of Lewis-Acid-Base (LAB)

interaction between clay lattice oxygens and MNP. The stronger [Clay-O:Cu^0] interaction was also reflected by a wider and asymmetric O1s signal for Cu/NaMt, as compared to Ag/NaMt.

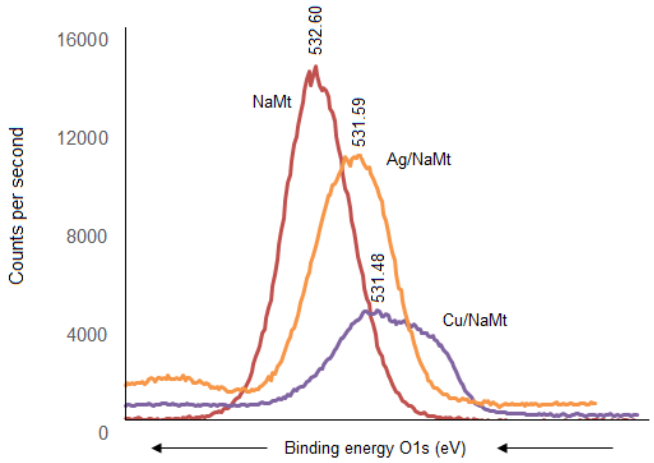

Figure 3.5. XPS signals for O1s electrons in NaMt and metal-loaded counterparts.

Signal deconvolution of this asymmetric signal for Cu/NaMt revealed three partially overlapped O1s signals, presumably due to multiple Cu^0 interactions with at least in-plane and out-of-plane silanols, with Si-O-Si groups and to a lesser extent with Al-OH groups (Aluminol). This explains somehow the higher dispersion of Cu^0 on NaMt as compared to Ag^0. Confirmation in this regard was provided by BE decrease for Si2s electrons from 154.55 eV to 152 eV, but slight Al 2p BE increase from 75.25 eV to 76.00 eV after Cu^0 incorporation. This indicates that Al-OH interaction with CuNP, if any, should have only weak contribution in copper retention. Interestingly, Ag^0 incorporation produced more pronounced Si2s BE decrease from 154.55 eV down to 149 eV but barely detectable Al2p shift from 75.25 eV to 74,99 eV. This is a precise indicator of the occurrence of stronger [Ag^0:Si] interaction without necessarily favoring silver dispersion on NaMt as compared to Cu^0, but almost negligible interaction with Al atoms.

3.2.8 Metal interaction in organic matrices

CT, H20 and their H20-CT composite showed XPS similar patterns with similar C1s signals at 288.91, 286.41 and 285.11 eV attributed to O-C=O, C-O-C and CC-groups, respectively (**Fig. 3.6**). The intensity of each C1s signal for H20-CT appears to be the sum of those of both organic components. No BE shift was detected suggesting that CT interaction with H20, if any should be negligible.

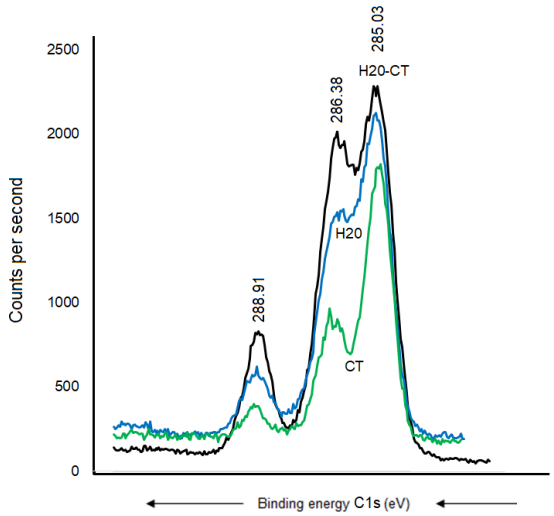

Figure 3.6. C1s XPS signals for metal-free CT, H20 and H20-CT

Cu^0 incorporation also induced no C1s BE shift in CT (**Fig. 3.7a**) but a pronounced BE decrease down to 285.71, 282.81 and 281.61 eV, respectively (**Fig. 3.7b**). Similar sequence was registered after AgNP insertion, providing evidence of strong [AgNP:H20-CT] interaction through the carbon atoms.

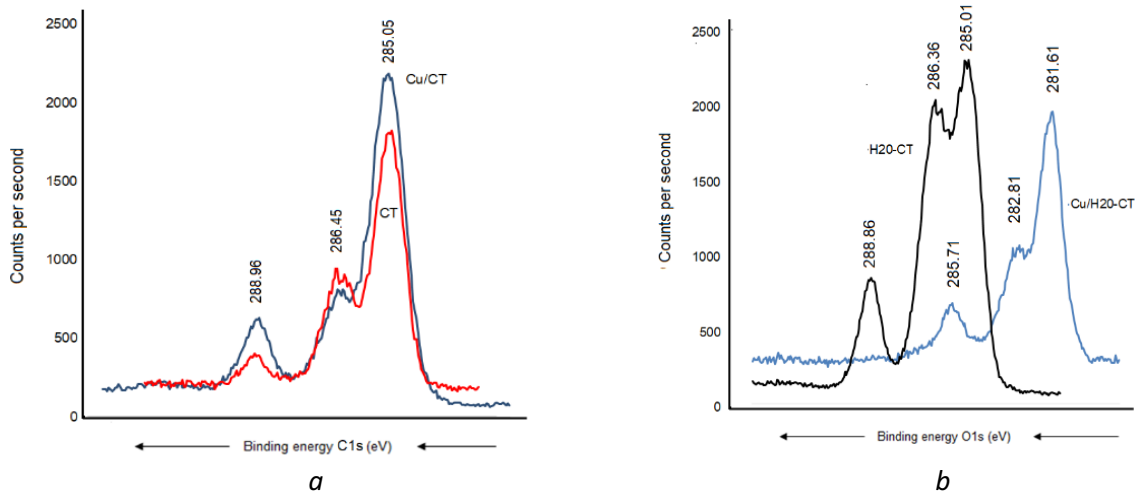

Figure 3.7. C1s XPS signals for Cu-loaded CT (a) and Cu-loaded H20-CT (b).

This marked BE shift for the C1s signal of more than 3 eV compared to the almost total lack of BE shift in CT alone accounts for a higher capacity of H20-CT to host MNP (**Fig. 3.6**). This is due to the contribution of the dendritic entanglement. The noticeable intensity decrease for the C1s signal of C-O-C and C-C groups (**Fig. 3.7b**) suggests a compaction of the dendritic entanglement around MNP.

3.2.9 Role of oxygen atom in metal-polymer interaction

Metal-matrices interaction should also involve the oxygen atoms of the polymers. No H-bridges seem to arise between CT and dendrimer H20, given the absence of detectable shift of the O1s signal at 532.71 eV (**Fig. 3.8a**). Nonetheless, CT was found interact with the incorporated Cu as supported by the O1s shift from 532.7 to 531.91 eV and appearance of a new signal at 533.31 eV assigned to the-C-O-H group (**Fig. 3.8b**). This is presumably due to the rise of [-HO:Cu] interaction.

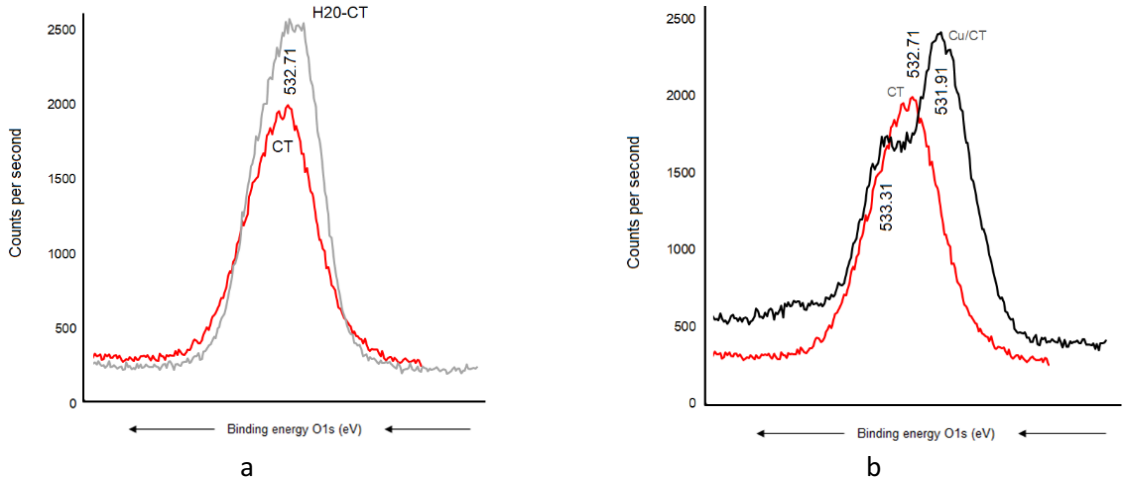

Figure 3.8. O1s XPS signals after CT loading by dendrimer H20 (a) and CuNP (b).

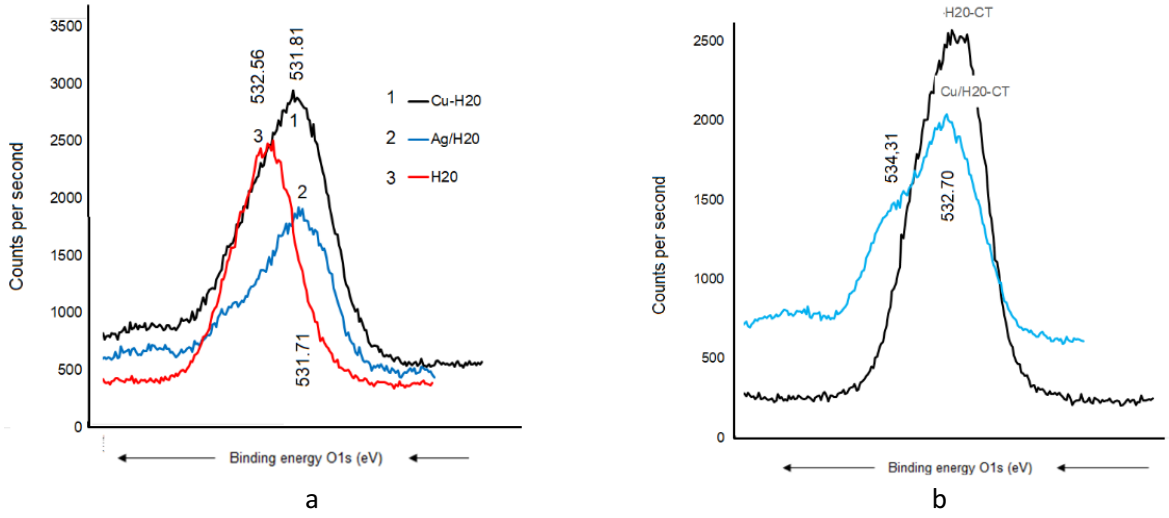

Figure 3.9. O1s signals for O1s electrons in CT alone (a) and dendrimer H20 alone (b).

A BE Shift from 532.56 eV down to 531.81 and a signal widening were observed after Cu^0 incorporation in dendrimer H20 alone. (**Fig. 3.9a**). The slightly higher BE decrease from 532.56 eV down to 531.71 eV registered after Ag^0 incorporation indicates a paradoxically stronger interaction of silver with the oxygen atoms of the dendrimer. Similar signal widening around 532.70 eV was observed for Cu^0/H20-CT with appearance of a second signal at 534.31 eV attributed to the -C-O-H group (**Fig. 3.9b**). Surprisingly, the higher density of hydroxyl groups in H20 as compared to CT gave only slightly higher signal. This may be due to signal mitigation by the effect of H20 entanglement compaction (Arus *et al.*, 2016a; Sennour *et al.*, 2017b; Tahir *et al.*, 2017). Here, the [-HO:MNP] interaction strength is expected to determine the entanglement compaction or, in contrast, MNP release according to the pH changes in aqueous media.

3.2.10 Antibacterial activity of metal-loaded NaMt

Triplicate incubation tests at 37 °C for 24 h of 74.10^6 CFU/mL populations of *E. coli* and *B. subtilis* strains revealed no antibacterial activity in the presence of metal-free NaMt, dendrimer H20, H20/NaMt and cellulose tissue. As compared to the starting NaMt, copper and silver-loaded montmorillonite (Cu^0/NaMt and Ag^0/NaMt) exhibited noticeable antibacterial activity against both bacteria strains as illustrated by marked increases in the diameter of the inhibition zone **(Fig. 3.10)**. This providing evidence of the beneficial effect of metal incorporation (Gordon *et al.*, 2010; Potera, 2012; Vincent *et al.*, 2018; Yun'an Qing *et al.*, 2018). Lower IZD was registered for Cu^0/NaMt (1.40 cm) as compared to Ag^0/NaMt (1.87 cm) in the presence of *E. coli* but comparable IZD (1.83 cm) were obtained for both Cu^0/NaMt and Ag^0/NaMt in the presence of *B. subtilis* (**Table S1**). This suggests a weaker antibacterial effect of CuNP on *E. Coli*.

Addition of dendrimer H20 on NaMt induced a visible improvement of the antibacterial activity, as illustrated by a larger inhibition zone (**Fig. S10**). This can be explained in terms of higher metal dispersion within the dendrimer entanglement bearing OH groups that act as chelating agents (Lewis base). The higher IZD values registered for Cu^0/H20-NaMt with both strains (1.77 and 1.83 cm versus 1.07 and 150 cm for Ag^0/H20-NaMt) indicate that Cu^0 is more effective than Ag^0, presumably due to: ***i.*** a higher dispersion by dendrimer H20 as revealed by TEM and; ***ii.*** an easier release of copper in the liquid media as a result of a higher dispersion of the material particles.

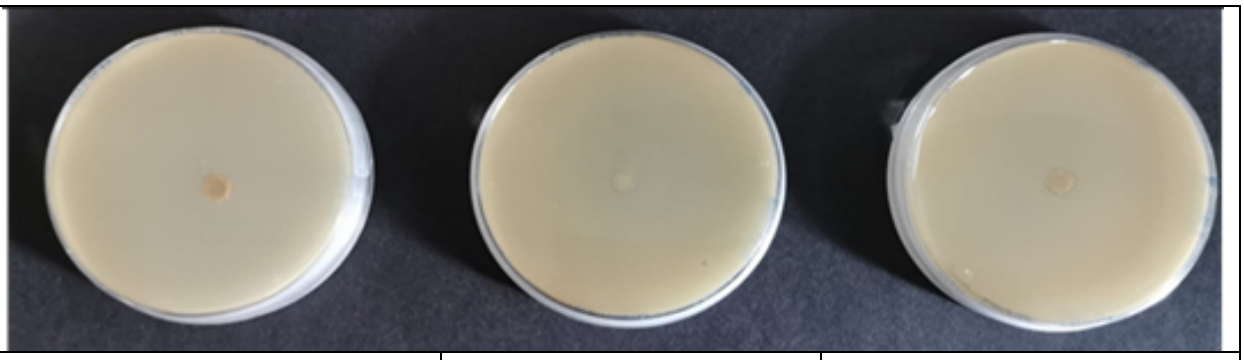

NaMt	Dendrimer H20	H20-NaMt

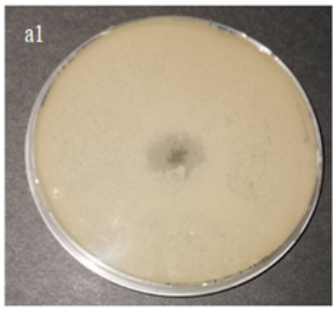

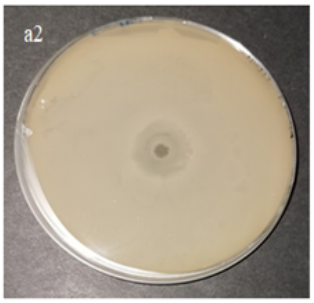

Cu^0/NaMt	Cu^0/NaMt

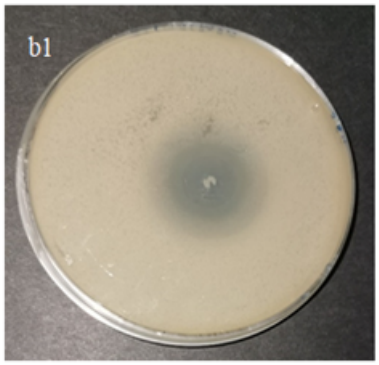

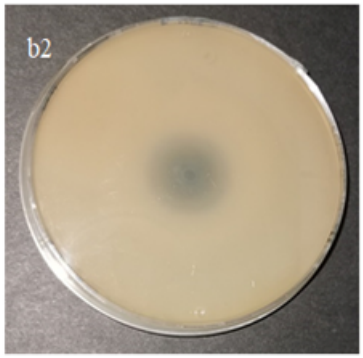

Ag^0/Mt	Ag^0/Mt
Escherichia coli DH5α	*Bacillus subtilis168*

Figure 3.10. Inhibition zones in the proliferation of both bacteria strains in the presence of NaMt and metal-loaded counterparts.

Besides, copper is also known to be more reactive than silver, generating oxygen reactive species (ROS) as in Fenton-like and Haber-Weiss processes. Other possible explanations should involve lower amounts of inserted Ag^0 atoms. This must be due to the lower reduction level of Ag^+ cations in agreement with XPS data and the large amount of non-dispersed rod-like silver salt crystals revealed by SEM images (**Fig. 3.1a**). The general tendency is that high antibacterial ability was observed against Gram-positive *B. subtilis,* as illustrated by the largest IZD values **(Table S1).** This can be due to the very structure of the *Bacillus* cell wall with peptidoglycan multilayers and an abundant amount of pores that confers them more sensitivity

to reactive species as compared to Gram-negative *E. coli* (Fu *et al.*, 2015). The high concordance between the material characterization data and antibacterial activity allows stating that judiciously tailored [Metal-Matrice] interaction allows designing effective antibacterial agents.

3.2.11 Effect of clay dispersion and particle size

The clay dispersion in water is expected to play a key-role in the antibacterial activity, because it is assumed to improve the contact surface available for MNP exchange with culture media. Clay material dispersion in water induced specific intrinsic pH levels. A correlation attempt from data summarized in **Table S1** showed that the average particle increasing pH from 6.01 up to 9.28 resulted in results in a marked decreased in particle size from 401.9 down to 127.6 µm (**Fig. 3.11a**). This accounts for a significant clay material dispersion in water most likely due to increasing repulsive forces between clay lamellae as supported by an increasing tendency of the negative value of Zeta potential (**Fig. 3.11b**). However, the occurrence of a maximum value of 38.12 mV for H20-NaMt indicates that increasing Zeta potential is not the sole factor of clay dispersion and that the modified clay structure also plays a role in this regard.

Interestingly, the highest dispersion grade, i.e. the lowest particle sizes were obtained for Ag^0/H20-NaMt (127.6 nm) and Ag^0/NaMt (152.7 nm), which displayed moderate Zeta potential of -27.21 and -28.31 mV, respectively (**Fig. 3.11c**). A possible explanation resides in a much weaker aggregation of clay or organoclay particles around AgNP.

As, expected, the particle size was found to exhibit a markedly favorable influence on the antibacterial activity, as supported by the decreasing tendency of the IZD with increasing particle size (**Fig. 3.11d**), thereby confirming the previous statement the key-role of the extent of the contact surface. This provides additional arguments in favor of the proof-of-concept that an optimal equilibrium between metal retention and release by the host-matrices is a key factor for high antibacterial activity. In other words, strong metal retention improves the carrier capacity of the host-matrices, but paradoxically easy metal release in the culture media improves the antibacterial activity. This simultaneously requires ***i:*** high metal dispersion and stabilization (fine particle size); ***ii:*** high matrix dispersion (Low material particle size) to improve the contact surface; and ***iii:*** modulable metal retention according the features of aqueous media.

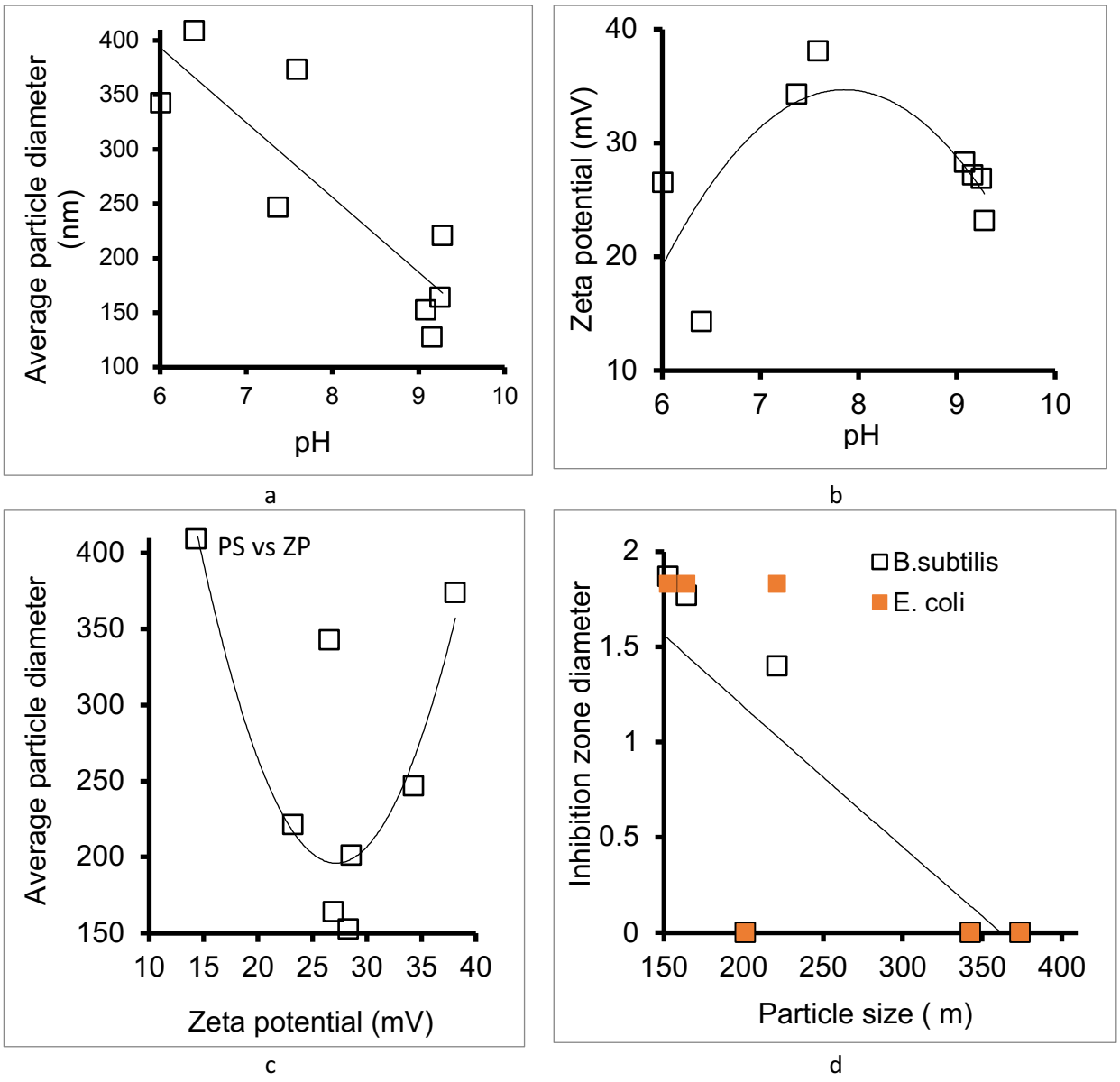

Figure 3.11. Effect of pH on the average particle size (a) and Zeta potential (b), their interdependence (c) and influence of the particle size on the IZD for both bacteria strains (d).

3.2.12 Effect of metal amount in clay samples

One of these features is undoubtedly the amount of incorporated metal, which appears to play a key-role in the effectiveness of the antibacterial agent. Deeper insights through different amounts of metal-loaded organoclays ranging from 1 to 9 mg revealed an almost proportional IZD increase for both strains *E. coli* and *B. subtilis* with increasing amounts of bactericidal agents up to a certain level (**Fig. 3.12**). Maximal

values of 2.5 and 3.5 cm for 9 mg of Cu^{2+}/NaMt-H20 and of 2.4 and 3 cm for the same amount of Cu^{0}/NaMt-H20 against *E. coli* and *B. subtilis,* were respectively attained (**Table S2**).

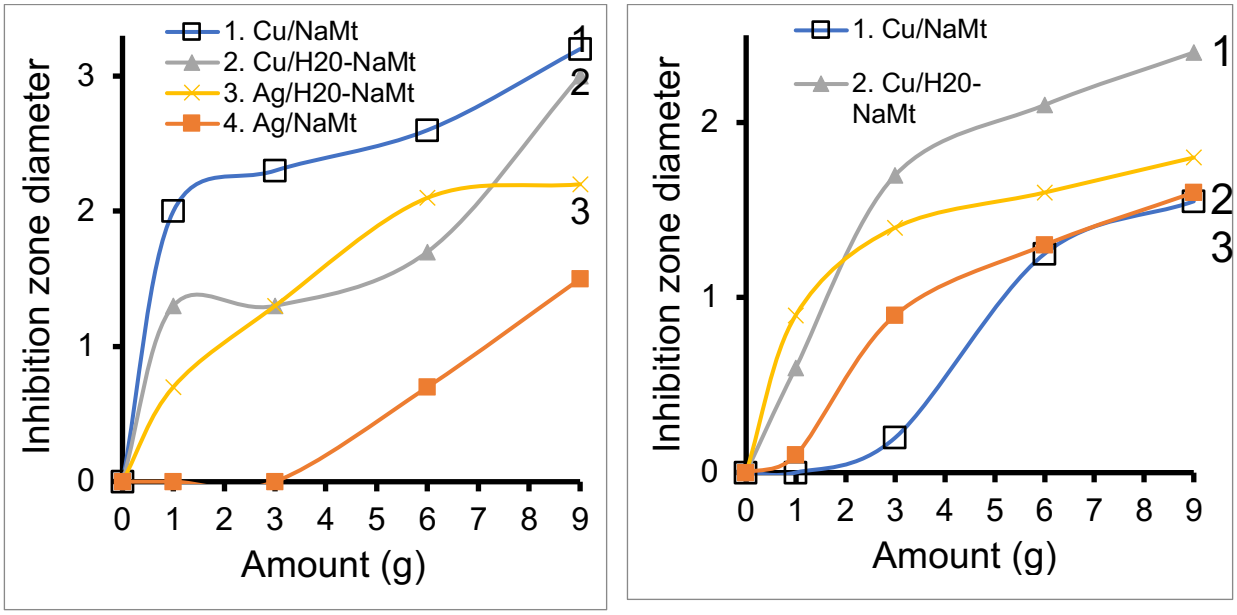

Bacillus subtilis168 *Escherichia coli DH5α*

Figure 3.12. Effect of the amount of antibacterial material on the inhibition zones diameter in Petri dishes pre-seeded by approximatively 74 x 10^6 colony forming units CFU/mL of each bacteria species with a cell optical density of 0.5 at 600 nm.

The general tendency is that higher IZD values were obtained with *B. subtilis* as compared to *E. coli*. This confirm the previous assertion of the higher sensitivity of *Bacillus subtilis* (Fu *et al.*, 2015). It is also worth mentioning that Cu^{0}/NaMt showed highest IZD values for *Bacillus subtilis168* but lowest values for *E. Coli*, in agreement with previous data (**Table S1**).

3.2.13 Effect of the solid surface

In order to investigated the role of the solid support, similar antibacterial tests performed with cellulose-based samples against both *E. coli* and *B. subtilis* revealed the absence of antibacterial activity for cellulose tissue (CT) and its polyol-functionalized counterpart (H20-CT). In contrast, Cu-loaded cellulose matrices exhibited strong activity of against bacteria as illustrated by significant IZD increase **(Table 3.3)**. This is a clear confirmation that the antibacterial activity is only due to metal incorporation regardless to the host-

matrix. The highest IZD values obtained for Cu^0/H20-CT (3.5 cm) must be due to both the beneficial role of dendrimer H20 and higher antibacterial activity of copper as compared to silver. Interestingly, this value is higher than those of 2.23 cm for *E. coli* and 2.73 cm for B. subtilis registered in the presence of Cu^{2+}/H20-NaMt (**Table S1**). Similar observations were made for Ag^0/H20-NaMt with a 0.90 cm IZD versus 2 cm for Ag^0/H20@CT.

Table 3.3. Inhibition zone diameter (cm) for metal-loaded CT-based materials

Samples	Inhibition zone diameter (cm)	
	B. subtilis 168	***E. coli DH5α***
CT	0	0
Boltorn™H20	0	0
H20@CT	0	0
Ag^0/CT	1	0
Cu^0/CT	1,6	0,5
Cu^0/H20@CT	3,5	1
Ag^0/H20@CT	2	0,9

The most plausible explanation resides in a higher metal dispersion in CT samples by all hydroxyls of dendrimer H20. Indeed, unlike on montmorillonite, the OH groups of H20 are expected to preponderantly interact with MNP at the expense H-bridges with the negligible amount of OH on CT surface, as supported by TPD measurements (**Fig. S7b**). This explains somehow the total absence of H20-CT interaction, in agreement with XPS data. This result if of great importance, because it clearly demonstrates that that the interaction of the polyol dendrimer with the solid surface are detrimental for MNP dispersion and antibacterial activity.

The effect of the surface charge and subsequently of the Zeta potential on the antibacterial activity should also be taken into account. The general tendency is that increase absolute value of the Zeta potential induced a marked decay of the antibacterial activity, as well illustrated by the visible IZD decrease (**Fig. 3.13**). This suggests a detrimental effect in higher density of negative charge on the solid surface that impede [Material:Bacteria wall] interaction through repulsive forces. The external side of the cell wall of both Gram-positive and Gram-negative bacteria bears negative charges (Ashmore *et al.*, 2018; Stensberg *et al.*, 2011).

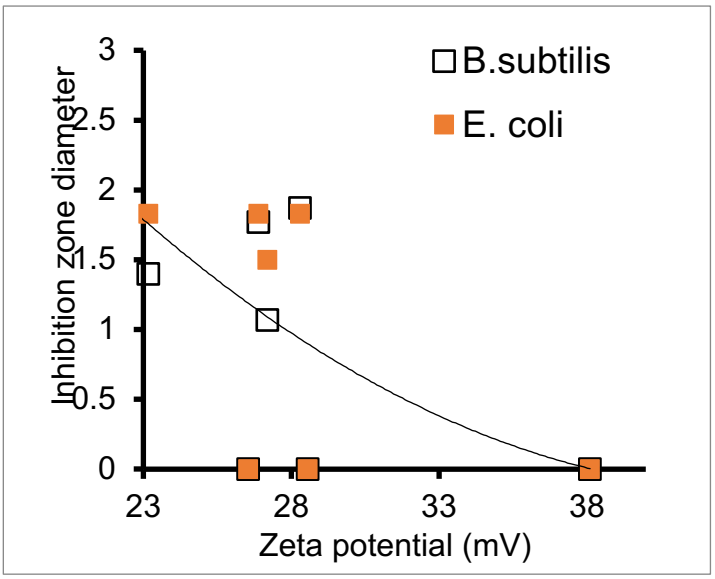

Figure 3.13. Effect of Zeta potential on the IZD for both bacteria strains.

Unlike with cations, negatively charged bacterial cell walls do not interact with negatively charged particles due to repulsive electrostatic forces. Decreasing Zeta potential is supposed to improve bacteria contact with solid surface, MNP release due to attractive Lewis base sites of the cell wall and further diffusion inside the cell (Stensberg *et al.*, 2011). Inside the cell, MNP can generate reactive oxygen species (ROS) like hydrogen peroxide (H_2O_2, superoxide anion ($\cdot O_2^-$), and hydroxyl radical $^{\bullet}OH$ (Gordon *et al.*, 2010; Yun'an Qing *et al.*, 2018) that alter the cell stability (Dakal *et al.*, 2016) via a wide variety of processes against bacteria (Dakal *et al.*, 2016; Losasso *et al.*, 2014; Yuan *et al.*, 2018). In spite of their antibacterial activity (Ávalos *et al.*, 2013), AgNP were found to be less effective than cations (El Badawy *et al.*, 2011), which are much more attracted by the negative charges of bacterial walls (Losasso *et al.*, 2014; Slavin *et al.*, 2017b; Yun'an Qing *et al.*, 2018). Similar observations can be made for CuNP (Chatterjee *et al.*, 2014; Sistemática *et al.*, 2016) whose concentration and dissolution in the bacterial membrane is known to induce potential and permeability changes, membrane alteration (Amro *et al.*, 2000; Azam *et al.*, 2012), production of ROS and other detrimental oxidative processes (Applerot *et al.*, 2012; Fang *et al.*, 2007), decay in intracellular ATP production and disruption of DNA replication (Kim *et al.*, 2007; Sondi et Salopek-Sondi, 2004), This should confer higher activity to CuNP against both bacteria compared to AgNP (Chudobová et Kizek, 2015), thereby explaining the higher performance of polyol dispersed copper reported herein.

3.3 Conclusion

Metal dispersion in the form of AgNP and CuNP with polyol dendrimer induced antibacterial activity on montmorillonite and cellulose tissue. Previous polyol incorporation induces no detectable antibacterial activity but provides additional hydroxyl groups that act as chelating agents for MNP. Strong [-HO:Metal interaction reduces MNP accessibility and affects the antibacterial activity. Weak -[-HO:Metal] interaction attenuates MNP retention and promotes the antibacterial activity. Optimal amount of metal-loaded polyol composites results in high biocidal through a compromise between structure compaction and MNP accessibility to bacteria cells. Polyol dendrimer interaction with the solid surface appears to be detrimental for MNP dispersion. High antibacterial activity involves a judicious compromise between strong metal retention to improve the carrier capacity of the host-matrices and easy metal release in the culture media. This requires high dispersion and low size of both metal particles and material grains to improve the contact surface. Modulable metal retention according the features of aqueous media appears to be a key factor in this regard. Higher density of negative charge on the solid surface impedes [Material:Bacteria wall] interaction through repulsive forces. These findings are essential requirements designing effective antibacterial matrices with natural and low-cost materials provided with modulable entanglement porosity,

Acknowledgements: *This work was supported by NSERC (To Pr. Mircea A. Mateescu). The authors appreciate the technical assistance of Dr. G. Chamoulaud (Nanoqam), Dr. Alain Adnot (Laval University) and Dainelys Guadarrama Bello (UdeM). A CRIPA-FRQNT scholarship granted to F. Noori is gratefully acknowledged.*

CHAPTER 4

SYNTHESIS OF METAL-LOADED CARBOXYLATED BIOPOLYMERS WITH ANTIBACTERIAL ACTIVITY THROUGH METAL SUBNANOPARTICLE INCORPORATION

Farzaneh Noori,[a] Meriem Megoura,[a] Marc-André Labelle,[a] Mircea Alexandru Mateescu,[a*] Abdelkrim Azzouz[a,b*]

[a] *Nanoqam, Department of Chemistry, Université du Québec à Montréal, QC, Canada H3C 3P8.*

[b] *École de Technologie Supérieure, Montréal, Québec, H3C 1K3, Canada.*

**Corresponding authors: Pr. Abdelkrim Azzouz & Pr. Mircea Alexandru Mateescu*

E-mail : azzouz.a@uqam.ca; Tel: 1 514 987 3000 Ext. 4119, Fax: 1 514 987 4054

E-mail: mateescu.m-alexandru@uqam.ca; Tel: 1 514 987 4319

Author contributions

Farzaneh Noori: Investigation, Data curation, Writing- Original draft preparation.

Meriem Megoura: Investigation, Data curation and contribution with antibacterial and viability tests.

Marc-André Labelle: Investigation, Data curation and contribution with DS determination.

Mircea Alexandru Mateescu: Supervision, Conceptualization, Methodology, Reviewing, corresponding author.

Abdelkrim Azzouz: Supervision, Conceptualization, Methodology, Manuscript writing, reviewing and editing, corresponding author.

Published by the Antibiotics on March 24th, 2022, *11*(4), p.439.

Abstract

Carboxymethylstarch (CMS) and carboxymethylcellulose (CMC) loaded by highly dispersed metal subnanoparticles (MSNP) showed antibacterial activity against *E. coli* and *B. subtilis* strains. Copper and silver were found to act in both cationic and zero-valence forms. The antibacterial activity depends on the metal species content but only up to a certain level. Silver cation (Ag^{+}) showed higher antibacterial activity as compared to Ag^{0}, which was however more effective than Cu^{0} due to weaker retention. The number of carboxyl groups of the biopolymers was found to govern the material dispersion in aqueous media, the metal retention strength and dispersion in the host-matrices. Cation and metal retention in both biopolymers was found to involve interactions with the oxygen atoms of both hydroxyl and carboxyl groups. There exists a ternary interdependence between the Zeta potential (ZP), pH induced by the biocidal agent and its particle size (PS). This interdependence is a key-factor in exchange processes with the surrounding species including bacteria. Clay mineral incorporation was found to mitigate material dispersion due to detrimental competitive Clay:Polymer interaction. This knowledge advancement opens promising prospects for manufacturing metal-loaded materials for biomedical applications.

Keywords: Carboxymethylstarch; Carboxymethylcellulose; Metal subnanoparticles; Antibacterial activity.

Highlights

1. Carboxymethyl-functionalized biopolymers act as host matrices for metal particles.
2. Carboxymethyl group density influences the metal dispersion and particle size.
3. Metal dispersion and stabilization involve interactions with matrices oxygen atoms.
4. Metal type, dispersion, valence and amount are key-factors in the antibacterial activity.
5. Highly dispersed copper and silver subnanoparticles show antibacterial activity.

Graphical abstract

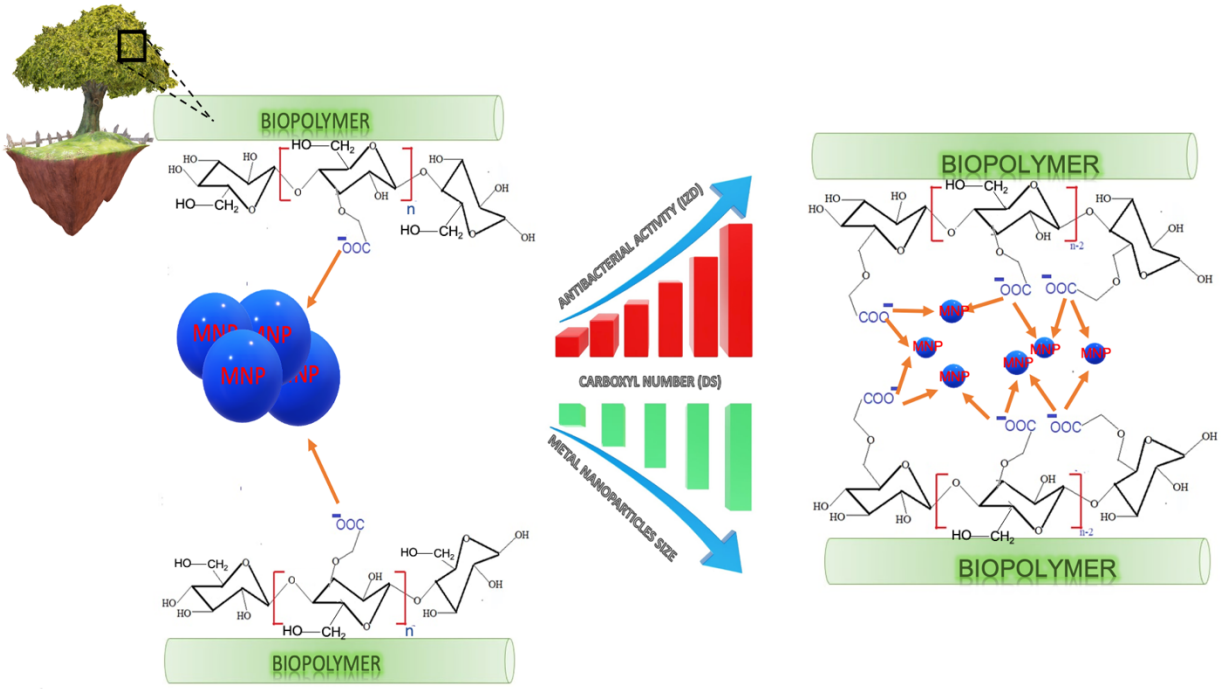

4.1 Introduction

Excessive use of conventional organic antibiotics was already recognized as favoring pathogenic micro-organism resistance with negative impact on animal and human health (Capita et Alonso-Calleja, 2013; Jansen *et al.*, 2006; Penesyan *et al.*, 2015; Roca *et al.*, 2015). Nowadays, this is regarded as being a major environmental issue. Metal nanoparticles (MNPs) have a broad-spectrum activity being efficient against both Gram positive and negative micro-organisms (Noori *et al.*, 2021; Sánchez-López *et al.*, 2020). Their non-selective toxicity arises from the production of a wide variety of reactive oxidative species (ROS) through the oxidative stress induced on micro-organisms.

Copper and silver already showed antibacterial activity (Bondarenko *et al.*, 2013; Harikumar et Aravind, 2016; Keshari *et al.*, 2020; Kim *et al.*, 2011; Noori *et al.*, 2021; Ramyadevi *et al.*, 2012) and anti-cancer properties (Faedmaleki *et al.*, 2014). These features were found to be improved by high contact surface with microorganisms, but their tendency to aggregate (Allen *et al.*, 2017; Kalsin *et al.*, 2006; Keller *et al.*, 2010) is known to affect their toxicity towards bacteria (De Souza *et al.*, 2019; Lin *et al.*, 2009). High dispersion into smallest particle size possible can allow overcoming this drawback by either using suitable host-matrices or surfactants bearing highly chelating groups (Diaz *et al.*, 2016; Furukawa *et al.*, 2009; Iqbal *et al.*, 2020; Kosakowska *et al.*, 2018; Le Ouay et Stellacci, 2015; Noori *et al.*, 2021; Pathak *et al.*, 2019; Tang et Zheng, 2018; Ujihara et Imae, 2010; Xiu *et al.*, 2012).

Biocompatibility is an essential requirement for such dispersing agents, and carboxymethylstarch (CMS) and carboxymethylcellulose (CMC) are low-cost and interesting polysaccharides for such a purpose. They are commonly used as drug carriers and other biomedical applications owing to their modification capability, non-toxicity, high biodegradability and biocompatibility and pH sensitivity (Javanbakht *et al.*, 2018; Javanbakht *et al.*, 2019; Labelle *et al.*, 2020; Ogushi *et al.*, 2007; Ounkaew *et al.*, 2020; Pal *et al.*, 2006; Wang *et al.*, 2018; Xu *et al.*, 2017). Upon chemical functionalization, they acquire different number of carboxymethyl (CM) groups that can capture metal cation via ion-exchange. The CM oxygen atoms should also provide electron pairs that are able to stabilize MNPs preventing their aggregation via Lewis acid-base interactions (Farrokhpay, 2009). Similar interactions were already reported for hydroxyl groups of polyol dendrimer and clay minerals (Arus *et al.*, 2016b; Bouazizi *et al.*, 2017a, 2018a; Noori *et al.*, 2021; Sennour *et al.*, 2017a; Tahir *et al.*, 2017).

However, unlike hydroxyls, which display amphoteric to weak basic character, CM groups are rather slightly acidic displaying a pH-dependent behavior. The latter is in turn expected to influence the metal retention strength and the dispersion of the metal within the host matrices and that of the biopolymer in aqueous media. These key-factors should influence not only the contact surface of the metal-loaded biopolymer with both the aqueous media and dispersed micro-organisms but also a possible metal release that seems to govern the antibacterial activity (Noori *et al.*, 2021). The study of these influences is the main objective of the present work.

Increasing the DS (degree of substitution: defined as number of carboxyl/glucose unit) is expected to favor metal dispersion through particle size reduction. In the meantime, high number of carboxyls is assumed to enhance the effect of pH on the aggregation-dispersion of the biopolymer entanglement in bacteria-infected media. Metal-cell interaction is known to result in an oxidative stress that unavoidably produces acidic species and fluctuations in metal-loaded biopolymer compaction-porosity grade that control the contact surface.

This interaction must also be influenced by competitive ones induced any HO-bearing species including water molecules and cell membrane. That's why a special interest was devoted to the role of solid particles bearing surface hydroxyl groups. For this purpose, CMS, CMC and their combinations with sodium montmorillonite (NaMt) were loaded with copper or silver particles. Comprehensive characterization through measurements of the zeta potential and particle size, analysis by X-ray photo-electron spectroscopy (XPS), Transmission Electron Microscopy (TEM) and Energy-dispersion X-ray fluorescence (ED-XRF) appears to be a judicious approach in this regard. The antibacterial activities to the host matrices before and after combination with the clay mineral and incorporation of Cu^0 and Ag^0 nanoparticles were evaluated in terms of inhibition zone diameter (IZD) on Gram-positive (*B. subtilis S*168) and Gram-negative (*E. coli DH5α*) bacterial species and correlated to the material features. Also, viability tests were carried out on *E. coli* as representative model.

4.2 Results and Discussion

4.2.1 Effects of biopolymer structure and clay addition

The starting CMC displayed higher zeta potential (ZP) value (-33.83 mV) as compared to CMS (-26.11 mV) due to a higher number of weakly acidic CM group expressed in terms of degree of substitution (DS) also reflected by a slightly lower pH (6.37 versus 6.50) (**Table 4.1**).

As expected, this resulted in a higher dispersion of CMC due to stronger electrostatic repulsion forces as suggested by the lower particle size (289.3 nm for CMC versus 350.2 nm for CMS). Montmorillonite incorporation was found to raise the ZP up to -48.36 for CMC/NaMt and up to -33.42 for CMS/NaMt, and, subsequently to reduce the particle size down to 266.6 nm and 299 nm, respectively. This can be explained by additional contributions of the exchangeable sites and deprotonated silanol groups of the clay mineral. This is in agreement with the slight pH decrease at pH from 6.37 and 6.56 down to 6.32 and 6.41 respectively.

Table 4.1. Some physico-chemical features of the investigation's materials

	Sample	Zeta potential (mV)	Particle size (nm)	Degree of substitution*	pH
Carboxymethyl cellulose	CMC	-33,83	289.30	0.3 (0.9/3)	6.37
	Cu^{2+}/CMC	-13.82	526.20		5.60
	Ag^{+}/CMC	-30.39	441.70		5.28
	Cu^{0}/CMC	-44.05	123.10		6.37
	Ag^{0}/CMC	-54.53	75.42		6.00
	CMC/NaMt	-48.36	266.60	-	6.32
	Cu^{2+}/CMC-NaMt	-23.74	605.50		5.66
	Ag^{+}/CMC-NaMt	-39.21	450.20		5.90
	Cu^{0}/CMC-NaMt	-48.36	206.25		6.90
	Ag^{0}/CMC-NaMt	-47.35	128.10		6.00
Carboxymethyl Starch	CMS	-26.11	350.20	0.17 (0.5/3)	6.56
	Cu^{2+}/CMS	-13.28	670.60		5.67
	Ag^{+}/CMS	-17.90	451.40		5.73
	Cu^{0}/CMS	-31.36	221.73		6.47
	Ag^{0}/CMS	-40.16	120.65		6.21
	CMS/NaMt	-33.42	299.00	-	6.41
	Cu^{2+}/CMS-NaMt	-17.89	596.30		5.90
	Ag^{+}/CMS-NaMt	-32.34	537.10		5.83
	Cu^{0}/CMS-NaMt	-34.12	213.10		6.37
	Ag^{0}/CMS-NaMt	-33.54	165.15		6.00

*Put here details about how DS was calculated.

4.2.2 Effect of metal incorporation

Incorporation of copper and silver cations into CMC and CMS induced a marked ZP decrease from -33.83 mV (CMC) and -26.11 mV (CMS) down to -13.82 mV for Cu^{2+}/CMC and -13.28 mV for Cu^{2+}/CMS as compared -30.39 mV for Ag^{+}/CMC and -17.9 for Ag^{+}/CMS. The simultaneous pH decrease, more pronounced with Cu^{2+} ions must be due to the Brønsted acidity induced by both cations retained by ion-

exchange and/or Lewis acid-base interactions (LAB) with the electron pairs of the oxygen atoms of the CM groups. The stronger effect of Cu^{2+} cation can be explained by its higher capacity to dissociate the surrounding water molecules as compared to Ag^{+} (***Reaction 1***). The consecutive H^{+} release unavoidably leads to carboxyl protonation and ZP decrease (***Reaction* 2**).

$$[M, nH_2O]^{2+} \leftrightharpoons [M, (n-1)H_2O, OH]^{+} + H^{+} \rightleftharpoons [M, (n-2)H_2O, OH]^{\circ} + H^{+} \qquad (1)$$

$$Biopolymer - COO^{-} \rightarrow Biopolymer - COOH \qquad Protonation \qquad (2)$$

This is in agreement with the higher polarizing power (PP) of Cu^{2+} (**Table S1**). This factor was found to reduce the ZP for both metal-loaded biopolymers regardless to the incorporated cation (**Fig. 4.1**). Less accentuated pH decreases down to 5.66-6.00 and 5.9-6.00 were observed after cation incorporation into CMC/NaMt and CMS/NaMt samples, most likely due to a compensating effect of CM group protonation at this pH value close to the pKa value.

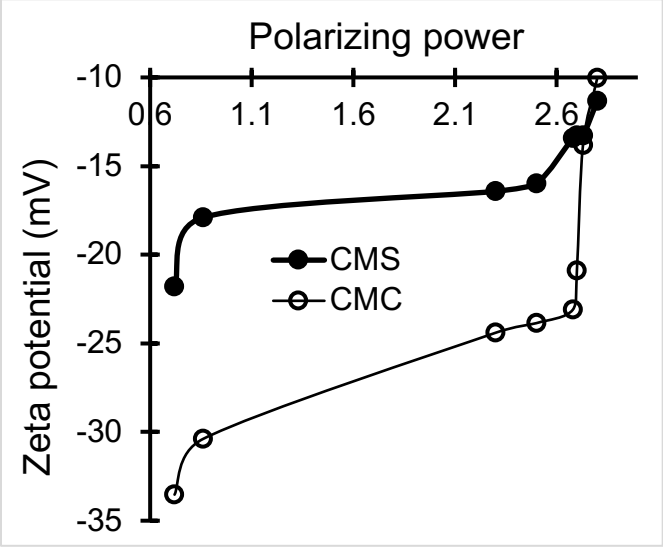

Figure 4.1 Influence of the polarizing power of the incorporated metal cation on the Zeta potential of metal-loaded CMC and CMS. The Zeta potential was measured for aqueous suspensions of CMC and CMS treated with aqueous solutions of different metal cations (Cu^{2+}, Ag^{+}, Zn^{2+}, Co^{2+}, Pt^{2+}, Ti^{2+} or Au^{+}).

Less accentuated pH decreases down to 5.66-6.00 and 5.9-6.00 were observed after cation incorporation into CMC/NaMt and CMS/NaMt samples, most likely due to a compensating effect of CM group protonation at this pH value close to the pKa value. Unlike cations, Zero-Valent Metals (ZVM) rather

induced ZP increase from -33.83 to -44.05 for Cu^0/loaded CMC and -54.53 for Ag^0/CMC, and from -26.11 up to -31.36 for Cu^0/loaded CMS and -40.16 for Ag^0/CMS. Here, MNP interaction with the electron pairs of the oxygen atoms in CM groups are expected to mitigate proton release, as reflected by weaker pH decrease down to 6.0 (Cu^0/CMC/NaMt), 6.0 (Ag^0/CMC/NaMt), 6.37 (Cu^0/CMS/NaMt) and 6.0 (Ag^0/CMS/NaMt).

4.2.3 Zeta potential - pH - material particle size interdependence

Changes in ZP and pH are almost linearly interdependent (**Fig. 4.2A**). In the meantime, increasing ZP enhances the repulsion forces and material dispersion that results in a decrease in material particle size (**Fig. 4.2B**). Subsequently, high intrinsic pH of the aqueous media appears to favor material dispersion through a decrease in particle size, as shown in **Fig. 4.2C**.

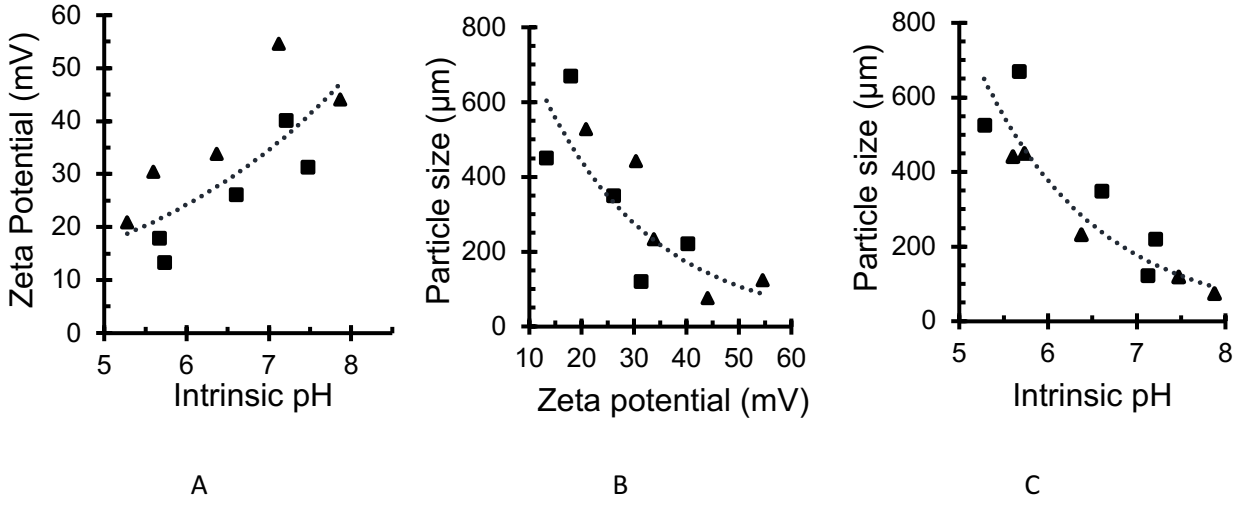

Figure 4.2. Relationship between zeta potential and pH (A), material particle size and Zeta potential (B) and material particle size and pH (C) of the dispersion media. In black square: CMC-based samples including CMC, Cu^{2+}/CMC, Cu^0/CMC, Ag^+/CMC and Ag^0/CMC. In black triangle: CMS-based samples including, CMS, Cu^{2+}/CMS, Cu^0/CMS, Ag^+/CMS and Ag^0/CMS.

This ternary interdependence is of great importance because it clearly demonstrates that the surface basicity of the antibacterial agent is a key-factor in the improvement of the contact surface and exchange processes with the targeted microorganisms. CMC and CMS and their NaMt-based composites have pH-sensitive chemical functions. The acid-base character can be modulated by the surface density of CM groups, lattice oxygen atoms, in-plane and out-of-plane silanols by means of suitable exchangeable cations.

4.2.4 XPS evidence of cation-matrix interactions

XPS measurements revealed noticeable changes in O_{1s} XPS signal after the incorporation of metal cation and MNP in both carboxymethylated biopolymers. The changes were reflected by higher signal intensity of 40000-100000 counts per seconds (CPS) for metal-loaded CMC (**Fig. S1-S2**) as compared to 15000-75000 CPS for metal-loaded CMS (**Fig. S3-S4**). This can be explained by the higher DS of 0.92 $\pm$ 0.01 for CMC versus 0.51 $\pm$ 0.01 for CMS, providing evidence of the involvement of the oxygen atoms of the CM groups in metal capture and stabilization. Weaker O_{1s} signal intensity was observed after Cu^{2+} incorporation as compared to Ag^{+} suggesting stronger compaction of the polymer entanglement that hinders electron release. This can be explained by the sandwiching effect of the positive charges of bivalent cations shared between two next-neighboring CM groups. Deeper insights into the O_{1S} XPS signals revealed BE shift for H-O-C:Cu^{2+} interaction of 1.3 eV in CMC (**Table S2**) and 1.0 eV in CMS (**Table S3**), i.e., stronger Cu^{2+} retention by H-O-C groups of CMC carboxyls (**Table 4.2**). These values are at least three times higher than those registered with Ag^{+} cation (0.3 in both CMC and CMS), indicating a much stronger retention of Cu^{2+} in both biopolymers as compared to silver.

As a general tendency, C_{1s} signals of C-O-C of glucose ring, C-C and O-C=O groups showed barely detectable BE shift not exceeding -0.3 eV in CMC (**Tables S2**) and -0.5 eV in CMS (**Tables S2**). This result is of great importance, because it demonstrates that: ***i.*** the carbon atoms do not directly interact with the incorporated metal species; ***ii.*** weak BE shifts, if any, are induced by next-neighboring oxygen atoms of the OH and carboxyl groups of both biopolymers.

Table 4.2. Binding energy (eV) shifts for key elements in the synthesized materials

XPS signal	Binding energy (eV)										
	CMC- Based samples						CMS-Based samples				
	Matrix	Alone	+ Cu^{2+}	+Cu^{0}	+Ag^{+}	+Ag^{0}	Alone	+ Cu^{2+}	+Cu^{0}	+Ag^{+}	+Ag^{0}
O_{1S}	O=C	530.68	530.28	529.89	530.18	529.38	530.78	530.08	529.88	530.28	529.98
	H-O-C	532.58	531.28	530.89	532.28	531.08	532.58	531.58	531.18	532.28	532.11
C_{1S}	C-O-C	286.18	286.28	287.08	286.38	286.22	286.18	286.28	285.98	286.29	286.37
	C-C	284.58	284.78	284.90	284.68	284.78	284.58	284.78	284.48	284.78	284.68
	O-C=O	287.58	287.88	287.98	287.68	287.78	287.68	288.18	288.10	287.98	287.78
$Cu2p_{3/2}$*	-	-	965.08	965.08	-	-	-	965.08	965.08	-	-
$Ag3d_{5/2}$*	-	-	-	-	380.08	380.08	-	-	-	380.08	380.08

* XPS data for pure zero-valent copper: $Cu2p_{3/2}$= 933 eV and for Cu^{2+} cation: $Cu2p_{3/2}$= 934.4 eV; XPS for pure zero-valent silver: $Ag3d_{5/2}$=368.2 eV.

Here also, the intensity decreases in C_{1s} XPS signals in CMC must be due to structure compaction that reduces electron release, given that entanglement compaction appears to lead to signal mitigation (Arus *et al.*, 2016a; Sennour *et al.*, 2017b; Tahir *et al.*, 2017). Surprisingly, CMS showed more pronounced C1s intensity decay in spite of its lower density of CM groups, suggesting accentuated biopolymer winding around the metal cation or MNP encapsulated. Cation retention and stabilization by carbonyl groups (C=O), if any, should involve only weaker interactions. This is supported by the lower BE shift observed for the O_{1S} signals of Cu^{2+}:O=C interaction (0.4 eV in CMC and 0.7 eV in CMS) and Ag^{+}:O=C interaction (0.5 eV in both CMC and CMS).

4.2.5 Biopolymer interaction with MNP and montmorillonite

MNP retention by the biopolymers appears to involve stronger -O:Metal interaction as compared to metal cation, given that CuNP insertion induced higher O_{1s} BE shift of 0.79 eV and 1.69 eV for Cu^0:O=C and Cu^0:H-O-C interactions in CMC and of 1.3 eV and 1.50 eV for Ag^0:O=C and Ag^0:H-O-C interactions in CMS (**Table S3)**. These values also indicates stronger interaction of Cu^0 and Ag^0 by hydroxyl groups than by C=O in the carboxyl groups. A similar phenomenon was noticed for Cu^0 but the reverse sequence was observed for Ag^0 in CMS, presumably due to a higher hydroxyl affinity towards CuNP as compared C=O in both polymers. Interestingly, AgNP appears to be selectively interact more with hydroxyls in CMC but with C=O in CMS, thereby confirming the key-role of the biopolymer structure.

NaMt/CMC and NaMt/CMS showed no noticeable BE shift of Si2s, Si2p and Al2p XPS signals after Cu^{2+} and Ag^{+} incorporation, in agreement with data on cellulose previously reported (Noori *et al.*, 2021). This is presumably because cation retention involves mainly ion exchange. This is even more plausible for the incorporated cation amount (1 mmol/g in CMC samples and 0.4 mmol/g in CMS), which is by far lower than the total cation-exchange capacity of the NaMt-modified biopolymers. However, NaMt addition to CMC and CMS induces new XPS signals mainly arising from MNP interaction with silanols and Si-O-Si groups, as already reported (Noori *et al.*, 2021). This was illustrated by BE shift of the O_{1s} signal from 532.6 (NaMt) down to 531.5 eV (Cu^0) and 531.6 (Ag^0). More pronounced BE shift was registered for the Si2s XPS signal from 154.55 eV to 152 eV (Cu^0) and 149 eV (Ag^0). No BE shift was noticed for Al2p XPS, suggesting at most negligible MNP:Al-OH interaction.

4.2.6 Zero-valent metal dispersion

TEM image of Cu^0/CMC displayed a uniform dispersion of pseudo-spherical 1-3 nm CuNP (**Fig. 4.3A, C**) and of subnanometric particles not exceeding 0.3 nm (**Fig. 4.3D, B**). Ag^0/CMC showed particle size below 6 nm, mostly (ca. 95%) below 4.0 nm, including 40% of 1.0–2.0 nm particles (**Fig. 4.4A, B**). Such a high dispersion must be due to the high density of potential chelating sites in CMC. Deeper insights through energy-dispersive X-ray spectroscopy (ED-XRF) of two different spots located in an apparently void area between AgNP (**Fig. 4.4A, C**) revealed AgNP contents of 84.3 wt.% in spot 1 and 28 wt.% in spot 2. This provides clear evidence of the occurrence of Ag^0 subnanoparticles (AgNP) barely detectable by TEM. Particle size assessment using Image-J software on magnified spot eds2 confirmed the existence of subnanometric AgNP in the range of 0.08 – 0.1 nm (**Fig. 4.4D**). Here, the higher CM group density of CMC appears to be responsible of its higher dispersion capacity as compared to CMS.

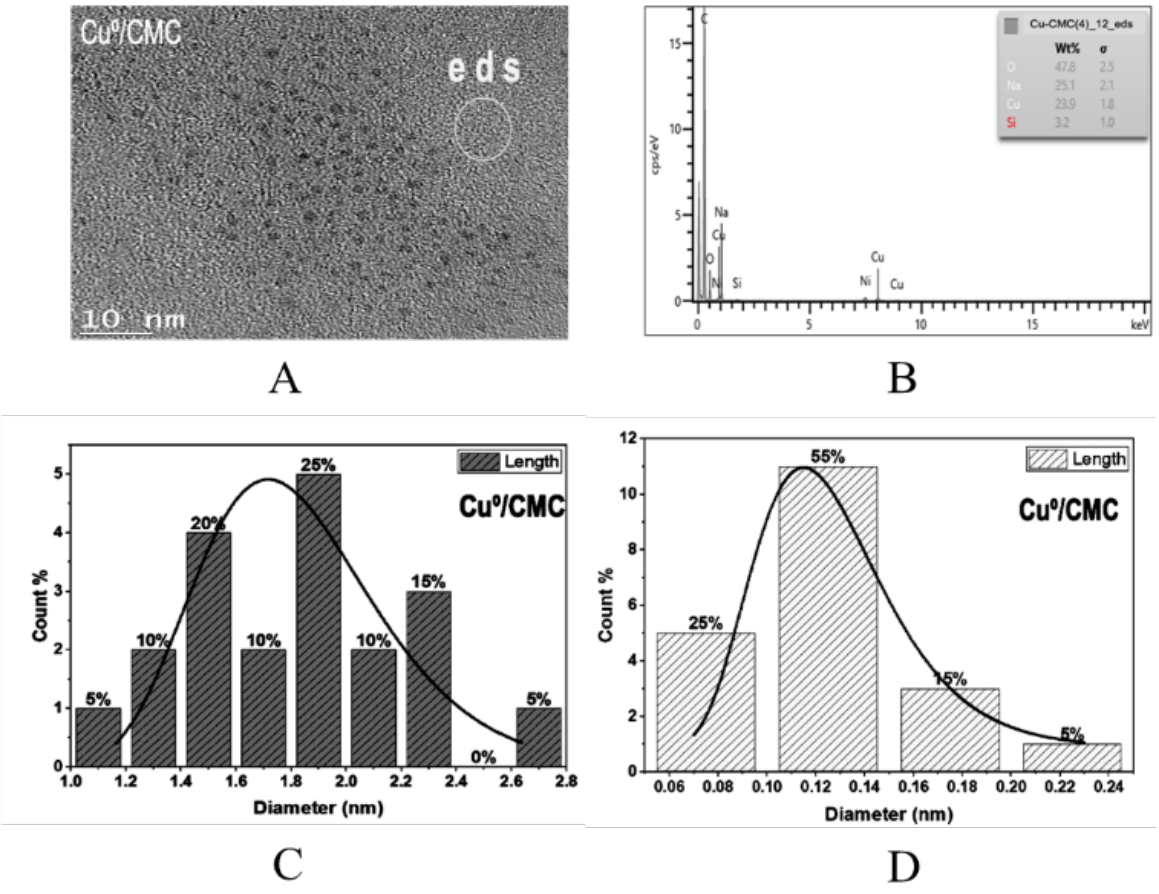

Figure 4.3. TEM image (A), ED-XRF spectrum (B) and Cu^0 particle size distribution in CMC (C,D)

As expected, bulkier MNP were obtained in CMS, since ca. 25 % of the incorporated AgNP displayed particle size ranging from 40 to 70 nm (**Fig. 4.4E**). NaMt incorporation was found to slightly affect the dispersion capacity of the host matrix as illustrated by the slight increase in particle size (**Fig. 4.5**). A possible explanation should consist in the appearance of competitive Clay:Polymer interaction that reduces the number of CM group available. More than 90 % of AgNP dispersed displayed an average particle size not exceeding 4 nm in CMC/NaMt (**Fig. 4.5A**) and 6 nm in CMC/NaMt (**Fig. 4.5B**). This confirms, once again, the key-roles of the biopolymer structure and density of chelating groups in metal dispersion and stabilization.

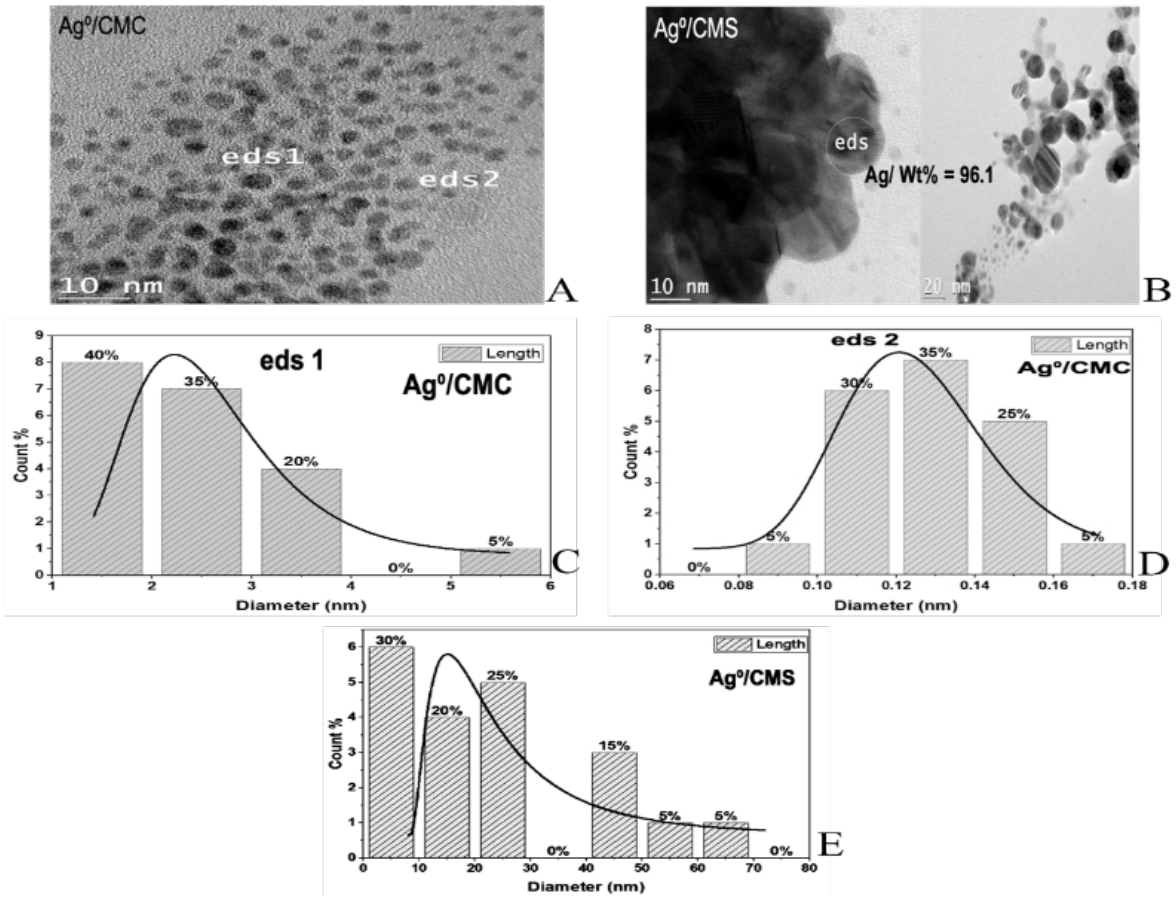

Figure 4.4. TEM images (A, B) and Ag^0 particle size distribution in CMC (C, D) and CMS (E).

4.2.7 Effect of biopolymer structure and metal incorporation on antibacterial activity

Triplicate antibacterial tests showed no antibacterial activity for the starting CMC and CMS biopolymers. A quick qualitative overview of the data obtained for modified biopolymers (**Fig. S6-S7**) revealed a

significant improvement of the antibacterial activity. The inhibition zone was not circular (due to the flowability of the MNP powders) and generated a low precision in graphical measurements of the inhibition zone diameter (IZD) (**Fig. S5**), but the use of Image-J software allowed reducing the standard deviation down to 1 % (**Table S4**). Quantitative IZD assessment showed a significant increase, providing evidence of the beneficial effect of a mere incorporation of the metal forms in agreement with previous data (Gordon *et al.*, 2010; Noori *et al.*, 2021; Potera, 2012; Vincent *et al.*, 2018; Yun'an Qing *et al.*, 2018). The relatively higher IZD values measured on ***B. subtilis S168*** indicate higher antibacterial activity as compared to ***E. coli DH5α*** for both metals in various investigated forms (**Table 4.3**). *B. subtilis* showed an IZD relatively higher compared to *E. coli*, suggesting a higher antibacterial activity on *Bacillus,* due to the Gram-positive cell wall structure with a thick peptidoglycan layer which prevents the leak of antibacterial agent once absorbed (Fu *et al.*, 2015).

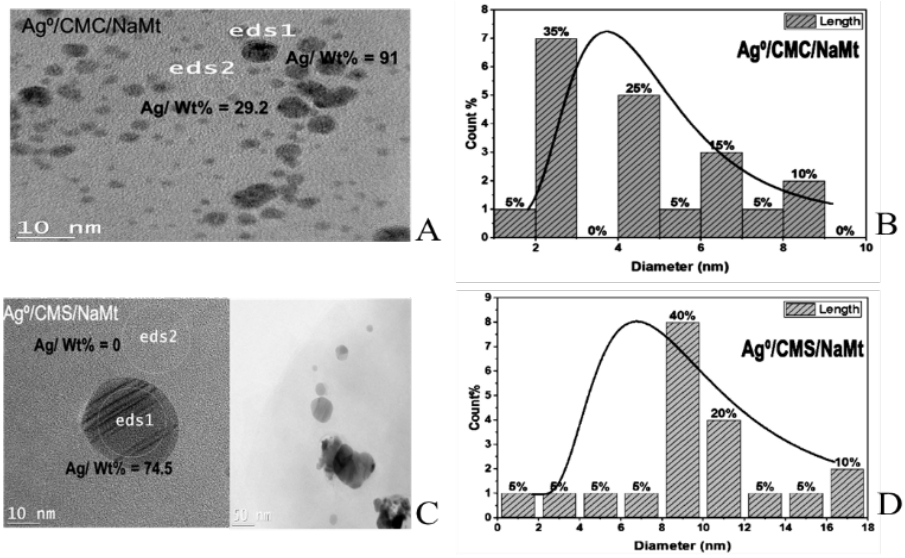

Figure 4.5. TEM images and Ag^0 particle size distribution in CMC/NaMt (A, B) and CMS/NaMt (C, D)

The IZD for both *E. coli DH5α* and *B. subtilis S168* strains in presence of Ag^+/CMC reached highest values of up to 4.36 and 5.40 cm, respectively. These values dropped drown to 3.81 and 4.70 cm, respectively for Ag^0/CMC. Similar decreases were registered from 3.06 and 5.00 cm for Ag^+/CMS to 2.54 and 3.81 cm for Ag^0/CMS. This turns out to be general tendency for silver-modified samples regardless to the matrix structure and composition, which reveals a stronger antibacterial activity of oxidized silver as compared to its zero-valent form regardless to the host-biopolymer. For copper-modified samples, this tendency was not maintained, and the antibacterial activity appears to depend on the sample type and composition. The

almost twice-higher IZD values registered for Ag^0/CMC (3.81 cm) as compared to Cu^0/CMC (1.7 cm) account for a higher antibacterial effectiveness of metal silver, presumably due to an easier release in the liquid media. This is in agreement with the weaker retention strength of AgNP as predicted by XPS measurements (**Tables 4.2, S2-S3**). From these data it appears that the IZD values when nanoparticles are formulated with the carboxylic polymers (in the range 1-5 cm) are higher than those found in a previous report (Noori *et al.*, 2021) with nanoparticles of the same metal species (Cu^0, Cu^{2+}, Ag^0, Ag^{2+}) with montmorillonite alone or associated with non-carboxylated cellulose (in the range 1-3 cm). This almost double diffusion zone indicates the major impact of association of metal subnanometric particles with the polycarboxylic biocompatible materials to improve their antibacterial efficiency.

Table 4.3. Inhibition zone diameter (IZD) for CMC- and CMS-based samples.

Biopolymer	Incorporated species	Samples	Inhibition zone diameter (IZD) (cm)*	
			E. coli DH5α	***B. subtilis S168***
CMC	None	CMC	0.00	0.00
	Metal cation	Cu^{2+}/CMC	2.12	3.81
		Ag^{+}/CMC	4.36	5.40
	Zero-valent metal	Cu^0/CMC	1.70	4.06
		Ag^0/CMC	3.81	4.70
	Montmorillonite	CMC/NaMt	0.00	0.00
	Metal cation	Cu^{2+}/CMC/NaMt	1.50	3.90
		Ag^{+}/CMC/NaMt	2.29	1.70
	Zero-valent metal	Cu^0/CMC/NaMt	1.27	3.81
		Ag^0/CMC/NaMt	2.11	1.27
CMS	None	CMS	0.00	0.00
	Metal cation	Cu^{2+}/CMS	1.82	3.80
		Ag^{+}/CMS	3.06	5.00
	Zero-valent metal	Cu^0/CMS	3.12	4.06
		Ag^0/CMS	2.54	3.81
	Montmorillonite	CMS/NaMt	0.00	0.00
	Metal cation	Cu^{2+}/CMS/NaMt	1.00	4.50
		Ag^{+}/CMS/NaMt	2.17	1.70
	Zero-valent metal	Cu^0/CMS/NaMt	1.52	3.30
		Ag^0/CMS/NaMt	1.20	0.20

*The inhibition zone diameter was assessed using Image-J software.

4.2.8 Effects of Cation amount and pH on antibacterial activity

The higher antibacterial effectiveness of Ag^{+}/CMC and Ag^{+}/CMS imposed deeper insights in the effect of cation content on their antibacterial activity (**Fig. 4.6**). The latter was found to increase as illustrated by increasing IZD with raising cation content. This increase reached a plateau at 0.2 mol/L with Ag^{+}/CMC and

Ag^+/CMS for maximal antibacterial activity in both strains. This surprising result clearly shows that low Ag^+ content is sufficiently effective to suppress the detrimental effect of the low retention capacity of CMS. This is not necessarily valid for other metals and other metal valence.

Deeper insights in the role of pH showed a beneficial effect of increasing initial pH on the antibacterial activity, as reflected by increasing IZD for silver-modified biopolymers (**Fig. 4.7a).** This result was somehow expected, given that increasing pH was already found to raise the Zeta potential thereby reducing the material particle size. This unequivocally demonstrates the beneficial of the high dispersion of the antibacterial agent and that the antibacterial activity is a surface phenomenon involving exchange processes between a solid surface, aqueous media and bacteria membrane.

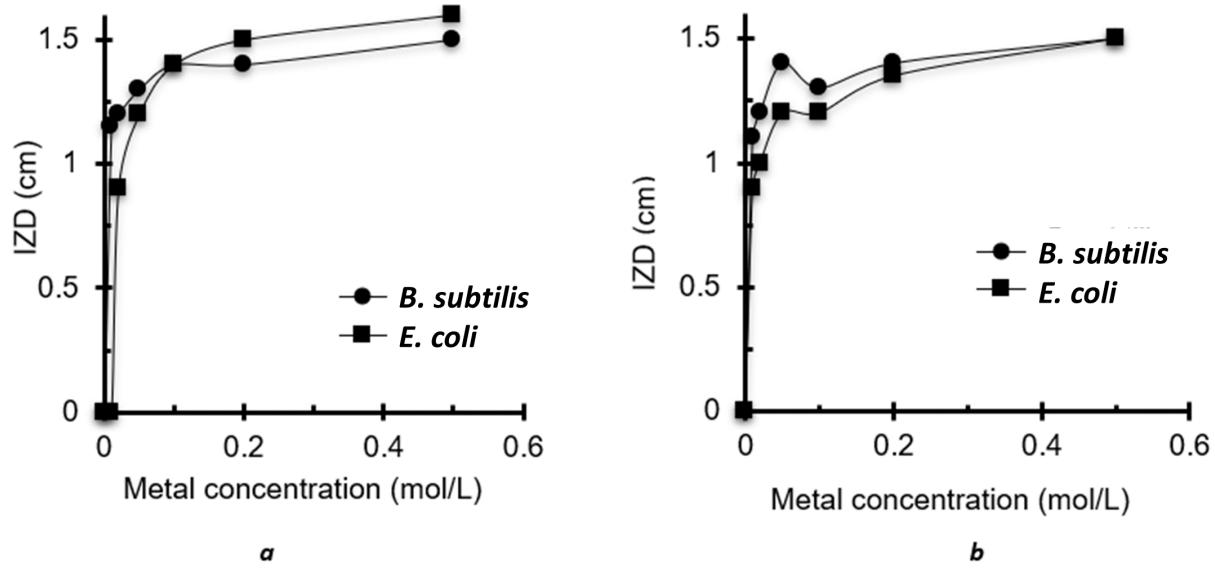

Figure 4.6. Inhibition zone diameter at different amounts of Ag^+-loaded CMC (a) and CMS (b).

This statement was confirmed by correlating the intrinsic initial pH induced by each antibacterial sample with the IZD (**Fig. 4.7b**). Indeed, beside the few exceptions arising from the roles of the structural and chemical composition and the investigated samples, it clearly appears that samples inducing higher pH in the culture broth exhibit highest antibacterial activity. This can explain at least partly the effect of pH, whose increase is expected to promote higher ionization of the carboxylic groups.

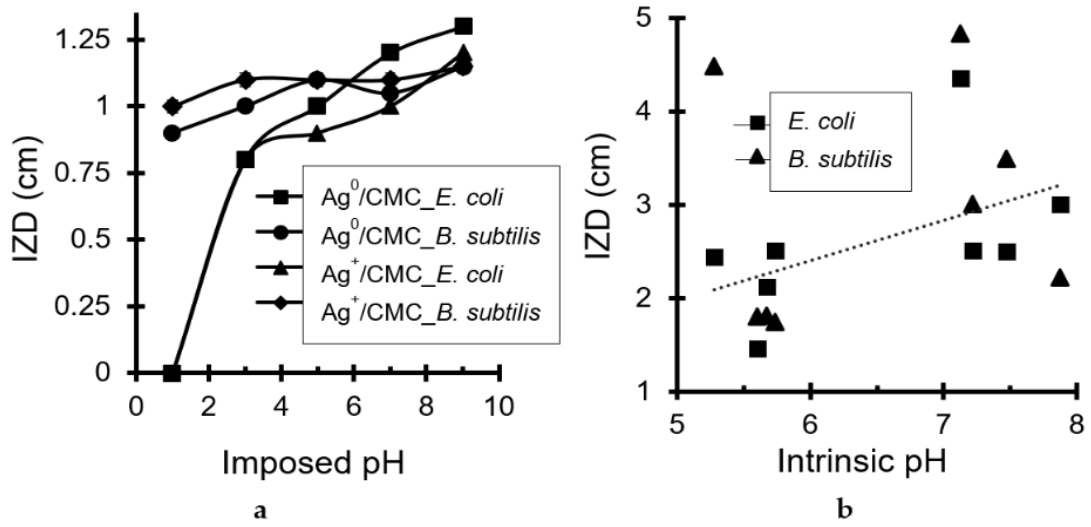

Figure 4.7. IZD dependence on imposed initial pH (a) and intrinsic pH of metal-loaded biopolymers (b)

4.2.9 Effects of material and metal dispersions on antibacterial activity

The antibacterial activity was found to strongly depend on the sample particle size, polymer degree of substitution (DS) and surface charges. As expected, the highest IZD were obtained for CMC samples with finest metal and material particle sizes (**Fig. 4.8A**). Samples with increased particle size resulted in lower IZD values. The most plausible explanation resides the higher capacity of CMC to disperse MNPs even at a subnanometric scale, as previously shown by TEM/ED-XRF (**Fig. 4.3-4**). This is in agreement with the general tendency on increasing IZD with increasing surface charge (**Fig. 4.8B**).

Additional viability tests performed on *E. coli*. with 0.1 and 1 mg/mL sample concentration showed a marked evolution in time of the antibacterial activity (**Fig. 4.9**). It clearly appears that raising the material concentration in the culture broth from 0.1 mg/mL up 1 mg/mL induced almost total bacteria depletion after 24 hours of incubation.

NaMt-biopolymer combination exhibited lower antibacterial activity than biopolymer-based samples as reflected by lower IZD values. This was previously explained in terms of competitive interactions between the clay mineral and polymer that involves partial involvement of CM groups in the formation of H-bridges.

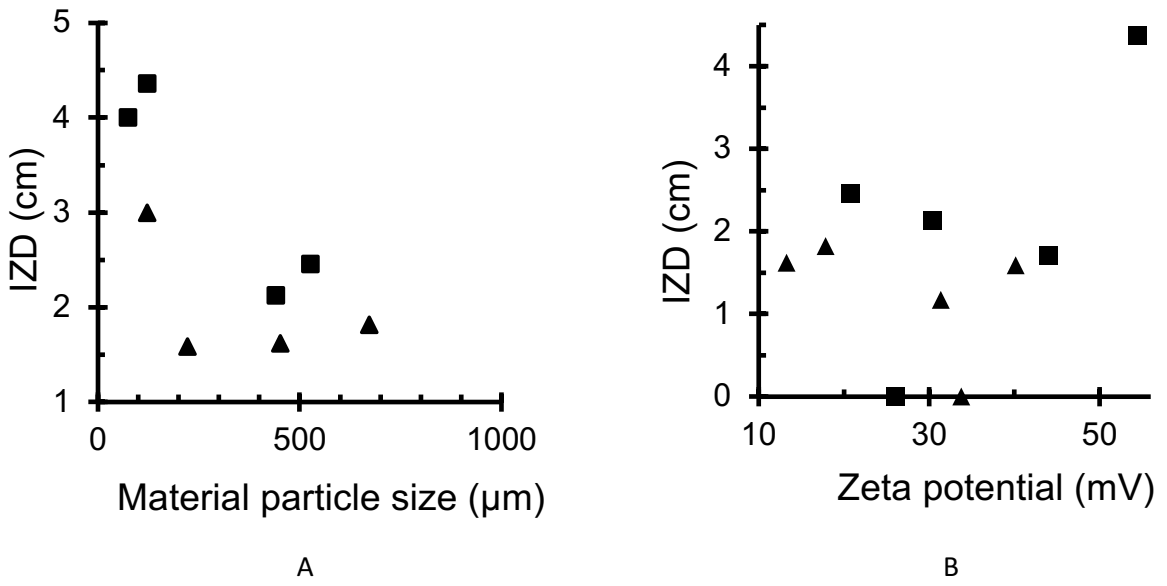

Figure 4.8. Effect of material particle size (A) and of zeta potential (B) on the inhibition zone diameter (IZD). In black square: CMC-based samples including $Cu^{2+/}$CMC, Cu^{0}/CMC, Ag^{+}/CMC and Ag^{0}/CMC. In black triangle: CMS-based samples including $Cu^{2+/}$CMS, Cu^{0}/CMS, Ag^{+}/CMS and Ag^{0}/CMS.

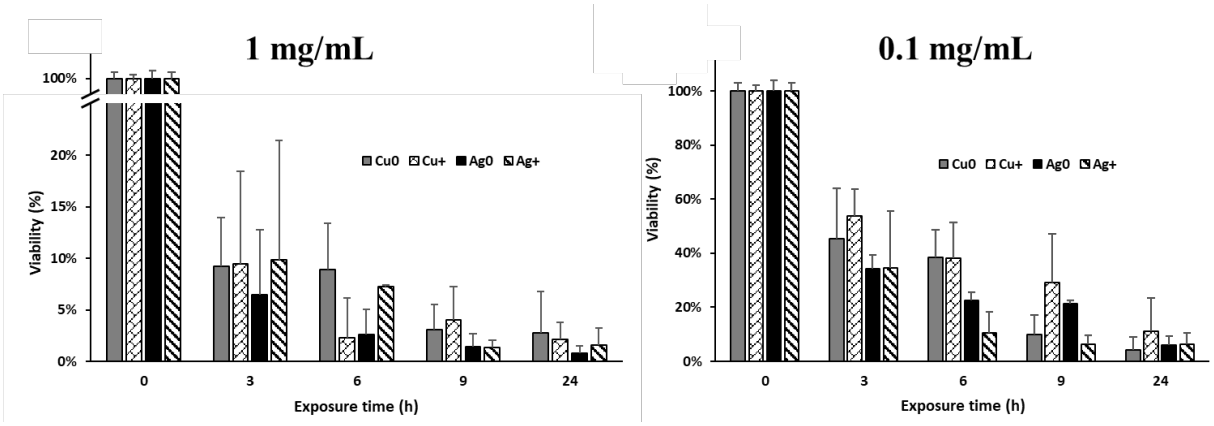

Figure 4.9. Time-course of *E. coli* viability in the presence of CMC samples.

This should result in favorable structure expansion that allows easy exchange with the impregnating media. However, this effect must be mitigated by the detrimental formation of bulkier MNPs, as already shown by TEM (**Fig. 4.5**). Almost similar phenomenon was noticed for CMS-based samples but with few exceptions. These exceptions may be due to the low number of CM groups, thereby demonstrating the

narrow interdependence between the biopolymer DS value and amounts of both incorporated metal and clay mineral. This remains to be elucidated through deeper investigations in this direction.

4.3 Conclusions

Copper and silver nanoparticles in both cation and zero-valent forms, when formulated with CM-cellulose or with CM-starch, present an antibacterial efficiency markedly higher in comparison with that of nanoparticles of the same metal species when they are not formulated with the polycarboxylic biomaterials. The carboxymethyl functions govern the surface charges that determine the biopolymer dispersion in aqueous media according to the pH. The density of these chelating groups strongly influences the metal retention strength and dispersion in the host-matrices. Cation:Biopolymer and MNP:Biopolymer interactions involve the oxygen atoms of the OH and carboxyl group. The dispersion of the modified biopolymers in the culture media also turned out to be a key-factor, by favoring exchange processes with the surrounding bacteria. Clay mineral incorporation was found to affect the dispersion capacity of the host matrix due to the appearance of competitive Clay:Polymer interaction. The antibacterial activity is strongly dependent on the amount of incorporated metal species but only at a certain level. Silver cation showed higher antibacterial activity as compared to its zero-valent form, which turned out to be more effective than zero-valent copper due to a weaker retention. These findings offer promising fundamentals for designing efficient metal-loaded biopolymers for biomedical and biotechnological purposes.

Acknowledgements: *This work was supported by NSERC (To Pr. Mircea A. Mateescu). The authors appreciate the technical assistance of Dr. Lihong Shang (McGill University) for XPS and Dr. Jean-Philippe Massé (Polytechnique Montreal) for TEM and ED-XRF.*

CHAPTER 5

GENERAL DISCUSSION

5.1 Results and discussion

The use of the well-known of metals toxicity towards living organisms was based on knowledge on their interactions with electron pair donor. This led to an approach that consists in designing matrices that host metal cation or zero-valent metal (SVM) through sufficiently strong interaction to ensure a high dispersion and stabilization but in the meantime, sufficiently weak to allow easy release in contact with membranes of living organisms for altering the behavior and stability of this membrane (Greiner *et al.*, 2012; Turel et Kljun, 2011). Silver and copper-loaded matrices turned out to act as surrogates to conventional antibiotics and address the issue of bacterial resistance (Pang *et al.*, 2019; Johanson et al., 2006; Khodakarami et al., 2021).The lower capacity of silver to undergo redox processes accounts for a lower amount of incorporated Ag^0NP, in agreement with its weaker antibacterial activity of as compared to their Cu-counterparts.

A first step of this research revealed higher capacity of montmorillonite-supported polyol dendrimer to host MNP as compared to cellulose counterpart. This arises from a higher density of OH groups of both clay surface and dendrimer branches in the formation of ternary [clay-polyol-MNP] interactions. Such interactions were found to generate metal sub-nanometric particles (MSNP) in Cu^0/H20-NaMt but neither in Ag^0/H20-NaMt nor in [clay-Cellulose-MNP]. This high metal dispersion resulted in high antibacterial activity against both non-pathogenic bacteria strains investigated. Therefore, the metal particle size was found to play a key-role, provided that the particle size of the host-matrices is sufficiently low to allow maximum exchange the aqueous infected media.

Changes in clay surface basicity and in the hydrophilic character and basicity of the host materials were induced by hydroxyl:metal interactions, inasmuch as slight shifts of thermal desorption peak of CO_2 towards higher temperatures. This a precise indicator of an enhancement and strengthening of the surface basicity, providing clear evidence of the occurrence of competitive interaction of CO_2 and metal with the clay surface, presumably via the lattice oxygen atoms (-Si-O-Si- with strong Lewis basicity), and to a lesser extent with the OH groups of both in-plane silanols and out-of-plane Si-OH of the surface (Sulpizi *et al.*,

2012). Stronger [AgNP:OH-] interaction indicates enhanced entrapment as compared to CuNP, explaining the lower antibacterial properties of Ag^0.

The hydrophilic character favors the material dispersion in aqueous media, and the antibacterial activity depends on the material affinity towards the bacteria-infected aqueous media. Incorporating CuNP reduces the hydrophilic character, as observed by thermal programmed-desorption tests on the moisture content but less in Ag^0-loaded matrices. Consecutive insertion of MNP in cellulose or polyol-cellulose composite resulted in an improvement of the hydrophilic character. Here, potential competitive [-HO:Metal] and [-HO:H_2O] interactions induce no alteration of the surface affinity towards water, most likely due to the mere presence of OH groups in the vicinity of MNP (Zhu, 1995). Here, a norrow interdependence between the hydrophilic character that favors the material dispersion in aqueous media and surface basicity that promotes the metal retention was suggested.

All metal-loaded host matrix showed antibacterial activity against E. coli and B. subtilis strains unlike the metal-free counterparts, thereby confirming the metal toxicity. (Gordon *et al.*, 2010; Potera, 2012; Vincent *et al.*, 2018; Yun'an Qing *et al.*, 2018). As expected, Cu^0 induced higher antibacterial activity than Ag^0, presumably due to a higher dispersion induced by multiple Cu^0 interactions with silanols and Si-O-Si groups, resulting in higher Cu^0 dispersion compared to Ag^0, an easier release of copper in the liquid media as a result of a higher dispersion of the material particles.

These results imposed deeper insights in the role of Metal:Surface interaction in the antibacterial activity against both investigated strains. This second part of the research showed that biocompatible biopolymers such as carboxymethyl-cellulose (CMC) and its starch counterpart (CMS) behave as more interesting host matrices for metals. This was explained in terms of a higher surface density of carboxyl groups and increased chelating capacity for both metal forms. The pH dependence of carboxyl groups made it possible that high intrinsic pH of the aqueous media favor material dispersion through a decrease in particle size.

The surface basicity of the antibacterial material appears to improve the contact surface with the targeted microorganisms, being narrowly dependent on the surface density of CM groups and other electron pair donor, if any. Incorporation of metal cation and MNP induced detectable and measurable XPS signal shifts for the electron pair donors such as the oxygen atoms. These signals displayed higher intensity in CMC as compared to CMS for due to its higher carboxyl surface density.

Cu^{2+} incorporation in the polymer resulted in weaker O1s signal intensity compared to Ag+, indicating stronger compaction and hindered electron release. The positive charges of bivalent cations shared between neighboring CM groups led to this effect. Deeper analysis revealed a higher Cu2+ retention by H-O-C groups in CMC carboxyls compared to Ag^{+}, suggesting a significantly stronger retention of Cu2+ in both biopolymers. XPS analysis provided evidence that the C, Si and Al atoms show no direct interactions with inserted metal species, but the interactions of next-neighboring oxygen atoms of the OH and carboxyl groups of both biopolymers appear to influence the biopolymer chain entanglement (Arus *et al.*, 2016a; Sennour *et al.*, 2017b; Tahir *et al.*, 2017).

Zero valent metals have stronger interactions with hydroxyl groups than with carbonyl groups compared to metal cations. Furthermore, AgNP selectively interacts more with hydroxyls in CMC and with carboxyl groups in CMS, highlighting the importance of biopolymer structure. CMC resulted in uniform and even subnanometric dispersion of both CuNP and AgNP the CMC owing to its higher density of chelating sites, while bulkier MNP were observed in CMS, thereby confirming the significant role of the chelating group density.

Higher antibacterial activity was registered on *Bacillus as* compared to *E. coli, most likely* due to the very structure of cell wall structure (Fu *et al.*, 2015) and for Ag^{0}, in agreement with its weaker retention strength of AgNP as predicted by XPS measurements. Interestingly, metal-loaded biopolymers showed higher antibacterial activity as compared to polyol, cellulose and montmorillonite combinations (Noori *et al.*, 2021). This was explained in terms of a higher dispersion of the metal with the host matrice and of the latter in the aqueous media.

This new approach in correlating the structure of metal-loaded materials to their antibacterial performances worth it being pursued by additional investigated that aim the explanation of the metal transfer between the matrices and the infected media. Some suggestions are provided below:

5.2 Recommendations

Further investigations on the mechanisms behind the superior dispersion of CuNPs compared to AgNPs in polyol-based matrices. Explore factors such as surface interactions, surface chemistry, and nanoparticle size that contribute to the observed differences.

Additional studies on the role of the dendrimer H20 in improving nanoparticle dispersion, particularly for CuNPs. Explore the specific mechanisms by which the dendrimer enhances dispersion and determine optimal conditions for its use.

Investigations on the impact of different surface functionalities and OH groups on the dispersion of nanoparticles. Explore the effect of varying concentrations and types of functional groups on the dispersion capacity of nanoparticles in polyol-based matrices.

Investigations on the potential of incorporating other types of nanoparticles or materials into the polyol-based matrices and investigate their dispersion behavior and resulting properties. Compare their dispersion characteristics with CuNPs and AgNPs to understand the generalizability of the findings.

Further investigations on the changes in basicity and hydrophilic nature of clay and cellulose tissue (CT) materials after incorporating nanoparticles. Explore the impact of these changes on other material properties and applications beyond antibacterial activity.

Additional studies to understand the long-term stability and durability of the modified biopolymer materials. Assess their performance under different environmental conditions, such as temperature, humidity, and exposure to various chemicals.

5.3 Limitations to overcome

The study focused on copper and silver nanoparticles and their dispersion in polyol-based matrices. The findings may not be directly applicable to other types of nanoparticles or matrices, and caution should be exercised when extrapolating the results.

The study primarily relied on microscopy techniques and spectroscopic analysis to assess dispersion and interactions between nanoparticles and the host material. Other characterization techniques, such as dynamic light scattering or rheological measurements, could provide additional insights into dispersion behavior.

The antibacterial activity of the materials was primarily evaluated qualitatively. Further quantitative assessments, such as minimum inhibitory concentration (MIC) or zone of inhibition measurements, could provide a more comprehensive understanding of the antibacterial efficacy.

The study focused on the effects of biopolymer structure and metal incorporation on the properties of the materials. However, other factors, such as processing conditions, nanoparticle concentration, and particle size, could also influence the final properties and should be considered in future studies.

The study did not extensively explore the potential cytotoxicity or biocompatibility of the modified materials. Further investigations are necessary to assess the safety and suitability of these materials for biomedical or other relevant applications.

The study did not consider potential environmental impacts or the recyclability of the modified materials. Future research should address the sustainability aspects of these materials and their potential for recycling or disposal.

CHAPTER 6

GENERAL CONCLUSION

The results of the present doctoral research allowed concluding that the main consisting in the synthesis of metal-loaded antibacterial material has been attained and that investigating the Metal-matrix interaction (MMI) and material behaviour in aqueous media turned out to be a judicious approach to understand the role of metals in the antibacterial activity. These results also provided evidence that the incorporation of both cationic and zero valence forms of both metals (Copper and silver) is responsible of the induced antibacterial activity, and that optimum MMI and material dispersions in the liquid media improve the contact surface. The latter appears to play the most important role in the antibacterial activity. The lower the particle size of the dispersed metals within the matrix and of the material in the aqueous media, the higher the inhibition zone diameter was found to be. Both the investigated metals in both their cationic and zero-valent form were found to interact as Lewis acids with the free electron pairs of the oxygen atoms belonging to -OH or CO_2H functional groups of host matrix. Optimum biocidal effect should be promoted by increased contact surface metal accessibility to the infected aqueous media. The antibacterial activity is explained in a term of optimum metal retention strength by host matrix to simultaneously avoid metal aggregation into bulkier clusters and allow easy metal release. Therefore, a judicious compromise between strong [–HO:metal] interaction that favors material stability for storage purposes and sufficiently strong [H_2O:metal] for higher material dispersion in the culture media and improved contact with bacteria cell wall. At this stage of the research, investigations are still in progress for determining whether the antibacterial activity requires metal release at the cell wall, inasmuch as the present results already provide evidence of the beneficial effect of weak metal retention strength by the matrix. Discovering the surface morphology and physicochemical properties of Na-montmorillonite and cellulose tissue used as host matrices was a key-step to correlate metal release, if any, with the antibacterial activity.

More specifically, the first step of this doctoral research provided valuable conclusions, among which the most important are the following:

Color change of the suspension of the metal-loaded materials and X-ray photoelectron spectroscopy provided clear evidence of the metal cation conversion into zero-valent forms in the presence of $NaBH_4$

The metal dispersion in both NaMt and CT was also confirmed by a transition of the host matrix surface morphology from soft to the appearance of spherical grains with a particle size smaller the 100 nm.

The non-uniform dispersion of metal grains in CT confirmed the occurrence of weak CT-MNP interaction due to the low surface density of hydroxyl groups.

Silver-based samples showed less antibacterial activity than copper counterparts

Incorporation of dendrimer Boltorn H20 in NaMt induced a marked improvement of metal dispersion by the OH groups of both the clay surface and dendrimer entanglement and formation of ternary [NaMt–polyol–MNP] interactions.

CuNP displayed higher dispersion capacity than AgNP with sub-nanosized particles smaller than 1 nm.

The contribution of NaMt in metal stabilization involves Lewis Acid-Base interaction of MNP with lattice oxygen atoms (–Si–O–Si– with strong Lewis basicity) and OH groups of the silanols (Si–OH) of the surface, as supported by XPS measurements.

The strong interaction between AgNP and OH groups and their lower antibacterial activity as compared to CuNP suggests a lower tendency to Ag^0 release.

Metal dispersion reduces the basicity and hydrophilic character of the host surface due to the involvement of the OH groups in metal stabilization.

Metal-NaMt interaction involves the electron pairs of lattice oxygen atoms in both siloxy (–Si–O–Si–) and silanol groups (Si–OH).

Asymmetric XPS signal for CuNP/NaMt revealed multiple Cu^0 interaction with NaMt functional groups.

CuNP show higher dispersion and lower particle size on NaMt as compared to AgNP.

The more pronounced decrease in the O1s binding energy induced by Ag^0 incorporation in H20 indicates a stronger retention in the dendrimer entanglement as compared to CuNP.

Both metals in both forms induced no C1s and O1s binding energy shift in CT-H20 composite, suggesting that MNP:CT and MNP:H20 interactions, if any, should be negligible.

Intensity decreases for the C1s signal of C–O–C and C–C groups account for a compaction of the dendritic entanglement around MNP.

CuNP incorporation in CT and Boltorn H20 reduces the O1s binding energy as a result of [–HO:Cu^0] interaction.

MNP insertion in dendrimer Boltorn H20 induced higher XPS signal intensity than in CT due to a higher density of hydroxyl groups.

[–HO:MNP] interaction appear to govern simultaneously MNP stabilization via entanglement compaction and MNP release via entanglement ''relaxation'' upon competitive [–HO:Water] interaction according to the pH of the aqueous media.

Metal-free NaMt, H20 and NaMt-H20 display no antibacterial activity but MNP incorporation turns out to be beneficial in this regard.

Both Cu^0/NaMt and Ag^0/NaMt show almost comparable antibacterial activity against *B. subtilis*, but lower for Cu^0/NaMt in the presence of *E. coli*.

MNP-loaded H20-NaMt composite show more enhanced antibacterial activity as compared to its separate components, due to a synergistic effect of dendrimer dispersion on the clay surface and MNP dispersion on both components.

Higher antibacterial activity was observed against Gram-positive *B. subtilis* as compared to Gram-negative *E. coli* presumably due to specific cell wall structure of *Bacillus* with a thick peptidoglycan layer and an abundant amount of pores.

The dispersion of the metal-loaded materials in water is a key factor to improve the contact surface between the stabilized metals and infected media.

Low particle sizes of both MNP and the suspension of the metal-loaded material in aqueous media appear to be an essential requirement for antibacterial activity enhancement.

High ZP improves the repulsion forces between clay particles and enhances material dispersion and antibacterial activity.

These findings paved the way for deeper insights into the effect of material and particle size for other metal-loaded host-matrices based on carboxylated biopolymers. In this regard, the first step of this doctoral research allowed not only confirming most of the previous conclusion but also providing additional findings, among which the most important are the following:

CM-cellulose and CM-starch act as efficient host matrices for highly dispersed SMNPs inducing a more marked improvement of the antibacterial activity as compared to NaMt, CT and CT-NaMt. This appear to be due to the particular structure of CM-biopolymers that contains both carboxymethyl and hydroxyl groups.

The biopolymer degree of substitution, defined as a number of CM groups governs the amount of incorporated metal, surface charges, and dispersion of both the metal with the biopolymer entanglement and metal-loaded biopolymer in aqueous media.

The dispersion of metal-loaded biopolymers in aqueous media turned out to be a key factor that promotes the antibacterial activity

Biopolymers combination with montmorillonite appears to affect the material dispersion in aqueous media most likely due to detrimental competitive Clay:Polymer interactions.

The higher zeta potential observed for CMC as compared to CMS is due to the high surface density of CM groups. This induces higher metal dispersion within the biopolymer entanglement and lower particle size of CMC as a result of stronger electrostatic repulsion forces.

Copper cation and to a lesser extent silver cation insertion, reduces the zeta potential and pH due to the higher polarizing power of Cu^{2+} to dissociate the surrounding water molecules generating additional protons.

Metal zero dispersion raises the Zeta potential as a result of induced increasing of ZP. LAB interaction of metals with the oxygen atoms of the CM groups that leads to their deprotonation.

There exists an almost linear proportionality between the Zeta potential and pH but a reverse proportionality with the particle size via enhanced repulsion forces and material dispersion.

The intensity increase of the O1s XPS signal induced by the incorporation of both metals in both valence forms is a precise indicator of the involvement of the oxygen atoms of CM groups in metal stabilization. This shift was more pronounced for CMC than CMS due to its higher density of CM groups.

The fact that the BE shifts of C1s signals for both CMC and CMS were negligible suggests no direct contribution of the carbon atoms in metal dispersion.

The pronounced C1s intensity decay observed for CMS suggests a pronounced biopolymer compaction around the encapsulated metal cation or MNP.

MNP dispersion, induced a more pronounced O1s BE shift and stronger [-O:Zero-Valent Metal] interaction as compared to metal cations.

XPS data allowed concluding that CuNP exhibit higher affinity towards hydroxyl as compared to C=O in both polymers, while AgNP selectively interacted with hydroxyls in CMC and with C=O groups in CMS.

The higher density of CM groups in CMC biopolymer resulted in higher metal zero dispersion even down to a sub-nanometric scale

NaMt-Biopolymer combination induced a slight increase in the metal particle size due to the rise of competitive [Clay:Biopolymer] interaction at the expense of [Metal:Biopolymer] one.

Incorporation of both Ag^0 and Cu^0 in the biopolymer was found to induce antibacterial activity.

As a general feature, both metal-loaded biopolymers exhibited higher antibacterial activity on *B. subtilis* S168 than *E. coli* DH5a. This activity appears to be enhanced by increasing metal content.

Cations showed higher antibacterial activity as compared to Ag^0 regardless to the biopolymer.

Weaker retention strength of AgNPs by CMC as assessed through XPS data produced higher antibacterial activity as compared to CuNPs.

The higher antibacterial activity of the metal -loaded biopolymers as compared to metal-loaded NaMt and metal-loaded NaMt- cellulose can be explained in terms of finer metal particle size mostly below 1 nm.

Increasing initial pH in the infect media in the presence of metal-loaded biopolymers was found to improve the antibacterial activity, but deeper insights in this direction are required for elucidating the contribution of decreasing particle size and/or of a biocidal effect of pH changes.

An optimum 1mg/mL concentration of metal-loaded biopolymers allowed achieving a total depletion of both bacteria strains.

Therefore, the antibacterial activity of the metal-loaded matrices turns out to be a surface phenomenon involving exchange processes between a solid surface, aqueous media and bacteria membrane. Such exchange processes require higher contact surfaces that strongly depend on material structure and behavior in aqueous media. All of these valuable findings that were published in the form of two articles along with deeper insights in surface exchange processes are expected to provide fundamental knowledge for designing efficient, low cost and biodegradable metal-loaded-host matrices for specific biomedical and

biotechnological purposes. Deeper insights in such exchange processes. Research should be pursued in this direction.

ANNEXE A

Supporting information for article 1

Insights in metal retention role on the antibacterial behavior of montmorillonite and cellulose tissue supported copper and silver nanoparticles

Farzaneh Noori et al.

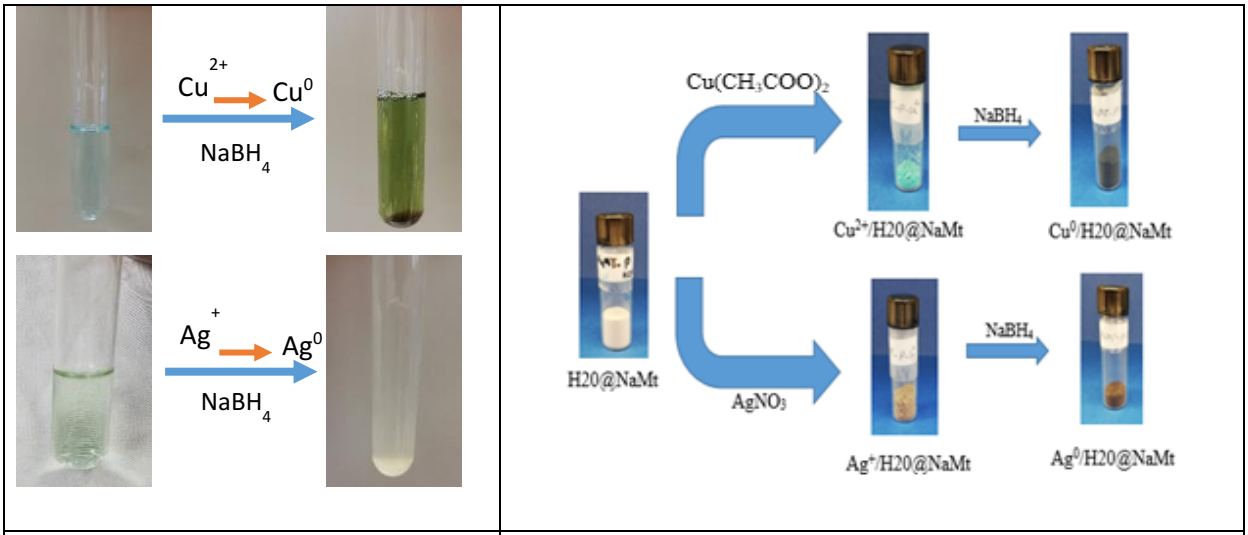

Fig. S1. Color changes after reduction of Cu^{2+} and Ag^{+} in the presence of $NaBH_4$ (a) and color changes of H20@NaMt composites after MNP_S and cation incorporation (b).

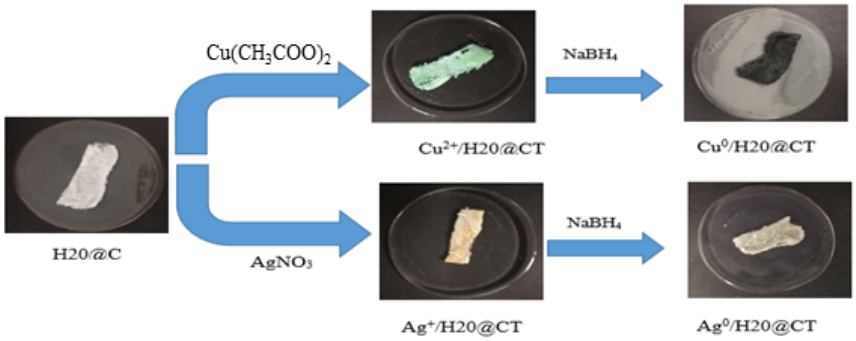

Fig. S2. Color changes of cellulose-based samples after the dispersion of metal cation and metal nanoparticles without or with the presence of $NaBH_4$ respectively.

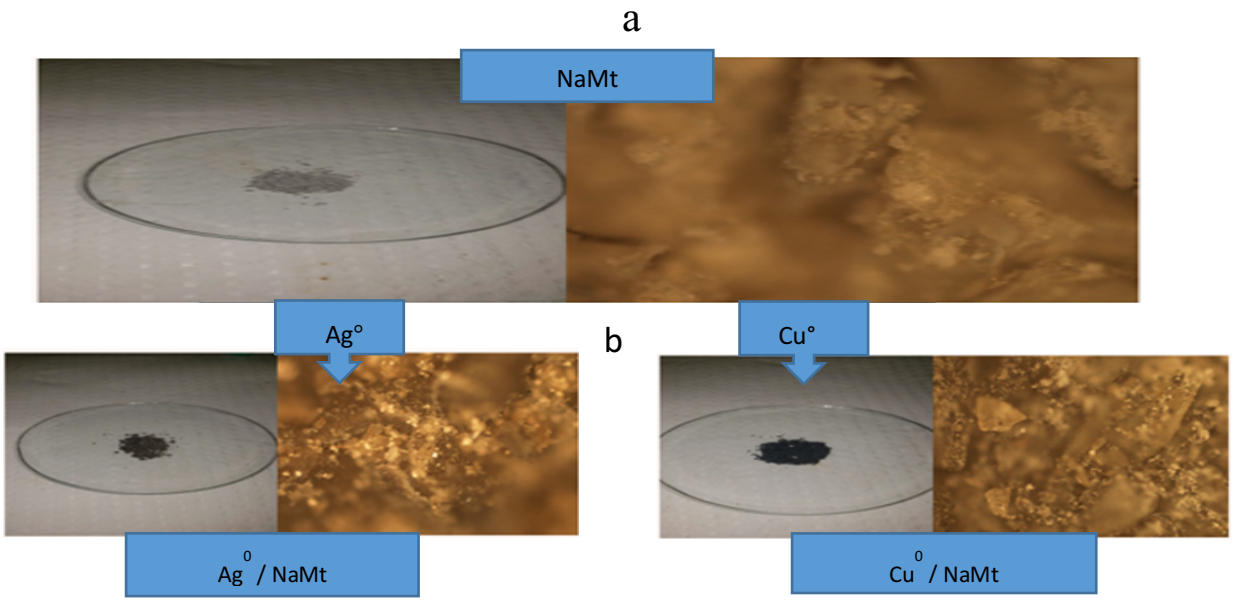

Fig. S3. Color changes and optical microscopy images of untreated NaMt (a) and MNPs-loaded NaMt (b).

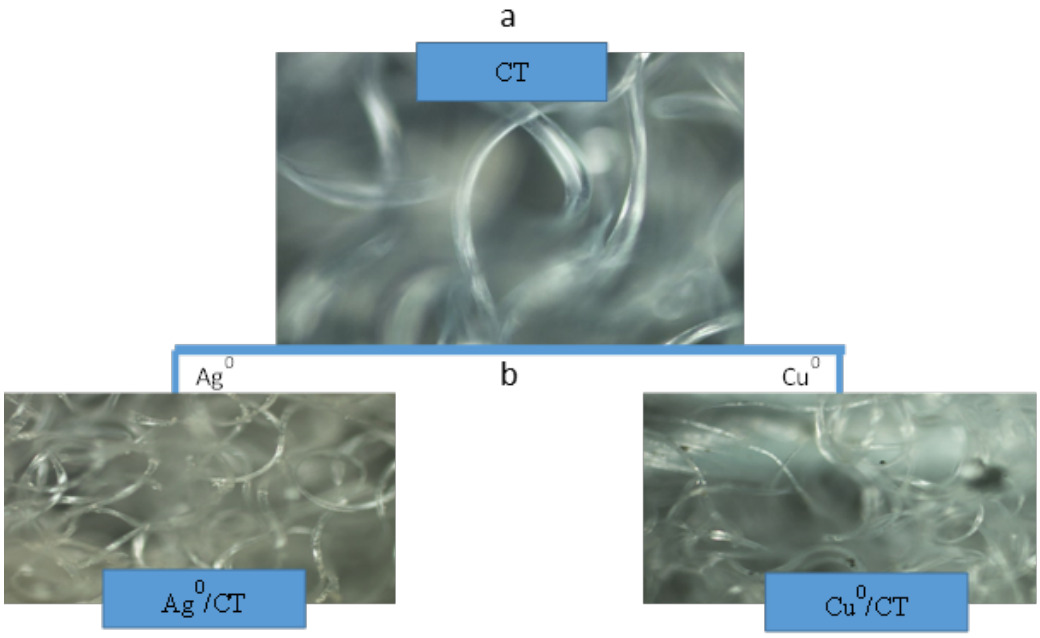

Fig. S4. Color changes and optical microscopy image of untreated CT (a) and MNPs-loaded CT (b).

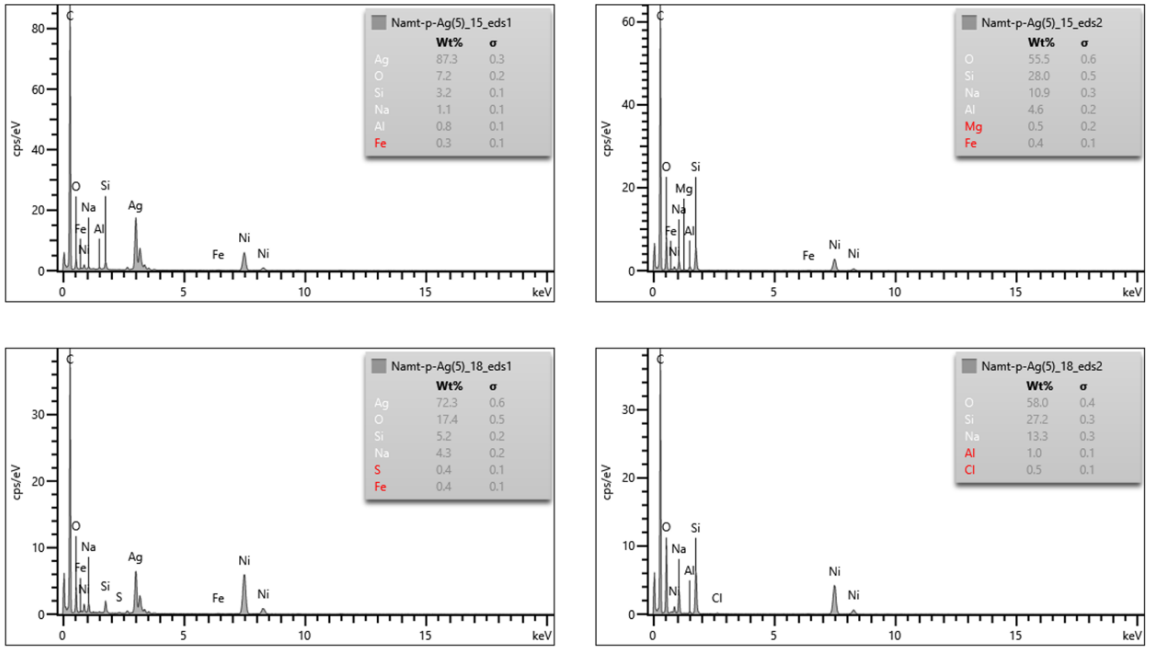

Fig. S5. ED-XRF spectra of some spots on SEM images of Ag^0/Boltorn H20-NaMt.

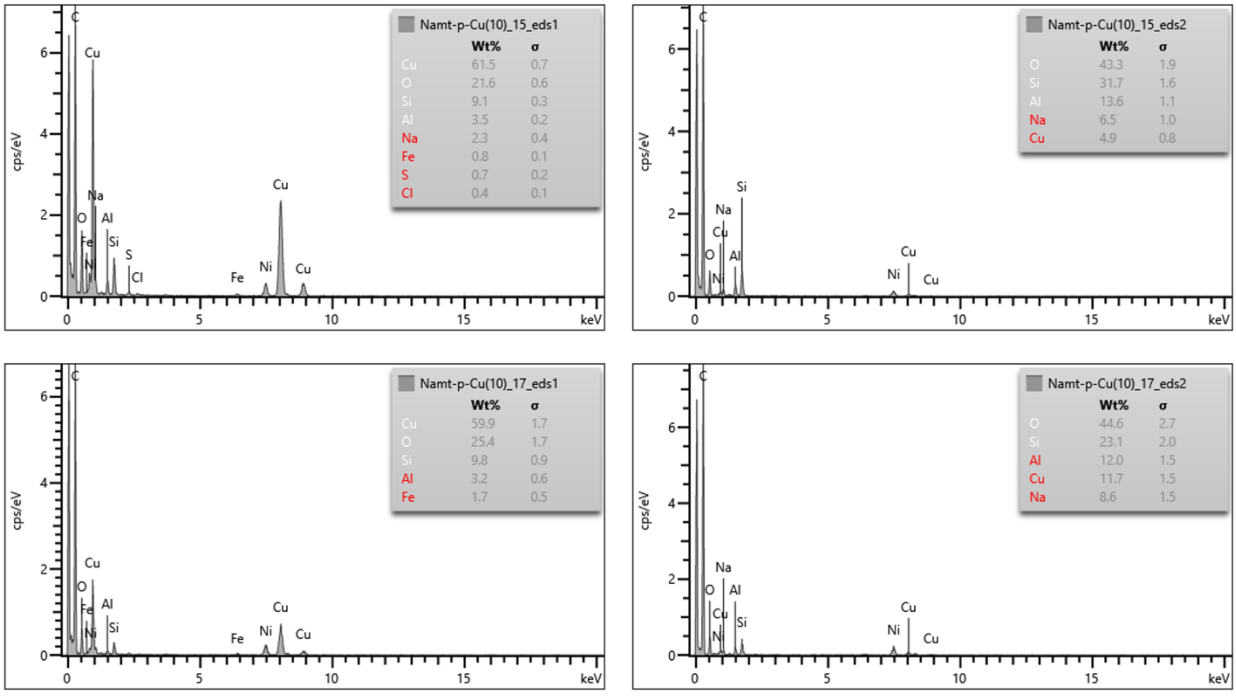

Fig. S6. ED-XRF spectra of some spots on SEM images of Cu^0/Boltorn H20-NaMt.

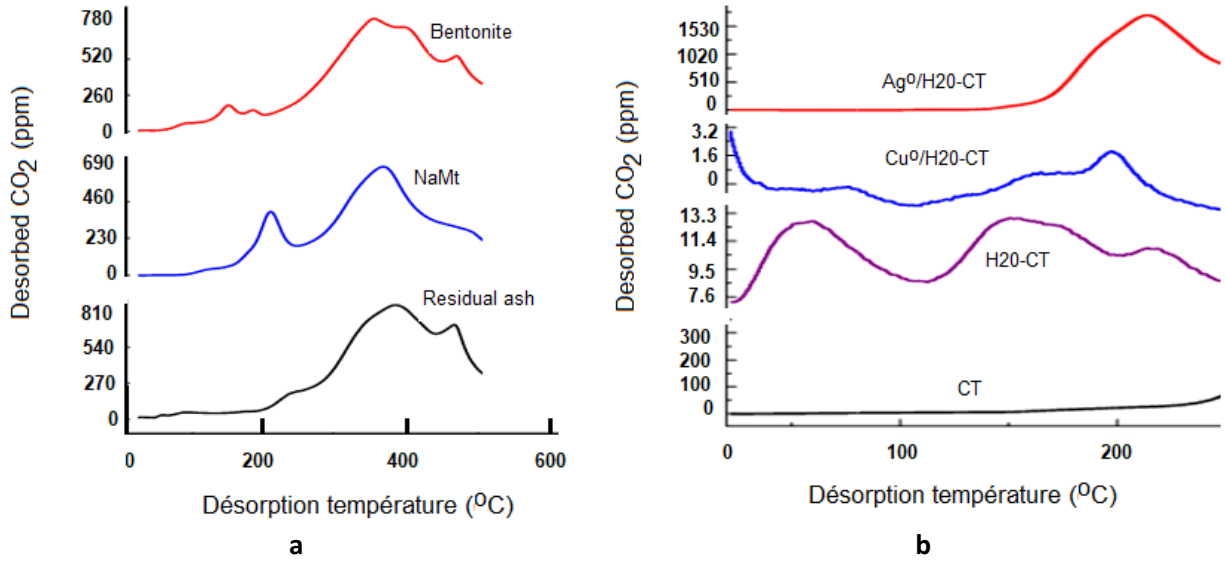

Fig. S7. CO_2-TPD patterns of clay-based samples (a) and CT-based samples (b).

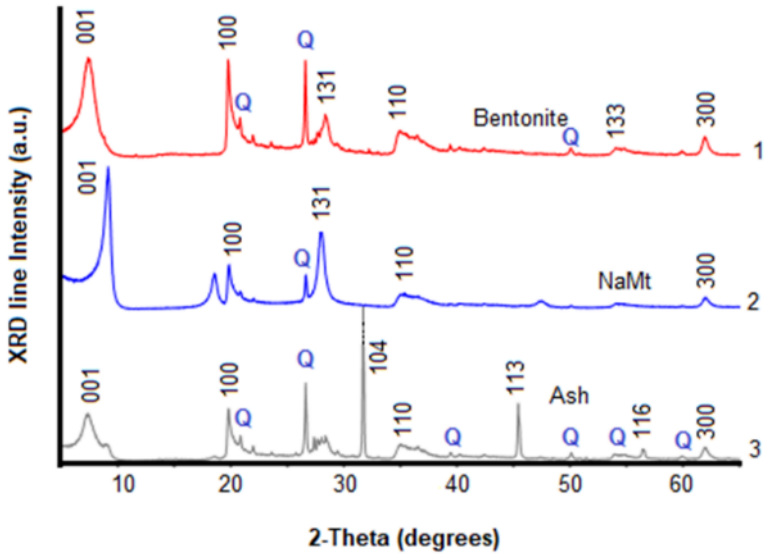

Fig. S8. XRD patterns of bentonite (1), NaMt (2) and residual ash from bentonite purification (3).

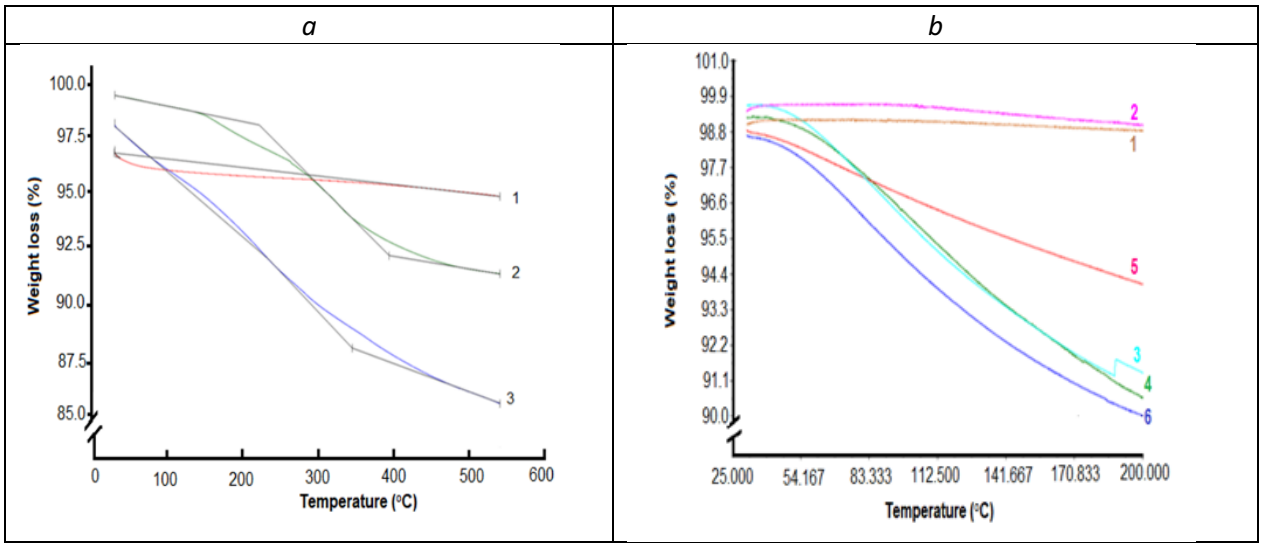

Fig. S9. TGA patterns of (a) clay-based samples: NaMt (1), Cu^0/NaMt (2) and Ag^0/NaMt (3) and of (b) Cellulose-based materials: CT (1), H20-CT (2), Cu^0/CT (3), Ag^0/CT (4), Cu^0/H20-CT (5) and Ag^0/H20-CT (6). TGA patterns were recorded between 25 and 700 °C for clay-based samples and between 25 and 200 °C for CT-based materials.

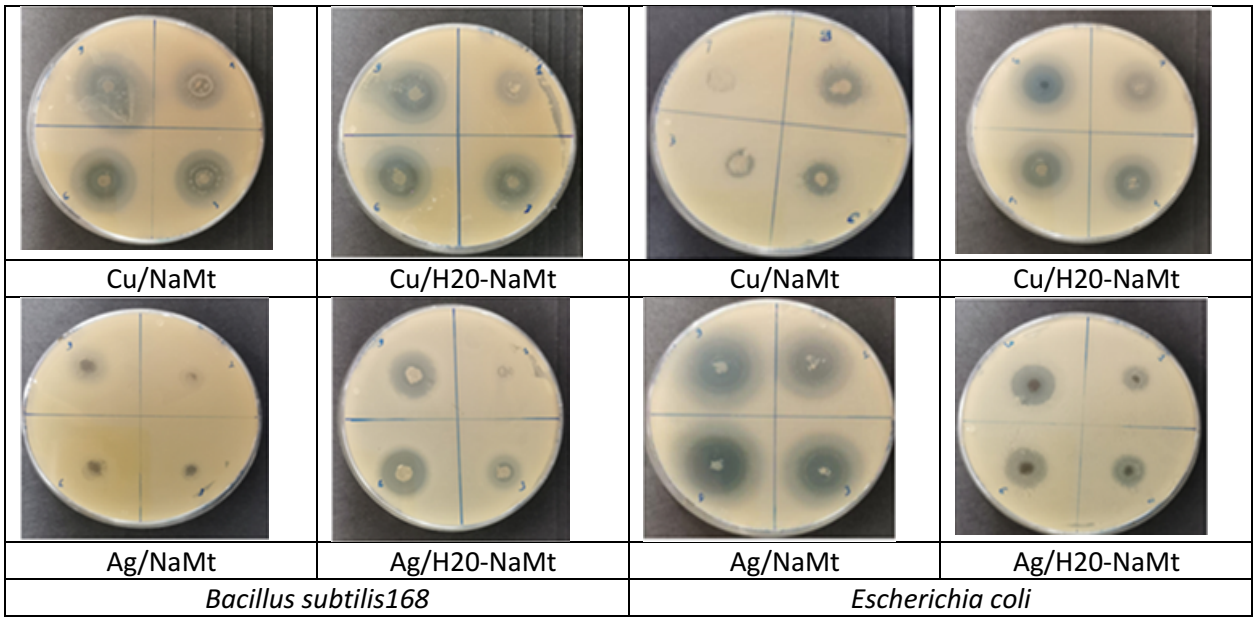

Fig. S10. Inhibition zones in *Bacillus subtilis168* proliferation in the presence of NaMt (a) and metal-loaded H20/NaMt composites (b).

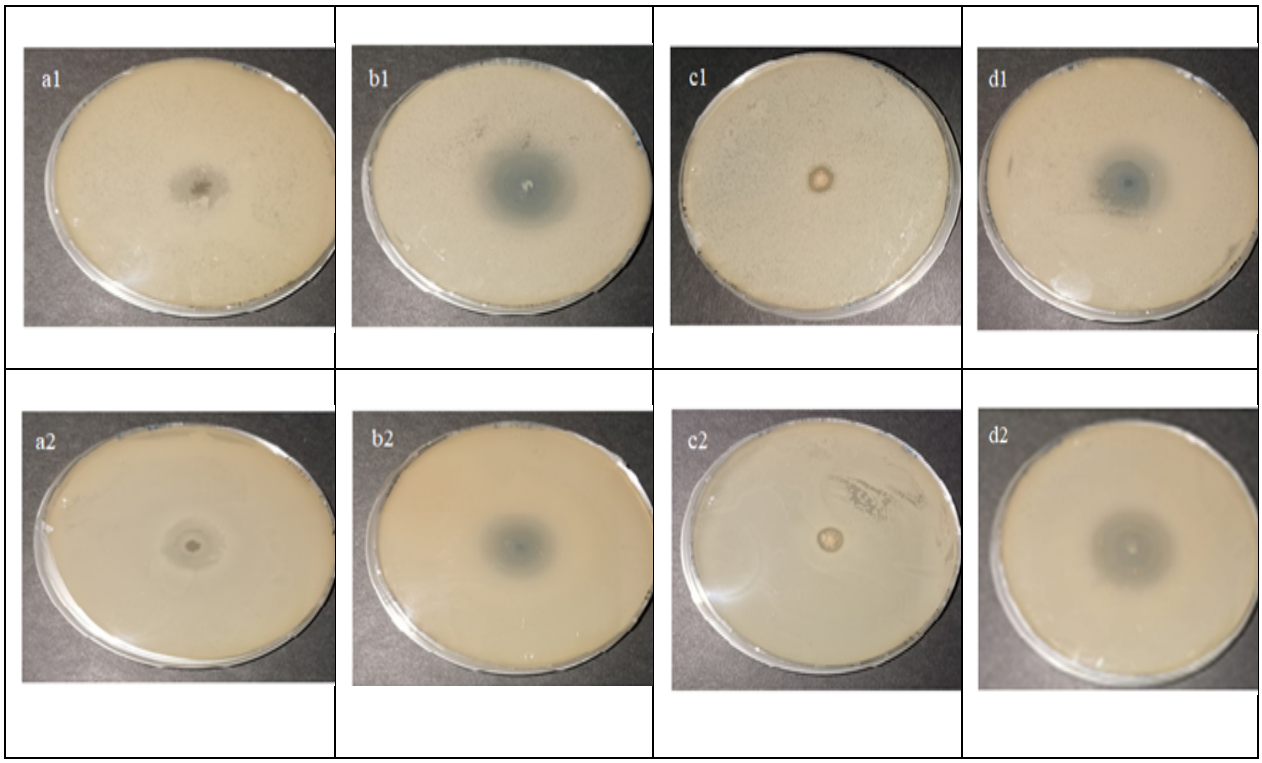

Fig. S11. Antibacterial test of MNP loaded in organoclay- based samples. *Escherichia coli* (a1, b1, c1 and d1), *Bacillus subtilis168* (a2, b2, c2 and d2) were incubated for 24h at 37 °C with 5 mg of Ag^0/H20@NaMt (a1-2); Cu^0/H20@NaMt (b1-2); Ag^+/H20@NaMt (c1-2) and Cu^{2+}/H20@NaMt (d1-2).

Table S1. Zeta potential, particle size and inhibition zone diameter for clay-based samples

Samples	Zeta potential (mV)*	Particle size (nm)**	pH	Inhibition zone diameter (cm)	
				E. coli DH5α	*B. subtilis 168*
NaMt	-26.56	342.7	6.01	0	0
Boltorn H20	-28.57	201.2	4.62	0	0
Cu^0/NaMt	-23.19	221.2	9.28	1.40	1.83
Ag^0/NaMt	-28.31	152.7	9.08	1.87	1.83
H20-NaMt	-38.12	373.7	7.59	0	0
Cu^0/H20-NaMt	-26.91	164.2	9.25	1.77	1.83
Ag^0/H20-NaMt	-27.21	127.6	9.16	1.07	1.50

*Average error on Zeta potential = 6.7%; **Average error on particle size = 5.7%.

Table S2. Inhibition zone diameters (cm) for different amounts of metal-loaded clay samples.

Samples	*B. subtilis 168*				*E. coli DH5α*			
Concentrations (mg powder)	1	3	6	9	1	3	6	9
NaMt-Cu^0	2.0	2.3	2.6	3.2	0	0.2	1.3	1.6
NaMt-Ag^0	0	0	0.7	1.5	0	0.9	1.3	1.6
Cu^0/NaMt@H20	1.3	1.3	1.7	3.0	0.6	1.7	2.1	2.4
Ag^0/NaMt@H20	0.7	1.3	2.1	2.2	0.9	1.4	1.6	1.8
Cu^{2+}/NaMt@H20	2.3	2.8	3.4	3.5	2.0	2.4	2.5	2.5
Ag^+/NaMt@H20	2.0	2.8	3.3	3.3	0.8	1.1	1.2	1.7

ANNEXE B
Supporting information for article 2

Synthesis of metal-loaded carboxylated biopolymers with antibacterial activity through metal subnanoparticle incorporation

Farzaneh Noori et al.

Table S1. Polarizing power (PP), ionic radius and Zeta potential of different metal cation loaded biopolymers

Cations	Polarizing power*	Ionic radius/pm	ZP (mV)	
			CMC	CMS
Ni^{2+}	2.80	70.	-10.05	-11.34
Cu^{2+}	2.73	73	-13.82	-13.28
Zn^{2+}	2.70	74.5	-20.90	-13.28
Co^{2+}	2.68	74	-23.10	-13.42
Pt^{2+}	2.50	80	-23.86	-15.98
Ti^{2+}	2.30	86	-24.40	-16.42
Ag^{+}	0.86	115	-30.39	-17.90
Au^{+}	0.72	137	-33.53	-21.81

*The polarizing power is a cation capacity to polarize the counter anion, i.e., the capacity to attract the electron cloud anion. This factor increases with increasing charge and decreasing size of the cation.

CMC alone	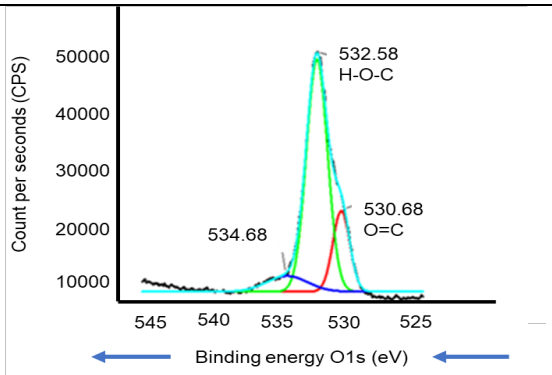
Cation-loaded CMC	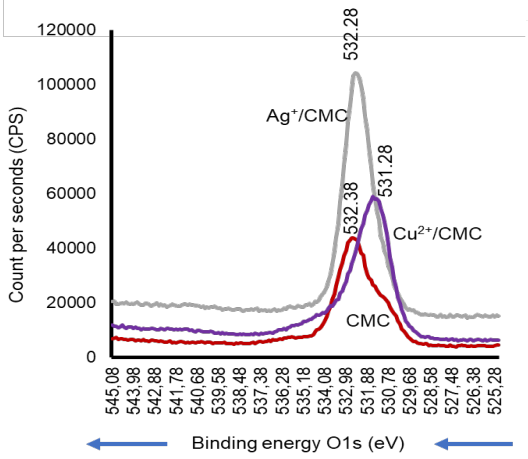
MNP-loaded CMC	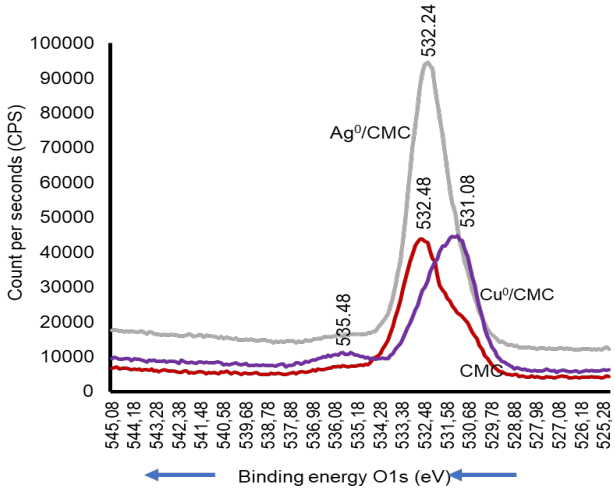

Fig. S1. O1s XPS spectra of CMC-based samples. The XPS spectra of the starting biopolymers are illustrated by red profiles. * The binding energy was assessed with absolution error below 0.05 eV.

CMC alone	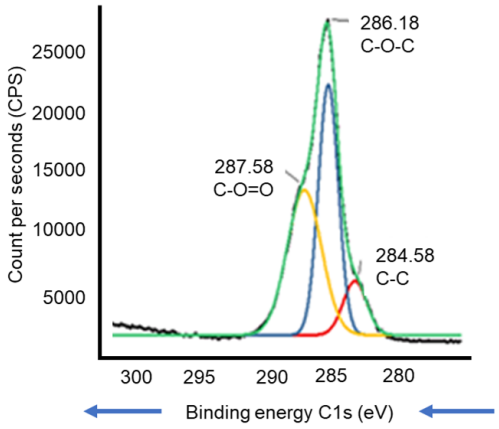
Cation-loaded CMC	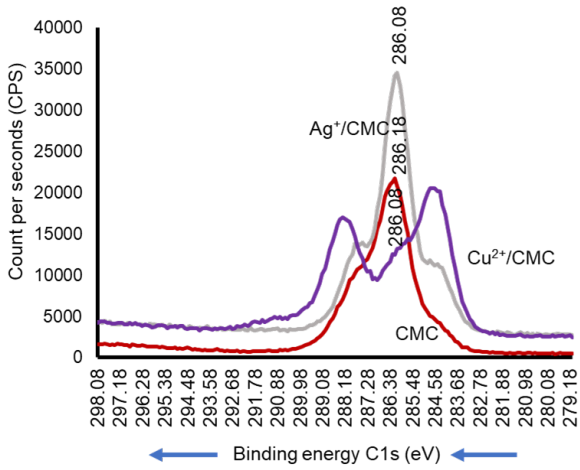
MNP-loaded CMC	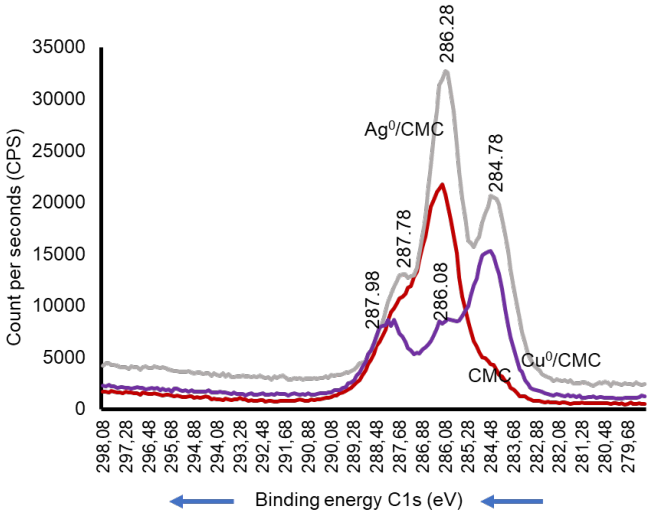

Fig. S2. C1s XPS spectra of CMC-based samples. The XPS spectra of the starting biopolymers are illustrated by red profiles. * The binding energy was assessed with absolution error below 0.05 eV.

CMS alone	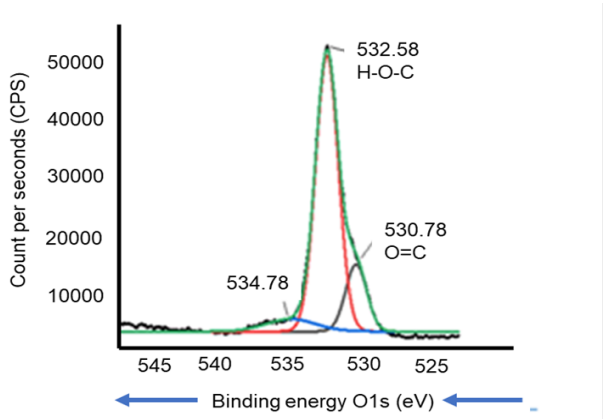
Cation-loaded CMS	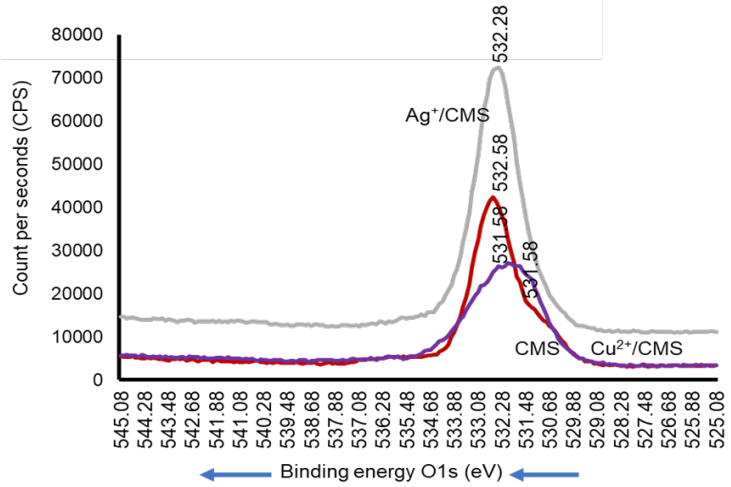
MNP-loaded CMS	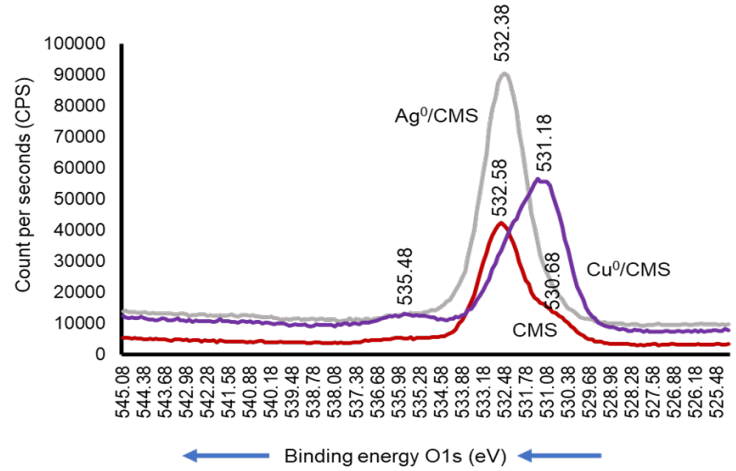

Fig. S3. O1s XPS spectra of CMS-based samples. The XPS spectra of the starting biopolymers are illustrated by red profiles. * The binding energy was assessed with absolution error below 0.05 eV.

CMS alone	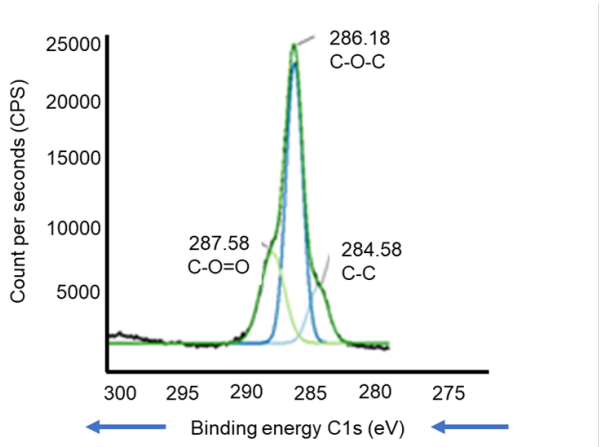
Cation-loaded CMS	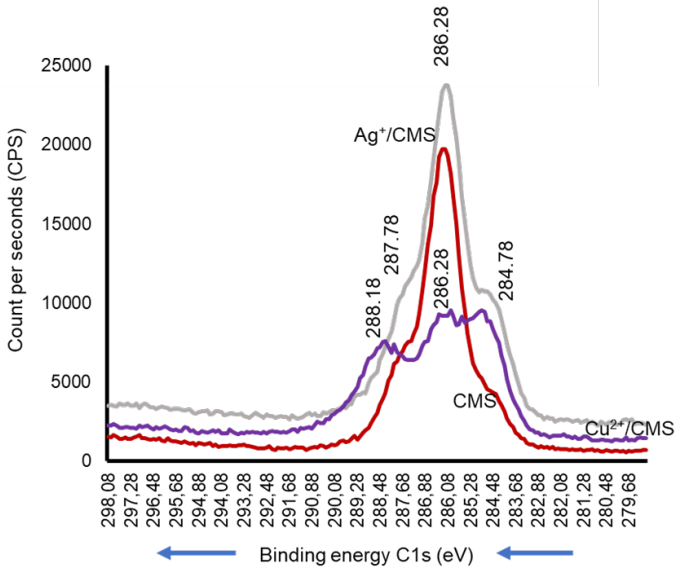
MNP-loaded CMS	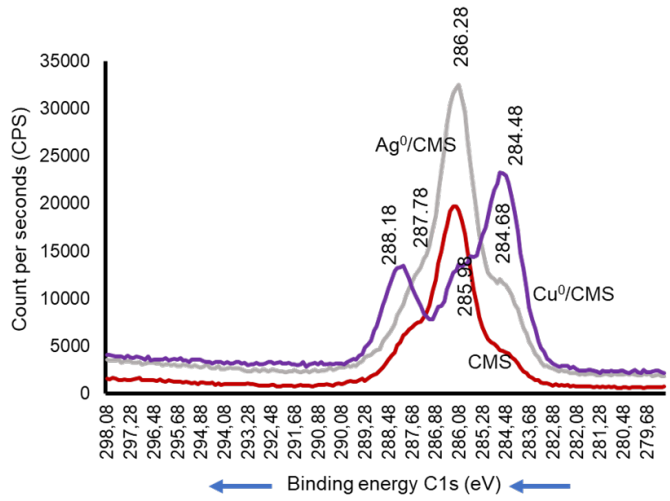

Fig. S4. C1s XPS spectra of CMS-based samples. The XPS spectra of the starting biopolymers are illustrated by red profiles. * The binding energy was assessed with absolution error below 0.05 eV.

Table S2. XPS BE shift in CMC-based samples.

XPS signal	Binding energy (eV) of CMC- Based samples (±0.05 eV)									
	Matrix	Alone	+ Cu^{2+}	Shift* (eV)	+Cu^{0}	Shift* (eV)	+Ag^{+}	Shift* (eV)	+Ag^{0}	Shift* (eV)
O_{1S}	O=C	530,68	530.28	0.40	529.89	0.79	530.18	0.50	529.38	1.30
	H-O-C	532.58	531.28	1.30	530.89	1.69	532.28	0.30	531.08	1.50
C_{1S}	C-O-C	286.18	286.28	-0.10	287.08	-0.90	286.38	-0.20	286.22	-0.04
	C-C	284.58	284.78	-0.20	284.9	-0.32	284.68	-0.10	284.78	-0.20
	O-C=O	287.58	287.88	-0.30	287.98	-0.40	287.68	-0.10	287.78	-0.20

* The BE shift was assessed as the difference between the BE values before and after metal loading.

Table S3. XPS BE shift in CMS-based samples.

XPS signal	Binding energy (eV) of CMC- Based samples (±0.05 eV)									
	Matrix	Alone	+ Cu^{2+}	Shift* (eV)	+Cu^{0}	Shift* (eV)	+Ag^{+}	Shift* (eV)	+Ag^{0}	Shift* (eV)
O_{1S}	O=C	530.78	530.08	0.70	529.88	0.90	530.28	0.50	529.98	0.80
	H-O-C	532.58	531.58	1.00	531.18	1.40	532.28	0.30	532.11	0.47
C_{1S}	C-O-C	286.18	286.28	-0.10	285.98	0.20	286.29	-0.11	286.37	-0.19
	C-C	284.58	284.78	-0.20	284.48	0.10	284.78	-0.20	284.68	-0.10
	O-C=O	287.68	288.18	-0.50	288.1	-0.42	287.98	-0.30	287.78	-0.10

* The BE shift was assessed as the difference between the BE values before and after metal loading.

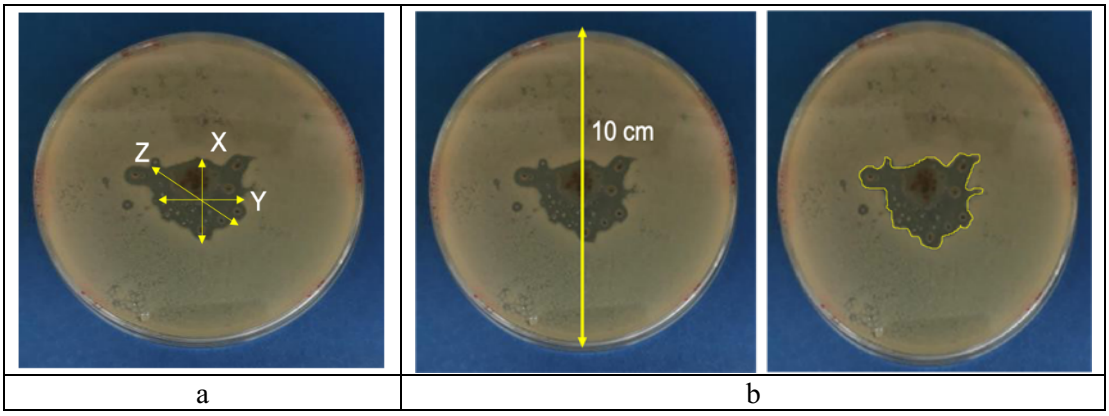

Fig. S5. Measuring the IZD graphically (a) or by using image j software (b).

Table S4. Relative standard deviation on IZD measurements by two different methods

Samples	Standard deviation (%)			
	E. coli DH5α		B. subtilis168	
	Graphically	Image-j	Graphically	Image-j
Ag/CMS	7.5	0.5	15.5	2.5
Ag^0/CMS	5.0	1.0	9.5	2.3
Ag/CMS/NaMt	6.5	0.5	4,0	1.5
Ag^0/CMS/NaMt	0.0	0.0	0.0	0.0
Cu^2/CMS	6.0	1.5	2.0	1.0
Cu^0/CMS	2.5	0.5	1.3	0.5
Cu^2/CMS/NaMt	5.0	0.5	15.5	2.5
Cu^0/CMS/NaMt	0.0	0.0	4.5	0.6

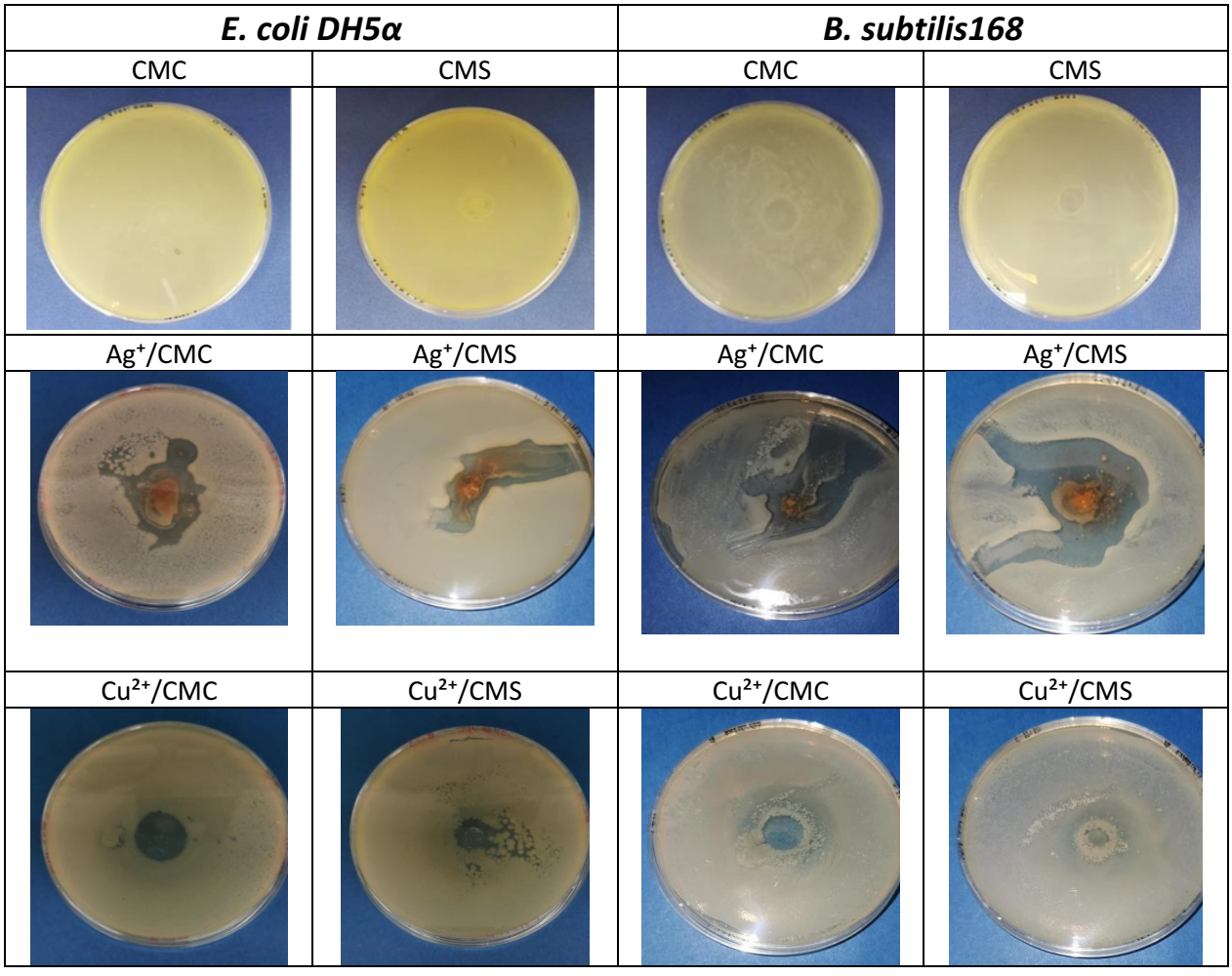

Fig. S6. Inhibition zones in the proliferation of both bacteria strains in the presence of CMC and CMS and metal cation-loaded counterparts. The irregular IZD shape is due to the heterogeneous flowability of the powders.

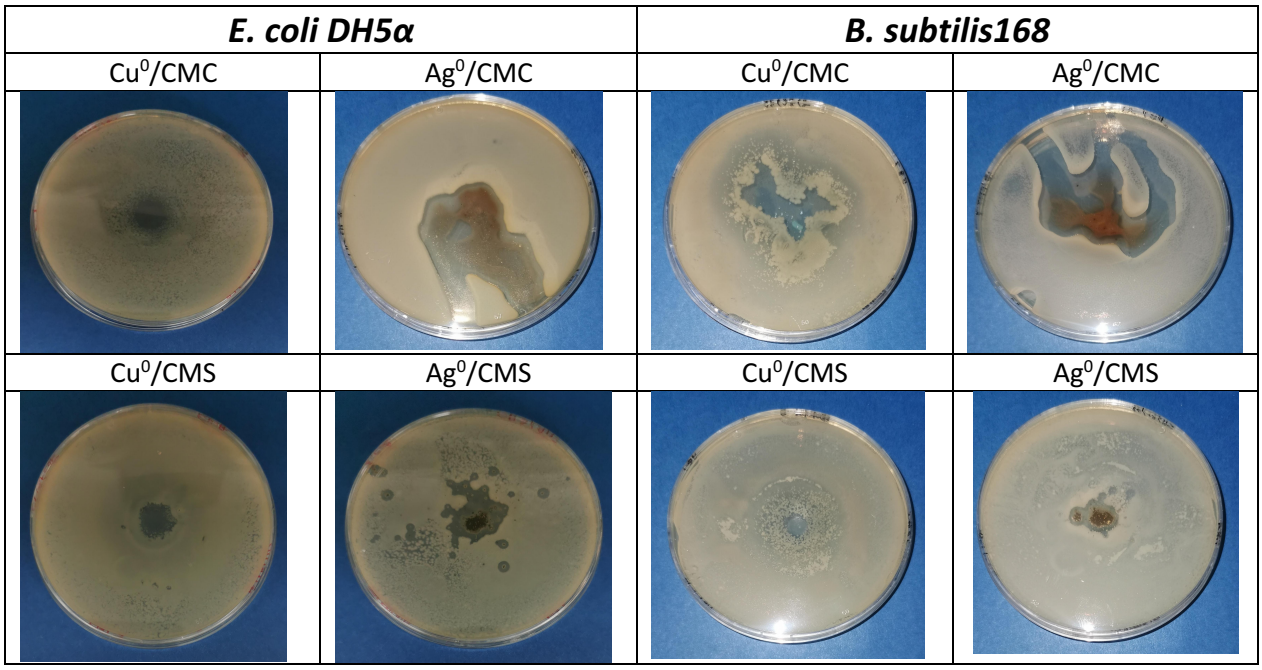

Fig. S7. Inhibition zones in the proliferation of both bacteria strains in the presence of CMC and CMS and metal zero-loaded counterparts. The irregular IZD shape is due to the heterogeneous flowability of the powders.

ANNEXE C

Preprint

Published by Authorea on July 7th, 2020

Metal-loaded porous polyhydroxylic matrices with improved antibacterial properties

Farzaneh Noori[1], Neree-Armelle Tchoumi[2], Meriem Megoura[2], Mircea Alexandu Mateescu[2], and Abdelkrim Azzouz[1]

[1]University of Quebec in Montreal
[2]University of Quebec at Montreal Department of Chemistry

July 7, 2020

Abstract

Metal-loaded porous matrices based on clay and cellulose materials displayed appreciable antibacterial activity against Escherichia coli DH5α and Bacillus subtilis 168. BoltornTMH20 polyol dendrimer supported by montmorillonite and cellulose turned out to be effective porous matrices for Cu0 and Ag0 nanoparticles dispersion. The resulting organoclay and polyol-coated cellulose were found to stabilize Cu0 and Ag0 nanoparticles through their terminal hydroxyl groups. This was explained in terms of Lewis Acid-Base interaction between the electron pair of the oxygen atom belonging to the terminal hydroxyl and metal species as supported by XPS data. The metal retention strength was found to correlate with the antibacterial activity, surface basicity and hydrophilic character. These findings are of great importance, because they open promising prospects for vegetal fibers and clay-supported drugs to treat dermatological and gastro-intestinal infections.

Keywords

Organoclays; Cellulose; Metal Nanoparticles, Porous Polyhydroxylic Matrices; Antibacterial Properties; X-ray Photoelectron Spectroscopy

Short running title

Novel metal-polyol-based antibacterial agents

Introduction

Resistance of pathogenic bacteria against antibiotics has become a major medical and pharmaceutical issue. Overuse of antibiotics has been identified as a main cause of pathogenic adaptation of bacteria. Numerous outbreaks of infectious diseases have been reported as a direct effect of antibiotic resistance (Levy, 1998), which still remains a major challenge to be addressed (Cragg & Newman, 2013). Metals are known as metabolism disturbing agents, some of them being harmful for animals and human (Martin & Griswold, 2009). Certain zero-valence metals (metal-zero) such as silver in high dispersion state have long been used in treating skin bacterial infections (Rai, Yadav, & Gade, 2009). Nanoparticles of gold, zinc and titanium have showed high bioactivity. In this context, silver (Ag) and copper (Cu) are also promising nanoparticles that have shown broad-spectrum activity against many species of Gram positive and Gram-negative bacteria (Carretero, 2002; Čık, Bujdáková, & Šeršeň, 2001; Čík et al., 2006; Costa, Conte, Buonocore, & Del Nobile, 2011; Dizman, Badger, Elasri, & Mathias, 2007; Gupta, Maynes, & Silver, 1998; Herrera, Burghardt, & Phillips, 2000).

Higher performant antibacterial activity is obtained if Ag and Cu nanoparticles are finely and uniformly sized (España, Sarkar, Biswas, Rusmin, & Naidu, 2019). When highly dispersed, metal nanoparticles (MNP) can

be active against pathogenic bacteria without inducing bacterial resistance (España et al., 2019). However, MNPs have a strong tendency to aggregate into bulky inactive clusters (Rees, Zhou, & Compton, 2011). Polyhydroxylated compounds and polyamines bear specific chemical groups that confer them chelating and stabilizing properties for metals (Crooks, Zhao, Sun, Chechik, & Yeung, 2001). Functionalized polymers could exhibit higher effectiveness when supported on solid surfaces (Hellmann et al., 1998). The resulting inorganic-organic matrices hosting metal nanoparticles **(Scheme 1)** are a novel class of antibacterial agents displaying high surface-to-volume ratio, chemical stability, thermal resistance, non-toxicity and recyclability (Bragg & Rainnie, 1974). Their synthesis has become the main target of the present research.

Scheme 1

The interest of this research consists in using inorganic natural alumino-silicates such as clay minerals, known to be harmless for human health and biodiversity. Among these, smectite-type sodium montmorillonite (NaMt) could be an interesting host matrice for metals due to its natural abundance, cost effectiveness, non-toxicity, chemical inertness, sorptive capabilities, large specific surface area (Komadel, 2016) and even beneficial medicinal effects (Carretero, 2002; Nadziakiewicza, Kehoe, & Micek, 2019). .

To overcome this problem, inorganic carriers such as clay minerals for metal nanoparticles have been investigated (Kim et al., 2007). Successful attempts against bacteria were already achieved using other clay minerals such as allophane and imogolite doped with metals like Ag, Cu, Co, Zn (Stavitskaya et al., 2019; Williams et al., 2011). Attempts were also achieved using functionalized clay minerals and vegetal fibers for the dispersion of silver and copper ions (Joshi, Purwar, Udakhe, & Sreedevi, 2015).

High adsorptive capabilities for metal nanoparticles in NaMt are largely responsible for the antimicrobial properties of the metal-clays. The adsorptive properties in NaMt are governed by a large specific surface area with increased net negative charges on the sheets that can be obtained by intercalation of NaMt with dendritic polyols like Boltorn^{TM} H20 (Vdović, Jurina, Škapin, & Sondi, 2010). Reportedly, eco-friendly and cost-effective cotton fabric–based composite materials doped with copper oxide showed antibacterial action against *Staphylococcus epidermis* and *Escherichia coli*(Nabil, Christine, Julien, & Abdelkrim, 2018). The aim of this work was to prepare organoclays and/or natural polymers for hosting metal nanoparticles with long-term antibacterial effects.

Deeper insights in metal-matrice interaction will allow tailoring optimal interactions with MNPs by modifying the type and number of chemical functions of the organic moiety. This is expected to influence the metal to be released, the release velocity and desired antibacterial activity. This concept allows envisaging diverse applications for controlled release of a wide variety and drugs and other medicinal molecules.

2. Materials and methods

2.1. Chemicals

All chemicals were of analytical grade and used without previous purification. Crude bentonite (Sigma-Aldrich, Oakville, Canada), sodium chloride (NaCl) (ACP chemicals, Montreal, Canada), copper acetate ($Cu(CH_3COO)_2$) (Fisher chemicals, Ottawa, Canada), silver nitrate ($AgNO_3$) (Fisher chemicals), sodium borohydride 98% ($NaBH_4$) (Acros organics, Ottawa, Canada), copper nitrate ($Cu(NO_3)_2$) (Anachemia VWR company, Montreal, Canada), Boltorn H20 (Perstorp, Malmo, Sweden), absolute methanol (MeOH) (Sigma-Aldrich), toluene (Sigma-Aldrich) were used. All experiments were performed in distilled water. Non-woven cellulose tissue (gauze) denoted as CT was purchased from PJC, Canada.

2.2. Polyol and metal dispersion

Sodium-montmorillonite (NaMt) was obtained through combined ion-exchange of crude bentonite (Aldrich) in aqueous NaCl solution using an effective procedure fully described elsewhere (**Scheme S1**) (Abdelkrim Azzouz et al., 2010; Thuc et al., 2010). This was followed by adding 200 g of NaMt to a 41.2:58.8 volume ratio $MeOH/H_2O$ mixture containing 200 mg of Boltorn H20 polyol dendrimer under continuous stirring for 1h at 40-60°C. The resulting organoclay, denoted as H20@NaMt was died overnight in a freeze-drying device.

Similarly, Boltorn H20 was also dispersed on cellulose tissue (CT) by impregnation in 20 mL of 0.01mol/L Boltorn^{TM}H20 aqueous solution at room temperature (RT) for 1h, resulting in a H20@CT composite.

An amount of 0.2 g of NaMt-H20 was slowly mixed in a 50 mL beaker with 15 mL (33.33% and 66.66% toluene/water) aqueous solution of 0.12mol/L Cu $(CH_3COO)_2$ and $(AgNO_3)$ under vigorous stirring for 2 h. Both organoclay suspensions were dried overnight at room temperature, resulting in a first series of cation-loaded organoclays denoted as Cu^{2+}/H20@NaMt and Ag^{+}/H20@NaMt. A second series of samples was prepared by dropwise adding 10 mL aqueous solution of $NaBH_4$(0.2mol/L) to both organoclay suspensions during 15 min under a nitrogen stream at ambient conditions (**Scheme S2**). The resulting metal-zero-loaded organoclays, denoted as Cu^0/H20@NaMt and Ag^0/H20@NaMt were further repeatedly washed with distilled water to eliminate the excess of Cu^{2+} and Ag^{+} cations and then dried overnight. Further, for the preparation of metal loaded H20@CT samples, 0.8g of $AgNO_3$ or 1.24g of $Cu(NO_3)_2$ were each dissolved in 30 mL of distilled water and mixed with 1g and 1.5g of $NaBH_4$, respectively in order to reduce Cu^{2+} and Ag^{+} into Cu^0 and Ag^0 nanoparticles (denoted as $AgNP_S$and $CuNP_S$,). This was achieved upon stirring for 5-6h at room temperature (RT), under nitrogen stream to prevent MNP oxidation. The resulting Ag^0/H20@CT and Cu^0/H20@CT samples were dried overnight at RT in a sealed enclosure containing dry O_2-free nitrogen dried with NaOH pellets.

2.3. Material characterization

The basicity and hydrophilic character of the as-prepared samples were assessed through TPD of CO_2 and water (A Azzouz et al., 2006; Beltrao-Nunes et al., 2019; Terrab et al., 2016). This was obtained by putting 45-50 mg of each sample at heating rate of 5 °C.min^{-1} from 20 °C to 450 °C and under a nitrogen stream of 5 mL.min^{-1} after saturation of each sample with $CO_{2\ gas}$ (**Scheme. S3**). Deeper insights into the structure of the as-synthesized MNP_S/H20@NaMt and MNP_S/H20@CT materials were achieved through TG Analysis (TA Instruments TGA (Q500)/Discovery MS equipment). For this purpose, 4-7 mg samples were heated in platinum (Pt) pan at a temperature range of 20-500 °C and 10 °C/min heating rate under 30 mL/min dry argon stream (**Fig. S1**). The particle morphology of the material was screened by SEM (Jeol JCM-6000 PLUS instrument). The samples were spread as powder on conductive double adhesive carbon tapes (**Fig. S2**). The SEM analysis of non-conductive samples was performed at 1.0 kV voltage, versus 15 kV for metal-containing materials (conductive). The crystalline structure was investigated by XRD in 2-Theta range 10-80, using CuK_{alpha} radiation (1.5406 Å) and XRD D8 Advance device (**Fig. S3**). Metal-matrices interactions were assessed through XPS of 7800 × 300 µm spots by means of an AXIS-ULTRA instrument (by KRATOS Analytical Ltd, UK) and a monochromatic Al-based X-ray source (260 watts in constant pass energy mode in two 160eV and 1eV steps).

2.4. Antibacterial tests

Approximatively 74 x 10^6 colony forming units CFU.mL^{-1} of each bacteria species (*E. coli* and*B. subtilis* 168) with a cell density of 0.5 at 600 nm was loaded on LBA plates. The antimicrobial behavior of the as-prepared samples was evaluated by diffusion and zone Inhibitory tests towards *E. coli*and *B. subtilis* bacterial strains. The assay is a semi-quantitative method where samples (1-9 mg) containing silver or copper metal were put in direct contact on LBA plate pre-seeded by bacteria strains. Negative controls were included in each assay. After 24 h of incubation at 37 °C, the diffusion zone where bacteria proliferation was inhibited was measured. The antibacterial property was evaluated by the application of 5 mg (Organoclays) or 1×0.5 mm^2 (CT) of the synthesized clay-based materials or tissue of cellulose-based samples, respectively. All experiments were performed in triplicate (three independent growth cultures) with at least two technical replicates.

3. RESULTS AND DISCUSSION

3.1. Changes upon metal incorporation

The formation of CuNPs and AgNPs dispersed into polyol-modified matrices was illustrated by marked color changes. The most visible changes took place from blue to black and accounts for Cu^{2+}conversion into Cu^0 in the presence of $NaBH_4$ as a reduction agent. However, a less visible color change was noticed for Ag^{+}

conversion into Ag^0 in the solution **(Fig. S4.a)** . These changes are much more pronounced in dry powders of H20@NaMt modified by Cu^0 and Ag^0 and their cationic forms (**Fig. S4.b**). The same results were observed for similar metal insertion in the presence of H20@CT-based samples. **(Fig. S5).**

Metal incorporation was confirmed by visible modification of the morphology of surface of the host-material. Preliminary observation through optical microscopy revealed a transition from a clean and almost soft surface of NaMt to the appearance of grains on the surfaces of both Cu^0/ NaMt and Ag^0/ NaMt (**Fig. S6**). This provides evidence of the formation of metal particles. Similar observations were made on CT-based materials (**Fig. S7**). This was confirmed by additional analysis through of SEM images of MNP-loaded NaMt and H20@CT (**Fig. 1.a)** . The appearance of grains smaller than 100 nm indicates that metal salt reduction using $NaBH_4$ effectively produced spheroidal nanoparticles with and without polyol as dispersing agent, as illustrated by the behavior of NaMt alone and H20-coated CT material. This can also be seen with CT alone **(Fig. S8).** The SEM images of NaMt showed specific morphology changes of lamellar structure according to the metal inserted (**Fig. 1.a**). Larger crystalline rods were observed on NaMt-Cu, presumably due to residual Cu^{2+} salt.

Figure 1

3.2. Effect polyol incorporation on metal dispersion

The non-uniform dispersion of MNPs must be due to the heterogeneous density of the small amount of hydroxyl groups belonging to the incorporated H20 poly dendrimer on the CT surface. Incorporation of polyol appears to act as the main dispersing agent of MNP, favoring complete metal entrapping by surrounding OH groups. This must take place through stronger Polyol-HO:Metal interaction that consumes all available OH groups of the inserted dendrimer at the expense of H20@CT surface association. This explains the presence of Polyol:MNP composite scales unstuck on the CT surface (**Fig. 1.b**). Similar observations can be made with Ag-modified materials, except the fact that metal salt needles apparently occur in much higher density. This corresponds to a relatively higher amount of residual unreduced Ag salt, i.e. less Ag^0 compared to copper-loaded materials. This lower reduction level of Ag^+ cations suggests a lower amount of Ag^0 atoms. This could explain somehow the paradoxically weaker antibacterial activity of Ag-based materials as compared to their Cu counterparts, given that silver is expected to display higher performance in this regard. A partial explanation resides in the stronger capacity of copper to undergo oxidative processes as compared to silver. The involvement of the OH groups in metal stabilization can be explained by changes in the hydrophilic character and basicity of the host materials. Deeper insights in this regard were achieved through TPD measurements.

3.3. Changes in clay surface basicity

The TPD patterns revealed the occurrence of at least four basicity strengths, namely weakly (below 100°C), medium (between 100 and 250°C), medium-to-strong (between 300 and 450°C) and strong basicity (between 450 and 550°C). The slight shift of the desorption peak from 60-200°C towards higher temperatures (170-220°C) was noticed from bentonite to NaMt (**Fig. S9-a**). This indicates a slight strengthening of the surface basicity, presumably due to the removal of acidic silica phases (quartz, sand, cristobalite). This agrees with the slight increase in the CRC value after bentonite purification from 2101 to 2261mmol.g^{-1} (**Table 1**) which indicates that bentonite purification induces a slightly higher number of stronger basic sites.

Table 1

This is well supported by the marked depletion of the XRD belonging to Quartz in bentonite and montmorillonite patterns (denoted as Q), and the presence of the main XRD lines of crystalline silica in the pattern of the residual ash (**Fig. S10**). A shift of the 001 XRD line from a 2ϑ value of 7.357@ for bentonite to 9.142@ was noticed for NaMt, indicating a decrease in the interlayer spacing. This shift is a special feature of the lamellar structure and is due to the replacement of bulky impurity particles by sodium cations. This was confirmed by the noticeable sharpening and increased intensity of the main XRD lines, which is a special feature of homo-ionic form of montmorillonite and almost perfect parallel arrangements of the clay sheets.

The Na^+ cation has a lower polarizing power and thereby lower intrinsic acidity and weaker capacity to attract water molecules than multivalent cations. This somehow explains the lower WRC value observed for NaMt compared to bentonite. MNP incorporation induced a marked decrease in CRC, due to at least two kinds of competitive interactions. Some MNP interactions occur with the lattice oxygen atoms (-Si-O-Si- with strong Lewis basicity). Other interactions take place between the OH groups of both terminal in-plane silanols and out-of-plane Si-OH with weaker basicity and MNPs on the surface (Sulpizi, Gaigeot, & Sprik, 2012).

3.4. Changes in CT surface basicity

The TDP measurements revealed no CO_2 desorption peak for untreated cellulose in the temperature range 20-100°C. Polyol incorporation induced a marked change in the TPD profile, mainly characterized by the appearance of a wide desorption peak between 20 and 110 °C (**Fig. S9.b**). This accounts for the rise of weakly basic adsorption sites, most likely amphoteric to slightly basic OH groups belonging to the inserted polyol dendrimer. OH groups were found to dramatically decline after CuNP insertion and totally disappear after AgNP incorporation. This is a confirmation of the appearance rise of novel HO:MNP interaction that seems to be stronger with AgNPs compared to CuNPs. Thus, CuNPs seem to be less entrapped by the dendrimer entanglement than AgNPs and more effective as antibacterial agent being less retained in the solid phase.

3.5. Thermal assessment of the affinity towards aqueous media

The antibacterial activity of MNP-loaded materials is often determined by their affinity towards aqueous media where bacteria live. This affinity towards water can be evaluated by TGA (Fu et al., 2015). The TGA patterns (**Fig. S11.a**) revealed a single and small weight loss (WL) of at most 0.7-0.8% for NaMt between 20 and 120°C. This corresponds to reversible dehydration, as shown by repeated TGA analysis of rehydrated samples. The total absence of other weight losses and more particularly of dehydroxylation (2 -Si-OH Si-O-Si- + H_2O) at higher temperature provided evidence that NaMt is stable throughout the entire range of temperature investigated. MNP insertion into NaMt gave rise to a marked endothermic process at ca. 140-480 °C for Cu^0/NaMt and 90-470 °C for Ag^0/NaMt. This accounts for 6.6 % and 9.4 % WL, respectively (**Table 2**).

Table 2

Within this temperature range, an initial mass loss was registered for NaMt-Cu^0 up to 180 °C, and must still be due to the dehydration process. This dehydration over a larger temperature range can be explained by an additional contribution of retained moisture on the incorporated metal. A second WL can be seen up to 470-480 °C and could be related to a dehydroxylation of terminal Metal-OH groups of possible metal oxide particles. The latter may unavoidably be produced during the synthesis procedure through slight metal oxidation when contacted to air. Another explanation should consist in a possible slow release of moisture from the internal surface the metal loaded clay mineral. Both WL were found to shift towards lower temperatures but with higher WL values in Ag^0/NaMt, indicating a higher hydrophilic character. In contrast, CT-based samples were mostly characterized by a much lower moisture loss **(Fig. S11.b)** , which indicates a much weaker hydrophilic character. This must be due to the fact that commercial untreated CT displays negligible surface density of hydroxyl groups. Polyol incorporation appeared to slightly improve this feature, by introducing high amount of OH groups. Incorporation of MNPs alone or accompanied by polyol H20 induced a marked enhancement of the hydrophilic character. This is supported by more pronounced weight loss in the temperature range of 47-200 °C up to 8.25 % (Cu^0/CT), 9.74 % (Ag^0/CT), 4.675 % (Cu^0/H20@CT) and 8.525 % (Ag^0/H20@CT) (**Table 2**).

3.6. Evidence of metal dispersion

Evidence of metal dispersion in the investigated materials was provided by X-Ray photoelectron spectroscopy (XPS). Changes in the binding energy (BE) of the electrons belonging to the material atoms involved in metal dispersion are expected to provide valuable information about the retention strength of MNP and

indirectly on the antibacterial activity. The presence of metal in the chemical compositions of NaMt and CT after metal incorporation was revealed by new XPS signals, i.e. Cu2p at 933 eV and Ag3d at 364 eV **(Fig. 2.a)** .

Fig. 2

Table 3

The most important XPS results reside in the shifts of the binding energy (BE) of the key elements (oxygen, silicon and aluminum)**(Table 3)** providing evidence of the occurrence of metal interaction with the host surface. For oxygen, the BE value decreased from 532.55 eV down to 531.00 eV and 527.00 eV upon Cu and Ag incorporation in NaMt samples, respectively. Similar sequence was noticed in H20@CT, but with much weaker BE decrease from 533.00 eV down to 531.65 eV and 531.74 eV after Cu and Ag incorporation. This suggests weaker metal retention in this organic composite. Such a BE weakening indicates lower electron binding to their parent-atom due to an attraction by next-neighboring species, and can be explained in terms of Lewis-Acid-Base (LAB) interaction between lattice oxygen and MNPs. This indicates weaker interaction with CuNPs as compared to AgNPs in both materials, and weaker retention strength of both metals in H20@CT.

BE decay was also noticed for Si and Al atoms from 1383.20 to 103 and 1411.29 to 75, respectively, suggesting additional MNP interactions with the aluminosilicate surface **(Fig. 2.b)** . The presence of a C1s signal in clay samples may be due to $CaCO_3$, as supported by the XRD pattern of bentonite with 113, 202 and 018 plane families between 40-45 degrees. XPS data, more particularly for cellulose-based samples (**Fig. S12**) showed no significant BE shift for C atom, indicating that carbon interaction with MNP, if any, is negligible.

3.7. Metal-induced antibacterial activity

E. coli DH5α and *B. subtilis* 168 were used as model species to evaluate mass transfer from the clay to bacteria. The 24 hours of incubation at 37 °C of untreated host matrices (NaMt, Boltorn^{TM}H20 and H20@NaMt) with a population of 74.10^6 CFU.mL^{-1} revealed no antibacterial activity in three independent experiments with both*E. coli* and *B. subtilis* strains. For conciseness, only data obtained with *B. subtilis* were mentioned herein (**Fig. 3.a)** . In contrast, copper-loaded (Cu/NaMt) and silver-loaded (Ag/NaMt) clays exhibited noticeable antibacterial activity **(Fig. 4)** , demonstrating that clay minerals can behave as MNP-hosting matrices**.** This improvement would be due to metal incorporation (Gordon et al., 2010; Potera, 2012; Vincent, Duval, Hartemann, & Engels-Deutsch, 2018; Yun'an Qing et al., 2018) but the mechanisms remain to be elucidated..

Fig. 4

3.8. Effect of metal dispersion upon dendrimer incorporation

The effect metal dispersion in dendrimer and their antibacterial activity were investigated by incubating silver and copper organoclay samples with bacteria. The results showed that the mere incorporation of metals regardless to the oxidation state induces antibacterial activity, slightly higher for the cationic form **(Fig. 5)** .

Fig. 5

The presence of dendrimer seems to play a key-role producing higher antibacterial activity as compared to Cu^0/NaMt and Ag^0/NaMt. This can be due to a higher metal dispersion within the dendrimer entanglement bearing OH groups that act as chelating agents (Lewis base) through their oxygen atoms. This was well supported by a marked increase in the inhibition zone diameter (**Table S1).** These data also revealed that both Cu^0 and Cu^{2+} are more effective than both silver forms. This can be explained by an easier release of copper (both zero and bivalent forms) in the liquid media due to lower BE shifts (as measured by XPS), as compared to silver. Also, copper is more reactive than silver, generating oxygen reactive species (ROS) as in Fenton-like and Haber-Weiss processes. Other possible contributions should be ascribed to lower amounts: ***(i)*** of inserted Ag^0 atoms probably because of the lower reduction level of Ag^+ cations and ***(ii)*** of dispersed

Ag^+ cation, chelated and stabilized by the polyol moiety. This was supported by SEM images (**Fig. 1.a**) that show large amount of non-dispersed rod-like silver salt crystals indicating a rigorous concordance between the material characterization data and antibacterial activity. Highest antibacterial ability was observed against Gram-positive *B. subtilis,* as illustrated by the largest inhibition zone diameter of 2.73±0.17cm **(Table S1).**This can be due to the very structure of the *Bacillus* cell wall with peptidoglycan multilayers and an abundant amount of pores that confers them more sensitivity to reactive species as compared to Gram-negative *E. coli* (Fu et al., 2015).

3.9. Effect of the amount of metal-loaded organoclay

Deeper insights through different amounts of metal-loaded organoclays ranging from 1 to 9 mg were achieved to confirm the effect of MNP insertion on their antibacterial activity. A first overview of the obtained results revealed that the bacterial growth was inhibited after an incubation with 1 mg antimicrobial agents **(Fig. 3.b)** . The average diameter of the inhibition zone was of 2-2.3 cm for Cu^{2+}/H20@NaMt and 0.8-2 cm Ag^+/H20@NaMt (**Table S2**). This result can be ascribed to the strong antibacterial capacity of metal-loaded organoclay matrices on *E. coli* and *Bacillus* . The appearance of antibacterial activity seems due to the metal incorporation, regardless to its oxidation state. In other words, the mere presence of metal species appears to promote an antibacterial activity. This is well argued by the fact that no antibacterial activity was found for both clay mineral and polyol alone **(Fig. 3.a)** . Therefore, the biocide effect of the as-synthesized samples should be due to the action of both MNPs and metal cations. The diameter of the inhibition zone of both strains *E. coli* and *B. subtilis* increased almost proportionally with increasing amount of bactericidal agents up to a certain level. Maximal values of 2.5 and 3.5 cm for 9 mg of Cu^{2+}/NaMt@H20 and of 2.4 and 3 cm for the same amount of Cu^0/NaMt@H20 against *E. coli* and *B. subtilis,* were respectively attained (**Table S2**).

Fig. 3

3.10. Effect of metal dispersion upon polyol-functionalized cellulose

Similar antibacterial tests were also performed with cellulose-based samples against both *E. coli* and *Bacillus* **(Fig. S13)** . Untreated cellulose denoted as CT and its polyol-functionalized counterpart (H20@CT) showed no antibacterial activity. Here also, the mere insertion of metal in both oxidation states induced antibacterial properties. The strong activity of Cu-loaded cellulose matrices against bacteria can be illustrated by inhibition zone diameters of 1.6 cm for Cu^0/CT and 1-3.5 cm for Cu^0/H20@CT**(Table 4)** . This confirms once again the beneficial role of dendrimer H20 incorporation favoring CuNP dispersion. Silver-based samples are less effective as antimicrobial agents against both *B. συβτιλις ανδ E. ϛολι ΔH5α, ω* hich can be related to a stronger HO:Ag interaction compared to HO:Cu interaction as supported by TPD measurements

Table 4

3.11. Action of Metal NPs against bacteria

The external side of the cell wall of both Gram-positive and Gram-negative bacteria bears negative charges due to the presence of functional groups like carboxyl and phosphate and hydroxyl (Ashmore et al., 2018). Gram-positive bacteria possess a thick peptidoglycan layer, which resides in linear chains alternating residues of N-acetylglucosamine (NAG) and N-acetylmuramic acid (NAM) linked together by a sequence of 3 to 5 amino acids that cross-link each other, giving rise to a cohesive mesh. Additionally, negatively charged teichoic acids (with high levels of phosphate groups) are spread from the cell wall to the surface of most Gram-positive bacteria **(Scheme S4.a)** . In contrast, Gram-negative bacteria display more complex structure with a thinner layer of peptidoglycan and a phospholipid outer membrane with partially phosphorylated lipopolysaccharides (LPS) that contribute to raise the negative surface charge **(Scheme S4.b)** (Stensberg et al., 2011).

Negatively charged bacterial cell walls interact with positively charged particles such as metal cations via electrostatic interactions. Cations may act through diverse pathways among which two seem to prevail in aqueous media: (i) strong electrostatic interaction that alter bacteria membrane equilibrium, and (ii) Lewis acid-base

interaction with water molecules that generates Bronsted acidity ($M^{n+} + xH_2O = [M(H_2O)_{(x-1)}OH]^{(n-1)+} + H^+$) that may alter bacteria membrane. The metal ions are then free to interact with cellular structures (*e.g.*,proteins, membranes, DNA), disrupting cell functions (Ashmore et al., 2018). In contrast, MNPs are supposed to interact via strong LAB interaction with atoms bearing available electron pairs (O, S, and N) that act as Lewis base. Such interactions are assumed to affect the normal cell exchange through bacteria membrane. Other mechanisms such MNP diffusion inside the cell and disrupt biological processes (Stensberg et al., 2011). Inside the cell, both metal cation and nanoparticles can generate reactive oxygen species (ROS) like hydrogen peroxide (H_2O_2, superoxide anion ($\cdot O_2^-$), and hydroxyl radical $^*OH$ (Gordon et al., 2010; Yun'an Qing et al., 2018). These species are assumed to bind to phosphate groups inhibiting protein phosphorylation frequently involved in enzymatic activation. This is expected to inhibit bacterial growth and cell cycle through the dephosphorylation of some important proteins for enzymatic activities (Dakal, Kumar, Majumdar, & Yadav, 2016). Given that metals bind to biomolecules through non-specific interactions, MNPs generally exhibit a wide variety of processes against bacteria **(Scheme S4.c)** (Yuan, Ding, Yang, & Xu, 2018).

Once inside the cell, both AgNPs and Ag^+ ions interact with diverse species resulting in cell dysfunction. Reportedly, AgNPs can act through four main mechanism pathways: (i) attraction on bacterial surface; (ii) destabilization of the bacterial cell wall and increase in membrane permeability even for larger AgNPs (Losasso et al., 2014); (iii) genesis of ROS and free radicals that induce toxicity and oxidative stress; (iv) modification of signal transduction pathways (Dakal et al., 2016). AgNP adsorption on the bacterial surface can be followed by diffusion of smaller particle inside the cell and retention of larger ones on the external side of the bacteria membrane. In spite of their antibacterial activity (Avalos, Haza, Mateo, & Morales, 2013), AgNPs were found to be less performant that cations (El Badawy et al., 2011). The latter are much more attracted by the negative charges of bacterial walls (Slavin, Asnis, Hafeli, & Bach, 2017). However, AgNPs may also act through partial dissolution into Ag^+ cations, as reported by many works. The Ag^+ cations act differently by binding to the cell membrane inducing changes in the membrane potential and proton leakage (Losasso et al., 2014). Reportedly, Ag^+ cation may intercalate DNA segments generating complexes with nucleotides and disrupting H-bonds between base pairs (Yun'an Qing et al., 2018). Similar observations were made for CuNPs where a Cu^{2+} release was found to be the main contribution to the high antibacterial activity (Chatterjee, Chakraborty, & Basu, 2014; Sistematica, Gabriela, Daniela, & Helia, 2016). As for silver, CuNP action may also involve diverse mechanisms, the most reported by the literature being: (i) CuNP concentration and dissolution in the bacterial membrane inducing potential and permeability changes, with unavoidable leak in lipopolysaccharides, membrane proteins, intracellular biomolecules and protons (Amro et al., 2000; Azam, Ahmed, Oves, Khan, & Memic, 2012). (ii) production of ROS, MNPs oxidation and dissolution into Cu^{2+} cation, with other detrimental oxidative processes (Fenton, Harber-Weiss) processes (Applerot et al., 2012; Fang, Lyon, Wiesner, Dong, & Alvarez, 2007); (iii) Accumulation of Cu^{2+} cation with decay in intracellular ATP production and disruption of DNA replication (Kim et al., 2007; Sondi & Salopek-Sondi, 2004). These pathways should confer higher activity to CuNPs against both bacteria compared with AgNPs (Chudobova & Kizek, 2015).

Conclusion

Metal dispersion in the form of AgNPs and CuNPs with polyol dendrimer resulted in higher antibacterial activity than merely spread on a solid surface of montmorillonite or cellulose fibers. Both cellulose and clay act as host matrices for MNP when previously coated by BoltornH20. Polyol dendrimer incorporation induces no detectable antibacterial activity but provides additional hydroxyl groups that act as chelating agents for both MNPs and metal cations. The strength of the –HO:Metal interaction plays a key-role in metal retention/release processes and, subsequently, in the antibacterial activity of the metal loaded polyol-clay or polyol-cellulose composite against both Gram-positive and Gram-negative bacteria. Weaker retention of CuNPs and its involvement in oxidative damage explains, at least in part, the higher antibacterial activity of CuNPs as compared to silver counterparts. The occurrence of an optimal amount of metal-loaded polyol composites for achieving a high biocidal effect is attributed to structure compaction and diffusion hindrance of metal species at abundant number of -OH groups incorporated. Research is still in progress for designing

even more effective antibacterial matrices with natural and low-cost materials and modulable entanglement porosity.

Acknowledgements: ***This work was supported by NSERC (To Pr. Mircea A. Mateescu). The authors appreciate the technical assistance of Dr. G. Chamoulaud (Nanoqam), Dr. Alain Adnot (Laval University) and Dainelys Guadarrama Bello (UdeM).***

References:

Amro, N. A., Kotra, L. P., Wadu-Mesthrige, K., Bulychev, A., Mobashery, S., & Liu, G.-y. (2000). High-resolution atomic force microscopy studies of the Escherichia coli outer membrane: structural basis for permeability. *Langmuir, 16* (6), 2789-2796.

Applerot, G., Lellouche, J., Lipovsky, A., Nitzan, Y., Lubart, R., Gedanken, A., & Banin, E. (2012). Understanding the antibacterial mechanism of CuO nanoparticles: revealing the route of induced oxidative stress. *Small, 8* (21), 3326-3337.

Ashmore, D. A., Chaudhari, A., Barlow, B., Barlow, B., Harper, T., Vig, K., . . . Pillai, S. (2018). Evaluation of E. coli inhibition by plain and polymer-coated silver nanoparticles. *Revista do Instituto de Medicina Tropical de Sao Paulo, 60* .

Avalos, A., Haza, A., Mateo, D., & Morales, P. (2013). Nanoparticulas de plata: aplicaciones y riesgos toxicos para la salud humana y el medio ambiente/Silver nanoparticles: applications and toxic risks to human heatlh and environment. *Revista Complutense de Ciencias Veterinarias, 7* (2), 1.

Azam, A., Ahmed, A. S., Oves, M., Khan, M., & Memic, A. (2012). Size-dependent antimicrobial properties of CuO nanoparticles against Gram-positive and-negative bacterial strains. *International journal of nanomedicine, 7* , 3527.

Azzouz, A., Assaad, E., Ursu, A.-V., Sajin, T., Nistor, D., & Roy, R. (2010). Carbon dioxide retention over montmorillonite–dendrimer materials. *Applied Clay Science, 48* (1-2), 133-137.

Azzouz, A., Nistor, D., Miron, D., Ursu, A., Sajin, T., Monette, F., . . . Hausler, R. (2006). Assessment of acid–base strength distribution of ion-exchanged montmorillonites through NH3 and CO2-TPD measurements.*Thermochimica Acta, 449* (1-2), 27-34.

Beltrao-Nunes, A.-P., Sennour, R., Arus, V.-A., Anoma, S., Pires, M., Bouazizi, N., . . . Azzouz, A. (2019). CO2 capture by coal ash-derived zeolites-roles of the intrinsic basicity and hydrophilic character.*Journal of Alloys and Compounds, 778* , 866-877.

Bragg, P., & Rainnie, D. (1974). The effect of silver ions on the respiratory chain of Escherichia coli. *Canadian journal of microbiology, 20* (6), 883-889.

Carretero, M. I. (2002). Clay minerals and their beneficial effects upon human health. A review. *Applied Clay Science, 21* (3-4), 155-163.

Chatterjee, A. K., Chakraborty, R., & Basu, T. (2014). Mechanism of antibacterial activity of copper nanoparticles. *Nanotechnology, 25* (13), 135101.

Chudobova, D., & Kizek, R. (2015). Nanotechnology in diagnosis, treatment and prophylaxis of infectious diseases. *Journal of Metallomics and Nanotechnologies, 2* , 67-69.

Čık, G., Bujdáková, H., & Šeršeň, F. (2001). Study of fungicidal and antibacterial effect of the Cu (II)-complexes of thiophene oligomers synthesized in ZSM-5 zeolite channels. *Chemosphere, 44* (3), 313-319.

Čík, G., Priesolová, S., Bujdáková, H., Šeršeň, F., Potheöová, T., & Krištín, J. (2006). Inactivation of bacteria G+-S. aureus and G–E. coli by phototoxic polythiophene incorporated in ZSM-5 zeolite.*Chemosphere, 63* (9), 1419-1426.

Costa, C., Conte, A., Buonocore, G. G., & Del Nobile, M. A. (2011). Antimicrobial silver-montmorillonite nanoparticles to prolong the shelf life of fresh fruit salad. *International Journal of Food Microbiology, 148* (3), 164-167.

Cragg, G. M., & Newman, D. J. (2013). Natural products: a continuing source of novel drug leads. *Biochimica et Biophysica Acta (BBA)-General Subjects, 1830* (6), 3670-3695.

Crooks, R. M., Zhao, M., Sun, L., Chechik, V., & Yeung, L. K. (2001). Dendrimer-encapsulated metal nanoparticles: synthesis, characterization, and applications to catalysis. *Accounts of chemical research, 34* (3), 181-190.

Dakal, T., Kumar, A., Majumdar, R., & Yadav, V. (2016). Mechanistic basis of antimicrobial actions of silver nanoparticles. Front Microbiol. 2016; 7: 1831. In.

Dizman, B., Badger, J. C., Elasri, M. O., & Mathias, L. J. (2007). Antibacterial fluoromicas: a novel delivery medium. *Applied Clay Science, 38* (1-2), 57-63.

El Badawy, A. M., Silva, R. G., Morris, B., Scheckel, K. G., Suidan, M. T., & Tolaymat, T. M. (2011). Surface charge-dependent toxicity of silver nanoparticles. *Environmental science & technology, 45* (1), 283-287.

Espana, V. A. A., Sarkar, B., Biswas, B., Rusmin, R., & Naidu, R. (2019). Environmental applications of thermally modified and acid activated clay minerals: current status of the art. *Environmental Technology & Innovation, 13* , 383-397.

Fang, J., Lyon, D. Y., Wiesner, M. R., Dong, J., & Alvarez, P. J. (2007). Effect of a fullerene water suspension on bacterial phospholipids and membrane phase behavior. *Environmental science & technology, 41* (7), 2636-2642.

Fu, F., Li, L., Liu, L., Cai, J., Zhang, Y., Zhou, J., & Zhang, L. (2015). Construction of cellulose based ZnO nanocomposite films with antibacterial properties through one-step coagulation. *ACS applied materials & interfaces, 7* (4), 2597-2606.

Gordon, O., Slenters, T. V., Brunetto, P. S., Villaruz, A. E., Sturdevant, D. E., Otto, M., . . . Fromm, K. M. (2010). Silver coordination polymers for prevention of implant infection: thiol interaction, impact on respiratory chain enzymes, and hydroxyl radical induction. *Antimicrobial agents and chemotherapy, 54* (10), 4208-4218.

Gupta, A., Maynes, M., & Silver, S. (1998). Effects of halides on plasmid-mediated silver resistance in Escherichia coli. *Appl. Environ. Microbiol., 64* (12), 5042-5045.

Hellmann, J., Hamano, M., Karthaus, O., Ijiro, K., Shimomura, M., & Irie, M. (1998). Aggregation of dendrimers with a photochromic dithienylethene core group on the mica surface-atomic force microscopic imaging. *Japanese journal of applied physics, 37* (7A), L816.

Herrera, P., Burghardt, R., & Phillips, T. (2000). Adsorption of Salmonella enteritidis by cetylpyridinium-exchanged montmorillonite clays. *Veterinary microbiology, 74* (3), 259-272.

Joshi, M., Purwar, R., Udakhe, J. S., & Sreedevi, R. (2015). Antimicrobial nanocomposite compositions, fibers and films. In: Google Patents.

Kim, J. S., Kuk, E., Yu, K. N., Kim, J.-H., Park, S. J., Lee, H. J., . . . Hwang, C.-Y. (2007). Antimicrobial effects of silver nanoparticles.*Nanomedicine: Nanotechnology, Biology and Medicine, 3* (1), 95-101.

Komadel, P. (2016). Acid activated clays: Materials in continuous demand. *Applied Clay Science, 131* , 84-99.

Levy, S. B. (1998). The challenge of antibiotic resistance.*Scientific American, 278* (3), 46-53.

Losasso, C., Belluco, S., Cibin, V., Zavagnin, P., Mičetić, I., Gallocchio, F., . . . Ricci, A. (2014). Antibacterial activity of silver nanoparticles: sensitivity of different Salmonella serovars.*Frontiers in microbiology, 5* , 227.

Martin, S., & Griswold, W. (2009). Human health effects of heavy metals. *Environmental Science and Technology briefs for citizens, 15* , 1-6.

Nabil, B., Christine, C., Julien, V., & Abdelkrim, A. (2018). Polyfunctional cotton fabrics with catalytic activity and antibacterial capacity. *Chemical Engineering Journal, 351* , 328-339.

Nadziakiewicza, M., Kehoe, S., & Micek, P. (2019). Physico-Chemical Properties of Clay Minerals and Their Use as a Health Promoting Feed Additive. *Animals, 9* (10), 714.

Potera, C. (2012). Understanding the germicidal effects of silver nanoparticles. In: National Institute of Environmental Health Sciences.

Rai, M., Yadav, A., & Gade, A. (2009). Silver nanoparticles as a new generation of antimicrobials. *Biotechnology advances, 27* (1), 76-83.

Rees, N. V., Zhou, Y. G., & Compton, R. G. (2011). The aggregation of silver nanoparticles in aqueous solution investigated via anodic particle coulometry. *ChemPhysChem, 12* (9), 1645-1647.

Sistemática, D. d. C. R. R., Gabriela, S.-S., Daniela, F.-R., & Helia, B.-T. (2016). Copper Nanoparticles as Potential Antimicrobial Agent in Disinfecting Root Canals. A Systematic Review. *Int. J. Odontostomat, 10* (3), 547-554.

Slavin, Y. N., Asnis, J., Häfeli, U. O., & Bach, H. (2017). Metal nanoparticles: understanding the mechanisms behind antibacterial activity. *Journal of nanobiotechnology, 15* (1), 65.

Sondi, I., & Salopek-Sondi, B. (2004). Silver nanoparticles as antimicrobial agent: a case study on E. coli as a model for Gram-negative bacteria. *Journal of colloid and interface science, 275* (1), 177-182.

Stavitskaya, A., Batasheva, S., Vinokurov, V., Fakhrullina, G., Sangarov, V., Lvov, Y., & Fakhrullin, R. (2019). Antimicrobial applications of clay nanotube-based composites. *Nanomaterials, 9* (5), 708.

Stensberg, M. C., Wei, Q., McLamore, E. S., Porterfield, D. M., Wei, A., & Sepúlveda, M. S. (2011). Toxicological studies on silver nanoparticles: challenges and opportunities in assessment, monitoring and imaging. *Nanomedicine, 6* (5), 879-898.

Sulpizi, M., Gaigeot, M. P., & Sprik, M. (2012). The Silica-Water Interface: How the Silanols Determine the Surface Acidity and Modulate the Water Properties. *J Chem Theory Comput, 8* (3), 1037-1047. doi:10.1021/ct2007154

Terrab, I., Boukoussa, B., Hamacha, R., Bouchiba, N., Roy, R., Bengueddach, A., & Azzouz, A. (2016). Insights in CO2 interaction on zeolite omega-supported polyol dendrimers. *Thermochimica Acta, 624* , 95-101.

Thuc, C.-N. H., Grillet, A.-C., Reinert, L., Ohashi, F., Thuc, H. H., & Duclaux, L. (2010). Separation and purification of montmorillonite and polyethylene oxide modified montmorillonite from Vietnamese bentonites.*Applied Clay Science, 49* (3), 229-238.

Vdović, N., Jurina, I., Škapin, S. D., & Sondi, I. (2010). The surface properties of clay minerals modified by intensive dry milling—revisited. *Applied Clay Science, 48* (4), 575-580.

Vincent, M., Duval, R. E., Hartemann, P., & Engels-Deutsch, M. (2018). Contact killing and antimicrobial properties of copper. *Journal of Applied microbiology, 124* (5), 1032-1046.

Williams, L. B., Metge, D. W., Eberl, D. D., Harvey, R. W., Turner, A. G., Prapaipong, P., & Poret-Peterson, A. T. (2011). What makes a natural clay antibacterial? *Environmental science & technology, 45* (8), 3768-3773.

Yuan, P., Ding, X., Yang, Y. Y., & Xu, Q. H. (2018). Metal nanoparticles for diagnosis and therapy of bacterial infection.*Advanced healthcare materials, 7* (13), 1701392.

Yun'an Qing, L. C., Li, R., Liu, G., Zhang, Y., Tang, X., Wang, J., . . . Qin, Y. (2018). Potential antibacterial mechanism of silver nanoparticles and the optimization of orthopedic implants by advanced modification technologies. *International journal of nanomedicine, 13* , 3311.

Tables

Table 1. CO_2 retention capacity (mmol.g^{-1}) for the synthesized clay and CT-based samples

Clay samples	CRC	WRC	CT samples	CRC
Bentonite	2101.082	1.2282E-05	CT	-
NaMt	2261.979	2.0257E-06	H20@CT	38.35921
Ash	1752.185	1.91539E-06	Cu^0/H20@CT	14.54479
Cu^0 /NaMt	55.418	-	Ag^0/H20@CT	5.661805
Ag^0 NaMt	662.8791	-		

Table 2. Weight loss of clay and cellulose-based samples for different temperature ranges.

Sample	Temperature (°C)	Wight loos (%)
NaMt	40-90	0.7-0.8
Cu^0/NaMt	140-480	6.6
Ag^0/NaMt	90-470	9.4
CT	47-130	0-0.1
H20@CT	47-185	0.275
Cu^0/CT	43-190	8.25
Ag^0/CT	47-200	8.74
Cu^0/H20@CT	32-200	4.675
Ag^0/H20@CT	40-200	8.525

Table 3. Binding energy (eV) shifts for key elements in the synthesized materials

Element's name	Binding energy (eV)	Binding energy (eV)	Binding energy (eV)	Binding energy (eV)	Binding ener
	NaMt	Cu^0/NaMt	Ag^0/NaMt	CT	H20@CT
O 1s	532.55	531	527	533	532
C 1s	285.55	285	285	285	285
Al 2s	115	85.6	75.55	-	-
Si 2s	154.55	103	149	-	-
Ag 3d	-	-	364	-	-
Cu 2p	-	933	-	-	-
Ca 2s	439.55	-	-		-
Fe 2p	714.55	-	709		-

Table 4. Bacterial inhibition diameters (cm) and antibacterial activity evaluation for various studied CT-based systems

Investigated system	CT	Boltorn^{TM}H20	H20@CT	Ag^0/CT	Cu^0/CT	Cu^0/H20@CT	Ag^0/H20@CT

Bacillus (cm)	-	-	-	1	1.6	3.5	2
Antibacterial activity	No	No	No	Strong	Strong	Strong	Strong
E. coli (cm)	-	-	-	-	0.5	1	0.9
Antibacterial activity	No	No	No	No	Weak	Strong	Weak

Figure & Scheme captions

Scheme 1. Schematic illustration of NaMt based samples before (H20@NaMt) and after metal dispersion (Metal/H20@NaMt) (a) and of CT based samples before (H20@CT) and after metal dispersion (Metal/H20@CT) (b).

Fig. 1. SEM of unloaded and of metal loaded NaMt and H20@CT (a) and of untreated cellulose (CT), polyol-functionalized cellulose (H20@CT), metal zero-loaded cellulose (MNPs/CT and MNPs/H20@CT) (b).

Fig. 2. XPS graphs of untreated NaMt and metal loaded counterparts (a) and of two key elements (Al2p, Si2p) for both NaMt and Ag^0/NaMt (b).

Fig. 3. Effect of untreated matrices on *Bacillus Subtilis168* proliferation . Bacteria strain was incubated for 24h at 37°C with 5 mg of untreated clays NaMt (left dish), Boltorn^{TM} H20 (middle dish) and H20@NaMt (right dish) (a). **Average diameter and dependence of inhibition zone of*E. coli* and *B. subtilis* treated with various amounts of antibacterial agents.** All Petri dishes were incubated for 24h at 37°C with a cell density of 0.5 at 600 nm (b).

Fig. 4. Antibacterial test of Ag^0/NaMt and Cu^0/NaMt clay- based samples . *Escherichia coli*(a1 and b1), *Bacillus subtilis168* (a2 and b2) were incubated for 24h at 37 °C with 5 mg of Cu^0/NaMt (a1-2) or Ag^0/NaMt (b1-2).

Fig. 5. Antibacterial test of MNP loaded in organoclay- based samples . *Escherichia coli* (a1, b1, c1 and d1),*Bacillus subtilis168* (a2, b2, c2 and d2) were incubated for 24h at 37 °C with 5 mg of Ag^0/H20@NaMt (a1-2); Cu^0/H20@NaMt (b1-2); Ag^+/H20@NaMt (c1-2) and Cu^{2+}/H20@NaMt (d1-2).

Hosted file

`Figures & Schemes.docx` available at https://authorea.com/users/338170/articles/464175-metal-loaded-porous-polyhydroxylic-matrices-with-improved-antibacterial-properties

BIBLIOGRAPHY

Abbanat, D., Morrow, B. et Bush, K. (2008). New agents in development for the treatment of bacterial infections. *Current opinion in pharmacology, 8*, p.582-92

Aberdein, J., Cole, J., Bewley, M., Marriott, H. et Dockrell, D. (2013). Alveolar macrophages in pulmonary host defence–the unrecognized role of apoptosis as a mechanism of intracellular bacterial killing. *Clinical & Experimental Immunology, 174*, p.193-202

Abou-Melha, K. S. (2008). Transition metal complexes of isonicotinic acid (2-hydroxybenzylidene) hydrazide. *Spectrochimica Acta Part A: Molecular and Biomolecular Spectroscopy, 70*, p.162-70

Adekunle, O. O. (2012). Mechanisms of antimicrobial resistance in bacteria, general approach. *International Journal of Pharma Medicine and Biological Sciences, 1*, p.166-87

Akhtar, M. S., Panwar, J. et Yun, Y.-S. (2013). Biogenic synthesis of metallic nanoparticles by plant extracts. *ACS Sustainable Chemistry & Engineering, 1*, p.591-602

Al-Obeid, S., Collatz, E. et Gutmann, L. (1990). Mechanism of resistance to vancomycin in Enterococcus faecium D366 and Enterococcus faecalis A256. *Antimicrobial Agents and Chemotherapy, 34*, p.252-6

Al-Sha'alan, N. H. (2007). Antimicrobial activity and spectral, magnetic and thermal studies of some transition metal complexes of a Schiff base hydrazone containing a quinoline moiety. *Molecules, 12*, p.1080-91

Alavi, M. et Rai, M. (2019). Recent advances in antibacterial applications of metal nanoparticles (MNPs) and metal nanocomposites (MNCs) against multidrug-resistant (MDR) bacteria. *Expert review of anti-infective therapy, 17*, p.419-28

Alavi, M. et Rai, M. (2020). Topical delivery of growth factors and metal/metal oxide nanoparticles to infected wounds by polymeric nanoparticles: an overview. *Expert Review of Anti-infective Therapy, 18*, p.1021-32

Ali, A., Shah, T., Ullah, R., Zhou, P., Guo, M., Ovais, M., Rui, Y. (2021). Review on recent progress in magnetic nanoparticles: Synthesis, characterization, and diverse applications. *Frontiers in Chemistry, 9*, p.629054

Allafchian, A. et Hosseini, S. S. (2019). Antibacterial magnetic nanoparticles for therapeutics: a review. *IET nanobiotechnology, 13*, p.786-99

Allan, D. L. et Jarrell, W. M. (1989). Proton and copper adsorption to maize and soybean root cell walls. *Plant Physiology, 89*, p.823-32

Allen, H. K., Donato, J., Wang, H. H., Cloud-Hansen, K. A., Davies, J. et Handelsman, J. (2010). Call of the wild: antibiotic resistance genes in natural environments. *Nature Reviews Microbiology, 8*, p.251-9

Allen, S. L., Sharma, J. N. et Zamborini, F. P. (2017). Aggregation-dependent oxidation of metal nanoparticles. *Journal of the American Chemical Society, 139*, p.12895-8

Allen, V. G., Seah, C., Martin, I. et Melano, R. G. (2014). Azithromycin resistance is coevolving with reduced susceptibility to cephalosporins in Neisseria gonorrhoeae in Ontario, Canada. *Antimicrob. Agents Chemother., 58*, p.2528-34

Alothman, M., Ispas-Szabo, P. et Mateescu, M. A. (2021). Design of Catalase Monolithic Tablets for Intestinal Targeted Delivery. *Pharmaceutics, 13*, p.69

Alsohaimi, I. H., Nassar, A. M., Elnasr, T. a. S. et Amar Cheba, B. (2020). A novel composite silver nanoparticles loaded calcium oxide stemming from egg shell recycling: a potent photocatalytic and antibacterial activities. *Journal of Cleaner Production, 248*, p.119274

Alswat, A. A., Ahmad, M. B., Saleh, T. A., Hussein, M. Z. B. et Ibrahim, N. A. (2016). Effect of zinc oxide amounts on the properties and antibacterial activities of zeolite/zinc oxide nanocomposite. *Materials Science and Engineering: C, 68*, p.505-11

Amabile-Cuevas, C. (2010). Antibiotic resistance in Mexico: a brief overview of the current status and its causes. *The Journal of Infection in Developing Countries, 4*, p.126-31

Amendola, V. et Meneghetti, M. (2009). Laser ablation synthesis in solution and size manipulation of noble metal nanoparticles. *Physical chemistry chemical physics, 11*, p.3805-21

Amro, N. A., Kotra, L. P., Wadu-Mesthrige, K., Bulychev, A., Mobashery, S. et Liu, G.-Y. (2000). High-resolution atomic force microscopy studies of the Escherichia coli outer membrane: structural basis for permeability. *Langmuir, 16*, p.2789-96

Anirudhan, T. et Parvathy, J. (2014). Novel semi-IPN based on crosslinked carboxymethylstarch and clay for the in vitro release of theophylline. *International Journal of Biological Macromolecules, 67*, p.238-45

Ansari, S. a. M. K., Ficiarà, E., Ruffinatti, F. A., Stura, I., Argenziano, M., Abollino, O., D'agata, F. (2019). Magnetic iron oxide nanoparticles: synthesis, characterization and functionalization for biomedical applications in the central nervous system. *Materials, 12*, p.465

Applerot, G., Lellouche, J., Lipovsky, A., Nitzan, Y., Lubart, R., Gedanken, A. et Banin, E. (2012). Understanding the antibacterial mechanism of CuO nanoparticles: revealing the route of induced oxidative stress. *Small, 8*, p.3326-37

Aree, T. (2019). Understanding structures and thermodynamics of beta-cyclodextrin encapsulation of chlorogenic, caffeic and quinic acids: Implications for enriching antioxidant capacity and masking bitterness in coffee. *Food Chemistry, 293*, p.550-60

Arus , A. V., Tahir, M. N., Sennour, R., Shiao, T. C., Sallam, L. M., Nistor, I. D., Azzouz, A. (2016a). Cu0 and Pd0 loaded Organo-Bentonites as Sponge–like Matrices for Hydrogen Reversible Capture at Ambient Conditions. *ChemistrySelect, 1*, p.1452-61

Arus , A. V., Tahir, M. N., Sennour, R., Shiao, T. C., Sallam, L. M., Nistor, I. D., Azzouz, A. (2016b). Cu0and Pd0loaded Organo-Bentonites as Sponge-like Matrices for Hydrogen Reversible Capture at Ambient Conditions. *ChemistrySelect, 1*, p.1452-61

Arus, V. A., Nousir, S., Sennour, R., Shiao, T. C., Nistor, I. D., Roy, R. et Azzouz, A. (2018). Intrinsic affinity of acid-activated bentonite towards hydrogen and carbon dioxide. *International Journal of Hydrogen Energy, 43*, p.7964-72

Ash, R. J., Mauck, B. et Morgan, M. (2002). Antibiotic resistance of gram-negative bacteria in rivers, United States. *Emerging infectious diseases, 8*, p.713

Ashmore, D. A., Chaudhari, A., Barlow, B., Barlow, B., Harper, T., Vig, K., Pillai, S. (2018). Evaluation of E. coli inhibition by plain and polymer-coated silver nanoparticles. *Revista do Instituto de Medicina Tropical de São Paulo, 60*, p.

Auría-Soro, C., Nesma, T., Juanes-Velasco, P., Landeira-Viñuela, A., Fidalgo-Gomez, H., Acebes-Fernandez, V., Fuentes, M. (2019). Interactions of nanoparticles and biosystems: microenvironment of nanoparticles and biomolecules in nanomedicine. *Nanomaterials, 9*, p.1365

Ávalos, A., Haza, A., Mateo, D. et Morales, P. (2013). Nanopartículas de plata: aplicaciones y riesgos tóxicos para la salud humana y el medio ambiente/Silver nanoparticles: applications and toxic risks to human heatlh and environment. *Revista Complutense de Ciencias Veterinarias, 7*, p.1

Azam, A., Ahmed, A. S., Oves, M., Khan, M. et Memic, A. (2012). Size-dependent antimicrobial properties of CuO nanoparticles against Gram-positive and-negative bacterial strains. *International journal of nanomedicine, 7*, p.3527

Azhar, A., Rasool, S., Haque, A., Shan, S., Saeed, M., Ehsan, B. et Haque, A. (2017). Detection of high levels of resistance to linezolid and vancomycin in Staphylococcus aureus. *J. Med. Microbiol., 66*, p.1328-31

Azmi, I. J., Khajanchi, B. K., Akter, F., Hasan, T. N., Shahnaij, M., Akter, M., Ahmed, M. K. (2014). Fluoroquinolone resistance mechanisms of Shigella flexneri isolated in Bangladesh. *PloS one, 9*, p.e102533

Azzouz, A., Aruş, V.-A., Platon, N., Ghomari, K., Nistor, I.-D., Shiao, T. C. et Roy, R. (2013a). Polyol-modified layered double hydroxides with attenuated basicity for a truly reversible capture of CO2. *Adsorption, 19*, p.909-18

Azzouz, A., Assaad, E., Ursu, A.-V., Sajin, T., Nistor, D. et Roy, R. (2010). Carbon dioxide retention over montmorillonite–dendrimer materials. *Applied Clay Science, 48*, p.133-7

Azzouz, A., Nistor, D., Miron, D., Ursu, A., Sajin, T., Monette, F., Hausler, R. (2006). Assessment of acid–base strength distribution of ion-exchanged montmorillonites through NH3 and CO2-TPD measurements. *Thermochimica Acta, 449*, p.27-34

Azzouz, A., Nousir, S., Bouazizi, N. et Roy, R. (2015). Metal–inorganic–organic matrices as efficient sorbents for hydrogen storage. *ChemSusChem, 8*, p.800-3

Azzouz, A., Nousir, S., Platon, N., Ghomari, K., Hersant, G., Bergeron, J.-Y., Roy, R. (2013b). Preparation and characterization of hydrophilic organo-montmorillonites through incorporation of non-ionic polyglycerol dendrimers derived from soybean oil. *Materials Research Bulletin, 48*, p.3466-73

Azzouz, A., Nousir, S., Platon, N., Ghomari, K., Shiao, T. C., Hersant, G., Roy, R. (2013c). Truly reversible capture of CO2 by montmorillonite intercalated with soya oil-derived polyglycerols. *International Journal of Greenhouse Gas Control, 17*, p.140-7

Azzouz, A., Platon, N., Nousir, S., Ghomari, K., Nistor, D., Shiao, T. C. et Roy, R. (2013d). OH-enriched organo-montmorillonites for potential applications in carbon dioxide separation and concentration. *Separation and Purification Technology, 108*, p.181-8

Bajpai, S., Chand, N. et Chaurasia, V. (2010). Investigation of water vapor permeability and antimicrobial property of zinc oxide nanoparticles-loaded chitosan-based edible film. *Journal of Applied Polymer Science, 115*, p.674-83

Bajpai, S. K., Chand, N. et Chaurasia, V. (2012). Nano zinc oxide-loaded calcium alginate films with potential antibacterial properties. *Food and Bioprocess Technology, 5*, p.1871-81

Bandla, M., Abbavaram, B. R., Kokkarachedu, V. et Sadiku, R. E. (2017). Silver nanoparticles incorporated within intercalated clay/polymer nanocomposite hydrogels for antibacterial studies. *Polymer Composites, 38*, p.E16-E23

Baranovskiy, A. G., Babayeva, N. D., Suwa, Y., Gu, J., Pavlov, Y. I. et Tahirov, T. H. (2014). Structural basis for inhibition of DNA replication by aphidicolin. *Nucleic Acids Res., 42*, p.14013-21

Barros, D., Pradhan, A., Mendes, V. M., Manadas, B., Santos, P. M., Pascoal, C. et Cássio, F. (2019). Proteomics and antioxidant enzymes reveal different mechanisms of toxicity induced by ionic and nanoparticulate silver in bacteria. *Environmental Science: Nano, 6*, p.1207-18

Baun, D. L. et Christensen, T. H. (2004). Speciation of heavy metals in landfill leachate: a review. *Waste management & research, 22*, p.3-23

Behrouzi, A., Vaziri, F., Rad, F. R., Amanzadeh, A., Fateh, A., Moshiri, A., Siadat, S. D. (2018). Comparative study of pathogenic and non-pathogenic Escherichia coli outer membrane vesicles and prediction of host-interactions with TLR signaling pathways. *BMC research notes, 11*, p.1-7

Beltrao-Nunes, A.-P., Sennour, R., Arus, V.-A., Anoma, S., Pires, M., Bouazizi, N., Azzouz, A. (2019). CO2 capture by coal ash-derived zeolites-roles of the intrinsic basicity and hydrophilic character. *Journal of Alloys and Compounds, 778*, p.866-77

Benjamin, J. S. (1970). Dispersion strengthened superalloys by mechanical alloying. *Metallurgical transactions, 1*, p.2943-51

Bergaya, F. et Lagaly, G. (2013). *Handbook of clay science*. Newnes

Biegański, P., Szczupak, Ł., Arruebo, M. et Kowalski, K. (2021). Brief survey on organometalated antibacterial drugs and metal-based materials with antibacterial activity. *RSC Chemical Biology, 2*, p.368-86

Biehl, P., Von Der Lühe, M., Dutz, S. et Schacher, F. H. (2018). Synthesis, characterization, and applications of magnetic nanoparticles featuring polyzwitterionic coatings. *Polymers, 10*, p.91

Bilal, M., Rasheed, T., Iqbal, H. M., Li, C., Hu, H. et Zhang, X. (2017). Development of silver nanoparticles loaded chitosan-alginate constructs with biomedical potentialities. *International journal of biological macromolecules, 105*, p.393-400

Binzet, G., Arslan, H., Flörke, U., Külcü, N. et Duran, N. (2006). Synthesis, characterization and antimicrobial activities of transition metal complexes of N, N-dialkyl-N'-(2-chlorobenzoyl) thiourea derivatives. *Journal of Coordination Chemistry, 59*, p.1395-406

Bondarenko, O., Ivask, A., Käkinen, A., Kurvet, I. et Kahru, A. (2013). Particle-cell contact enhances antibacterial activity of silver nanoparticles. *PLoS One, 8*, p.e64060

Bouazizi, N., Barrimo, D., Nousir, S., Ben Slama, R., Shiao, T. C., Roy, R. et Azzouz, A. (2017a). Metal-loaded polyol-montmorillonite with improved affinity towards hydrogen. *Journal of the Energy Institute, 402*, p.314–22

Bouazizi, N., Barrimo, D., Nousir, S., Ben Slama, R., Shiao, T. C., Roy, R. et Azzouz, A. (2018a). Metal-loaded polyol-montmorillonite with improved affinity towards hydrogen. *Journal of the Energy Institute, 91*, p.110-9

Bouazizi, N., Barrimo, D., Nousir, S., Slama, R. B., Roy, R. et Azzouz, A. (2017b). Montmorillonite-supported Pd0, Fe0, Cu0 and Ag0 nanoparticles: properties and affinity towards CO2. *Applied Surface Science, 402*, p.314-22

Bouazizi, N., Barrimo, D., Nousir, S., Slama, R. B., Shiao, T., Roy, R. et Azzouz, A. (2018b). Metal-loaded polyol-montmorillonite with improved affinity towards hydrogen. *Journal of the Energy Institute, 91*, p.110-9

Bragg, P. et Rainnie, D. (1974). The effect of silver ions on the respiratory chain of Escherichia coli. *Canadian journal of microbiology, 20*, p.883-9

Bruggraber, S. F., French, G., Thompson, R. P. et Powell, J. J. (2004). Selective and effective bactericidal activity of the cobalt (II) cation against Helicobacter pylori. *Helicobacter, 9*, p.422-8

Butler, M. S. et Buss, A. D. (2006). Natural products—the future scaffolds for novel antibiotics? *Biochem. Pharmacol., 71*, p.919-29

Byarugaba, D. (2004). Antimicrobial resistance in developing countries and responsible risk factors. *International journal of antimicrobial agents, 24*, p.105-10

Cai, X., Wang, Y., Du, X., Xing, X. et Zhu, G. (2020). Stability of pH-responsive Pickering emulsion stabilized by carboxymethylstarch/xanthan gum combinations. *Food Hydrocolloids, 109*, p.106093

Camilli, R., Del Grosso, M., Iannelli, F. et Pantosti, A. (2008). New genetic element carrying the erythromycin resistance determinant erm (TR) in Streptococcus pneumoniae. *Antimicrob. Agents Chemother., 52*, p.619-25

Capita, R. et Alonso-Calleja, C. (2013). Antibiotic-resistant bacteria: a challenge for the food industry. *Critical reviews in food science and nutrition, 53*, p.11-48

Carbone, M., Donia, D. T., Sabbatella, G. et Antiochia, R. (2016). Silver nanoparticles in polymeric matrices for fresh food packaging. *Journal of King Saud University-Science, 28*, p.273-9

Carretero, M. I. (2002). Clay minerals and their beneficial effects upon human health. A review. *Applied Clay Science, 21*, p.155-63

Casaburi, A., Rojo, Ú. M., Cerrutti, P., Vázquez, A. et Foresti, M. L. (2018). Carboxymethylcellulose with tailored degree of substitution obtained from bacterial cellulose. *Food Hydrocolloids, 75*, p.147-56

Cerri, G., Farina, M., Brundu, A., Gavini, E., Salis, A. et Dathe, W. (2021). Antibacterial activity of Zn-loaded Cuban zeolite against Helicobacter pylori in comparison to its Na-loaded and unmodified counterparts. *Environmental Geochemistry and Health, 43*, p.2037-48

Chacko, S. M., Thambi, P. T., Kuttan, R. et Nishigaki, I. (2010). Beneficial effects of green tea: A literature review. *Chin. Med., 5*, p.13

Chatterjee, A. K., Chakraborty, R. et Basu, T. (2014). Mechanism of antibacterial activity of copper nanoparticles. *Nanotechnology, 25*, p.135101

Chaurasia, V., Chand, N. et Bajpai, S. (2010). Water sorption properties and antimicrobial action of zinc oxide nanoparticles-loaded cellulose acetate films. *Journal of Macromolecular Science, Part A: Pure and Applied Chemistry, 47*, p.309-17

Chen, J., Fan, L., Yang, C., Wang, S., Zhang, M., Xu, J. et Luo, S. (2020). Facile synthesis of Ag nanoparticles-loaded chitosan antibacterial nanocomposite and its application in polypropylene. *International Journal of Biological Macromolecules, 161*, p.1286-95

Chen, Y., Li, Y., Dai, L., Qin, G., Guo, J., Zhang, Q., Zhang, S. (2021). High-efficiency Pd nanoparticles loaded porous organic polymers membrane catalytic reactors. *Chemical Communications, 57*, p.3131-4

Chinedum, I. E. (2005). Microbial resistance to antibiotics. *African journal of Biotechnology, 4*, p.

Chudobová, D. et Kizek, R. (2015). Nanotechnology in diagnosis, treatment and prophylaxis of infectious diseases. *Journal of Metallomics and Nanotechnologies, 2*, p.67-9

ČíK, G., Bujdáková, H. et Šeršeň, F. (2001). Study of fungicidal and antibacterial effect of the Cu (II)-complexes of thiophene oligomers synthesized in ZSM-5 zeolite channels. *Chemosphere, 44*, p.313-9

Čík, G., Priesolová, S., Bujdáková, H., Šeršeň, F., Potheöová, T. et Krištín, J. (2006). Inactivation of bacteria G+-S. aureus and G–-E. coli by phototoxic polythiophene incorporated in ZSM-5 zeolite. *Chemosphere, 63*, p.1419-26

Costa, C., Conte, A., Buonocore, G. G. et Del Nobile, M. A. (2011). Antimicrobial silver-montmorillonite nanoparticles to prolong the shelf life of fresh fruit salad. *International Journal of Food Microbiology, 148*, p.164-7

Courvalin, P. (1994). Transfer of antibiotic resistance genes between gram-positive and gram-negative bacteria. *Antimicrobial agents and chemotherapy, 38*, p.1447-51

Cragg, G. M. et Newman, D. J. (2013). Natural products: a continuing source of novel drug leads. *Biochimica et Biophysica Acta (BBA)-General Subjects, 1830*, p.3670-95

Cronholm, P., Karlsson, H. L., Hedberg, J., Lowe, T. A., Winnberg, L., Elihn, K., Möller, L. (2013). Intracellular uptake and toxicity of Ag and CuO nanoparticles: a comparison between nanoparticles and their corresponding metal ions. *Small, 9*, p.970-82

Crooks, R. M., Zhao, M., Sun, L., Chechik, V. et Yeung, L. K. (2001). Dendrimer-encapsulated metal nanoparticles: synthesis, characterization, and applications to catalysis. *Accounts of chemical research, 34*, p.181-90

Dakal, T., Kumar, A., Majumdar, R. et Yadav, V. (2016). *Mechanistic basis of antimicrobial actions of silver nanoparticles. Front Microbiol. 2016; 7: 1831*.

Davidson, C. M., Thomas, R. P., Mcvey, S. E., Perala, R., Littlejohn, D. et Ure, A. M. (1994). Evaluation of a sequential extraction procedure for the speciation of heavy metals in sediments. *Analytica Chimica Acta, 291*, p.277-86

De Souza, T. a. J., Souza, L. R. R. et Franchi, L. P. (2019). Silver nanoparticles: An integrated view of green synthesis methods, transformation in the environment, and toxicity. *Ecotoxicology and environmental safety, 171*, p.691-700

Decastro, C. et Mitchell, B. (2012). *Nanoparticles from mechanical attrition, in Synthesis, Functionalization, and Surface Treatment of Nanoparticles* : American Scientific Publishers California.

Decastro, C. L. et Mitchell, B. S. (2002). Nanoparticles from mechanical attrition. *Synthesis, functionalization, and surface treatment of nanoparticles, 5*, p.

Diaz, C., Barrientos, L., Carrillo, D., Valdebenito, J., Valenzuela, M. L., Allende, P., O'dwyer, C. (2016). Solvent-less method for efficient photocatalytic α-Fe 2 O 3 nanoparticles using macromolecular polymeric precursors. *New Journal of Chemistry, 40*, p.6768-76

Dizman, B., Badger, J. C., Elasri, M. O. et Mathias, L. J. (2007). Antibacterial fluoromicas: a novel delivery medium. *Applied clay science, 38*, p.57-63

Drlica, K. et Franco, R. J. (1988). Inhibitors of DNA topoisomerases. *Biochemistry, 27*, p.2253-9

Dumitrache, F., Morjan, I., Alexandrescu, R., Ciupina, V., Prodan, G., Voicu, I., Sandu, I. (2005). Iron–iron oxide core–shell nanoparticles synthesized by laser pyrolysis followed by superficial oxidation. *Applied Surface Science, 247*, p.25-31

Duruibe, J. O., Ogwuegbu, M. et Egwurugwu, J. (2007). Heavy metal pollution and human biotoxic effects. *International Journal of physical sciences, 2*, p.112-8

Effenberger, F. B., Couto, R. A., Kiyohara, P. K., Machado, G., Masunaga, S. H., Jardim, R. F. et Rossi, L. M. (2017). Economically attractive route for the preparation of high quality magnetic nanoparticles by the thermal decomposition of iron (III) acetylacetonate. *Nanotechnology, 28*, p.115603

Eirish, M. et Tret'yakova, L. (1970). The role of sorptive layers in the formation and change of the crystal structure of montmorillonite. *Clay Minerals, 8*, p.255-66

El-Eskandarany, M. S. (2001). *Mechanical alloying: For fabrication of advanced engineering materials*. William Andrew

El Badawy, A. M., Silva, R. G., Morris, B., Scheckel, K. G., Suidan, M. T. et Tolaymat, T. M. (2011). Surface charge-dependent toxicity of silver nanoparticles. *Environmental science & technology, 45*, p.283-7

España, V. a. A., Sarkar, B., Biswas, B., Rusmin, R. et Naidu, R. (2019). Environmental applications of thermally modified and acid activated clay minerals: current status of the art. *Environmental Technology & Innovation, 13*, p.383-97

Esteban-Cubillo, A., Pecharromán, C., Aguilar, E., Santarén, J. et Moya, J. S. (2006). Antibacterial activity of copper monodispersed nanoparticles into sepiolite. *Journal of materials science, 41*, p.5208-12

Faedmaleki, F., F, H. S., Salarian, A. A., Ahmadi Ashtiani, H. et Rastegar, H. (2014). Toxicity Effect of Silver Nanoparticles on Mice Liver Primary Cell Culture and HepG2 Cell Line. *Iran J Pharm Res, 13*, p.235-42

Fang, J., Lyon, D. Y., Wiesner, M. R., Dong, J. et Alvarez, P. J. (2007). Effect of a fullerene water suspension on bacterial phospholipids and membrane phase behavior. *Environmental science & technology, 41*, p.2636-42

Farrell, D., Morrissey, I., Bakker, S. et Felmingham, D. (2002). Molecular characterization of macrolide resistance mechanisms among Streptococcus pneumoniae and Streptococcus pyogenes isolated from the PROTEKT 1999-2000 study. *J. Antimicrob. Chemother., 50*, p.39-47

Farrokhpay, S. (2009). A review of polymeric dispersant stabilisation of titania pigment. *Advances in Colloid and Interface Science, 151*, p.24-32

Feng, Q. L., Wu, J., Chen, G. Q., Cui, F., Kim, T. et Kim, J. (2000). A mechanistic study of the antibacterial effect of silver ions on Escherichia coli and Staphylococcus aureus. *Journal of biomedical materials research, 52*, p.662-8

Fernández, L. et Hancock, R. E. (2012). Adaptive and mutational resistance: role of porins and efflux pumps in drug resistance. *Clin. Microbiol. Rev., 25*, p.661-81

Franklin, T. et Snow, G. (1989). Inhibitors of protein synthesis. Dans *Biochemistry of Antimicrobial Action* (p. 112-36) : Springer.

Fu, F., Li, L., Liu, L., Cai, J., Zhang, Y., Zhou, J. et Zhang, L. (2015). Construction of cellulose based ZnO nanocomposite films with antibacterial properties through one-step coagulation. *ACS applied materials & interfaces, 7*, p.2597-606

Fujimoto, T., Terauchi, S.-Y., Umehara, H., Kojima, I. et Henderson, W. (2001). Sonochemical preparation of single-dispersion metal nanoparticles from metal salts. *Chemistry of Materials, 13*, p.1057-60

Furukawa, Y., Watkins, J. L., Kim, J., Curry, K. J. et Bennett, R. H. (2009). Aggregation of montmorillonite and organic matter in aqueous media containing artificial seawater. *Geochemical transactions, 10*, p.1-11

Gabrielyan, L. et Trchounian, A. (2019). Antibacterial activities of transient metals nanoparticles and membranous mechanisms of action. *World Journal of Microbiology and Biotechnology, 35*, p.1-10

Galletta, M., Reekie, T. A., Nagalingam, G., Bottomley, A. L., Harry, E. J., Kassiou, M. et Triccas, J. A. (2020). Rapid Antibacterial activity of cannabichromenic acid against methicillin-resistant Staphylococcus aureus. *Antibiotics, 9*, p.523

Gallo, G. et Schillaci, D. (2021). Bacterial metal nanoparticles to develop new weapons against bacterial biofilms and infections. *Applied Microbiology and Biotechnology, 105*, p.5357-66

Gandra, S., Barter, D. et Laxminarayan, R. (2014). Economic burden of antibiotic resistance: how much do we really know? *Clinical microbiology and infection, 20*, p.973-80

García-Ivars, J., Corbatón-Báguena, M.-J. et Iborra-Clar, M.-I. (2019). Development of mixed matrix membranes: Incorporation of metal nanoparticles in polymeric membranes. Dans *Nanoscale materials in water purification* (p. 153-78) : Elsevier.

Gericke, M. et Pinches, A. (2006). Biological synthesis of metal nanoparticles. *Hydrometallurgy, 83*, p.132-40

Ghomari, K., Benhamou, A., Hamacha, R., Bengueddach, A., Nousir, S., Shiao, T. C., Azzouz, A. (2015). TPD and DSC insights in the basicity of MCM-48-like silica and modified counterparts. *Thermochimica Acta, 600*, p.52-61

Ghomari, K., Boukoussa, B., Hamacha, R., Bengueddach, A., Roy, R. et Azzouz, A. (2017). Preparation of dendrimer polyol/mesoporous silica nanocomposite for reversible CO2 adsorption: Effect of pore size and polyol content. *Separation Science and Technology, 52*, p.2421-8

Ghooi, R. et Thatte, S. (1995). Inhibition of cell wall synthesis—is this the mechanism of action of penicillins? *Medical hypotheses, 44*, p.127-31

Glauert, A. M. et Thornley, M. J. (1969). The topography of the bacterial cell wall. *Annual review of microbiology, 23*, p.159-98

Godoy-Gallardo, M., Eckhard, U., Delgado, L. M., De Roo Puente, Y. J., Hoyos-Nogués, M., Gil, F. J. et Perez, R. A. (2021). Antibacterial approaches in tissue engineering using metal ions and nanoparticles: From mechanisms to applications. *Bioactive Materials, 6*, p.4470-90

Gold, K., Slay, B., Knackstedt, M. et Gaharwar, A. K. (2018). Antimicrobial activity of metal and metal-oxide based nanoparticles. *Advanced Therapeutics, 1*, p.1700033

Gong, C.-P., Luo, Y. et Pan, Y.-Y. (2019). Novel synthesized zinc oxide nanoparticles loaded alginate-chitosan biofilm to enhanced wound site activity and anti-septic abilities for the management of complicated abdominal wound dehiscence. *Journal of Photochemistry and Photobiology B: Biology, 192*, p.124-30

Gordon, O., Slenters, T. V., Brunetto, P. S., Villaruz, A. E., Sturdevant, D. E., Otto, M., Fromm, K. M. (2010). Silver coordination polymers for prevention of implant infection: thiol interaction, impact on respiratory chain enzymes, and hydroxyl radical induction. *Antimicrobial agents and chemotherapy, 54*, p.4208-18

Greiner, M. T., Chai, L., Helander, M. G., Tang, W. M. et Lu, Z. H. (2012). Transition metal oxide work functions: the influence of cation oxidation state and oxygen vacancies. *Advanced Functional Materials, 22*, p.4557-68

Griffith, J. et Orgel, L. (1957). Ligand-field theory. *Quarterly Reviews, Chemical Society, 11*, p.381-93

Groot, M. J. et Van't Hooft, K. E. (2016). The hidden effects of dairy farming on public and environmental health in the Netherlands, India, Ethiopia, and Uganda, considering the use of antibiotics and other agro-chemicals. *Frontiers in public health, 4*, p.12

Grün, I. et Dirr, K. (1967). The differentiation of pathogenic and nonpathogenic staphylococci by estimation of the reduction of amido-blue-black and methylene blue. *International Journal of Systematic and Evolutionary Microbiology, 17*, p.391-4

Gu, H., Xu, K., Xu, C. et Xu, B. (2006). Biofunctional magnetic nanoparticles for protein separation and pathogen detection. *Chemical Communications*, p.941-9

Guglielmi, P., Pontecorvi, V. et Rotondi, G. (2020). Natural compounds and extracts as novel antimicrobial agents. *Expert Opinion on Therapeutic Patents, 30*, p.949-62

Gunasundari, E., Senthil Kumar, P., Christopher, F. C., Arumugam, T. et Saravanan, A. (2017). Green synthesis of metal nanoparticles loaded ultrasonic-assisted spirulina platensis using algal extract and their antimicrobial activity. *IET Nanobiotechnology, 11*, p.754-8

Gupta, A., Maynes, M. et Silver, S. (1998). Effects of halides on plasmid-mediated silver resistance in Escherichia coli. *Appl. Environ. Microbiol., 64*, p.5042-5

Guzmán, M. G., Dille, J. et Godet, S. (2009). Synthesis of silver nanoparticles by chemical reduction method and their antibacterial activity. *Int J Chem Biomol Eng, 2*, p.104-11

Hachemaoui, M., Boukoussa, B., Mokhtar, A., Mekki, A., Beldjilali, M., Benaissa, M., Sassi, M. (2020). Dyes adsorption, antifungal and antibacterial properties of metal loaded mesoporous silica: effect of metal and calcination treatment. *Materials Chemistry and Physics, 256*, p.123704

Hakenbeck, R., Grebe, T., Zähner, D. et Stock, J. B. (1999). β-Lactam resistance in Streptococcus pneumoniae: penicillin-binding proteins and non-penicillin-binding proteins. *Mol. Microbiol., 33*, p.673-8

Hancock, R. E. (1998). Resistance mechanisms in Pseudomonas aeruginosa and other nonfermentative gram-negative bacteria. *Clin. Infect. Dis., 27*, p.S93-S9

Harikumar, P. et Aravind, A. (2016). Antibacterial activity of copper nanoparticles and copper nanocomposites against Escherichia coli bacteria. *Int J Sci, 5*, p.83-90

Hart, C. et Kariuki, S. (1998). Antimicrobial resistance in developing countries. *Bmj, 317*, p.647-50

Harun, N. H., Mydin, R. B. S., Sreekantan, S., Saharudin, K. A., Basiron, N., Aris, F., Seeni, A. (2020). Bactericidal capacity of a heterogeneous TiO2/ZnO nanocomposite against multidrug-resistant and non-multidrug-resistant bacterial strains associated with nosocomial infections. *ACS omega, 5*, p.12027-34

Hellmann, J., Hamano, M., Karthaus, O., Ijiro, K., Shimomura, M. et Irie, M. (1998). Aggregation of dendrimers with a photochromic dithienylethene core group on the mica surface-atomic force microscopic imaging. *Japanese journal of applied physics, 37*, p.L816

Herrera, P., Burghardt, R. et Phillips, T. (2000). Adsorption of Salmonella enteritidis by cetylpyridinium-exchanged montmorillonite clays. *Veterinary microbiology, 74*, p.259-72

Hornischer, K. et Häußler, S. (2016). Diagnostics and resistance profiling of bacterial pathogens. *How to Overcome the Antibiotic Crisis*, p.89-102

Hrenović, J., Dekić, S., Dikić, J., Kazazić, S., Durn, G. et Rajić, N. (2020). Metal-loaded zeolite remediation of soils contaminated with pandrug-resistant. *Archives of Industrial Hygiene and Toxicology, 71*, p.146-51

Hsu, L.-Y., Tan, T.-Y., Tam, V. H., Kwa, A., Fisher, D. A. et Koh, T.-H. (2010). Surveillance and correlation of antibiotic prescription and resistance of Gram-negative bacteria in Singaporean hospitals. *Antimicrobial agents and chemotherapy, 54*, p.1173-8

Iqbal, T., Irfan, M., Ramay, S. M., Mahmood, A., Saleem, M. et Siddiqi, S. A. (2020). ZnO–PVA Polymer Matrix with Transition Metals Oxide Nano-fillers for High Dielectric Mediums. *Journal of Polymers and the Environment, 28*, p.2422-32

Iszatt, J. J., Larcombe, A. N., Chan, H.-K., Stick, S. M., Garratt, L. W. et Kicic, A. (2021). Phage therapy for multi-drug resistant respiratory tract infections. *Viruses, 13*, p.1809

Jamkhande, P. G., Ghule, N. W., Bamer, A. H. et Kalaskar, M. G. (2019). Metal nanoparticles synthesis: An overview on methods of preparation, advantages and disadvantages, and applications. *Journal of drug delivery science and technology, 53*, p.101174

Jansen, W., Van Der Bruggen, J., Verhoef, J. et Fluit, A. (2006). Bacterial resistance: a sensitive issue: complexity of the challenge and containment strategy in Europe. *Drug Resistance Updates, 9*, p.123-33

Jarosz, M., Keppler, B. K. et Timerbaev, A. R. (2022). Current and emerging mass spectrometry methods for the preclinical development of metal-based drugs: a critical appraisal. *Analytical and Bioanalytical Chemistry, 414*, p.95-102

Javanbakht, S., Pooresmaeil, M., Hashemi, H. et Namazi, H. (2018). Carboxymethylcellulose capsulated Cu-based metal-organic framework-drug nanohybrid as a pH-sensitive nanocomposite for ibuprofen oral delivery. *International journal of biological macromolecules, 119*, p.588-96

Javanbakht, S., Pooresmaeil, M. et Namazi, H. (2019). Green one-pot synthesis of carboxymethylcellulose/Zn-based metal-organic framework/graphene oxide bio-nanocomposite as a nanocarrier for drug delivery system. *Carbohydrate polymers, 208*, p.294-301

Ji, G. et Silver, S. (1995). Bacterial resistance mechanisms for heavy metals of environmental concern. *Journal of industrial microbiology, 14*, p.61-75

Jiang, W., Yang, H.-C., Yang, S.-Y., Horng, H.-E., Hung, J., Chen, Y. et Hong, C.-Y. (2004). Preparation and properties of superparamagnetic nanoparticles with narrow size distribution and biocompatible. *Journal of Magnetism and Magnetic Materials, 283*, p.210-4

Johanson, P. (2006). *Copper*. The Rosen Publishing Group, Inc

Joshi, M., Purwar, R., Udakhe, J. S. et Sreedevi, R. (2015). *Antimicrobial nanocomposite compositions, fibers and films* : Google Patents.

Kalsin, A. M., Pinchuk, A. O., Smoukov, S. K., Paszewski, M., Schatz, G. C. et Grzybowski, B. A. (2006). Electrostatic Aggregation and Formation of Core− Shell Suprastructures in Binary Mixtures of Charged Metal Nanoparticles. *Nano letters, 6*, p.1896-903

Karbowniczek, J., Cordero-Arias, L., Virtanen, S., Misra, S. K., Valsami-Jones, E., Tuchscherr, L., Czyrska-Filemonowicz, A. (2017). Electrophoretic deposition of organic/inorganic composite coatings containing ZnO nanoparticles exhibiting antibacterial properties. *Materials Science and Engineering: C, 77*, p.780-9

Karkman, A., Do, T. T., Walsh, F. et Virta, M. P. (2018). Antibiotic-resistance genes in waste water. *Trends in microbiology, 26*, p.220-8

Keller, A. A., Wang, H., Zhou, D., Lenihan, H. S., Cherr, G., Cardinale, B. J., Ji, Z. (2010). Stability and aggregation of metal oxide nanoparticles in natural aqueous matrices. *Environmental science & technology, 44*, p.1962-7

Keshari, A. K., Srivastava, R., Singh, P., Yadav, V. B. et Nath, G. (2020). Antioxidant and antibacterial activity of silver nanoparticles synthesized by Cestrum nocturnum. *Journal of Ayurveda and integrative medicine, 11*, p.37-44

Khameneh, B., Diab, R., Ghazvini, K. et Bazzaz, B. S. F. (2016). Breakthroughs in bacterial resistance mechanisms and the potential ways to combat them. *Microb. Pathog., 95*, p.32-42

Khodakarami, M. et Bagheri, M. (2021). Recent advances in synthesis and application of polymer nanocomposites for water and wastewater treatment. *Journal of Cleaner Production, 296*, p.126404

Khorsandi, K., Hosseinzadeh, R., Sadat Esfahani, H., Keyvani-Ghamsari, S. et Ur Rahman, S. (2021). Nanomaterials as drug delivery systems with antibacterial properties: Current trends and future priorities. *Expert Review of Anti-infective Therapy, 19*, p.1299-323

Khurana, C., Vala, A. K., Andhariya, N., Pandey, O. et Chudasama, B. (2014). Antibacterial activity of silver: the role of hydrodynamic particle size at nanoscale. *Journal of Biomedical Materials Research Part A, 102*, p.3361-8

Kim, J. S., Kuk, E., Yu, K. N., Kim, J.-H., Park, S. J., Lee, H. J., Hwang, C.-Y. (2007). Antimicrobial effects of silver nanoparticles. *Nanomedicine: Nanotechnology, Biology and Medicine, 3*, p.95-101

Kim, S.-H., Lee, H.-S., Ryu, D.-S., Choi, S.-J. et Lee, D.-S. (2011). Antibacterial activity of silver-nanoparticles against Staphylococcus aureus and Escherichia coli. *Microbiology and Biotechnology Letters, 39*, p.77-85

Knapp, C. W., Dolfing, J., Ehlert, P. A. et Graham, D. W. (2010). Evidence of increasing antibiotic resistance gene abundances in archived soils since 1940. *Environmental science & technology, 44*, p.580-7

Kolář, M., Urbanek, K. et Látal, T. (2001). Antibiotic selective pressure and development of bacterial resistance. *Int. J. Antimicrob. Agents, 17*, p.357-63

Komadel, P. (2016). Acid activated clays: Materials in continuous demand. *Applied Clay Science, 131*, p.84-99

Kosakowska, K. A., Casey, B. K., Albert, J. N., Wang, Y., Ashbaugh, H. S. et Grayson, S. M. (2018). Synthesis and Self-Assembly of Amphiphilic Star/Linear–Dendritic Polymers: Effect of Core versus Peripheral Branching on Reverse Micelle Aggregation. *Biomacromolecules, 19*, p.3177-89

Kotov, Y. A. (2003). Electric explosion of wires as a method for preparation of nanopowders. *Journal of nanoparticle research, 5*, p.539-50

Kurose, A., Tanaka, T., Huang, X., Traganos, F. et Darzynkiewicz, Z. (2006). Synchronization in the cell cycle by inhibitors of DNA replication induces histone H2AX phosphorylation: an indication of DNA damage. *Cell proliferation, 39*, p.231-40

Labelle, M. A., Ispas-Szabo, P. et Mateescu, M. A. (2020). Structure-Functions Relationship of Modified Starches for Pharmaceutical and Biomedical Applications. *Starch-Stärke, 72*, p.2000002

Lapasam, A., Dkhar, L., Joshi, N., Poluri, K. M. et Kollipara, M. R. (2019). Antimicrobial selectivity of ruthenium, rhodium, and iridium half sandwich complexes containing phenyl hydrazone Schiff base ligands towards B. thuringiensis and P. aeruginosa bacteria. *Inorganica Chimica Acta, 484*, p.255-63

Le Ouay, B. et Stellacci, F. (2015). Antibacterial activity of silver nanoparticles: a surface science insight. *Nano today, 10*, p.339-54

Lemire, J. A., Harrison, J. J. et Turner, R. J. (2013). Antimicrobial activity of metals: mechanisms, molecular targets and applications. *Nature Reviews Microbiology, 11*, p.371-84

Levy, C., Minnis, D. et Derrick, J. P. (2008). Dihydropteroate synthase from Streptococcus pneumoniae: structure, ligand recognition and mechanism of sulfonamide resistance. *Biochemical Journal, 412*, p.379-88

Levy, S. B. (1992). Active efflux mechanisms for antimicrobial resistance. *Antimicrob. Agents Chemother., 36*, p.695-703

Levy, S. B. (1998). The challenge of antibiotic resistance. *Scientific American, 278*, p.46-53

Li, F.-T., Ran, J., Jaroniec, M. et Qiao, S. Z. (2015). Solution combustion synthesis of metal oxide nanomaterials for energy storage and conversion. *Nanoscale, 7*, p.17590-610

Lima, T. B., Pinto, M. F. S., Ribeiro, S. M., De Lima, L. A., Viana, J. C., Júnior, N. G., Franco, O. L. (2013). Bacterial resistance mechanism: what proteomics can elucidate. *The FASEB Journal, 27*, p.1291-303

Lin, C., Fugetsu, B., Su, Y. et Watari, F. (2009). Studies on toxicity of multi-walled carbon nanotubes on Arabidopsis T87 suspension cells. *Journal of Hazardous Materials, 170*, p.578-83

Linder, M. C. (2001). Copper and genomic stability in mammals. *Mutation Research/Fundamental and Molecular Mechanisms of Mutagenesis, 475*, p.141-52

Liu, Y. et Breukink, E. (2016). The membrane steps of bacterial cell wall synthesis as antibiotic targets. *Antibiotics, 5*, p.28

Londono, S. C., Hartnett, H. E. et Williams, L. B. (2017). Antibacterial activity of aluminum in clay from the Colombian Amazon. *Environmental Science & Technology, 51*, p.2401-8

Longley, D. et Johnston, P. (2005). Molecular mechanisms of drug resistance. *The Journal of Pathology, 205*, p.275-92

Lorenz, B., Ali, N., Bocklitz, T., Rösch, P. et Popp, J. (2020). Discrimination between pathogenic and non-pathogenic E. coli strains by means of Raman microspectroscopy. *Analytical and Bioanalytical Chemistry, 412*, p.8241-7

Losasso, C., Belluco, S., Cibin, V., Zavagnin, P., Mičetić, I., Gallocchio, F., Ricci, A. (2014). Antibacterial activity of silver nanoparticles: sensitivity of different Salmonella serovars. *Frontiers in microbiology, 5*, p.227

Lou, G. et Huang, P. (1988). Hydroxy-aluminosilicate interlayers in montmorillonite: Implications for acidic environments. *Nature, 335*, p.625-7

Macone, A., Caruso, B., Leahy, R., Donatelli, J., Weir, S., Draper, M., Levy, S. (2014). In vitro and in vivo antibacterial activities of omadacycline, a novel aminomethylcycline. *Antimicrob. Agents Chemother., 58*, p.1127-35

Makwana, D., Castano, J., Somani, R. S. et Bajaj, H. C. (2020). Characterization of Agar-CMC/Ag-MMT nanocomposite and evaluation of antibacterial and mechanical properties for packaging applications. *Arabian Journal of Chemistry, 13*, p.3092-9

Malla, P., Ravindranathan, P., Komarneni, S. et Roy, R. (1991). Intercalation of copper metal clusters in montmorillonite. *Nature, 351*, p.555-7

Mamaghani, A. H., Haghighat, F. et Lee, C.-S. (2019). Hydrothermal/solvothermal synthesis and treatment of TiO2 for photocatalytic degradation of air pollutants: Preparation, characterization, properties, and performance. *Chemosphere, 219*, p.804-25

Mani, R. (2018). Hard Soft Acid Base Theory (Hsab Theory) of Ralph Pearson. *Int. J. Sci. Res, 7*, p.29-31

Mao, A., Xiang, H., Ran, X., Li, Y., Jin, X., Yu, H. et Gu, X. (2019). Plasma arc discharge synthesis of multicomponent Co-Cr-Cu-Fe-Ni nanoparticles. *Journal of Alloys and Compounds, 775*, p.1177-83

Markley, J. L. et Wencewicz, T. A. (2018). Tetracycline-Inactivating Enzymes. *Frontiers in Microbiology, 9*, p.1058

Marquez, B. (2005). Bacterial efflux systems and efflux pumps inhibitors. *Biochimie, 87*, p.1137-47

Martin, S. et Griswold, W. (2009). Human health effects of heavy metals. *Environmental Science and Technology briefs for citizens, 15*, p.1-6

Martinez-Gutierrez, F., Boegli, L., Agostinho, A., Sánchez, E. M., Bach, H., Ruiz, F. et James, G. (2013). Anti-biofilm activity of silver nanoparticles against different microorganisms. *Biofouling, 29*, p.651-60

Mazel, D. et Davies, J. (1999). Antibiotic resistance in microbes. *Cellular and Molecular Life Sciences CMLS, 56*, p.742-54

Mcgowan Jr, J. E. (2006). Resistance in nonfermenting gram-negative bacteria: multidrug resistance to the maximum. *American journal of infection control, 34*, p.S29-S37

Mcmanus, M. C. (1997). Mechanisms of bacterial resistance to antimicrobial agents. *American Journal of Health-System Pharmacy, 54*, p.1420-33

Mello-Filho, A. C. et Meneghini, R. (1991). Iron is the intracellular metal involved in the production of DNA damage by oxygen radicals. *Mutation Research/Fundamental and Molecular Mechanisms of Mutagenesis, 251*, p.109-13

Milenkovic, J., Hrenovic, J., Matijasevic, D., Niksic, M. et Rajic, N. (2017). Bactericidal activity of Cu-, Zn-, and Ag-containing zeolites toward Escherichia coli isolates. *Environmental Science and Pollution Research, 24*, p.20273-81

Mittapally, S., Taranum, R. et Parveen, S. (2018). Metal ions as antibacterial agents. *Journal of Drug Delivery and Therapeutics, 8*, p.411-9

Moellering Jr, R. C. (2014). Tedizolid: a novel oxazolidinone for Gram-positive infections. *Clinical Infectious Diseases, 58*, p.S1-S3

Moghaddam, V. A., Kasmaeifar, V., Mahmoodi, Z., Ghafouri, H., Saberi, O. et Mohammadi, A. (2021). A novel sulfamethoxazole derivative as an inhibitory agent against HSP70: a combination of computational with in vitro studies. *International Journal of Biological Macromolecules, 189*, p.194-205

Moloney, M. G. (2016). Natural products as a source for novel antibiotics. *Trends in Pharmacological Sciences, 37*, p.689-701

Mosayebi, J., Kiyasatfar, M. et Laurent, S. (2017). Synthesis, functionalization, and design of magnetic nanoparticles for theranostic applications. *Advanced Healthcare Materials, 6*, p.1700306

Motshekga, S. C., Pillai, S. K., Sinha Ray, S., Jalama, K. et Krause, R. (2012). Recent trends in the microwave-assisted synthesis of metal oxide nanoparticles supported on carbon nanotubes and their applications. *Journal of Nanomaterials, 2012*, p.

Motshekga, S. C., Ray, S. S., Onyango, M. S. et Momba, M. N. (2013). Microwave-assisted synthesis, characterization and antibacterial activity of Ag/ZnO nanoparticles supported bentonite clay. *Journal of hazardous materials, 262*, p.439-46

Mouton, J. (1999). Combination therapy as a tool to prevent emergence of bacterial resistance. *Infection, 27*, p.S24-S8

Nabil, B., Christine, C., Julien, V. et Abdelkrim, A. (2018). Polyfunctional cotton fabrics with catalytic activity and antibacterial capacity. *Chemical Engineering Journal, 351*, p.328-39

Nadziakiewicza, M., Kehoe, S. et Micek, P. (2019). Physico-chemical Properties of Clay Minerals and Their Use as a Health Promoting Feed Additive. *Animals, 9*, p.714

Namivandi-Zangeneh, R., Wong, E. H. et Boyer, C. (2021). Synthetic antimicrobial polymers in combination therapy: tackling antibiotic resistance. *ACS Infectious Diseases, 7*, p.215-53

Nanda, M., Kumar, V. et Sharma, D. (2019). Multimetal tolerance mechanisms in bacteria: The resistance strategies acquired by bacteria that can be exploited to 'clean-up'heavy metal contaminants from water. *Aquatic toxicology, 212*, p.1-10

Nawar, N. et Hosny, N. M. (1999). Transition metal complexes of 2-acetylpyridine o-hydroxybenzoylhydrazone (APo-OHBH): Their preparation, characterisation and antimicrobial activity. *Chemical and pharmaceutical bulletin, 47*, p.944-9

Noori, F., Megoura, M., Labelle, M.-A., Mateescu, M. A. et Azzouz, A. (2022). Synthesis of Metal-Loaded Carboxylated Biopolymers with Antibacterial Activity through Metal Subnanoparticle Incorporation. *Antibiotics, 11*, p.439

Noori, F., Neree, A. T., Megoura, M., Mateescu, M. A. et Azzouz, A. (2021). Insights into the metal retention role in the antibacterial behavior of montmorillonite and cellulose tissue-supported copper and silver nanoparticles. *Rsc advances, 11*, p.24156-71

Noori, F., Tchoumi, N.-A., Megoura, M., Mateescu, M. A. et Azzouz, A. (2020). Metal-loaded porous polyhydroxylic matrices with improved antibacterial properties. *Authorea Preprints*, p.

Nouri, A., Yaraki, M. T., Ghorbanpour, M., Agarwal, S. et Gupta, V. K. (2018). Enhanced Antibacterial effect of chitosan film using Montmorillonite/CuO nanocomposite. *International Journal of Biological Macromolecules, 109*, p.1219-31

Nousir, S., Arus, V.-A., Shiao, T. C., Bouazizi, N., Roy, R. et Azzouz, A. (2019). Organically modified activated bentonites for the reversible capture of CO2. *Microporous and Mesoporous Materials, 290*, p.109652

Nousir, S., Ghomari, K., Roy, R. et Azzouz, A. (2013a). [Polyol-clay matrices with improved hydrophilic character and affinity towards CO2 - Attempts to CO2 concentration at room temperature]. CTSI-Cleantech 2013.

Nousir, S., Platon, N., Ghomari, K., Sergentu, A.-S., Shiao, T. C., Hersant, G., Azzouz, A. (2013b). Correlation between the hydrophilic character and affinity towards carbon dioxide of montmorillonite-supported polyalcohols. *Journal of Colloid and Interface Science, 402*, p.215-22

Nousir, S., Sergentu, A.-S., Shiao, T. C., Roy, R. et Azzouz, A. (2014). Hybrid Clay Nanomaterials with Improved Affinity for Carbon Dioxide through Chemical Grafting of Amino Groups. *International Journal of Environmental Pollution and Remediation*, p.

Noussir, S., Yemelong, G. T., Bouguedoura, S., Chabre, Y. M., Shiao, T. C., Roy, R. et Azzouz, A. (2017). Improved carbon dioxide storage over clay-supported perhydroxylated glucodendrimer. *Canadian Journal of Chemistry*, p.

Odularu, A. T. (2018). Metal nanoparticles: thermal decomposition, biomedicinal applications to cancer treatment, and future perspectives. *Bioinorganic chemistry and applications, 2018*, p.

Ogushi, Y., Sakai, S. et Kawakami, K. (2007). Synthesis of enzymatically-gellable carboxymethylcellulose for biomedical applications. *Journal of bioscience and bioengineering, 104*, p.30-3

Ounkaew, A., Kasemsiri, P., Jetsrisuparb, K., Uyama, H., Hsu, Y.-I., Boonmars, T., Chindaprasirt, P. (2020). Synthesis of nanocomposite hydrogel based carboxymethylstarch/polyvinyl alcohol/nanosilver for biomedical materials. *Carbohydrate Polymers, 248*, p.116767

Özdemir, G. et Yapar, S. (2020). Preparation and characterization of copper and zinc adsorbed cetylpyridinium and N-lauroylsarcosinate intercalated montmorillonites and their antibacterial activity. *Colloids and Surfaces B: Biointerfaces, 188*, p.110791

Pal, K., Banthia, A. et Majumdar, D. (2006). Development of carboxymethylcellulose acrylate for various biomedical applications. *Biomedical Materials, 1*, p.85

Pang, Z., Raudonis, R., Glick, B. R., Lin, T.-J. et Cheng, Z. (2019). Antibiotic resistance in Pseudomonas aeruginosa: mechanisms and alternative therapeutic strategies. *Biotechnology advances, 37*, p.177-92

Parashar, M., Shukla, V. K. et Singh, R. (2020). Metal oxides nanoparticles via sol–gel method: a review on synthesis, characterization and applications. *Journal of Materials Science: Materials in Electronics, 31*, p.3729-49

Park, H.-J., Kim, J. Y., Kim, J., Lee, J.-H., Hahn, J.-S., Gu, M. B. et Yoon, J. (2009). Silver-ion-mediated reactive oxygen species generation affecting bactericidal activity. *Water research, 43*, p.1027-32

Patel, S., Singh, D., Srivastava, S., Singh, M., Shah, K., Chauahn, D. N. et Chauhan, N. S. (2017). Nanoparticles as a platform for antimicrobial drug delivery. *Adv Pharmacol Pharm, 5*, p.31-43

Pathak, T. K., Kroon, R., Craciun, V., Popa, M., Chifiriuc, M. et Swart, H. (2019). Influence of Ag, Au and Pd noble metals doping on structural, optical and antimicrobial properties of zinc oxide and titanium dioxide nanomaterials. *Heliyon, 5*, p.e01333

Penesyan, A., Gillings, M. et Paulsen, I. T. (2015). Antibiotic discovery: combatting bacterial resistance in cells and in biofilm communities. *Molecules, 20*, p.5286-98

Peng, C., Tong, H., Yuan, P., Sun, L., Jiang, L. et Shi, J. (2019). Aggregation, sedimentation, and dissolution of copper oxide nanoparticles: influence of low-molecular-weight organic acids from root exudates. *Nanomaterials, 9*, p.841

Pfeifer, Y., Cullik, A. et Witte, W. (2010). Resistance to cephalosporins and carbapenems in Gram-negative bacterial pathogens. *Int. J. Med. Microbiol., 300*, p.371-9

Phan, D.-N., Dorjjugder, N., Saito, Y., Khan, M. Q., Ullah, A., Bie, X., Kim, I.-S. (2020). Antibacterial mechanisms of various copper species incorporated in polymeric nanofibers against bacteria. *Materials Today Communications, 25*, p.101377

Pitton, J.-S. (1972). Mechanisms of bacterial resistance to antibiotics. *Ergebnisse der Physiologie Reviews of Physiology, Volume 65*, p.15-93

Pooresmaeil, M. et Namazi, H. (2021). Developments on carboxymethylstarch-based smart systems as promising drug carriers: A review. *Carbohydrate Polymers, 258*, p.117654

Potera, C. (2012). *Understanding the germicidal effects of silver nanoparticles* : National Institute of Environmental Health Sciences.

Prathna, T., Chandrasekaran, N. et Mukherjee, A. (2011). Studies on aggregation behaviour of silver nanoparticles in aqueous matrices: effect of surface functionalization and matrix composition. *Colloids and Surfaces A: Physicochemical and Engineering Aspects, 390*, p.216-24

Qureshi, M. A., Nishat, N., Jadoun, S. et Ansari, M. Z. (2020). Polysaccharide based superabsorbent hydrogels and their methods of synthesis: A review. *Carbohydrate Polymer Technologies and Applications, 1*, p.100014

Rahman, S., Huang, Y., Zhu, L., Feng, S., Khan, I., Wu, J., Wang, X. (2018). Therapeutic Role of Green Tea Polyphenols in Improving Fertility: A Review. *Nutrients, 10*, p.834-

Rai, M., Yadav, A. et Gade, A. (2009). Silver nanoparticles as a new generation of antimicrobials. *Biotechnology advances, 27*, p.76-83

Rai, M. K., Deshmukh, S., Ingle, A. et Gade, A. (2012). Silver nanoparticles: the powerful nanoweapon against multidrug-resistant bacteria. *J. Appl. Microbiol., 112*, p.841-52

Raman, N., Dhaveethu Raja, J. et Sakthivel, A. (2007). Synthesis, spectral characterization of Schiff base transition metal complexes: DNA cleavage and antimicrobial activity studies. *Journal of Chemical sciences, 119*, p.303-10

Ramasamy, M. et Lee, J. (2016). Recent nanotechnology approaches for prevention and treatment of biofilm-associated infections on medical devices. *BioMed Research International, 2016*, p.

Ramyadevi, J., Jeyasubramanian, K., Marikani, A., Rajakumar, G. et Rahuman, A. A. (2012). Synthesis and antimicrobial activity of copper nanoparticles. *Materials letters, 71*, p.114-6

Rao, Z., Ge, H., Liu, L., Zhu, C., Min, L., Liu, M., Li, D. (2018). Carboxymethylcellulose modified graphene oxide as pH-sensitive drug delivery system. *International journal of biological macromolecules, 107*, p.1184-92

Ravindran, A., Chandran, P. et Khan, S. S. (2013). Biofunctionalized silver nanoparticles: advances and prospects. *Colloids and Surfaces B: Biointerfaces, 105*, p.342-52

Rees, N. V., Zhou, Y. G. et Compton, R. G. (2011). The aggregation of silver nanoparticles in aqueous solution investigated via anodic particle coulometry. *ChemPhysChem, 12*, p.1645-7

Ren, B., Kandjani, A. E., Chen, M., Field, M. R., Oppedisano, D. K., Bhargava, S. K. et Jones, L. A. (2019). Preparation of Au nanoparticles on a magnetically responsive support via pyrolysis of a Prussian blue composite. *Journal of colloid and interface science, 540*, p.563-71

Reygaert, W. C. (2018). An overview of the antimicrobial resistance mechanisms of bacteria. *AIMS microbiology, 4*, p.482

Ribeiro, A. I., Dias, A. M. et Zille, A. (2022). Synergistic effects between metal nanoparticles and commercial antimicrobial agents: A Review. *ACS Applied Nano Materials, 5*, p.3030-64

Robertson, G. T., Bonventre, E. J., Doyle, T. B., Du, Q., Duncan, L., Morris, T. W., Lynch, A. S. (2008). In vitro evaluation of CBR-2092, a novel rifamycin-quinolone hybrid antibiotic: studies of the mode of action in Staphylococcus aureus. *Antimicrob. Agents Chemother., 52*, p.2313-23

Roca, I., Akova, M., Baquero, F., Carlet, J., Cavaleri, M., Coenen, S., Heure, O. (2015). The global threat of antimicrobial resistance: science for intervention. *New microbes and new infections, 6*, p.22-9

Rudramurthy, G. R., Swamy, M. K., Sinniah, U. R. et Ghasemzadeh, A. (2016). Nanoparticles: alternatives against drug-resistant pathogenic microbes. *Molecules, 21*, p.836

Saboktakin, M. R., Maharramov, A. et Ramazanov, M. A. (2009). Synthesis and characterization of superparamagnetic nanoparticles coated with carboxymethylstarch (CMS) for magnetic resonance imaging technique. *Carbohydrate polymers, 78*, p.292-5

Sahraei, R. et Ghaemy, M. (2017). Synthesis of modified gum tragacanth/graphene oxide composite hydrogel for heavy metal ions removal and preparation of silver nanocomposite for antibacterial activity. *Carbohydrate polymers, 157*, p.823-33

Sánchez-López, E., Gomes, D., Esteruelas, G., Bonilla, L., Lopez-Machado, A. L., Galindo, R., Souto, E. B. (2020). Metal-Based Nanoparticles as Antimicrobial Agents: An Overview. *Nanomaterials (Basel), 10*, p.292

Sandeep Kumar, V. (2013). Magnetic nanoparticles-based biomedical and bioanalytical applications. *J Nanomed Nanotechol, 4*, p.e130

Saravanan, A., Kumar, P. S., Devi, G. K. et Arumugam, T. (2016). Synthesis and characterization of metallic nanoparticles impregnated onto activated carbon using leaf extract of Mukia maderasapatna: Evaluation of antimicrobial activities. *Microbial pathogenesis, 97*, p.198-203

Saravanan, R. et Ravikumar, L. (2015). The use of new chemically modified cellulose for heavy metal ion adsorption and antimicrobial activities. *Journal of water resource and protection, 7*, p.530

Saravolatz, L. D., Stein, G. E. et Johnson, L. B. (2009). Telavancin: a novel lipoglycopeptide. *Clinical Infectious Diseases, 49*, p.1908-14

Saravolatz, L. D., Stein, G. E. et Johnson, L. B. (2011). Ceftaroline: a novel cephalosporin with activity against methicillin-resistant Staphylococcus aureus. *Clinical Infectious Diseases., 52*, p.1156-63

Sarwat, S. G. (2017). Contamination in wet-ball milling. *Powder Metallurgy, 60*, p.267-72

Scalbert, A. et Williamson, G. (2000). Dietary Intake and Bioavailability of Polyphenols. *J Nutr, 130*, p.2073S--85S

Seiler, C. et Berendonk, T. U. (2012). Heavy metal driven co-selection of antibiotic resistance in soil and water bodies impacted by agriculture and aquaculture. *Frontiers in microbiology, 3*, p.399

Seipenbusch, M. et Binder, A. (2009). Structural stabilization of metal nanoparticles by chemical vapor deposition-applied silica coatings. *The Journal of Physical Chemistry C, 113*, p.20606-10

Sekkal, K. N. E. H., Ouargli-Saker, R., Lachachi, A. K., Zekkari, M., Beltrao-Nunes, A.-P., Michelin, L., Azzouz, A. (2021). Effect of copper dispersion on SBA-15 and SBA-16 affinity towards carbon dioxide—an approach through thermal programmed desorption. *Journal of Nanoparticle Research, 23*, p.154

Sennour, R., Shiao, T. C., Arus, V. A., Tahir, M. N., Bouazizi, N., Roy, R. et Azzouz, A. (2017a). Cu0-Loaded organo-montmorillonite with improved affinity towards hydrogen: an insight into matrix-metal and non-contact hydrogen-metal interactions. *Physical Chemistry Chemical Physics, 19*, p.29333-43

Sennour, R., Shiao, T. C., Arus, V. A., Tahir, M. N., Bouazizi, N., Roy, R. et Azzouz, A. (2017b). Cu 0-Loaded organo-montmorillonite with improved affinity towards hydrogen: an insight into matrix–metal and non-contact hydrogen–metal interactions. *Physical Chemistry Chemical Physics, 19*, p.29333-43

Shah, M., Fawcett, D., Sharma, S., Tripathy, S. K. et Poinern, G. E. J. (2015). Green synthesis of metallic nanoparticles via biological entities. *Materials, 8*, p.7278-308

Shaheen, B. W., Nayak, R., Foley, S. L. et Boothe, D. M. (2013). Chromosomal and plasmid-mediated fluoroquinolone resistance mechanisms among broad-spectrum-cephalosporin-resistant Escherichia coli isolates recovered from companion animals in the USA. *J. Antimicrob. Chemother., 68*, p.1019-24

Sharma, R. K. et Agrawal, M. (2005). Biological effects of heavy metals: an overview. *Journal of environmental Biology, 26*, p.301-13

Shin, D., Matsuda, Y. et Bernstein, E. (2004). On the iron oxide neutral cluster distribution in the gas phase. II. Detection through 118 nm single photon ionization. *The Journal of chemical physics, 120*, p.4157-64

Shortridge, V. D., Flamm, R. K., Ramer, N., Beyer, J. et Tanaka, S. K. (1996). Novel mechanism of macrolide resistance in Streptococcus pneumoniae. *Diagn. Microbiol. Infect. Dis., 26*, p.73-8

Sistemática, D. D. C. R. R., Gabriela, S.-S., Daniela, F.-R. et Helia, B.-T. (2016). Copper Nanoparticles as Potential Antimicrobial Agent in Disinfecting Root Canals. A Systematic Review. *Int. J. Odontostomat, 10*, p.547-54

Sköld, O. (2001). Resistance to trimethoprim and sulfonamides. *Vet. Res., 32*, p.261-73

Slavin, Y. N., Asnis, J., Häfeli, U. O. et Bach, H. (2017a). Metal nanoparticles: understanding the mechanisms behind antibacterial activity. *Journal of nanobiotechnology, 15*, p.1-20

Slavin, Y. N., Asnis, J., Häfeli, U. O. et Bach, H. (2017b). Metal nanoparticles: understanding the mechanisms behind antibacterial activity. *Journal of nanobiotechnology, 15*, p.65

Soler-Illia, G. J. et Azzaroni, O. (2011). Multifunctional hybrids by combining ordered mesoporous materials and macromolecular building blocks. *Chemical Society Reviews, 40*, p.1107-50

Sondi, I. et Salopek-Sondi, B. (2004). Silver nanoparticles as antimicrobial agent: a case study on E. coli as a model for Gram-negative bacteria. *Journal of colloid and interface science, 275*, p.177-82

Spychaj, T., Zdanowicz, M., Kujawa, J. et Schmidt, B. (2013). Carboxymethylstarch with high degree of substitution: synthesis, properties and application. *Polimery, 58*, p.503-11

Staroń, A. et Długosz, O. (2021). Antimicrobial properties of nanoparticles in the context of advantages and potential risks of their use. *Journal of Environmental Science and Health, Part A, 56*, p.680-93

Stavitskaya, A., Batasheva, S., Vinokurov, V., Fakhrullina, G., Sangarov, V., Lvov, Y. et Fakhrullin, R. (2019). Antimicrobial applications of clay nanotube-based composites. *Nanomaterials, 9*, p.708

Stensberg, M. C., Wei, Q., Mclamore, E. S., Porterfield, D. M., Wei, A. et Sepúlveda, M. S. (2011). Toxicological studies on silver nanoparticles: challenges and opportunities in assessment, monitoring and imaging. *Nanomedicine, 6*, p.879-98

Stepanov, A., Hole, D. et Townsend, P. (2000). Excimer laser annealing of glasses containing implanted metal nanoparticles. *Nuclear Instruments and Methods in Physics Research Section B: Beam Interactions with Materials and Atoms, 166*, p.882-6

Stojanović, Ž., Jeremić, K. et Jovanović, S. (2000). Synthesis of carboxymethylstarch. *Starch-Stärke, 52*, p.413-9

Stojanović, Ž., Jeremić, K., Jovanović, S. et Lechner, M. D. (2005). A comparison of some methods for the determination of the degree of substitution of carboxymethylstarch. *Starch-Stärke, 57*, p.79-83

Stubenrauch, C., Wielpütz, T., Sottmann, T., Roychowdhury, C. et Disalvo, F. J. (2008). Microemulsions as templates for the synthesis of metallic nanoparticles. *Colloids and Surfaces A: Physicochemical and Engineering Aspects, 317*, p.328-38

Su, J.-F., Huang, Z., Yuan, X.-Y., Wang, X.-Y. et Li, M. (2010). Structure and properties of carboxymethylcellulose/soy protein isolate blend edible films crosslinked by Maillard reactions. *Carbohydrate polymers, 79*, p.145-53

Suleiman, H. a. H. L. A. et Haddadin, R. (2019). Antimicrobial Activity of Metal-Loaded Zeolites Against S. aureus and E. coli. *Jordan Journal of Chemistry (JJC), 14*, p.61-8

Sulpizi, M., Gaigeot, M. P. et Sprik, M. (2012). The Silica-Water Interface: How the Silanols Determine the Surface Acidity and Modulate the Water Properties. *Journal of chemical theory and computation, 8*, p.1037-47

Sultan, I., Rahman, S., Jan, A. T., Siddiqui, M. T., Mondal, A. H. et Haq, Q. M. R. (2018). Antibiotics, resistome and resistance mechanisms: a bacterial perspective. *Front Microbiol, 9*, p.2066

Susanti, D., Aminudin, N. I., Ismail, M. W., Taher, M., Shafiee, S. A., Danial, W. H. et Hamzah, N. (2022). Nanotechnology-based approaches for antitubercular drug delivery. Dans *Emerging Nanomaterials and Nano-Based Drug Delivery Approaches to Combat Antimicrobial Resistance* (p. 365-94) : Elsevier.

Suzuki, T., Yamate, T., Hara, J., Wada, K. et Niinae, M. (2021). Inactivation of bacteria using Fe3+-loaded montmorillonite. *Journal of Environmental Chemical Engineering, 9*, p.105637

Tahir, M. N., Sennour, R., Arus, V. A., Sallam, L. M., Roy, R. et Azzouz, A. (2017). Metal organoclays with compacted structure for truly physical capture of hydrogen. *Applied Surface Science, 398*, p.116-24

Tan, J., Liu, R., Wang, W., Liu, W., Tian, Y., Wu, M. et Huang, Y. (2010). Controllable aggregation and reversible pH sensitivity of AuNPs regulated by carboxymethylcellulose. *Langmuir, 26*, p.2093-8

Tang, S. et Zheng, J. (2018). Antibacterial activity of silver nanoparticles: structural effects. *Advanced healthcare materials, 7*, p.1701503

Tenover, F. C. (2006). Mechanisms of antimicrobial resistance in bacteria. *The American journal of medicine, 119*, p.S3-S10

Terrab, I., Boukoussa, B., Hamacha, R., Bouchiba, N., Roy, R., Bengueddach, A. et Azzouz, A. (2016). Insights in CO2 interaction on zeolite omega-supported polyol dendrimers. *Thermochimica acta, 624*, p.95-101

Thakkar, K. N., Mhatre, S. S. et Parikh, R. Y. (2010). Biological synthesis of metallic nanoparticles. *Nanomedicine: nanotechnology, biology and medicine, 6*, p.257-62

Theophanides, T. et Anastassopoulou, J. (2002). Copper and carcinogenesis. *Critical reviews in oncology/hematology, 42*, p.57-64

Thuc, C.-N. H., Grillet, A.-C., Reinert, L., Ohashi, F., Thuc, H. H. et Duclaux, L. (2010). Separation and purification of montmorillonite and polyethylene oxide modified montmorillonite from Vietnamese bentonites. *Applied Clay Science, 49*, p.229-38

Turel, I. et Kljun, J. (2011). Interactions of metal ions with DNA, its constituents and derivatives, which may be relevant for anticancer research. *Current topics in medicinal chemistry, 11*, p.2661-87

Uddin, F. (2018). *Montmorillonite: An introduction to properties and utilization*. IntechOpen London, UK

Uddin, T. M., Chakraborty, A. J., Khusro, A., Zidan, B. R. M., Mitra, S., Emran, T. B., Sahibzada, M. U. K. (2021). Antibiotic resistance in microbes: History, mechanisms, therapeutic strategies and future prospects. *Journal of Infection and Public Health, 14*, p.1750-66

Ujihara, M. et Imae, T. (2010). Hierarchical structures of dendritic polymers. *Polymer international, 59*, p.137-44

Van Duijkeren, E., Schink, A.-K., Roberts, M. C., Wang, Y. et Schwarz, S. (2018). Mechanisms of bacterial resistance to antimicrobial agents. *Microbiology spectrum, 6*, p.6.2. 14

Van Goethem, M. W., Pierneef, R., Bezuidt, O. K., Van De Peer, Y., Cowan, D. A. et Makhalanyane, T. P. (2018). A reservoir of 'historical'antibiotic resistance genes in remote pristine Antarctic soils. *Microbiome, 6*, p.1-12

Varadwaj, G. B. B. et Parida, K. (2013). Montmorillonite supported metal nanoparticles: an update on syntheses and applications. *Rsc Advances, 3*, p.13583-93

Vázquez, D. (2012). Inhibitors of protein biosynthesis. p.

Velkov, T. et Roberts, K. D. (2019). Discovery of novel polymyxin-like antibiotics. *Polymyxin Antibiotics: From Laboratory Bench to Bedside*, p.343-62

Verma, R., Pathak, S., Srivastava, A. K., Prawer, S. et Tomljenovic-Hanic, S. (2021). ZnO nanomaterials: Green synthesis, toxicity evaluation and new insights in biomedical applications. *Journal of Alloys and Compounds, 876*, p.160175

Vincent, M., Duval, R. E., Hartemann, P. et Engels-Deutsch, M. (2018). Contact killing and antimicrobial properties of copper. *Journal of applied microbiology, 124*, p.1032-46

Wakshlak, R. B.-K., Pedahzur, R. et Avnir, D. (2015). Antibacterial activity of silver-killed bacteria: the" zombies" effect. *Scientific reports, 5*, p.1-5

Wan, F., Draz, M. S., Gu, M., Yu, W., Ruan, Z. et Luo, Q. (2021). Novel strategy to combat antibiotic resistance: a sight into the combination of CRISPR/Cas9 and nanoparticles. *Pharmaceutics, 13*, p.352

Wang, C. Y., Makvandi, P., Zare, E. N., Tay, F. R. et Niu, L. N. (2020). Advances in antimicrobial organic and inorganic nanocompounds in biomedicine. *Advanced Therapeutics, 3*, p.2000024

Wang, J., Ji, B., Shu, Y., Chen, W., Zhu, L. et Chen, F. (2018). Cr (VI) Removal from Aqueous Solution Using Starch and Sodium Carboxymethylcellulose-Coated Fe and Fe/Ni Nanoparticles. *Polish Journal of Environmental Studies, 27*, p.

Wang, Z., Lee, Y.-H., Wu, B., Horst, A., Kang, Y., Tang, Y. J. et Chen, D.-R. (2010). Anti-microbial activities of aerosolized transition metal oxide nanoparticles. *Chemosphere, 80*, p.525-9

Widdowson, C. A., Adrian, P. V. et Klugman, K. P. (2000). Acquisition of chloramphenicol resistance by the linearization and integration of the entire staphylococcal plasmid pC194 into the chromosome of Streptococcus pneumoniae. *Antimicrob. Agents Chemother., 44*, p.393-5

Williams, L. B., Metge, D. W., Eberl, D. D., Harvey, R. W., Turner, A. G., Prapaipong, P. et Poret-Peterson, A. T. (2011). What makes a natural clay antibacterial? *Environmental science & technology, 45*, p.3768-73

Witte, W. (2000). Selective pressure by antibiotic use in livestock. *Int. J. Antimicrob. Agents, 16*, p.19-24

Wolter, N., Smith, A. M., Farrell, D. J., Schaffner, W., Moore, M., Whitney, C. G., Klugman, K. P. (2005). Novel mechanism of resistance to oxazolidinones, macrolides, and chloramphenicol in ribosomal protein L4 of the pneumococcus. *Antimicrob. Agents Chemother., 49*, p.3554-7

Wright, G. D. (2010). Q&A: Antibiotic resistance: where does it come from and what can we do about it? *BMC Biol., 8*, p.1-6

Wu, K., Su, D., Liu, J., Saha, R. et Wang, J.-P. (2019). Magnetic nanoparticles in nanomedicine: A review of recent advances. *Nanotechnology, 30*, p.502003

Xiu, Z.-M., Zhang, Q.-B., Puppala, H. L., Colvin, V. L. et Alvarez, P. J. (2012). Negligible particle-specific antibacterial activity of silver nanoparticles. *Nano letters, 12*, p.4271-5

Xu, L., Chen, G., Peng, C., Qiao, H., Ke, F., Hou, R., Wan, X. (2017). Adsorptive removal of fluoride from drinking water using porous starch loaded with common metal ions. *Carbohydrate Polymers, 160*, p.82-9

Yamanaka, M., Hara, K. et Kudo, J. (2005). Bactericidal actions of a silver ion solution on Escherichia coli, studied by energy-filtering transmission electron microscopy and proteomic analysis. *Applied and environmental microbiology, 71*, p.7589-93

Yan, A. et Chen, Z. (2019). Impacts of silver nanoparticles on plants: a focus on the phytotoxicity and underlying mechanism. *International Journal of Molecular Sciences, 20*, p.1003

Yan, H., Chen, X., Bao, C., Yi, J., Lei, M., Ke, C., Lin, Q. (2020a). Synthesis and assessment of CTAB and NPE modified organo-montmorillonite for the fabrication of organo-montmorillonite/alginate based hydrophobic pharmaceutical controlled-release formulation. *Colloids and Surfaces B: Biointerfaces, 191*, p.110983

Yan, Z., Zhong, Y., Duan, Y., Chen, Q. et Li, F. (2020b). Antioxidant mechanism of tea polyphenols and its impact on health benefits. *Anim. Nutr., 6*, p.115-23

Yang, Z., Zhao, T., Huang, X., Chu, X., Tang, T., Ju, Y., Gao, S. (2017). Modulating the phases of iron carbide nanoparticles: from a perspective of interfering with the carbon penetration of Fe@ Fe 3 O 4 by selectively adsorbed halide ions. *Chemical science, 8*, p.473-81

Yu, S.-J., Chao, J.-B., Sun, J., Yin, Y.-G., Liu, J.-F. et Jiang, G.-B. (2013). Quantification of the uptake of silver nanoparticles and ions to HepG2 cells. *Environmental science & technology, 47*, p.3268-74

Yu, Y., Xu, Q., He, S., Xiong, H., Zhang, Q., Xu, W., Yu, Z. (2019). Recent advances in delivery of photosensitive metal-based drugs. *Coordination Chemistry Reviews, 387*, p.154-79

Yuan, P., Ding, X., Yang, Y. Y. et Xu, Q. H. (2018). Metal nanoparticles for diagnosis and therapy of bacterial infection. *Advanced Healthcare Materials, 7*, p.1701392

Yun'an Qing, L. C., Li, R., Liu, G., Zhang, Y., Tang, X., Wang, J., Qin, Y. (2018). Potential antibacterial mechanism of silver nanoparticles and the optimization of orthopedic implants by advanced modification technologies. *International journal of nanomedicine, 13*, p.3311

Zahid, M., Nadeem, N., Hanif, M. A., Bhatti, I. A., Bhatti, H. N. et Mustafa, G. (2019). Metal ferrites and their graphene-based nanocomposites: synthesis, characterization, and applications in wastewater treatment. Dans *Magnetic nanostructures* (p. 181-212) : Springer.

Zapun, A., Contreras-Martel, C. et Vernet, T. (2008). Penicillin-binding proteins and beta-lactam resistance. *FEMS Microbiol Rev, 32*, p.361-85

Zare-Akbari, Z., Farhadnejad, H., Furughi-Nia, B., Abedin, S., Yadollahi, M. et Khorsand-Ghayeni, M. (2016). PH-sensitive bionanocomposite hydrogel beads based on carboxymethylcellulose/ZnO nanoparticle as drug carrier. *International journal of biological macromolecules, 93*, p.1317-27

Zhang, C. X. et Lippard, S. J. (2003). New metal complexes as potential therapeutics. *Current opinion in chemical biology, 7*, p.481-9

Zhang, J., Guo, W., Li, Q., Wang, Z. et Liu, S. (2018). The effects and the potential mechanism of environmental transformation of metal nanoparticles on their toxicity in organisms. *Environmental Science: Nano, 5*, p.2482-99

Zhang, P., Zhang, Y., Gao, M. et Zhang, X. (2016). Dendrimer-assisted hydrophilic magnetic nanoparticles as sensitive substrates for rapid recognition and enhanced isolation of target tumor cells. *Talanta, 161*, p.925-31

Zhang, W. (2014). Nanoparticle aggregation: principles and modeling. *Nanomaterial*, p.19-43

Zhao, Q., Wendlandt, S., Li, H., Li, J., Wu, C., Shen, J., Wang, Y. (2014). Identification of the novel lincosamide resistance gene lnu (E) truncated by IS Enfa5-cfr-IS Enfa5 insertion in Streptococcus suis: de novo synthesis and confirmation of functional activity in Staphylococcus aureus. *Antimicrob. Agents Chemother., 58*, p.1785-8

Zhu, S.-B. (1995). Interactions of water, ions, and atoms with metal surfaces. *Surface Science, 329*, p.276-84